Current Based Fault Detection and Diagnosis of Induction Motors

Adaptive Mixed-Residual Approach for Fault Detection and Diagnosis of Rotor, Stator, Bearing and Air-Gap Faults in Induction Motors Using a Fuzzy Logic Classifier with Voltage and Current Measurement Only

by

William John BRADLEY, MEng.

Thesis submitted in fulfilment of the requirement for the degree of

Doctor of Philosophy

School of Engineering, Design and Technology

University of Bradford

2013

Abstract

Current Based Fault Detection and Diagnosis of Induction Motors
William John BRADLEY

Keywords: Condition based maintenance, induction motor, fault detection and diagnosis, parameter estimation, fuzzy logic, modelling, speed estimation

Induction motors (IM) find widespread use in modern industry and for this reason they have been subject to a significant amount of research interest in recent times. One particular aspect of this research is the fault detection and diagnosis (FDD) of induction motors for use in a condition based maintenance (CBM) strategy; by effectively tracking the condition of the motor, maintenance action need only be carried out when necessary. This type of maintenance strategy minimises maintenance costs and unplanned downtime. The benefits of an effective FDD for IM is clear and there have been numerous studies in this area but few which consider the problem in a practical sense with the aim of developing a single system that can be used to monitor motor condition under a range of different conditions, with different motor specifications and loads.

This thesis aims to address some of these problems by developing a general FDD system for induction motor. The solution of this problem involved the development and testing of a new approach; the adaptive mixed-residual approach (AMRA). The main aim of the AMRA system is to avoid the vast majority of unplanned failures of the machine and therefore as opposed to tackling a single induction motor fault, the system is developed to detect all four of the most statistically prevalent induction motor fault types; rotor fault, stator fault, air-gap fault and bearing fault. The mixed-residual fault detection algorithm is used to detect these fault types which includes a combination of spectral and model-based techniques coupled with particle swarm optimisation (PSO) for automatic identification of motor parameters. The AMRA residuals are analysed by a fuzzy-logic classifier and the system requires only current and voltage inputs to operate. Validation results indicate that the system performs well under a range of load torques and different coupling methods proving it to have significant potential for use in industrial applications.

Acknowledgements

This piece of research would not have been possible without the continued assistance of the Engineering, Design and Technology (EDT) staff. Developing and operating the test rig was a significant challenge and could not have been accomplished without the help of Hybrid Powertrain Engineering Research Centre (HyperC) and workshop staff in particular Didge Chavda and Chib Mistry.

I would also like to thank Moftah Binhasan for his support and Keith Harrison of the Bradford Armature and Winding Company (BAWCO) for kindly offering his time at the beginning of the project.

Special thanks go to my industrial supervisor Charles Pestell and the support of S&I Ltd, and, my academic supervisors Kambiz Ebrahimi and John Victory. Without the expertise and support of John and Kambiz in particular I would have found it impossible to make it this far.

Most importantly I want to thank my parents for their continued support and help towards payment of fees, and finally my wife, Hannah, for putting up with me over the past 4 years whilst I worked towards completing this piece of work.

Table of Contents

List of Figures

List of Tables

Nomenclature

a	Wavelet scale parameter
b	Wavelet time parameter (s)
D_b	Diameter of rolling element or ball (m)
D_c	Diameter of cage (m)
$\boldsymbol{e}$	Error
F_c	Cage defect characteristic frequency (Hz)
F_O	Outer-race defect characteristic frequency (Hz)
F_I	Inner-race defect characteristic frequency (Hz)
F_R	Rolling element defect characteristic frequency (Hz)
f_{ecc}	Eccentricity related frequency components (Hz)
f_0	Supply frequency (Hz)
f_r	Mechanical rotational speed (Hz)
f_{har}	Harmonic frequency (Hz)
f_{rotor}	Rotor rotational frequency (Hz)
f_s	Supply frequency (Hz)
i_A	Line current (A)
i_D	Line current referred to D-axis (A)
i_Q	Line current referred to D-axis (A)
i_{as}	Stator current (A)
i_{ar}	Rotor cage current (A)
I_R	Equivalent circuit rotor current (A)
$\boldsymbol{i}_s^{abc}\boldsymbol{i}_r^{abc}$	Stator and rotor current matrices on ABC axes (A)
$\boldsymbol{i}_s^{qd0}, \boldsymbol{i}_r^{qd0}$	Stator current matrix in QD0 reference frame (A)
i_{ds}, i_{qs}	Stator current in direct and quadrature axes (A)
i_{dr}, i_{qr}	Rotor current in direct and quadrature axes (A)
$i_{(p,t)-sim}$	‘t’th sample of the simulated line current on line p
$i_{(p,t)-mes}$	‘t’th sample of the measured line current on line p
J_{eq}	Combined equivalent inertia of motor and load (kg/ms^2)
$\boldsymbol{L}_{ss}^{abc}$	Stator self inductance matrix on ABC axes (H)
$\boldsymbol{L}_{sr}^{abc}\boldsymbol{L}_{rs}^{abc}$	Stator-rotor mutual inductance matrices on ABC axes (H)
$\boldsymbol{L}_{rr}^{abc}$	Rotor self inductance matrix on ABC axes (H)
$L_{ls},\ L_{lr}$	Stator and rotor leakage inductances (H)
L_{ss}, L_{rr}	Stator and rotor self inductances (H)

L_{sm}, L_{rm}	Stator and rotor magnetizing inductances (H)
L_{11}	Stator inductance matrix element (row ‘i’, column ‘k’) (H)
$n_{a,b,c}$	Number of shorted turns on ‘a’, ‘b’ and ‘c’ windings
$n_{ST-a,b,c}$	Proportion of healthy turns on the ‘a’, ‘b’ and ‘c’ windings
n_{BB}	Number of broken rotor bars
N_{RB}	Number of rotor bars
N	Number of rotor bars
n	Rotor bar harmonic
n_e	Rotor eccentricity harmonic
n_{ws}	Stator MMF harmonic
P	Active power (kW)
P_{mech}	Mechanical power (kW)
P, p	Number of pole pairs
$P_{apparent}$	Apparent power (kW)
P_{active}	Active power (kW)
P_{IN}	Input power (kW)
$P_{IN.R}$	Rated input power (kW)
P_R	Rated power (kW)
R	Equivalent circuit combined resistance (Ω)
r_r	Rotor cage resistance (Ω)
r_s	Stator winding resistance (Ω)
$\boldsymbol{r}_s^{abc}$	Stator resistance matrix on ABC axes (Ω)
$\boldsymbol{r}_r^{abc}$	Rotor resistance matrix on ABC axes (Ω)
ΔR	Change in resistance (Ω)
$r_{ri,k}$	Rotor resistance matrix element (row ‘i’, column ‘k’) (Ω)
$\Delta r_{a,b,c}$	Change in resistance on ‘a’, ‘b’ and ‘c’ winding (Ω)
$\boldsymbol{r}_s^{qd0}, \boldsymbol{r}_r^{qd0}$	Stator resistance matrix for the QD0 axes (Ω)
R_s, R_r	Equivalent circuit stator and rotor resistances (Ω)
R_R	Equivalent circuit rotor resistance (Ω)
RF_{res}	Rotor fault residual (dB)
$Rfault_{i-sim}$	Simulated rotor fault value on line 1 (dB)
$Rfault_{i-mes}$	Actual rotor fault value on line 1 (dB)
$Rfault_1$	Rotor fault value on line 1 (dB)
s	Slip
S	Apparent power (kW)

$Sfault$	Stator fault value
$SBP_{line-1U}$	Upper sideband peak value line (dB)
$SBP_{line-1L}$	Lower sideband peak value line (dB)
T_{em}	Electromagnetic torque (Nm)
T_{est}	Estimated torque (Nm)
T_L	Load torque (Nm)
$T_{qd0}(\theta_d)$	ABC-to-QD0 axes transformation
T_R	Rated torque (Nm)
v_{ar}	Rotor cage voltage (V)
v_{as}	Stator voltage (V)
$\boldsymbol{v}_s^{qd0}, \boldsymbol{v}_r^{qd0}$	Stator and rotor voltage matrices QD0 reference frame (V)
$\boldsymbol{X}$	Measured data
X	Equivalent circuit combined reactance
$\widehat{\boldsymbol{X}}$	Simulated data
X_1	Equivalent circuit stator reactance
X_2	Equivalent circuit rotor reactance
$x(t)$	Waveform signal
Z_{fl}	Full load combined impedance (Ω)
Z	Impedance (Ω)
β	Contact angle between ball and raceway (º)
η_B	Proportion of damaged rotor bars
θ_d	Rotor angular position with respect to the direct axis (rad)
θ_r	Rotor angular position with respect to winding A (rad)
λ_{0s},λ_{0r}	0-axis flux in stator windings and rotor cage (Wb)
λ_{as}	Stator winding flux (Wb)
λ_{ar}	Rotor cage flux (Wb)
$\boldsymbol{\lambda}_s^{abc}$	Stator winding flux matrix on ABC axes (Wb)
$\boldsymbol{\lambda}_r^{abc}$	Rotor cage flux matrix on ABC axes (Wb)
$\boldsymbol{\lambda}_s^{qd0}, \boldsymbol{\lambda}_r^{qd0}$	Stator and rotor flux matrix in QD0 reference frame (Wb)
μ_x	Degree of membership for fuzzy set ‘x’
φ_R	Rated power factor angle (rad)
φ	Power factor angle (rad)
ψ_{qs}	Rate of change of flux of stator referred to quadrature axis (Wb/s)
ψ_{qr}	Rate of change of flux of stator referred to direct axis (Wb/s)
ψ_{0s}	Rate of change of flux of stator referred to zero axis (Wb/s)

$\psi(.)$	Wavelet transform
ω_b	Base frequency (Hz)
ω_d	Direct axis rotational speed (rad/s)
ω_{est}	Estimated mechanical rotational speed (rad/sec)
ω_m	Mechanical rotational speed of the rotor (rad/sec)
ω_r	Electrical rotational speed of the rotor (rad/sec)
ω_{sync}	Synchronous mechanical rotational speed (rad/sec)

Abbreviations

AE	Acoustic Emission
AMRA	Adaptive Mixed-Residual Approach
ANN	Artificial Neural Network
AR	Auto-Regressive
ARMA	Auto-Regressive Moving Average
CBM	Condition Based Maintenance
CM	Condition Monitoring
CMM	Co-ordinate Measuring Machine
CoV	Coefficient of Variation
DAQ	Data Acquisition
DE	Dynamic Eccentricity
DE	Drive End
DOL	Direct On-Line
DoM	Degree of Membership
DQ	Direct-Quadrature (axes)
EKF	Extended Kalman Filter
EMF	Electro-Motive Force
EPVA	Extended Park's Vector Approach
ES	Evolution Strategy
ES	Expert System
ETA	Event Tree Analysis
FDA	Fisher Discriminant Analysis
FDD	Fault Detection and Diagnosis
FDS	Fault Diagnosis System
FLC	Full Load Current
FOS	Fast Orthogonal Search
FFT	Fast Fourier Transform
FTA	Fault Tree Analysis
GA	Genetic Algorithm
HV	High Voltage
IM	Induction Motor
LDR	Laser Doppler Velocimetry
LRC	Locked Rotor Current
LS	Local Search

LV	Low Voltage
MCC	Motor Control Centre
MCSA	Motor Current Signature Analysis
MMF	Magneto-Motive Force
MRAS	Model Reference Adaptive System
NDE	Non-Drive End
NM	Nelder-Mead
NN	Neural Network
NS	Negative Sequence
PCA	Principal Component Analysis
PD	Partial Discharge
PF	Power Factor
PS	Pattern Search
PSO	Particle Swarm Optimisation
PWM	Pulse-Width Modulated
QD0	Quadrature-Direct-Zero (axes)
RBF	Radial Basis Function
RBPF	Rotor Bar Pass Frequency
RSH	Rotor Slot Harmonics
RW	Random Walk
SA	Simulated Annealing
SE	Static Eccentricity
SEA	Spectral Energy Analyser
STFT	Short-Time Fourier Transform
SVAnF	Space Vector Angular Fluctuation
SVAmF	Space Vector Amplitude Fluctuation
TSE	Total Spectral Energy
UMP	Unbalanced Magnetic Pull
VSD	Variable Speed Drive
WFA	Winding Function Approach
WPT	Wavelet Packet Transform
ZCT	Zero-Crossing Time
3P+E+N	Three Phase, Earth and Neutral

Chapter 1. Introduction

The inevitable and continual deterioration of every physical system eventually results in system failure; the point at which the system no longer performs the function it was designed to. Engineers develop solutions to these problems by creating more robust and reliable solutions with ever increasing mean time between failures (MTBF) but failures still occur and cause significant problems when they do occur. System failures must be dealt with in a suitable manner with the overall objective of reducing the amount of time that the system is malfunctioning, and by minimising this downtime the efficiency (proportion of time spent producing the desired output or product) of the system is maximised. This makes the method by which system failures are addressed, known as maintenance, highly important; effective maintenance is the key to maximising efficiency.

Within the field of maintenance there are three commonly applied approaches which find applications in modern industrial environments, the aim of each strategy to keep the plant operating as close to maximum efficiency as possible. The simplest maintenance strategy is reactive maintenance (also known as run-to-failure, breakdown or unplanned maintenance [1]). The concept of this approach is to operate or use a component or system until it fails [2], where a failure is defined as the point at which the system can no longer perform the function it was designed to perform. With reactive maintenance, upon failure the device is either repaired or replaced by a similar component held in reserve. Unfortunately reactive maintenance suffers from the unavoidable fact that considerable downtime occurs due to the unforeseen nature of the failures

which occur with relatively high frequency due to the lack of other types of maintenance. When applying this form of maintenance failures cannot be predicted and thus cause extended delays due to the additional time required to find the failure, shutdown the process safely and repair any secondary damage or disruption to the production line. The significant time delays associated with these activities lead to excessive plant downtime which results in poor overall efficiencies. Run-to-failure maintenance strategies usually involve a standby spare to replace the faulty component or alternatively duplex systems can be employed; utilising primary and secondary (standby) components in a single system to ensure a redundant component is available should the active component fail. Redundant systems and large spares inventories obviously have an associated cost in terms of initial capital required to purchase and install and also the cost associated with the constant monitoring and management of the spare inventory as units fail and need replacement.

A logical improvement of this type of maintenance is to conduct repairs or replacements at regular intervals. This strategy is known as preventative maintenance [3]. Regular repairs and inspections are carried out in an effort to prevent the failures from occurring, with the maintenance exercise carried out regardless of whether the item is faulty or not. It is clear that this form of maintenance is highly inefficient because, on one hand, if scheduled too frequently there is an increase in plant downtime (during repair/replacement operations) and maintenance costs and on the other if scheduled too infrequently there is an increase in the chance of motor failure.

Each of these types of maintenance has its drawbacks and it is for this reasons that recently interest has grown in a third area of maintenance; that of predictive maintenance or condition based maintenance (CBM) [1], [2], [4].

CBM is based around the concept of condition monitoring (CM). A system is observed over time in order to detect incipient faults before they develop into system failures. The CBM procedure can be broken down into three stages [1]:

1. Information Collection. This stage involves data acquisition using suitable instrumentation.
2. Information Handling. The acquired data and signals are processed to make them more useful for the diagnosis procedures (feature extraction).
3. Decision Making. Using the processed data the maintenance system determines the faulty components (and in some cases recommends maintenance action).

In summary, a CBM system should detect faults *before* they turn into system failures. CBM overcomes the problems of both preventative and reactive maintenance by only scheduling maintenance when it is necessary. This minimises the downtime associated with both planned maintenance activities and also unplanned downtime due to system failures making CBM the most efficient and cost effective maintenance strategy. Initial costs for a CBM system depend on the quantity which is monitored and sensors required for measuring this variable, and also the software which is used to measure, process and analyse these quantities and finally the hardware on which the software is to be executed. This may seem prohibitive for some applications and in many cases it is (which is why reactive and preventative maintenance strategies can still be found), however, quantities which contain useful information on system

condition are often already measured for control or protection purposes and thus only the software to record, process and analyse these variables is all that is required to implement a CBM strategy on an existing process.

1.1 The three-phase induction motor

The modern industrial plant or factory is a suitable candidate for the implementation of a CBM strategy. In these environments there are numerous mechanical, electrical, hydraulic and pneumatic systems which must be functioning correctly for the plant or factory to produce a useful product or output. Amongst these systems there is one device which finds extensive use and can be used in any number of purposes (driving pumps, fans, conveyors, etc); this device is the induction motor.

Commonly described as the workhorse of modern industry the induction motor (IM) is an established technology that is rugged, provides good performance and is relatively inexpensive [5]. The IM is an asynchronous, alternating current machine which can be driven by single-phase, for smaller power requirements, or 3-phase power for more general applications. The alternating current is spread around the periphery of the machine via the stator windings in order to create a rotating magnetic field which induces currents in the rotor squirrel-cage; a number of bars shorted by two end rings. The currents in the rotor generate a magnetic field which interacts with the stator field in order to produce a torque on the rotor output shaft. Since the currents are induced in the rotor there is no requirement for the mechanical contacts or ‘brushes’ required by direct current (DC) machines. The moving parts (rotor assembly) of the machine are enclosed within the stator housing and sealed by the end-plates making the IM suitable for use in harsh environments.

The IM is thus a reliable and robust machine however it is inevitable that, like any physical system, during operation the component parts of the machine will develop faults at some time which will eventually propagate into system failures.

The induction motor can fail in a number of different ways. Two leading studies have been conducted on the statistics of motor failures and these studies are cited in [2]. These investigations aimed at identifying the different types of motor failure; one study was conducted by IEEE-IGA and the other by General Electric Co. The results of these studies can be found in Table 1.1.

Table 1.1 Statistics of induction motor failure types (source [2]***)***

Fault Type	Percentage of Total Failures (%)	
	IEEE-IGA Study	GE Study
Bearing	42	40
Stator	28	38
Rotor	8	10
Other	22	12

The most prevalent failures are associated with the shaft bearings, stator windings and rotor cage of the machine; it follows that faults in these areas will be those that a IM monitoring system should be, as a priority, able to reliably detect in order to provide the maximum benefit to the plant maintenance effectiveness. The ‘other’ category includes air-gap eccentricity faults and bent shaft faults (a type of eccentricity) amongst other less prevalent faults, and thus air-gap eccentricity faults (static and dynamic) make up the final member of the top 4 prevalent fault types. These four fault zones (stator, rotor, air-gap and bearing) are the most prevalent sources of IM failures [6], and therefore must be reliably detected by a IM fault detection and diagnosis (FDD) system if it is to be suitable for use in a CBM scheme.

The induction motor is the subject of this thesis and the development of FDD tool to be used with induction motors will be documented in the remainder of this document. The FDD tool is aimed at enabling a CBM strategy to be applied in industrial environments with respect to induction motors.

1.2 Fault detection and diagnosis (FDD)

Fault detection and diagnosis is the process of identifying deviation from healthy condition (change detection) and from these detected changes identifying which type of fault has occurred (diagnosis). The process of FDD provides the input data on which a CBM strategy operates; the FDD process identifies a specific fault and then the CBM strategy is used to track this fault over time and schedule an appropriate maintenance activity at an appropriate time with the aim of bringing the process or system back to a healthy state with the minimum amount of disruption. This process is depicted in Figure 1.1.

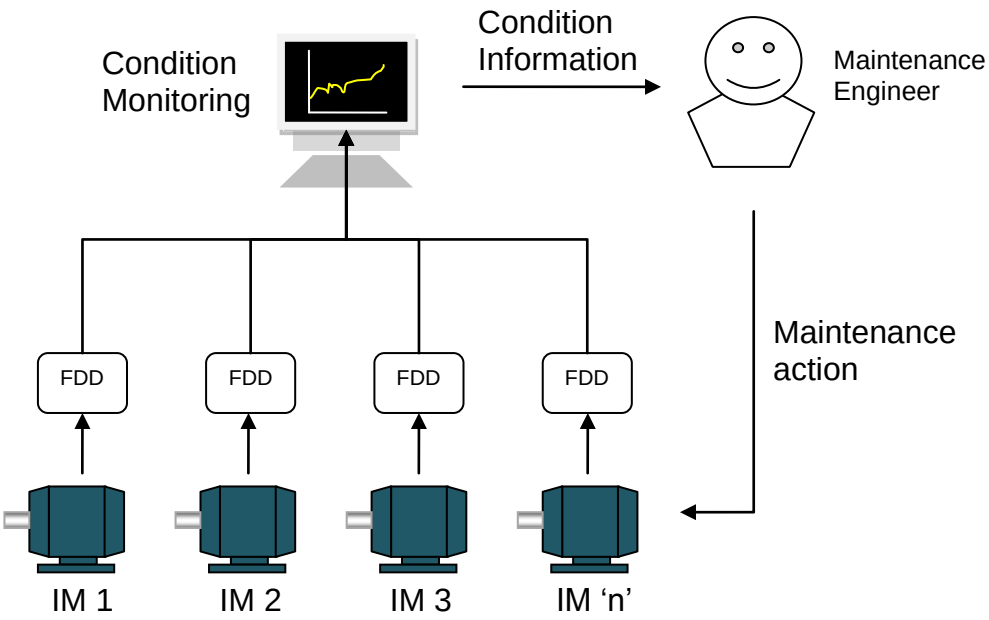

Figure 1.1 FDD as part of a CBM system

The process of fault detection involves performing some form of processing on measured process (system) variables. The aim of the processing is to produce

some ‘features’ which are compared in faulty and healthy cases to generate ‘residuals’ and are sensitive to one or more fault cases. Limit value checking, correlation functions, frequency spectra, variances, amplitudes, state and parameter estimations, parity equations are all examples of methods that can be used to generate the features which indicate the presence of a particular fault [4].

The process of fault diagnosis is the determination of the type of fault and other details relating to the fault such as fault magnitude, fault location and the time of detection. Diagnosis systems can be implemented in a number of different ways and can utilise several different techniques with fault trees, digraphs, model-based methods, knowledge-based systems and neural approaches have been used for the purpose of fault diagnosis [7]. When combined, the fault detection and diagnosis elements result in a system which provides useful data on the health of a process which can be used as the input to a CBM programme.

Figure 1.2 shows a flow chart which describes the key components of a FDD system.

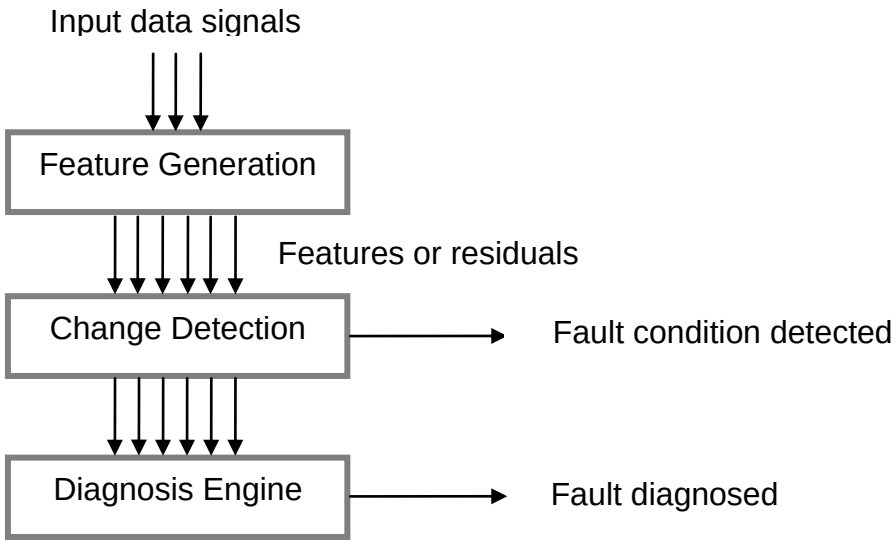

Figure 1.2 FDD system flow chart

As mentioned previously the input data can take the form of raw measured variables or could be parameter or state estimates, etc. These different data types are processed in order to generate a number of ‘features’ or ‘residuals’ which are analysed by some form of change detection. Since the raw data can be analysed in a number of different ways multiple features can be generated from one input data source to provide a better overall view of the system. Variation in the residuals is tracked in order to detect a fault condition has occurred and the diagnosis engine analyses these residuals in order to diagnose the details of the fault; which type of fault has occurred, fault severity, time of occurrence, etc. An overview of various FDD methods and techniques which can be applied for these purposes is found in Figure 1.3.

1.3 The ‘Adaptive Mixed-Residual Approach’ (AMRA) for universal induction motor fault detection and diagnosis

The method developed and validated in this dissertation is the adaptive mixed-residual approach for universal induction motor fault detection and diagnosis. This method utilises a diverse set of residuals (features) which are derived using both model-based and model-free techniques. This allows the system to utilise the power of model-based methods where a model is appropriate, and in cases where model parameters are too complex to identify, the model-based approaches are supplemented with a range of data processing based residuals such as specific spectral components.

The usage of these different fault indicator methods results in a set of residuals which range from parameter estimates of complex models and simple comparisons of the current signals features. When these residuals are combined the information they provide can be used to produce more accurate

FDD results if analysed by a suitable diagnosis component, such as a fuzzy logic algorithm. The fuzzy logic provides the diagnosis aspect of the system using the mixed residuals as inputs and reaching a diagnosis for each of the four motor subsystems; bearing, air-gap, stator and rotor.

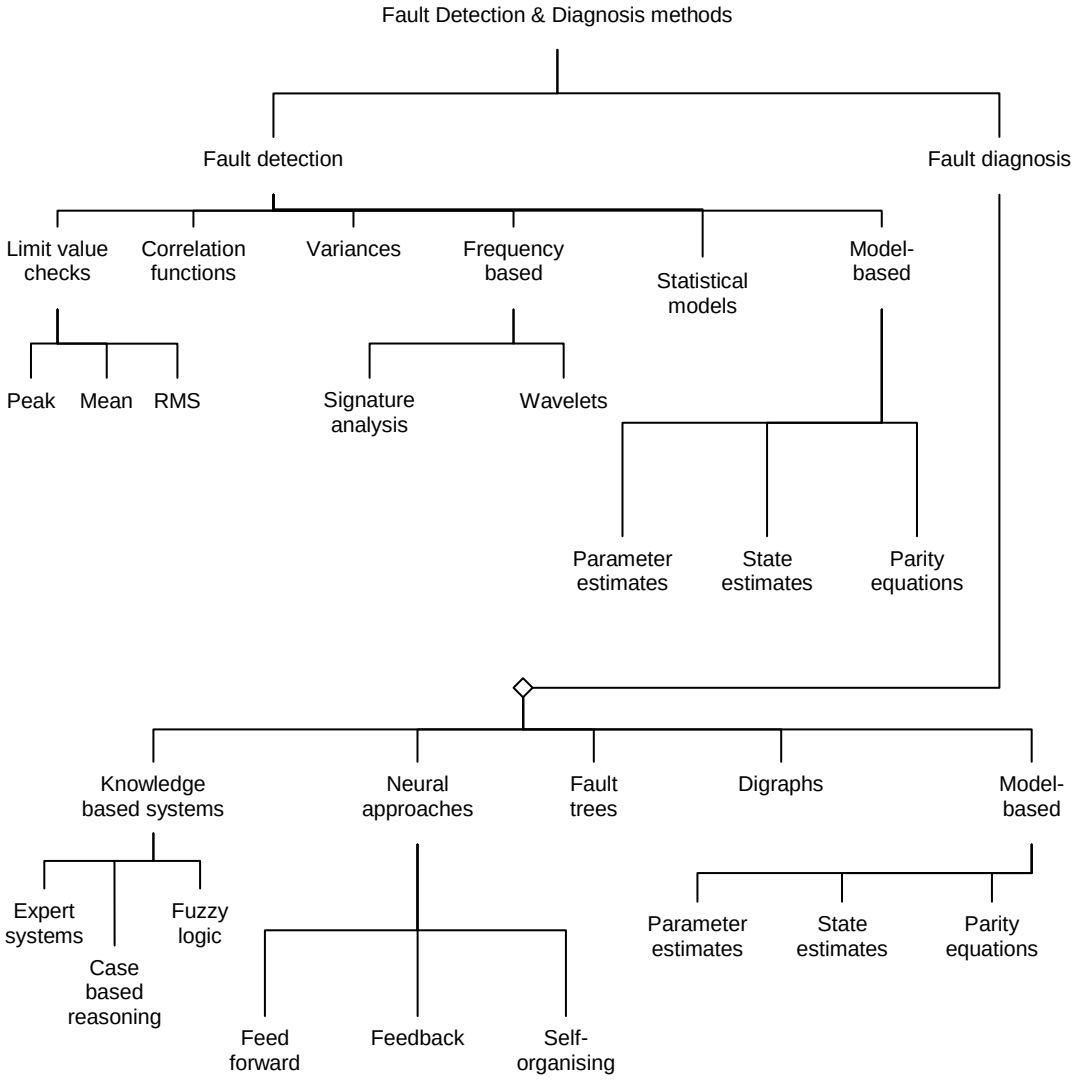

Figure 1.3 An overview of fault detection and diagnosis techniques

The mixed residual set provides a large amount of information on many aspects of machine operation and thus when combined with the fuzzy logic classifier it has the ability to detect and diagnose the four most prevalent motor faults. Since these faults are the cause of the vast majority of machine failures the

system can provide universal FDD by considering several faults and not just one or two.

In addition, the system utilises only current and voltage signals and requires only the freely available nameplate data as inputs. No detailed machine knowledge is required. Beyond this all information is gathered automatically by the system, including a PSO based parameter estimation routine which identifies the motor model and development of a ‘baseline’ for the motor which acts as a birth case state against which subsequent FDD results are compared. By using a baseline and the parameter estimation routine the algorithm has the ability to adapt itself to a range of motors, loads, operating conditions, load connections, motor speeds, etc allowing the algorithm be deployed on a vast range of motors and applications. An overview of the system operation is given in Figure 1.4.

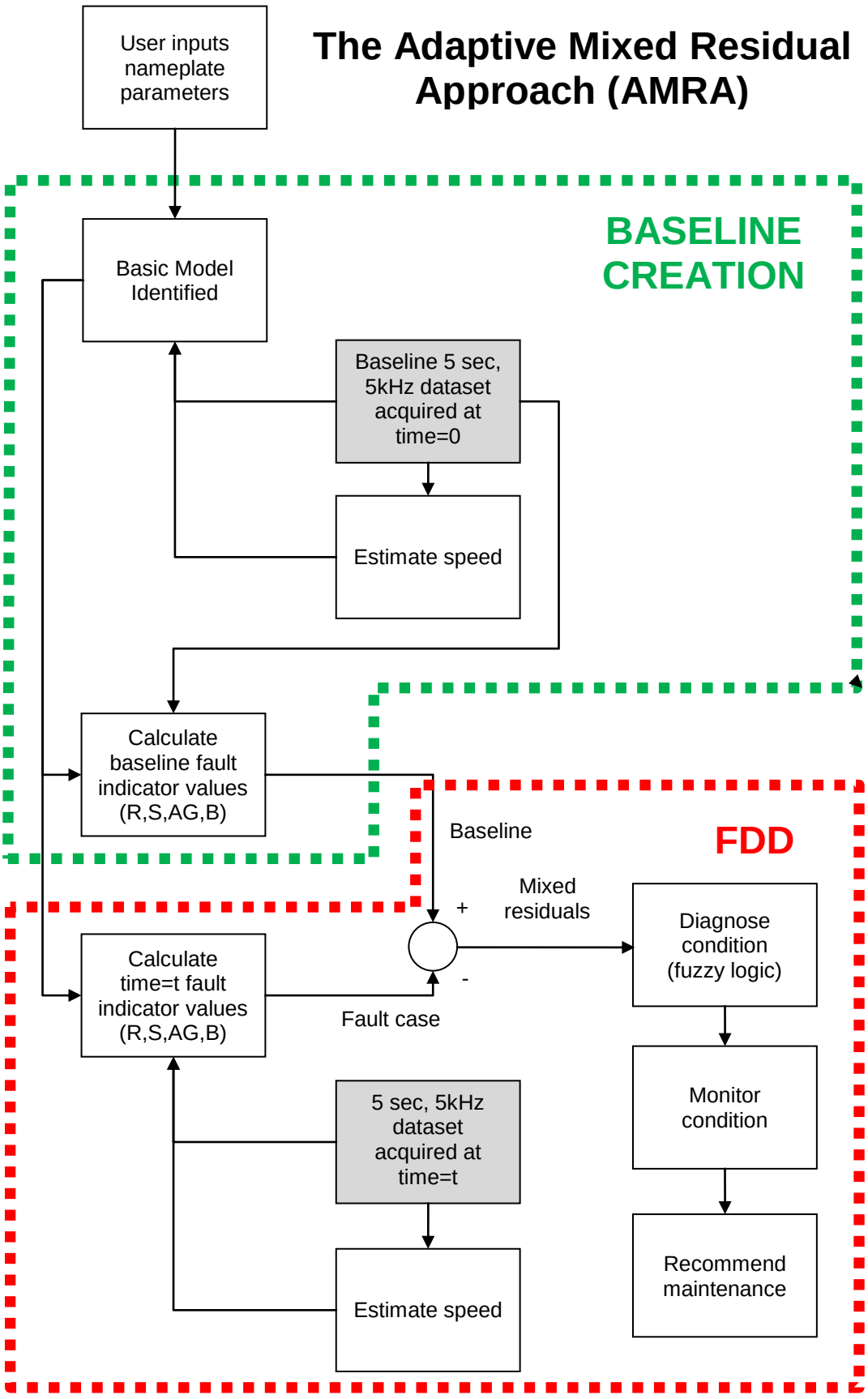

Figure 1.4 Overview of the Adaptive Mixed-Residual Approach (AMRA)

1.4 Problem statement

Considerable research effort has been invested in the area of induction motor fault detection and diagnosis over recent years. This research effort has focused on a range of fault types and the detection and diagnosis methods have wide variety too.

The majority of research interest focuses on one or two specific faults and how to develop a system that is suitable for detecting this specific fault. In addition to this many fault detection and diagnosis algorithms require a detailed knowledge of the machine that is being monitored, for example, details of the winding layout, bearing type, or number of rotor bars. Some methods are inherently simple whereas others require models with simulation times of several hours.

The problem with these approaches is that in practical terms these systems are of minor use in industrial environments. Detecting only one or two fault types without even considering the other fault types makes missing detection of an induction motor fault highly probable. In order for a system to be useful it must attempt to detect the vast majority of possible faults in order to pre-empt as many failures as possible.

In addition to this, the average maintenance technician will not have access to detailed internal dimensions of the machine including details such as the number of stator turns, number of coils, number and electrical characteristics of the rotor bars, contact angles within the bearings, number of rolling elements, etc. In any given plant or factory tens or hundreds of machines will be operated and thus there will be huge range of required motor parameters. Hence an IM FDD system that requires detailed knowledge of the machine construction is prohibitive due to the difficulties in obtaining and inputting the long list of

required parameters. For a system to be feasible in a modern plant or factory it should have some form of self-learning requiring at most the motor characteristics that can be easily noted down from the nameplate (e.g. rated speed, load torque, current, etc). An IM FDD system must also be general, i.e. it must be applicable to a wide range of different motor sizes and types, the algorithms must adapt to the motor in question and be flexible enough to adapt to differing conditions whilst still maintaining the ability to detect and diagnose a range of faults.

The implementation of IM FDD systems need to consider how they will be deployed in practice. IM motors operate in the harshest of industrial environments and developing a system that requires a quad-core PC running a MATLAB programme with a number of National Instruments acquisition cards supporting several types of sensory equipment is simply not feasible in practice. These systems would be hugely expensive to purchase and challenging to install and maintain. There needs to be a system which requires minimal sensory equipment and that can be deployed to a microprocessor unit (i.e. C code or some equivalent) since microprocessor devices are the commonly used technology for motor switchgear control and protection devices (motor management). Therefore a problem exists in designing a system which utilises the minimum number of inputs (measured variables) and also uses inputs which require minimum changes to the plant instrumentation and can be deployed to a microprocessor device. By deploying control and monitoring functionality as close to the measurement point as possible implementation costs are reduced and the overall monitoring system reliability is improved [8].

The previous paragraphs describe the problem; much IM FDD theory exists and piecemeal or highly specific solutions have been developed which are suitable for laboratory use only in their basic form. Therefore the specific problem statement is as follows: *The need for the development of a general FDD system which is suitable for microprocessor deployment and utilises only measured current and voltage as system inputs. The system must have the flexibility to be applied to a range of motor types and sizes, not require detailed knowledge of machine construction and have the ability to differentiate between stator, rotor, air-gap eccentricity and bearing faults. The system should be designed to monitor faults within DOL (direct on-line) motors running at steady-state.*

A system of this type would provide the most value for use in a CBM strategy in order to maximise the effectiveness of modern industrial plants or factories.

1.5 Contributions

The contributions of this piece of research are as follows:

1. Development of the overall adaptive mixed-residual (AMRA) CM strategy.
2. Developed a particle swarm optimisation (PSO) driven parameter identification algorithm for estimation of all of the basic motor model parameters using current and voltage signals alone.
3. Developed a new induction motor model for simulation of rotor and stator faults which contains no algebraic loops and is thus suitable for code generation purposes (and therefore microprocessor deployment).
4. Coupled the rotor and stator fault model with a Nelder-Mead optimiser to provide rotor broken bar and stator turn-to-turn fault detection via parameter estimation.

5. Developed a speed estimation algorithm based on rotor bar pass frequencies (RBPF) in the current spectrum.
6. Developed a fuzzy logic algorithm to diagnose and isolate all the major IM fault types (stator, rotor, air-gap and bearing faults) based on the outputs of point (3) and the outputs of spectral bearing and air-gap feature generation algorithm.
7. Compared the current signals due to stator, rotor, air-gap and bearing faults for both directly coupled and belt coupled loads and developed the FDD system to be tolerant of these differences.

1.6 Dissertation outline

The dissertation is organised as follows and dissertation structure is shown in Figure 1.5.

Chapter 2 reviews the state-of-the-art of the field of induction motor fault detection and diagnosis and assesses the practical issues associated with implementing the different techniques.

Chapter 3 details the development of the basic QD0 model of the squirrel cage induction motor [9] and an extension of this model to allow motors with damaged rotor bars and stator turn-to-turn winding faults to be simulated. The model is then modified in order to remove all algebraic loops making it suitable for code generation purposes.

Chapter 4 describes the development of speed estimation algorithm based on the content of the current spectrum. A brief review of IM speed estimation is included in addition to the development and testing of a new speed estimation algorithm.

Chapter 5 explains the experimental setup used to test the motors. This includes both belt coupled and direct shaft coupled loads.

Chapter 6 reviews literature on induction motor parameter estimation and describes the development of the PSO based optimisation procedure used for the motor system identification process.

Chapter 7 details the validation of the optimisation procedure and basic (healthy) model.

Chapter 8 investigates the most prevalent induction motor failure modes and the incipient faults which lead to these failures. The development and symptoms of the faults are reviewed.

Chapter 9 proposes four different fault detection methods. These methods include model-based and model-free methods specifically chosen or developed to be fit for purpose in this type of IM FDD system. The performance of the fault detection methods is presented in this chapter.

Chapter 10 explains the fuzzy logic system used to analyse the results of the fault detection methods in addition to other variables in order to diagnose the overall machine condition and the condition of the four key subsystems (stator, rotor, air-gap and bearings). The full dataset results are presented here based on the collection of algorithms developed in previous chapters.

Chapter 11 provides a summary of the work included in this dissertation and makes some concluding remarks. Suitable topics for further work are recommended.

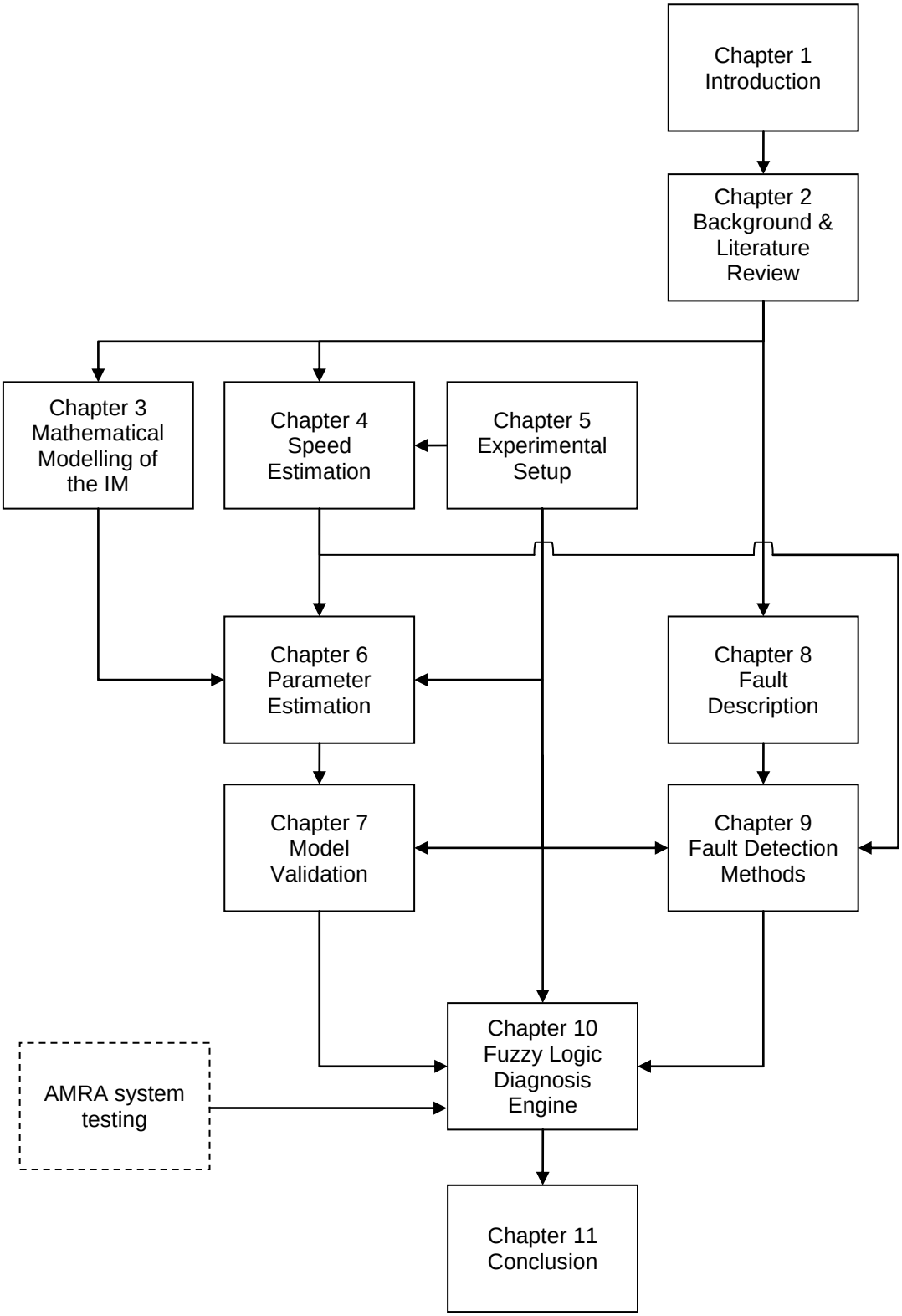

Figure 1.5 Structure of the dissertation

Chapter 2. Literature Review & Background

This chapter will give an introduction to the theories and applications found in literature regarding the development of induction motor (IM) fault detection and diagnosis (FDD) systems.

2.1 Input measurement types for IM FDD

The FDD algorithms which are used rely on some form of input data and this section will explore the types of input data which have been used in the area of IM FDD.

2.1.1 Vibration

Vibration of the motor can be measured by fitting accelerometers to the motor. Accelerometers can be fitted in order to measure vibration signals in the x, y and z directions; this results in signals being measured which correspond to vibration in the direction of the shaft and also in the horizontal and vertical planes [10]. Vibrations in the motor structure are detected using vibration transducers using strain gauge, piezoelectric, capacitive, electro-dynamic or electromagnetic principles of operation. Piezoelectric sensors are by far the most common as they can be designed to be small in size and weight, robust, and insensitive to external disturbances such as temperature variation, magnetic fields and airborne sound [11]. Piezoelectric accelerometers coupled with charge amplifiers are commonly used allowing the piezoelectric sensor charge output to be converted to an output voltage that can be easily measured. Once the vibration signal has been captured it can be filtered to extract frequencies of particular interest for detection of specific faults [12].

Accelerometers can be fitted directly onto the main stator housing of the motor, for example on a cooling fin [13], fitted onto the end-plates which house the bearings [14], or attached to motor mounting brackets [15]. The sensors can be attached magnetically [16] or simply be glued in place. Fibre-optic displacement sensors can also be mounted directly inside the bearing housing and used to track the deformation of the outer race of the bearing; this eliminates the extraneous vibration of the housing but is complex to install [17]. In addition to fixed and continuous measurement accelerometers, hand-held periodic vibration sensors can be utilised [15], however these require maintenance personnel to carry-out manual measurements and thus would not form part of a automated CBM scheme. The accelerometer output signals can be used to measure acceleration directly or, via integration of the signals, velocity and displacement can also be calculated and used for IM FDD. Non-contact optical vibration probes are also available [6,4]; these sensors use laser Doppler velocimetry (LDR) technology to eliminate the need for physical contact between sensor and system and avoid the installation constraints and electromagnetic noise that can affect piezoelectric sensors [19].

2.1.2 Current

The alternating current signals of the power supply to the motor or the current flowing through the stator windings (dependent on winding configuration) can be used as an FDD input. Current can be measured using Hall effect sensors [20] which output a second current signal proportional to the measured current value. Typical current sensors are relatively cheap and be combined easily with voltage sensors on compact printed circuit board (PCB) layouts [21]; the acquisition of these signals allows calculation of power based quantities. The

unobtrusive nature and ease of installation of current sensors gives current measurement a significant advantage over other input types and has led to an increase in the popularity of current based techniques such as motor current signature analysis (MCSA) [22]. Similar to vibration measurement, handheld devices exist for measuring voltage, current and power quality, however, they require plant operatives to carry-out manual maintenance rounds in order to gather the data. Current sensors are suitable for FDD applications due to their reliability, sensitivity and ease of accessibility [23]. In fact, current and voltage measurements will generally require no additional instrumentation to be added since the terminal voltages and currents will typically be available in the motor control centre (MCC) [24]. Thus the major benefit of current measurements is that in the majority of cases additional instrumentation will not be required since voltage and current measurements will already be available as they are used for motor protection and control purposes.

2.1.3 Flux

The fundamental principle of operation of an IM requires the creation of defined flux fields within the motor. If these magnetic fields change then they can indicate changes to the machine condition such as stator faults [25]. Axial flux can be measured using coils wound around the shaft of the machine and stray flux using search coils positioned around the machine [6], [26]. The search coils are non-invasive, however it may be impractical to install the sensors into a position where they obtain a reliable signal [27].

2.1.4 Partial discharge

As insulation breaks down small electrical discharges are created due to ionization of insulation under extreme voltages and these discharges can be detected using a partial discharge (PD) analyser [28]. At present this technology is limited to high voltage (HV) machines but work is being carried out to investigate usage of the technique on low voltage (LV) machines [29].

2.1.5 Temperature

The addition of internal or external thermocouples allows for the measurement of machine temperature, for example, temperature of the stator winding which is related to insulation life [14,21]. The temperature of the winding can be measured by embedding a thermocouple within the stator but this requires invasive modifications of the stator housing and would require installation during the winding process.

2.1.6 Shaft speed

The rotational speed of the shaft can be measured using laser encoders, shaft mounted optical encoders or magnetic pick-ups [31] and if the application involves a variable speed drive (VSD) shaft speed can be estimated by the drive algorithms (sensor-less). Incremental optical encoders are available with different angular fidelities based on the number of pulses per revolution and can easily be fitted on to the non-drive end of the motor by modifying the fan guard, however, the wiring (encoder power supply and signal transmission) must be considered. An additional channel can be included on the encoder which provides one pulse per revolution allowing positional information to be obtained in addition to speed.

2.1.7 Acoustics & Acoustic Emissions (AE)

The acoustic noise emitted by the machine can be measured in order to provide information on the condition of the machine, and an operator simply listening to a machine can be sufficient to detect faults such as bearing problems. For use in a automated system however acoustic emission (AE) transducers are available and can be used in conjunction with a pre-amplifier to provide continuous acoustic measurement [32]. Acoustic emissions will also include ventilation noise due to the operation of the fan which is dependent on shaft speed [28] and this (in addition to other ambient noise pollution) may need filtering out for acoustic emissions measurements to be effective.

2.1.8 Torque

Torque can be measured directly by a shaft torque transducer or dynamometer or estimated using advanced electric algorithms in modern VSDs. When sampled at a sufficient rate a spectrum of load torque can be derived that can provide information on the frequency content of the torque signal which since provides useful information on the operation of a rotating machine.

2.2 Fault detection techniques

The previous section describes the variables which can be used for a FDD system for induction motors. This section will describe the various techniques which convert these inputs into useful features in order for fault detection to take place.

2.2.1 Spectral analysis

Due to the nature of rotating machines analysing the frequency spectrum of measured time series variables can provide additional information that can be used to indicate the presence of a fault condition. The time series variables are converted to frequency data by applying fast Fourier transforms (FFT) to the data. Vibration, flux, acoustic and current spectra have all been proven to be sensitive to one or more fault types [17], [28], [32], [33].

Depending on the type and location of the fault a ‘characteristic frequency’ can be calculated for a given running speed; examples of bearing [24], air-gap [24], rotor [34], and stator fault [28] detection using spectral components can be found in the literature.

Mechanical faults such as eccentric air-gap and bearing defects cause a change in the forces on the shaft and rotor during rotation, for example, if a defect occurs on the outer race of the bearing a repeated impact will occur as each rolling element within the bearing interacts with the spall or pit in the raceway [35]. This leads to a periodic variation in load torque, the frequency of which is dependent on the location of the fault be that inner race, outer race, cage or rolling element. The characteristic frequencies can be calculated for several different fault types and, as an example, the equations used to calculate bearing related characteristic frequencies in the vibration spectrum are given below [29]:

$$F_c = \frac{1}{2} F_R \left\{ 1 - \frac{D_b cos\beta}{D_c} \right\} \qquad (2.1)$$

$$F_O = \frac{N_B}{2} F_R \left\{ 1 - \frac{D_b cos\beta}{D_c} \right\} \qquad (2.2)$$

$$F_I = \frac{N_B}{2} F_R \left\{1 + \frac{D_b cos\beta}{D_c}\right\} \quad (2.3)$$

$$F_B = \frac{D_c}{D_b} F_R \left\{1 - \left(\frac{D_b cos\beta}{D_c}\right)^2\right\} \quad (2.4)$$

where F_c is the cage fault frequency, F_I the inner raceway fault frequency, F_R is the rotational frequency of the inner race with respect to the outer race, F_O the outer raceway fault frequency, F_B the ball fault frequency, D_b the ball diameter, D_c the pitch diameter, N_B the number of rolling elements and β the contact angle between the ball and raceway. Electrical faults, such as stator winding issues or broken rotor bars, can also be detected via vibration spectrum since these factors cause an asymmetry in the machine fluxes which causes unbalanced magnetic forces across the air-gap of the machine which in turn translate into vibrations that propagate through the machine [28].

In addition to causing variations in machine vibration the four major fault types also effect the flux and current of the machine and can therefore be detected using the spectra of these variables. In terms of electrical faults, both the stator and rotor faults lead to a change in the electrical parameters of the machine (inductance and resistance) and therefore faults in these areas can be readily detected in the current or flux spectrum via predictable characteristic frequencies in a similar manner to the vibration based methods [29], [26], [36]. The effect of mechanical faults can also be observed in the current spectrum due to the air-gap modulation that takes place under these conditions (air-gap eccentricity or bearing faults). Air-gap eccentricity faults cause a periodic variation in the air-gap between the rotor and stator which is dependent on the type of eccentricity that is present; static eccentricity, dynamic eccentricity or a combination of the two. The air-gap variation during shaft rotation causes a non-

uniform airgap permeance between stator and rotor which modulates the flux density across the air-gap [37]. This variation in flux density goes on to alter the current flowing in each of the phase windings. In fact, any vibrations and imbalances that are present in the motor will modulate the rotating flux to some extent and lead to a modulated current signal [27].

Thus by converting current signals into the frequency domain a number of frequency components relating to each of the four major fault types can be detected. This has led to the development of one of the most popular IM FDD techniques; Motor Current Signature Analysis (MCSA) [2], [6], [38], [39]. This is a specific type of spectrum (signature) analysis which is focussed specifically on frequency components in the line currents supplying the motor. This method has been proved successful in industry and case studies can be found in the literature proving the accuracy of this technique in detecting a range of faults [27], [40].

The studies into MCSA indicate that any change in the operating characteristics of the motor will be reflected in the motor current signal. It is for this reason that MCSA can offer the same detection capabilities as vibration analysis. Traditionally, spectral components of a signal are identified using the Fast Fourier Transform (FFT). This method works well when the motor is in steady-state. Case studies indicate that it has been possible to detect broken rotor bars, air-gap eccentricity and shorted turns in the stator using FFT of the stator current [39], [31], [38]. Pre-processing can be used to increase the robustness of an MCSA detection algorithm. Pre-processing usually involves filtering out information from the current signal that does not aid the detection of certain

faults [18]. This leaves behind only the components (or features) of the signal that relate to the fault, making the algorithm more robust.

One drawback of signature analysis is that the motor operating speed and detailed knowledge of the machine's construction is required for most of the fault frequency calculations. Another consideration when using FFT is that the motor needs to be sufficiently loaded and operating in steady-state in order for fault frequencies to be reliably detected. This is problematic for machines that may be lightly loaded or operate transiently (e.g. wind turbines) [41]. When an induction machine is unloaded or lightly loaded the motor slip is small causing fault frequencies to be masked by the supply frequency or supply frequency harmonics [42], [43]. Additionally, the FFT transform sums frequency components over the entire time period therefore there is no indication of which frequencies were present at a certain moment in time. This makes FFT unsuitable for the spectral analysis of transients, e.g. start-up or variable loads.

Motor vibration spectra are also used heavily in the field of induction motor monitoring and when compared to current analysis often provides more reliable data from which FDD activities can be performed. Bearing defects will generally appear clearly in the vibration spectrum [44] whereas they may have very little impact on the current spectrum [45]; thus, for the bearing fault, vibration spectrum based detection is often preferred [24], [32]. The difficulties in obtaining information on bearing faults from the current spectrum is perhaps highlighted by a review of MCSA applications [36] indicating that despite the fact there is considerable research interest in the area of current signature analysis very few of these papers feature bearing fault detection. Research into the area of MCSA for bearing faults continues but vibration spectral analysis

continues to find the most widespread use due to the improved sensitivity of this method to bearing faults [29].

Finally, the rotational speed spectrum has been used for IM FDD. Angular speed variations have been proven to be sensitive to broken rotor bar faults [31]. The rotor fault leads to a pulsating torque due to flux differences dependent on rotor angular position. The frequency spectra of these angular speed differences are reported to indicate broken rotor bar faults with accuracy greater than that of MCSA. To date, this method has only been applied to rotor bar faults.

2.2.2 Wavelet transforms

One of the major drawbacks of the FFT based spectral techniques is that they only provide useful results if the rotational speed of the machine is constant. This has lead to the introduction of wavelet transform techniques which allow detection of faults during start-up transients and non-stationary aspects of the measured input signals of a FDD system [46]. Wavelet transforms can also provide improved performance in cases where background noise is significant since the wavelet transforms behave like filters allowing extraction of useful features on which to perform FDD [47].

Wavelet analysis involves analysing a number of windows in time (time splitting) thus offering information on time based variations in frequency content which is useful for rotational speed transients. These time windows are passed separately to a wavelet analyser which determines a set of wavelet coefficients that provide best correlation different wavelets to the measured signal. The

coefficients which are used to fit the wavelets most effectively are outputted by the algorithm and can be used as features in a FDD system [48].

The basic form of the continuous wavelet transform is as follows [1]:

$$W(a,b) = \frac{1}{\sqrt{a}} \int_{-\infty}^{\infty} x(t).\psi^* \left(\frac{t-b}{a}\right) dt \qquad (2.5)$$

where $x(t)$ is the waveform signal, a is the scale parameter, b is the time parameter and $\psi(.)$ is the wavelet. The wavelet analysis expresses a waveform as a series of oscillations of different frequency and at different time dilations using wavelet types such as Morlet, Mexican hat and Haar [1].

The analysis of small sections of a signal independently allows information on time and frequency to be derived thus mapping a signal into a two-dimensional function of frequency and time; this result can also be achieved via the short time Fourier transform (STFT), however if wavelet analysis is applied the problems associated with the limited precision of the STFT can be overcome by allowing variable length time windows [36]. Since the wavelet provides information on time and frequency it can provide an effective method of analysing frequency changes during transients, however, when compared to FFT techniques it has the drawback of increased computational complexity and is thus not suited to real-time applications [49].

At start-up the conditions imposed on the motor can lead to the occurrence of fault signals that are not present in steady-state operation. Wavelets have been used to analyse the start-up transient signal of a motor and successfully detect broken rotor bar faults [42]. This method is successful regardless of load level

(unlike MCSA) and can be used at start-up and for transiently operated machines.

In [35] it is noted that the stator current signals are non-stationary by nature (due to, for example, varying load conditions or power supply fluctuations [50]). The wavelet packet transform (WPT) can be used to analyse non-stationary signals and can split a spectra into frequency bands so that only the fault frequencies of interest are analysed. This has the effect of creating more robust detection algorithms. Bearing faults [35], broken rotor bar and eccentric air-gap faults [50] have been successfully detected using this technique and there is also evidence of applications for gearbox problems and other mechanical issues [1].

2.2.3 Park's vector approach

Park's vector approach is a technique used to represent the three dimensional line current signals in two dimensions by performing a mathematical transform given below [51]:

$$i_D = \sqrt{\frac{2}{3}}\, i_A - \sqrt{\frac{1}{6}}\, i_B - \sqrt{\frac{1}{6}}\, i_c \qquad (2.6)$$

$$i_Q = \sqrt{\frac{1}{2}}\, i_B - \sqrt{\frac{1}{2}}\, i_c \qquad (2.7)$$

The transform results in a 'direct' component, i_D, and a 'quadrature' component, i_Q where i_A, i_B, and i_C are the motor line currents. If these two components are plotted against each other they result in a number of overlapping geometric loci. In ideal conditions (balanced and sinusoidal voltages) the locus traced out will

be a perfect circle thus any deviation from balanced and perfect sinusoid current signals will result in a change in shape of the locus.

These loci can then be analysed directly from the plot (manually) or via taking an FFT of the radius; this method is known as the Extended Park's Vector Approach (EPVA) [51]. This technique has been proven to highlight stator turn-to-turn faults with an increase in energy at twice the supply frequency being the symptom of this particular fault. This method is advantageous as it does not require knowledge of the number of poles, winding arrangement or slip and only utilises frequencies up to twice supply frequency therefore noise can be easily filtered. Direct analysis of the DQ vector locus can be achieved by a trained expert or alternatively a neural network trained to detect specific fault features which eliminate the need for any further processing (e.g. FFT). Automated analysis of the Park vector plots has been achieved using a radial basis function (RBF) neural network (NN) [52].

The Park vector approach has been proven to respond to stator turn-to-turn faults [51], rotor bar damage and voltage unbalance [36], air-gap eccentricity [53], and bearing outer race point faults [54].

2.2.4 Physics-based models

Physics-based models can be used for FDD purposes using the technique of analytical redundancy; the process of comparing the outputs of a system with the output of a mathematical model in order deviations from a healthy condition. Using the input and output signals of a process, comparisons are made in order to highlight faults in the actual process. This requires that the process is modelled with a reasonable degree of accuracy.

Obtaining accurate models can be achieved through utilising in-depth and verified mathematical relationships or determining certain physical characteristics of the system using identification techniques [55]. The comparison of the mathematical model of the system with the actual system generates ‘residuals’ which allow for the diagnosis of faults [56]. In theory, when faults are present the residual values will be large and when the system is healthy the residuals will be small. The three popular ways to generate residuals are [57]:

1. Parameter Estimation. Generates residuals that are the difference of healthy model parameters and model parameters estimated from system input/output relationships.
2. Observers. Observers estimate the output of the system. Residuals are generated from the difference between measured and estimated signals.
3. Parity Relations. The residuals are generated by direct comparison of the model and system outputs.

The direct-quadrature (DQ) induction motor model in DQ [21] or DQ0 [9] form finds widespread use in the field of induction motor modelling [9], [21], [58]–[70] . In addition to the DQ transform the Concordia transform also results in a two-

axis model which can then be used for simulation purposes [71], [72]. The model is obtained by transforming the three-phase system into a two-phase system using a transform similar to the Park transform (see previous section). The DQ model is relatively simple to implement in modern software [9] and compared to some of the more complex motor models has a minor computational burden.

The simple DQ0 model in its most basic form has no ability to simulate faulty machines since it assumes sinusoidal balanced winding distributions in the stator and sinusoidal balanced *equivalent* windings for the rotor. The rotor cage is simulated as a three-phase set of windings since the magnet-motive force (MMF) distribution of a rotor cage approximates a sinusoidal distribution. Several extensions to the basic DQ0 model introduce the capability to simulate motors in unbalanced modes of operation i.e. operation in the presence of faults, and also simulate machines taking into account the non-uniform distribution of conductors in the stator and rotor which makes the DQ0 model suitable for use in a model-based IM FDD system.

The DQ0 balanced rotor equivalent windings can be replaced by a detailed model of the rotor including equivalent circuits for each of the individual rotor loops (two adjacent bars and a section of each end-ring) [21]. The inductance and resistance terms for a given number of loops can then be modified to simulate damage or complete bar breakages. This method has also been applied to an ABC (3 axis) reference frame model [73]. An additional feature of the detailed rotor loop model is the ability to locate the angular position of the rotor fault with respect to some arbitrary reference angle [74]. In research terms this is an interesting development but offers little practical use since the

absolute position of the rotor will not be tracked over time nor will it be recorded when the machine is assembled, therefore knowledge of the location of the rotor fault is largely irrelevant.

If the detailed rotor cage model is coupled with a winding function approach (WFA) model of the stator winding then the DQ0 model gains the ability to simulate rotor slot harmonics (RSH) [59]. The rotor slot harmonics are generated as the rotor bars pass the individual winding coils. The WFA model replaces the sinusoidal stator winding distributions with a ‘winding function’ which provides information on the density of conductors as a function of angular position, these parameters then dictate the air-gap field strength. For this kind of model a detailed knowledge of the machine construction is required including information regarding the air-gap width, number of stator coils, number of turns per coil and the number of rotor bars. This information is not commonly available and can only be obtained direct from the manufacturer by special request which makes techniques requiring a large number of detailed machine parameters such as this prohibitive. The DQ0 model including RSH does however provide very useful information since the RSH are useful for two key purposes; speed estimation and eccentric air-gap fault detection [75].

Winding function methods calculate machine inductances based on the stator winding layout, rotor cage dimensions and electrical parameters. The inductances are also a function of the air-gap permeance. Furthermore, the air-gap permeance is a function of air-gap width and thus if the air-gap width is provided as a function of stator and rotor angular positions then the conditions for both static and dynamic eccentricity faults can be modelled [76], [77].

Stator winding turn-to-turn faults can be modelled by including parameters in the model which allow modification of the stator inductance and resistance matrices; this creates a set of electrically unbalanced stator windings which simulate the stator turn-to-turn winding fault [9]. The most commonly applied method used to extend the simple IM to a stator fault model is to include parameters which define the number or percentage of shorted turns in one winding. The magnitude of this parameter then modifies the inductance and resistance terms for that particular winding. Some stator fault models exist which allow for localization of the fault by including an angle parameter estimating the mechanical angle between the inter-turn short and the stator winding a-axis [74]. The modifications that are made to the stator inductance and resistance matrices are applied to the ABC 3-axis model then, depending on whether the 2-axis or 3-axis model is to be simulated, the matrices are inputted directly into the simulation [78] or are converted to 2 axes (DQ0 model) by applying the mathematical transform [9].

The final major fault zone, the shaft bearings require additional information on the dimensions of the machine. These parameters are crucial for effective modelling, namely; contact angle, inner race diameter, outer race diameter and number of rolling elements. Once these details have been included in the model, periodic frequencies relating to the impacts between bearing contact surfaces and a bearing fault (inner race, outer race, cage or rolling element) can be predicted. This information can then be used to simulate the periodic changes in load torque and air-gap width (and thus air-gap permeance) which allows the effect of bearing fault on the motor line currents to be modelled [79]. More advanced bearing models have been developed which allow modelling of bearing dynamics under high frequency resonant conditions by including the

effects of the stiffness of the bearing supports, components and the shaft, masses of the individual components and also measured vibration responses [80]. Clearly several additional parameters are required for inclusion of bearing subsystems within a motor model adding to the complexity and creating an issue as to how the values for these parameters are obtained or estimated.

The preceding paragraphs highlight the common approaches used to create and simulate physical models of the induction motor in healthy configuration and also in the presence of rotor, air-gap eccentricity, stator and bearing faults. In addition there is a description of the techniques that utilise these models to provide useful 'features' for use in a FDD system, namely, parameter estimations, observers, or parity relations. If enough information can be obtained on a given induction motor the modelling approach provides a powerful method of detecting and diagnosing a fault easily since the variation in specific parameters and states can be linked directly to specific faults.

2.2.5 Analytical symptom generation

These methods involve processing measured data for a given system or process to develop quantifiable, analytical information in the form of characteristic values [4] and can be achieved via adaptive filtering, variable threshold logic, statistical decision theory and statistical models [55]. Using the input and output signals of a process, comparisons are made using the model and actual process in order to highlight faults in the actual process. This requires that the process is modelled with a reasonable degree of accuracy. Once useful features are being generated the process of change detection is needed. Detected changes in these features can be done using simple thresholds, adaptive thresholds or using statistical analysis. Trending of the

residuals can be implemented in order to detect slowly developing faults. Fixed thresholds define a pre-set and stationary boundary between faulty and fault-free conditions. Due to their simplicity they provide computationally efficient algorithms but they can be problematic due to the diverse nature of machines and operating conditions – over a wide operating range the thresholds may no longer correctly define the difference between faulty and healthy [81]. Adaptive thresholding can overcome some of the problems fixed thresholding suffers from. When the machine is running in different parts of its operating range different thresholds are required. Using heuristics the thresholds can be varied for the different conditions e.g. low temperature, medium temperature and high temperature. These terms define a numerical regions for which the thresholds apply [81].

Vibration and current features have be used to provide information on IM faults by using a set of analytical features such as mean, root mean square (RMS), shape factor, kurtosis, crest factor, entropy error, etc. These calculations can be applied to current or vibration data in order to generate a set of feature values for both healthy and faulty cases. The quantities listed above have been used successfully to detect bowed rotor, air-gap eccentricity, bearing point faults, broken rotor bars and phase unbalance [10]. Correct selection of the relevant features is the challenging aspect of these types of methods [53] and will be considered in the diagnosis section of this chapter.

Auto-regressive (AR) and auto-regressive moving average models (ARMA) can be used to model time series data. Using input data such as measured vibration signals a model is fitted and it is the coefficients which are used to fit the model which are then used as the features to drive the analytic FDD algorithms [1].

ARMA models can also be used for FDD purposes by utilising them in simple parity equations [7].

2.3 Fault diagnosis techniques

The preceding section identified the wide range of available techniques for fault detection and also the application of these techniques within the field of IM FDD. These fault detection techniques generate the features (symptoms) which are analysed by the fault diagnosis aspects of the system in order to provide a diagnosis on machine condition. The fault detection aspect determines whether there is a fault or not and the fault diagnosis aspect determines the location of the fault (i.e. which fault is present). This section will examine various fault diagnosis methods and review fault diagnosis applications for IM.

Following successful detection of signals that can indicate faults these signals need to be analysed in order to determine the type of fault that is present in the induction motor. Isermann [82] defines fault diagnosis as the determination of the kind, size, location and time of detection of a fault. If the FDD system can successfully diagnose the fault then not only does the process operator know that there is a problem with the system (fault detection) he also knows details about the specific fault (fault diagnosis) which will allow him to repair or replace parts in order to bring the machine back to a healthy state with minimal disruption to the industrial plant.

2.3.1 Reasoning methods

For the majority of technical processes some knowledge will usually exist regarding the link between specific faults and specific symptoms and these

casual relationships can be used to develop reasoning methods to diagnose faults [4].

2.3.1.1 Expert systems

An expert system or ‘ES’ (also known as the Knowledge Based System) creates a representation of the system or process based upon knowledge-based rules. The system consists of a knowledge base, which contains a set of rules and an inference mechanism which chooses how to use the stored knowledge in order to reach the required goal [83].

An expert system (ES) involves capturing the knowledge of a domain expert and converting this into a set of rules and using these rules the system makes decisions based on the measured system variables. The rule sets are designed to replicate the expert’s decision making process based on the information captured in the knowledgebase. The rule set can contain heuristic rules based on experience or symptom-fault links based on measured fault histories [84]. The key features of an expert system can be summarised as follows [29]:

1. emulation and implementation of human expertise
2. building and maintenance of a knowledge base
3. signal filtering and feature extraction
4. inclusion of user feedback
5. extending the knowledgebase using results of experiments and simulations
6. fault diagnosis and classification

A knowledge-base is essentially a list of if-then-else rules and therefore suffers from the occurrence of new situations since no fundamental knowledge of the underlying physics of the system is captured [85]. For this reason expert systems are suited specialized applications in narrow areas of expertise only

[86]. Developing a comprehensive knowledgebase is time-consuming since the expert's in-depth understanding of the particular process takes time to be properly captured. This makes the knowledge acquisition and verification process difficult especially considering that experienced engineers and technicians may not be able to easily explain their knowledge explicitly and accurately [47]. In addition, ES suffer from the problem of combinatorial explosion with the number of rules (and effort required to derive these rules) increasing exponentially with the number of variables [1].

2.3.1.2 Decision trees

Standard inference methods (if-then rules) can be combined to form complex decision trees to perform diagnosis of faults. Classical fault tree analysis considers binary inputs and Boolean equations to reach a diagnosis verdict [57]. Within a fault tree there are a number of different layers or nodes; at each node a logic operation is performed (e.g. AND, OR, NOR, etc) and based on these logic operation events are analysed as control propagates through the tree to different nodes eventually resulting in a conclusion or diagnosis verdict being reached. This process of linking a set of symptoms with a specific fault is known as event tree analysis (ETA) or fault tree analysis (FTA) [4]. In order to properly construct a fault tree the analyst must have a complete understanding of the system and then work backwards from a top level event (e.g. occurrence of a fault) through a series of events linked by the logic operations [85]. This will result in a series of events (inputs) contained within a logic network which are evaluated in order until a specific conclusion is reached.

2.3.1.3 Fuzzy logic

Fuzzy logic is a rule-based expert system in which the input to these rules does not have to be exactly defined. This allows the system to accommodate situations it was not programmed for, much like the human brain [83]. Decisions are made based on vague input data by mimicking the human reasoning process. This technique replaces the traditional logic states of '0' and '1' with continuous variables and linguistic describing terms. Fuzzy logic is particularly suited to machine condition monitoring since in practice operators are concerned with the condition of the motor in terms of linguistic variables, e.g. is the machine condition 'healthy, or 'damaged' or 'seriously damaged' [45].

Fuzzy logic applications have been applied to IM FDD using simple comparisons of line current amplitudes to detect stator faults [23]. In [45] a general method for detection of induction motor faults was developed using a fuzzy logic inference system. This type of system successfully interpreted MCSA and imbalance data to detect and diagnose stator and rotor faults.

2.3.2 Classification methods

When little or no knowledge exists regarding the link between symptoms (features) and faults for a given process or system, then pattern recognition or classification techniques can be used to determine the relationship between the faults and symptoms [4]. Classification methods are trained based on symptoms that were recorded under a number of different fault conditions for a given system. By using measured data in this way a fundamental understanding of the physics of the process is not required.

2.3.2.1 Pattern classification

Pattern classification is the process of determining the relationship between some observation vector and a range of classes – for example, different types of fault. This process involves the use of a discriminant function which quantifies the relationship between the observation vector and a given class [81]. The observation vector consists of a set of features which contain useful information with respect to the system being diagnosed (see section 2.2 for a review of features which are applicable to IM FDD).

The pattern classification approach is basically a multivariate clustering process which is intended to maximise the difference between different classes. Classes are usually grouped based on distance measures or discriminant functions such as Euclidian distance, Mahlanobis distance, Kullback-Liebler distance or Bayesian distance [1].

Principle Component Analysis (PCA) and Fisher Discriminant Analysis (FDA) are two techniques which utilise dimensionality reduction in order to perform fault diagnosis via classification. These dimensionality reduction techniques allow the problem of fault diagnosis to be simplified by reducing the number of inputs being considered and then identifying regions within this lower-dimensional space which are indicative of specific faults. Alternatively, a PCA/FDA can be generated for each specific fault then statistical analyses can be performed to determine which fault most likely occurred [81]. PCA has been applied to machine FDD to simply reduce the dimensionality of the problem (diagnosis performed via a different method) and has also be used to perform the fault detection and diagnosis procedure alone [1].

2.3.2.2 Neural networks

Artificial neural networks (ANN) are computer model equivalents of processes occurring in the human brain. Knowledge is built up in the ANN by 'training' using inputs and outputs and comparing the ANN outputs with the real outputs in order to generate weightings on parts of the calculation [83].

The ANN is built up by processing elements called artificial neurons whose output is calculated based on a number of inputs which are modified by individual weightings and bias offsets. Once these modifiers have been applied to the inputs, all terms are summed and passed to the activation function. The activation function can be a simple linear function, a logistic function, a hyperbolic function, a threshold function, etc [87]. The operation of an artificial neuron is shown in the equation below:

$$y = f\left\{\sum_{k=1}^{n}(x_k w_k + b_k)\right\} \qquad (2.8)$$

where:

x_k The k[th] input
w_k The weight applied to the k[th] input
b_k The value of the bias applied to the k[th] input

Neurons are linked together to form layers and these layers are then combined to form a network; the network is the processing structure which is designed to replicate the chosen process or system. ANN have been used to model induction motors [88], identify model parameters [89], estimate motor running speed [90] and detect and diagnose a variety of motor faults [26], [52], [91]–[97].

The application of ANN to bearing FDD was demonstrated in [52] where a ANN is used to diagnose the outputs of a Park's Vector method. MCSA and vibration data have been successfully used to train a ANN to detect bearing, stator and rotor faults [95]. In this study the data was pre-processed to remove components of the data that did not characterise the faults. This was seen to simplify the network and lower its training times. In [97] a wavelet transform is applied to the motor current, a number of frequency features are extracted. These features are analysed by a genetic algorithm which selects the most significant features for fault detection. The features are then those that are used to optimise the structure of the ANN to be sensitive to faults.

Although ANN has been proven to be a suitable CM tool in some situations they do have some drawbacks. ANN applications require training and there can be problems when an ANN is exposed to new conditions – standard NNs can struggle to carry out learning without forgetting previously acquired knowledge (stable training). This inhibits their ability to adapt in 'on-line' mode; they have to be re-trained with the entire dataset off-line. There are also problems associated with choosing the right inputs and structure for a ANN – the configuration of the network needs to be compact and receive useful inputs in order to obtain good results whilst keeping computational time to a minimum [97].

2.3.3 Model reference methods

The model-based fault detection techniques also lend themselves to fault diagnosis since the variation of specific model parameters can be explicitly linked to a specific fault. Thus the model-based detection and diagnosis aspects are closely coupled. An example of this could be the estimation of a parameter

which indicates the number of shorted turns in a stator winding. If the parameter estimate increases significantly then the fault can be diagnosed as a shorted turn directly without any need for a complicated inference tree, statistical clustering technique, NN, etc.

An in-depth review of model-based approaches for fault detection and diagnosis along with several applications in the field of IM FDD can be found in section 2.2.4.

2.4 Discussion & summary

This chapter presents the state-of-the-art for the different measurement types, techniques and methods commonly used to detect and diagnose faults in induction motors. Detailed descriptions of induction motor fault types and propagation, modelling methods and parameter estimation techniques have been omitted from this chapter for clarity and will be included in the relevant chapters later in the dissertation.

Firstly, the different measurement types applicable to IM FDD were reviewed. Of the numerous input measurement types, vibration and current are the most popular at the time of writing. Of these two data sources vibration-based data is arguably the most sensitive to machine faults, however, current-based techniques are non-invasive and will usually require no additional hardware since motor supply current and voltages will usually already be measured for protection and/or control purposes.

This chapter indicates the extensive nature of condition monitoring techniques available and highlights the applications specific to induction motors. There are a wide variety of possible approaches that have been documented in literature.

Analytic methods, spectral analysis, wavelet transforms, Park vector methods and model based approaches have been reviewed as the major techniques applicable to fault detection. For fault diagnosis, expert systems, decision trees, fuzzy logic, neural networks and pattern classification were described in detail.

As far as current-based methods are concerned there are two stand-out solutions to the fault detection problem; motor current signature analysis (MCSA) and model-based techniques.

MCSA offers the prospect of proven detection of all the major faults (bearing, air-gap, stator and rotor) but it can be difficult to interpret spectra in the presence of noise and overlapping characteristic fault frequencies. It is the individual properties unique to each motor and operating environment that make MCSA problematic; unique characteristics may be wrongly diagnosed as faults if each motor is treated in a similar way. On the other hand, model based methods provide useful indications of which parameters are varying and this can aid with the diagnostic process. Additionally, models can be used to capture the 'healthy' state of the motor including in-built asymmetries and characteristics. Unfortunately, detailed model based methods require significant computational effort, and there are only a few applications of model-based approaches that have demonstrated detection ability for all fault types.

For these reasons, it is suggested that a combination of model-based and frequency-domain approaches to FDD would be a more suitable approach. The flexibility of the model-based approaches can be combined with the proven detection capabilities of the spectral methods (such as MCSA) to create a robust and computationally efficient fault detection algorithm. Combining these two approaches should help to counteract their individual deficiencies.

For diagnosis there are three types of methods that are commonly applied; reasoning, classification and model-based. Classification (pattern matching or neural network) are ill-suited to this application since it is difficult to generate the required amount of data to properly train these methods in the laboratory. The laboratory testing can however generate a limited number of cases for healthy and faulty motor configurations and in addition allow experiments to be conducted in order to understand the system and fault mechanisms in detail, and produce and validate motor models under a variety of fault conditions. For these reasons the problem lends itself to reasoning and model-based diagnosis techniques since an in-depth understanding of the process will be available via experimental investigations and literature reviews. This knowledge can then be captured in some form of expert system (e.g. fuzzy logic) in order to perform the diagnosis task.

The information collected and conclusions made in this chapter were used to develop the research aims stated in the previous chapter.

Chapter 3. Mathematical Modelling of the Induction Motor

The first part of this chapter describes the system of differential equations used to model the induction motor in the ‘ABC’ reference frame as a set of six magnetically coupled circuits. Then the ‘ABC’ to ‘QD0’ transformation is explained. This allows the system of equations to be transformed into a form which is easier to model and more computationally efficient. The resulting ‘QD0’ reference frame model is then presented. This ‘healthy case’ model of the induction motor is based on the motor model developed in reference [98].

The second part of this chapter describes the theory for modelling stator and rotor faults which results in the extended ‘QD0’ reference frame model. This model allows simulation of induction motors with stator turn-to-turn winding faults and/or damaged rotor bars. This ‘faulty case’ model of the induction motor is based on the motor model developed in reference [9], which is itself an extension of the ‘healthy case’ motor model.

Finally, the process of rewriting the modelling equations to eliminate algebraic loops is presented. This results in a third motor model which is suitable for conversion to C code for faster simulation on a PC or use on a microprocessor based device.

The models developed in this chapter are used to generate the model-based residual values to be used as part of the AMRA system. These model based residuals are supplemented by model-free residuals described in subsequent chapters to provide a set of mixed residuals which offer a better perfromance for detection of a wide range of faults.

3.1 The coupled magnetic circuit approach

The squirrel cage induction motor can be modelled by considering a system of six electrical circuits which are magnetically coupled. This approach, used to describe the induction motor in this chapter, is known as the coupled magnetic circuit approach [98].

The six circuits consist of three stator windings and three rotor 'equivalent windings'. Induction motors are designed to have as close to a sinusoidally distributed conductor density in the stator windings as possible. This leads to a sinusoidally distributed MMF in the airgap. Equivalent windings (rather than individual rotor bars) can be used for the rotor since the currents in the rotor bars also induce a sinusoidally distributed MMF [99]. Replacing the rotor squirrel cage with 3 equivalent winding simplifies the modelling equations.

The relationship between the stator windings and rotor equivalent windings is shown in Figure 3.1.

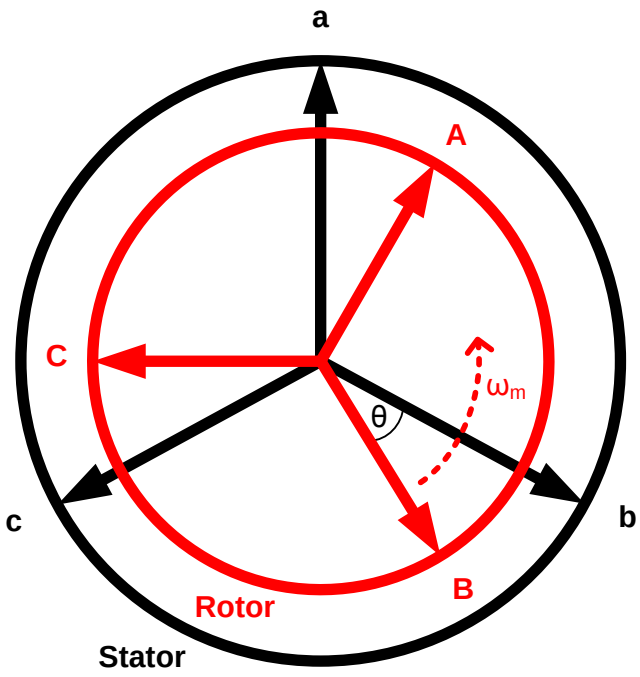

Figure 3.1 Diagram showing the realtionship between the stator windings (a-b-c) and rotor 'equivalent' windings (A-B-C)

The separate circuits are coupled with one another via inductance terms which are dependent on the angular position of the windings with respect to each other. As the rotor equivalent windings rotate with respect to the stator windings the angular relationship changes which results in time-varying inductances.

The six circuits can be represented by a system of first-order differential equations and these equations are said to be in the 'ABC' reference frame. This requires each of the equations to be referenced to the 'a', 'b' or 'c' winding of the stator.

In order to develop the governing equations several assumptions are made:

- The permeability of the stator magnetic material is assumed to be infinite
- The permeability of the rotor magnetic material is assumed to be infinite
- Saturation effects are neglected
- Iron losses are neglected
- End-winding effects are ignored
- Slotting effects are ignored (sinusoidally distributed windings)

These assumptions introduce only small errors to the model that are not significant enough to affect the model's potential for fault diagnosis applications.

The relationship between the windings can be defined by six voltage equations and six flux linkage equations. Firstly, the voltage equations can be written:

$$v_{as} = i_{as} r_s + \frac{d\lambda_{as}}{dt} \tag{3.1a}$$

$$v_{bs} = i_{bs} r_s + \frac{d\lambda_{bs}}{dt} \tag{3.1b}$$

$$v_{cs} = i_{cs} r_s + \frac{d\lambda_{cs}}{dt} \tag{3.1c}$$

where $v_{a,b,c\,s}$ represent the stator winding voltages, $i_{a,b,c\,s}$ represent the stator winding currents, $\lambda_{a,b,c\,s}$ represent the stator flux linkages, and r_s is the stator winding resistance per phase.

Similarly, rotor voltage equations are given by:

$$v_{ar} = i_{ar} r_r + \frac{d\lambda_{ar}}{dt} \tag{3.2a}$$

$$\mathrm{v_{br}} = \mathrm{i_{br} r_r} + \frac{\mathrm{d\lambda_{br}}}{\mathrm{dt}} \tag{3.2b}$$

$$\mathrm{v_{cr}} = \mathrm{i_{cr} r_r} + \frac{\mathrm{d\lambda_{cr}}}{\mathrm{dt}} \tag{3.2c}$$

Combining these equations into a single matrix equation gives:

$$\begin{bmatrix} \mathrm{v_s} \\ \mathrm{v_r} \end{bmatrix} = \begin{bmatrix} \mathrm{r_s} & 0 \\ 0 & \mathrm{r_r} \end{bmatrix} \begin{bmatrix} \mathrm{i_s} \\ \mathrm{i_r} \end{bmatrix} + \frac{\mathrm{d}}{\mathrm{dt}} \begin{bmatrix} \lambda_\mathrm{s} \\ \lambda_\mathrm{r} \end{bmatrix} \tag{3.3}$$

The stator and rotor resistance matrices are given by:

$$\mathrm{r_s^{abc}} = \begin{bmatrix} \mathrm{r_s} & 0 & 0 \\ 0 & \mathrm{r_s} & 0 \\ 0 & 0 & \mathrm{r_s} \end{bmatrix} \qquad \mathrm{r_r^{abc}} = \begin{bmatrix} \mathrm{r_r} & 0 & 0 \\ 0 & \mathrm{r_r} & 0 \\ 0 & 0 & \mathrm{r_r} \end{bmatrix} \tag{3.4}$$

For squirrel cage induction motors (SCIM) there is no voltage input to the rotor cage, therefore, $v_{a,b,c\,r}$ are all equal to zero.

The six circuits are coupled by flux linkages connecting the different windings. The relationship between the flux linkages of stator and rotor windings and the stator and rotor currents is given by:

$$\begin{bmatrix} \lambda_\mathrm{s}^\mathrm{abc} \\ \lambda_\mathrm{r}^\mathrm{abc} \end{bmatrix} = \begin{bmatrix} \mathrm{L_{ss}^{abc}} & \mathrm{L_{sr}^{abc}} \\ \mathrm{L_{rs}^{abc}} & \mathrm{L_{rr}^{abc}} \end{bmatrix} \begin{bmatrix} \mathrm{i_s^{abc}} \\ \mathrm{i_r^{abc}} \end{bmatrix} \tag{3.5}$$

where:

$$\lambda_\mathrm{s}^\mathrm{abc} = \begin{bmatrix} \lambda_\mathrm{as} \\ \lambda_\mathrm{bs} \\ \lambda_\mathrm{cs} \end{bmatrix} \tag{3.6a}$$

$$\lambda_r^{abc} = \begin{bmatrix} \lambda_{ar} \\ \lambda_{br} \\ \lambda_{cr} \end{bmatrix} \tag{3.5b}$$

$$i_s^{abc} = \begin{bmatrix} i_{as} \\ i_{bs} \\ i_{cs} \end{bmatrix} \tag{3.5c}$$

$$i_r^{abc} = \begin{bmatrix} i_{ar} \\ i_{br} \\ i_{cr} \end{bmatrix} \tag{3.5d}$$

The inductance sub-matrices (stator-stator and rotor-rotor) given by:

$$L_{ss}^{abc} = \begin{bmatrix} L_{ls} + L_{ss} & L_{sm} & L_{sm} \\ L_{sm} & L_{ls} + L_{ss} & L_{sm} \\ L_{sm} & L_{sm} & L_{ls} + L_{ss} \end{bmatrix} \tag{3.7}$$

$$L_{rr}^{abc} = \begin{bmatrix} L_{lr} + L_{rr} & L_{rm} & L_{rm} \\ L_{rm} & L_{lr} + L_{rr} & L_{rm} \\ L_{rm} & L_{rm} & L_{lr} + L_{rr} \end{bmatrix} \tag{3.8}$$

The mutual inductances between stator and rotor are given as a function of rotor angle, *θr*:

$$\begin{aligned} \left[L_{sr}^{abc}\right] &= \left[L_{rs}^{abc}\right]^T \\ &= L_{sr} \begin{bmatrix} \cos\theta_r & \cos\left(\theta_r + \frac{2\pi}{3}\right) & \cos\left(\theta_r - \frac{2\pi}{3}\right) \\ \cos\left(\theta_r - \frac{2\pi}{3}\right) & \cos\theta_r & \cos\left(\theta_r + \frac{2\pi}{3}\right) \\ \cos\left(\theta_r + \frac{2\pi}{3}\right) & \cos\left(\theta_r - \frac{2\pi}{3}\right) & \cos\theta_r \end{bmatrix} \end{aligned} \tag{3.9}$$

where L_{ls} is the per phase stator leakage inductance, L_{lr} is the per phase rotor leakage inductance, L_{ss} is the stator winding self-inductance, L_{rr} is the rotor winding self inductance, L_{sm} is the mutual inductance between stator windings, L_{sr} is the stator-to-rotor mutual inductance and L_{rm} is the mutual inductance between the rotor windings.

This section provides an overview of the coupled magnetic circuit approach which defines the relationship between voltage, current and flux within the IM.

The motor is represented by six first-order differential equations with each differential equation representing one winding. The next section will explain how this theoretical analysis is built upon in order to develop an IM model in Simulink.

3.2 The QD0 reference frame induction motor model

In this section the ‘QD0’ reference frame mathematical model of the induction motor will be described.

As mentioned in the previous section, the ABC reference frame model contains position-varying inductance terms, see Equation (3.9). By applying the ‘QD0’ transformation the 3-axis system is effectively transformed to a 2-axis system and the inductance become constant (as opposed to the time varying inductances in the ABC reference frame model). This results in the ‘QD0’ reference frame model of the motor.

The ‘QD0’ reference frame model has become popular due to the fact that it is simpler to solve than the ABC reference frame model and it also allows flux and torque to be controlled independently in dynamic conditions which is important for AC motor control [99].

The model consists of several parts that will be explained in the following subsections. The model used here is based on the method found in [98].

3.2.1 ABC-to-QD0 reference frame transformation

The ABC-to-QD0 transform is used to simplify the system of differential equations by removing time (position) varying inductances. The QD0 axis system consists of two orthogonal axes; the Q and D axes. Since these axes are orthogonal to each other there is no flux linkage between the Q and D

windings. The '0' axis is included to allow the transformation to be bidirectional. The ABC-to-QD0 transformation matrix is given by:

$$\left[T_{qd0}(\theta_d)\right] = \frac{2}{3}\begin{bmatrix} \cos\theta_d & \cos\left(\theta_d - \frac{2\pi}{3}\right) & \cos\left(\theta_d + \frac{2\pi}{3}\right) \\ -\sin\theta_d & -\sin\left(\theta_d - \frac{2\pi}{3}\right) & \sin\left(\theta_d - \frac{2\pi}{3}\right) \\ \frac{1}{2} & \frac{1}{2} & \frac{1}{2} \end{bmatrix} \tag{3.10}$$

where θ_d is the angle between the d-axis and the a-axis.

This transformation is used to convert the 'ABC' reference frame variables and equations to the 'QD0' reference frame. Once the 'QD0' reference frame equations have been solved the reverse transformation can be applied to calculate the resulting currents and flux linkages in the 'ABC' reference frame.

For all the models developed in this thesis the d-axis is kept stationary and aligned with the a-axis i.e. θ_d is always equal to zero. This is the 2-axis stationary reference frame approach.

3.2.2 Voltage equations in the QD0 reference frame

If equations (3.1b), (3.1b) and (3.1c) are written in matrix form the 'ABC' reference frame voltage equations become:

$$v_s^{abc} = \frac{d}{dt}\lambda_s^{abc} + r_s^{abc} i_s^{abc} \tag{3.11}$$

The stator and rotor resistance matrices are given by:

$$r_s^{abc} = \begin{bmatrix} r_s & 0 & 0 \\ 0 & r_s & 0 \\ 0 & 0 & r_s \end{bmatrix} \qquad r_r^{abc} = \begin{bmatrix} r_r & 0 & 0 \\ 0 & r_r & 0 \\ 0 & 0 & r_r \end{bmatrix} \tag{3.12}$$

The ABC-to-QD0 transform (with the arbitrary reference frame angle set to 0) is applied to equation (3.11) to give the 'QD0' reference frame voltage equation (see Appendix C):

$$v_s^{qd0} = \frac{d}{dt}\lambda_s^{qd0} + r_s^{qd0} i_s^{qd0} \tag{3.13}$$

$$v_r^{qd0} = \begin{bmatrix} 0 & -\omega_r & 0 \\ \omega_r & 0 & 0 \\ 0 & 0 & 0 \end{bmatrix} \lambda_r^{qd0} + \frac{d}{dt}\lambda_r^{qd0} + r_r^{qd0} i_r^{qd0} \tag{3.14}$$

where $\boldsymbol{r}_s^{qd0}$ is the stator resistance matrix, $\boldsymbol{r}_r^{qd0}$ is the rotor resistance matrix, ω_r is the rotational speed of the motor shaft in electrical radians per second, $\boldsymbol{\lambda}_s^{qd0}$ is the stator flux linkage, and $\boldsymbol{\lambda}_r^{qd0}$ is the rotor flux linkage (all quantities in the QD0 reference frame).

The stator and rotor resistance matrices are given by:

$$r_s^{qd0} = \begin{bmatrix} r_s & 0 & 0 \\ 0 & r_s & 0 \\ 0 & 0 & r_s \end{bmatrix} \qquad r_r^{qd0} = \begin{bmatrix} r_r & 0 & 0 \\ 0 & r_r & 0 \\ 0 & 0 & r_r \end{bmatrix} \tag{3.15}$$

3.2.3 Flux linkage equations in the QD0 reference frame

The reference frame transformation is also applied to the flux linkage equation (3.5) to give the QD0 reference frame flux linkage equations (see Appendix D):

$$\begin{bmatrix} \lambda_s^{qd0} \\ \lambda_r^{qd0} \end{bmatrix} = \begin{bmatrix} L_{ls} + L_m & 0 & 0 & L_m & 0 & 0 \\ 0 & L_{ls} + L_m & 0 & 0 & L_m & 0 \\ 0 & 0 & L_{ls} & 0 & 0 & 0 \\ L_m & 0 & 0 & L_{lr}' + L_m & 0 & 0 \\ 0 & L_m & 0 & 0 & L_{lr}' + L_m & 0 \\ 0 & 0 & 0 & 0 & 0 & L_{lr}' \end{bmatrix} \begin{bmatrix} i_s^{qd0} \\ i_r^{qd0} \end{bmatrix} \tag{3.16}$$

where primed terms indicate the parameter is referred to the stator side. As mentioned previously, one of the benefits of the QD0 axes system is that there is no mutual magnetic coupling between the D and Q axis due to the fact that the two axes are orthogonal. This is demonstrated by observing the inductance

matrix of equation (3.16). The zero terms indicate that a flux linkage on the q-axis cannot induce a current on the d-axis (or 0-axis), and vice-versa.

If the inductance matrix is inverted the stator and winding currents can be calculated from the winding fluxes.

3.2.4 Calculation of electromagnetic torque

Torque is generated by the interaction of the flux linkages. The torque generated by the simulation model can be calculated using the instantaneous power supplied to all six of the stator and rotor windings. Using this approach leads to the following equation for electromagnetic torque (see Appendix D):

$$\mathrm{T_{em}} = \frac{3}{2}\frac{\mathrm{P}}{2}\mathrm{L_m}\left(\mathrm{i'_{dr}i_{qs}} - \mathrm{i'_{qr}i_{ds}}\right) \tag{3.17}$$

where P is the number of poles ($\mathrm{P} \geq 2$).

3.2.5 Calculation of the mechanical speed of the rotor

Having calculated the electromagnetic torque generated by the motor it is possible to determine the mechanical speed of the rotor using the following relationship:

$$\frac{\mathrm{d}}{\mathrm{dt}}(\omega_\mathrm{r}) = \frac{\mathrm{T_{em}} - \mathrm{T_L}}{\mathrm{J_{eq}}} \tag{3.18}$$

where T_L is the load torque, J_{eq} is the combined inertia of the load and motor, and ω_r is the mechanical rotational speed of the rotor in electrical radians per second.

In order to calculate the mechanical rotational speed of the rotor (i.e. the actual shaft speed) the speed value needs to be converted from electrical radians per second to mechanical radians per second. The conversion to mechanical speed is as follows:

$$\omega_{\mathrm{m}} = \left(\frac{2}{\mathrm{P}}\right)\omega_{\mathrm{r}} \tag{3.19}$$

where ω_r is the rotational speed in electrical radians per second, ω_m is the rotational speed in mechanical radians per second and P is the number of poles.

3.2.6 Exclusion of the '0' axis

Due to the fact that the healthy model of the induction motor is assumed to be mechanically and electrically symmetrical, simulation the '0' axis is not required. The '0' axis becomes important for unbalanced (faulty) induction motors so that when simulating the stator and rotor fault cases the '0' axis must be included in the model.

When modelling the healthy motor the '0' axis can be removed and only the 'Q' and 'D' axis need to be modelled. This results in the 'QD' reference frame model which requires less computational processing but produces identical results to the 'QD0' reference frame model when simulating balanced (healthy) motors.

This is important if (as in this case) the model is to be used for an iterative parameter identification process. Small improvements in processing time are magnified since the model will go through thousands of simulation runs during the optimisation of machine parameters. This leads to significant time savings during the baseline parameter identification process.

The 'DQ' reference frame model developed in Simulink is shown in Figure 3.2.

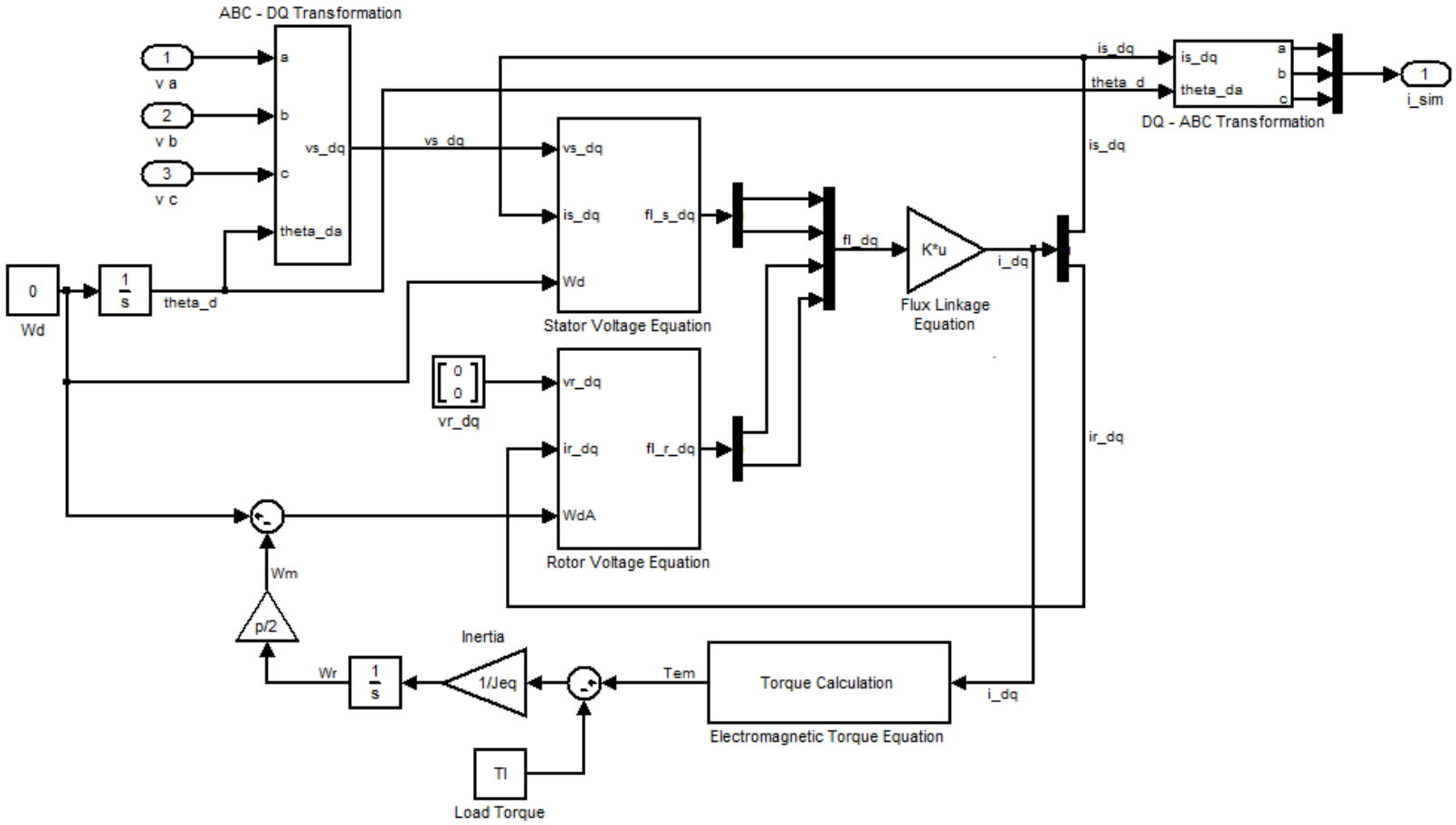

Figure 3.2 The Simulink 'DQ' reference frame model of the induction motor for simualtion of healthy (balanced) induction motors

3.2.7 Model parameters

The model contains the following parameters:

1. Stator Winding Electrical Resistance, R_S. This parameter defines the value of the resistance of the stator windings.
2. Rotor Cage Electrical Resistance, R_R. This parameter defines the resistance of the equivalent rotor windings.
3. Stator Winding Inductance, L_S. This parameter defines the combined inductance (leakage and magnetising) of the stator windings.
4. Rotor Winding Inductance, L_R. This parameter defines the combined inductance (leakage and magnetising) the equivalent rotor windings.
5. Magnetising Inductance, L_M. This parameter defines the inductance component that produces flux linkages between rotor and stator, i.e. the magnetising inductance.
6. Combined Motor and Load Equivalent Inertia, J_{eq}. This parameter defines the equivalent inertia of the motor and load seen by the motor.
7. Number of poles, P. This parameter defines the number of poles in the machine (p/2 = pole pairs).

3.3 The modified QD0 reference frame motor model for simulation of rotor and stator faults

In this section the model required for simulation of induction motors with rotor or stator faults will be presented. The presence of rotor and stator faults results in an unbalanced machine (in terms of resistances and inductances). To model this effect the resistance and inductance matrices are modified. In order to model machine in the ‘QD’ reference frame the ‘0’ axis must now be included since the modified resistance and inductance matrices can be asymmetrical.

3.3.1 Modelling the rotor fault

The rotor of a squirrel cage induction motor consists of a number of parallel rotor bars connected via circular end rings. If one or more of the conducting bars is broken, cracked or contains a casting void, the resistance and inductance of that particular bar will be modified resulting in an electrically unbalanced rotor squirrel cage.

The modelling technique used in this thesis – 'QD0' reference frame modelling – uses three 'equivalent' windings to model the rotor cage (see previous section). In order to model a bar break, the resistance of one of these rotor equivalent windings is modified. When modelling a rotor fault in this way, only changes to the resistance of the rotor need to be considered (changes to rotor inductance are neglected). The rotor fault can be successfully modelled by varying resistance only as the effect of a broken bar on rotor inductance is negligible in comparison to effect on rotor resistance [2,5,6].

If the actual rotor cage has N_{RB} rotor bars then there will be $N_{RB}/3$ rotor bars in each equivalent rotor winding (the rotor bars are shared equally between the 3 rotor equivalent windings). If the number of broken bars is represented by n_{BB} then the proportion of broken rotor bars to total rotor bars in one equivalent rotor winding is given by [74]:

$$\eta_B = \frac{3n_{BB}}{N_{RB}} \tag{3.20}$$

where n_{BB} is the number of broken bars and N_{RB} is total number of rotor bars. Using this value, the change in resistance of the faulty rotor equivalent winding (ΔR) can be calculated:

$$\Delta R = \eta_B r_r = \left(\frac{3n_{BB}}{N_{RB}}\right) r_r \tag{3.21}$$

where r_r is the rotor equivalent winding resistance referred to the stator.

This increment due to rotor bar breaks is included in equation (3.4) by modifying to rotor resistances from r_r to $(r_r + \Delta R)$.

Then the ABC-to-QD0 reference frame transformation is applied to the rotor resistance matrix including the fault parameters for equivalent rotor resistance. The balanced (healthy) case equivalent rotor resistance given in equation (3.12) is replaced by the following (faulty) equivalent rotor resistance matrix:

$$r_{r(fault)}^{qd0} = \begin{bmatrix} r_r + r_{r11} & r_{r12} & r_{r13} \\ r_{r21} & r_r + r_{r22} & r_{r23} \\ r_{r31} & r_{r32} & r_r + r_{r33} \end{bmatrix} \tag{3.22}$$

The rotor resistance matrix values are given by:

$$\begin{aligned}
r_{r11} &= \frac{1}{3}(\Delta r_a + \Delta r_b + \Delta r_c) + \frac{1}{6}(2\Delta r_a - \Delta r_b - \Delta r_c) \\
&\quad + \frac{\sqrt{3}}{6}(\Delta r_b - \Delta r_c) \\
r_{12} = r_{21} &= -\frac{1}{6}(2\Delta r_a - \Delta r_b - \Delta r_c)\sin(2\theta_r) + \frac{\sqrt{3}}{6}(\Delta r_b \\
&\quad - \Delta r_c)\cos(2\theta_r) \\
r_{13} = 2r_{31} &= \frac{1}{3}(2\Delta r_a - \Delta r_b - \Delta r_c)\sin(2\theta_r) \\
&\quad + \frac{\sqrt{3}}{6}(\Delta r_b - \Delta r_c)\sin\theta_r \\
r_{22} &= \frac{1}{3}(\Delta r_a + \Delta r_b + \Delta r_c) - \frac{1}{6}(2\Delta r_a - \Delta r_b - \Delta r_c) + \frac{\sqrt{3}}{6}(\Delta r_b - \Delta r_c) \\
r_{23} = 2r_{32} &= \frac{-1}{3}(2\Delta r_a - \Delta r_b - \Delta r_c)\sin(2\theta_r) \\
&\quad - \frac{\sqrt{3}}{3}(\Delta r_b - \Delta r_c)\sin\theta_r \\
r_{33} &= \frac{1}{3}(\Delta r_a + \Delta r_b + \Delta r_c)
\end{aligned} \tag{3.23}$$

3.3.2 Modelling the stator fault

Having completed the rotor fault model the stator fault model can now be considered. The stator fault model allows simulation of stator windings with turn-to-turn winding faults.

Unlike modelling the rotor fault, the variation in inductance cannot be ignored, therefore a modified inductance and resistance matrix for the stator windings is required to fully model the stator turn-to-turn fault [9].

The inductance and resistance of a given stator winding depends on the number of 'turns' (conductor loops) in each phase winding; in its healthy case the induction motor will have an equal number of turns in each stator phase winding. When a stator turn-to-turn fault develops the insulation between two adjacent turns is broken down which provides a short-circuited path through the winding. This effectively removes a number of stator turns from the winding (the number may be one or more since the turns are randomly wound within the stator slots therefore turn 'n' is not necessarily physically adjacent to turn 'n+1').

If n_{ST-a} , n_{ST-b} , and n_{ST-c} represent the percentage of turns which have been shorted on the 'a', 'b', and 'c' stator windings respectively, then the proportion of remaining turns is given by:

$$\mathrm{n_a} = 1 - \mathrm{n_{ST-a}} \tag{3.24}$$

$$\mathrm{n_b} = 1 - \mathrm{n_{ST-b}} \tag{3.25}$$

$$\mathrm{n_c} = 1 - \mathrm{n_{ST-c}} \tag{3.26}$$

It follows that in the case where there is no fault then n_a, n_b, and n_c are equal to 1; the stator winding is healthy (no shorted turns). By incorporating these stator fault parameters into the basic ABC reference frame model, stator turn-to-turn winding faults can be simulated.

Firstly, these fault terms are introduced into the ABC reference frame model and then transformed into the QD0 reference frame. The rotor resistance matrix of equation (3.4) is modified to include the parameters for representing the proportion of healthy turns in the rotor resistance matrix:

$$r_{s(abc)} = \begin{bmatrix} n_a r_s & 0 & 0 \\ 0 & n_b r_s & 0 \\ 0 & 0 & n_c r_s \end{bmatrix} \tag{3.27}$$

The resistance is modified proportionally according to the number of turns e.g. 100% healthy turns give 100% of the nominal resistance, 50% healthy turns give 50% of the nominal resistance.

As mentioned earlier in this section, the inductance matrix must also be modified. Since the inductance between two windings is proportional to the product of the number of turns on each winding [99], the stator inductances (self and mutual) are modified according to the number of healthy turns on each winding. This results in the modified stator-to-stator inductance matrix:

$$L_{ss}^{abc} = \begin{bmatrix} n_a^2(L_{ls} + L_{ss}) & n_a n_b L_{sm} & n_a n_c L_{sm} \\ n_b n_a L_{sm} & n_b^2(L_{ls} + L_{ss}) & n_b n_c L_{sm} \\ n_c n_a L_{sm} & n_c n_b L_{sm} & n_c^2(L_{ls} + L_{ss}) \end{bmatrix} \tag{3.28}$$

where L_{sm} is the mutual inductance between stator windings and L_{ss} is the self inductance of a stator winding.

The stator-to-rotor inductance matrix becomes:

$$L_{sr}^{abc} = \begin{bmatrix} n_a \cos\theta_r & n_a\left(\cos\theta_r + \frac{2\pi}{3}\right) & n_a\left(\cos\theta_r - \frac{2\pi}{3}\right) \\ n_b\left(\cos\theta_r - \frac{2\pi}{3}\right) & n_b \cos\theta_r & n_b\left(\cos\theta_r + \frac{2\pi}{3}\right) \\ n_c\left(\cos\theta_r + \frac{2\pi}{3}\right) & n_c\left(\cos\theta_r - \frac{2\pi}{3}\right) & n_c \cos\theta_r \end{bmatrix} \tag{3.29}$$

The rotor-to-stator mutual inductance is given by:

$$L_{rs}^{abc} = \left[L_{sr}^{abc}\right]^{T} \tag{3.30}$$

These equations fully define the modifications required to model the stator turn-to-turn fault in the ABC reference frame. The next stage is to use the ABC-to-QD0 transformation to convert the modified matrices to the QD0 reference frame for simulation.

Note: to simplify the mathematics the stator fault is only considered occurring on the 'a' phase. Therefore, only n_a appears in the following equations. This will have no effect on the accuracy of the method. In order to test for faults on other stator phase windings, the order of the voltages applied to the model is varied (i.e. the model phase ordering is modified so that the simulated fault phase moves to one of the other two windings).

Applying the ABC-to-QD0 reference frame transformation to the modified resistance matrix results in the QD0 reference frame resistance matrix:

$$r_s^{qd0} = r_s \begin{bmatrix} r_{s11} & 0 & r_{s13} \\ 0 & r_{s22} & 0 \\ r_{s31} & 0 & r_{s33} \end{bmatrix} \tag{3.31}$$

where the QD0 resistance matrix coefficients are given by:

$$\begin{aligned} r_{s11} &= \frac{1}{3}(2n_a + 1) \\ r_{s13} &= \frac{2}{3}(n_a - 1) \\ r_{s22} &= 1 \\ r_{s31} &= \frac{1}{3}(n_a - 1) \\ r_{s33} &= \frac{1}{3}(n_a + 1) \end{aligned} \tag{3.32}$$

Finally, the QD0 flux linkage equation (including the stator fault QD0 inductance matrix) is given by:

$$\begin{bmatrix}\lambda_{qs}\\ \lambda_{ds}\\ \lambda_{0s}\\ \lambda_{qr}\\ \lambda_{dr}\\ \lambda_{0r}\end{bmatrix}=\begin{bmatrix}L_{11} & 0 & L_{13} & L_{14} & 0 & 0\\ 0 & L_{22} & 0 & 0 & L_{25} & 0\\ L_{31} & 0 & L_{33} & L_{34} & 0 & 0\\ L_{41} & 0 & L_{43} & L_{44} & 0 & 0\\ 0 & L_{52} & 0 & 0 & L_{55} & 0\\ 0 & 0 & 0 & 0 & 0 & L_{66}\end{bmatrix}\begin{bmatrix}i_{qs}\\ i_{ds}\\ i_{0s}\\ i_{qr}\\ i_{dr}\\ i_{0r}\end{bmatrix} \tag{3.33}$$

where the inductance matrix coefficients are given by:

$$\begin{aligned}
L_{11} &= \frac{1}{3}(2n_a^2+1)L_{ls}+\frac{1}{9}(2n_a+1)^2L_m\\
L_{13} &= \frac{2}{3}(n_a^2-1)L_{ls}+\frac{2}{9}(2n_a^2-n_a-1)L_m\\
L_{14} &= L_{41}=\frac{1}{3}(2n_a^2+1)L_m\\
L_{22} &= L_{ls}+L_m\\
L_{25} &= L_{52}=L_m\\
L_{31} &= \frac{1}{3}(n_a^2-1)L_{ls}+\frac{1}{9}(2n_a^2-n_a-1)L_m\\
L_{33} &= \frac{1}{3}(n_a^2+2)L_{ls}+\frac{2}{9}(n_a^2-2n_a-1)L_m\\
L_{34} &= \frac{1}{2}L_{43}=\frac{1}{3}(n_a-1)L_m\\
L_{44} &= L_{55}=L_{lr}+L_m\\
L_{66} &= L_{lr}
\end{aligned} \tag{3.34}$$

This completes the theoretical development of the induction motor model. The model now has the ability to simulate induction motors with both rotor and stator faults.

3.3.3 QD0 reference frame fault model

Figure 3.3**,** Figure 3.4**,** Figure 3.5 and Figure 3.6 describe the QD0 reference frame fault model. The top-level Simulink view (overview) of the QD0 reference frame model of the faulty model is shown in Figure 3.3. This figure demonstrates the added complexity the fault modelling introduces. The complexity of the model is increased further due to the fact that the ‘0’ axis must

now been included (since the motor inductances and resistances will be unbalanced).

The ‘Q Axis Flux and Current’ subsystem is shown in Figure 3.4. The ‘D’ and ‘0’ axis equations are modelled using the same structure as the Q axis block (shown as the example).

The ‘Torque and Speed Calculation Block’ is shown in Figure 3.5.

The ‘ABC-to-QD0 transformation Block’ is shown in Figure 3.6.

The model parameters and input data (measured voltage/current) are prepared in the MATLAB workspace then loaded into the Simulink before a simulation run commences.

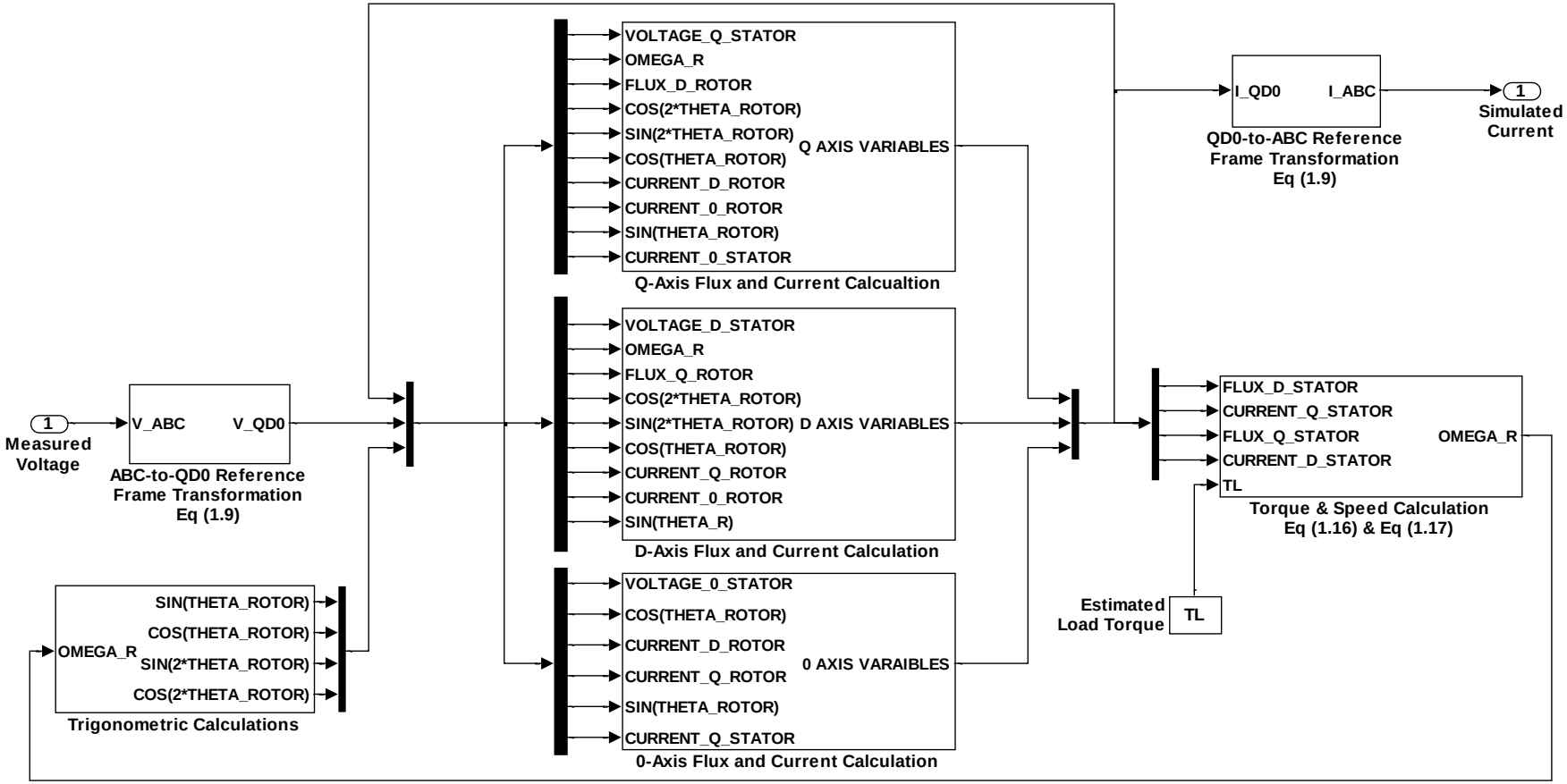

Figure 3.3 Simulink representation of the induction motor model in the QD0 reference frame

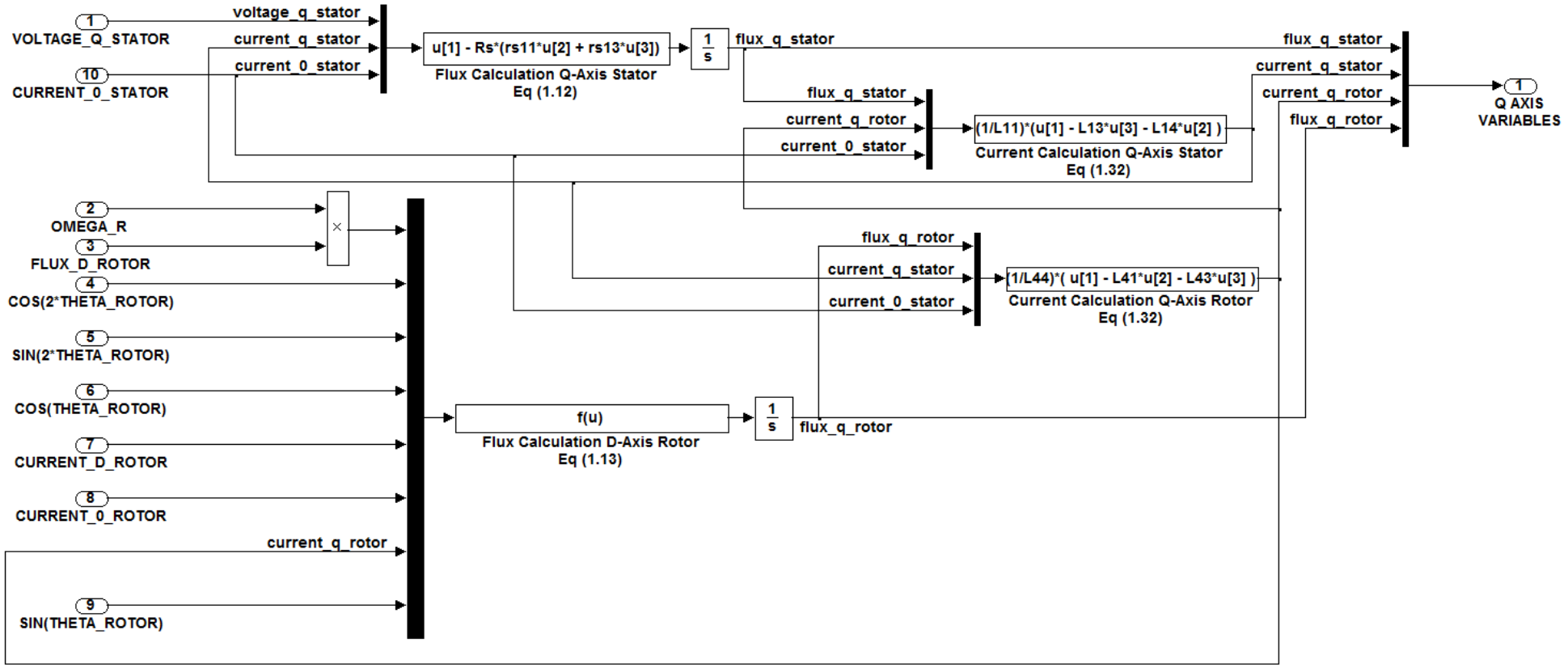

Figure 3.4 Simulink block diagram of the 'Q-Axis flux and current calculation block'

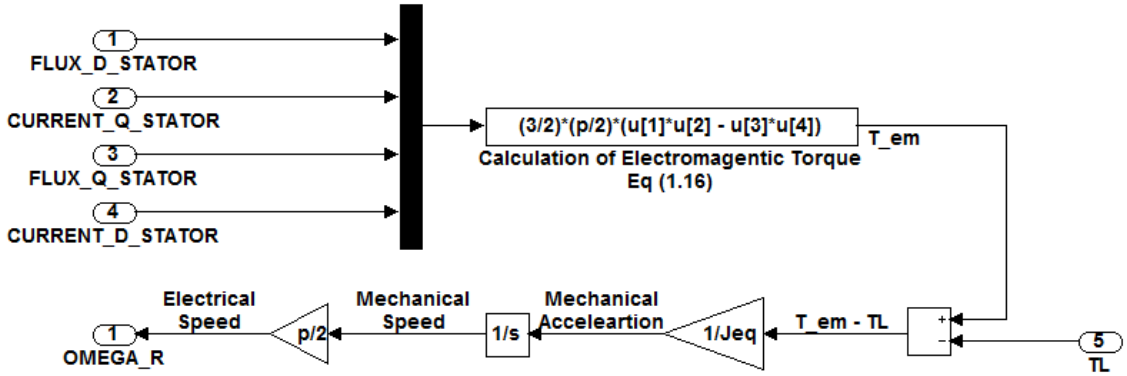

Figure 3.5 Simulink block diagram of the torque and speed calculation

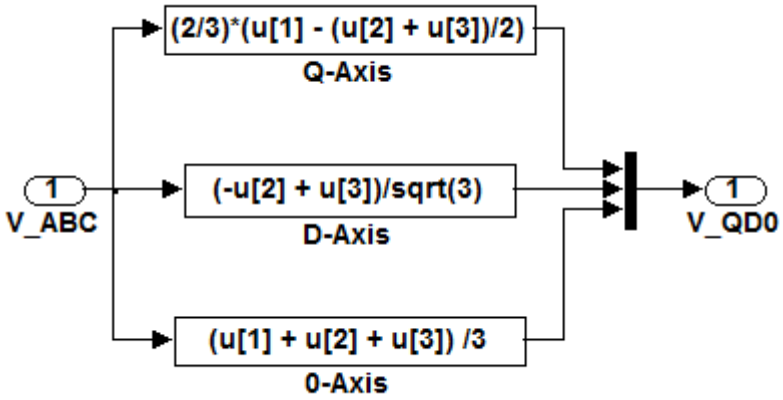

Figure 3.6 Simulink block diagram of the ABC-to-DQ0 transformation

3.4 Developing a model suitable for industrial deployment

The QD0 reference frame model described in the previous section is suitable for simulation from within MATLAB/Simulink. In a typical industrial environment the hardware/software available on the shop-floor (i.e. the switchgear room, switchgear rack, or plant control panel) will not have access to MATLAB/Simulink software package and even if this was the case, purchasing MATLAB/Simulink licenses for each running motor would be prohibitive. In addition to this MATLAB/Simulink is computationally more demanding than, for example, C code.

If a MATLAB/Simulink based monitoring algorithm is to be of any practical use it must be developed with code generation in mind. Code generation is the process of converting MATLAB/Simulink software and models into another

software language. C code allows the algorithm to be executed on a PC but more importantly on it also allows the code to be downloaded to an embedded microprocessor based device. This type of device is common in industrial applications (motor management devices) and may form part of the motor switchgear unit or be a separate panel-mounted unit. Hence, in order for a condition monitoring algorithm to be truly useful for industrial deployment it should be written in a common embedded software language e.g. C.

MATLAB/Simulink provides functionality which allows conversion of scripts and models into C code. This functionality is provided by the Simulink Coder (formerly Real-Time Workshop).

A prerequisite of model conversion using the Real-Time Workshop is the models must not contain any algebraic loops. An algebraic loop occurs when an input port (with direct feed through) is driven by the output of the same block via a feedback path of direct feed through blocks. The fault model described in the previous section (originally presented in reference [9]) contains algebraic loops and therefore cannot be converted into C-code directly using the Real-Time Workshop packages supplied by Mathworks. In order to allow development of algorithms in MATLAB/Simulink and deployment in C, the algebraic loops must be removed.

This process of re-organising the system of differential equations representing the motor results in a third model; the QD0 reference frame model of the faulty induction motor with no algebraic loops.

The algebraic loops are due to the ‘Current Calculation Blocks’ – equation (3.33). The inputs to these blocks include current signals from equivalent blocks on the other two axes which create a set of algebraic loops. In order to eliminate

the loops these equations must be re-written in terms of flux linkages only (or alternatively flux linkages per second) i.e. eliminate current signals from the block inputs. Figure 3.7 shows the algebraic loops in the ‘Q’ axis subsystem as an example.

The model free from algebraic loops is derived by re-writing the original current equations in terms of flux only on each of the 3 axes. Once this is done the equations can be worked through and simplified. This creates equations that are rather complex combinations of inductance terms but only require flux values as inputs. The algebraic loop free equations are derived in Appendix B.

Having derived the new algebraic loop free equations they can then be integrated with the existing Simulink model. The updated ‘Q’ axis subsystem is given as an example of this new format in Figure 3.8. This new fault model without algebraic loops produces identical results to the existing model but is now in a form which can be easily converted to C code making it ideal for industrial deployment.

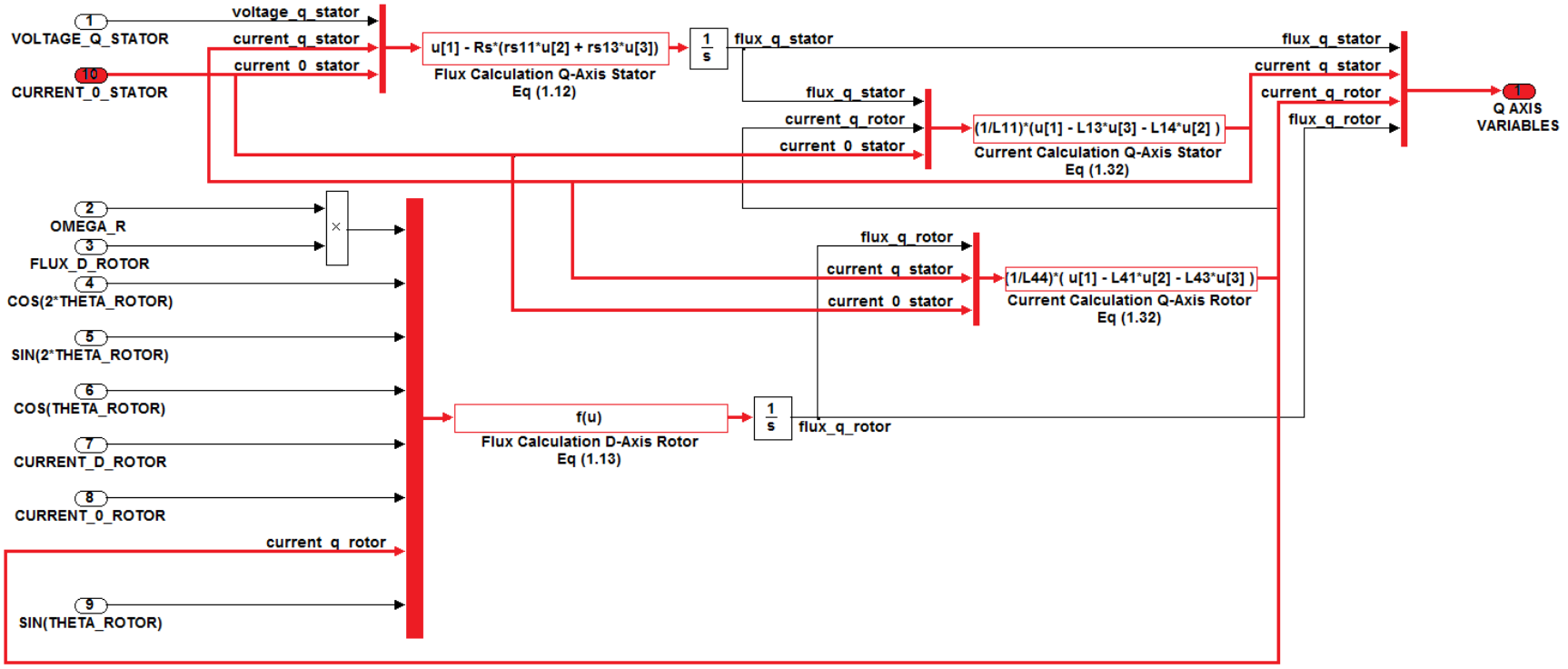

Figure 3.7 QD0 reference frame model showing signals involved in the algebriac loops (highlighted in red)

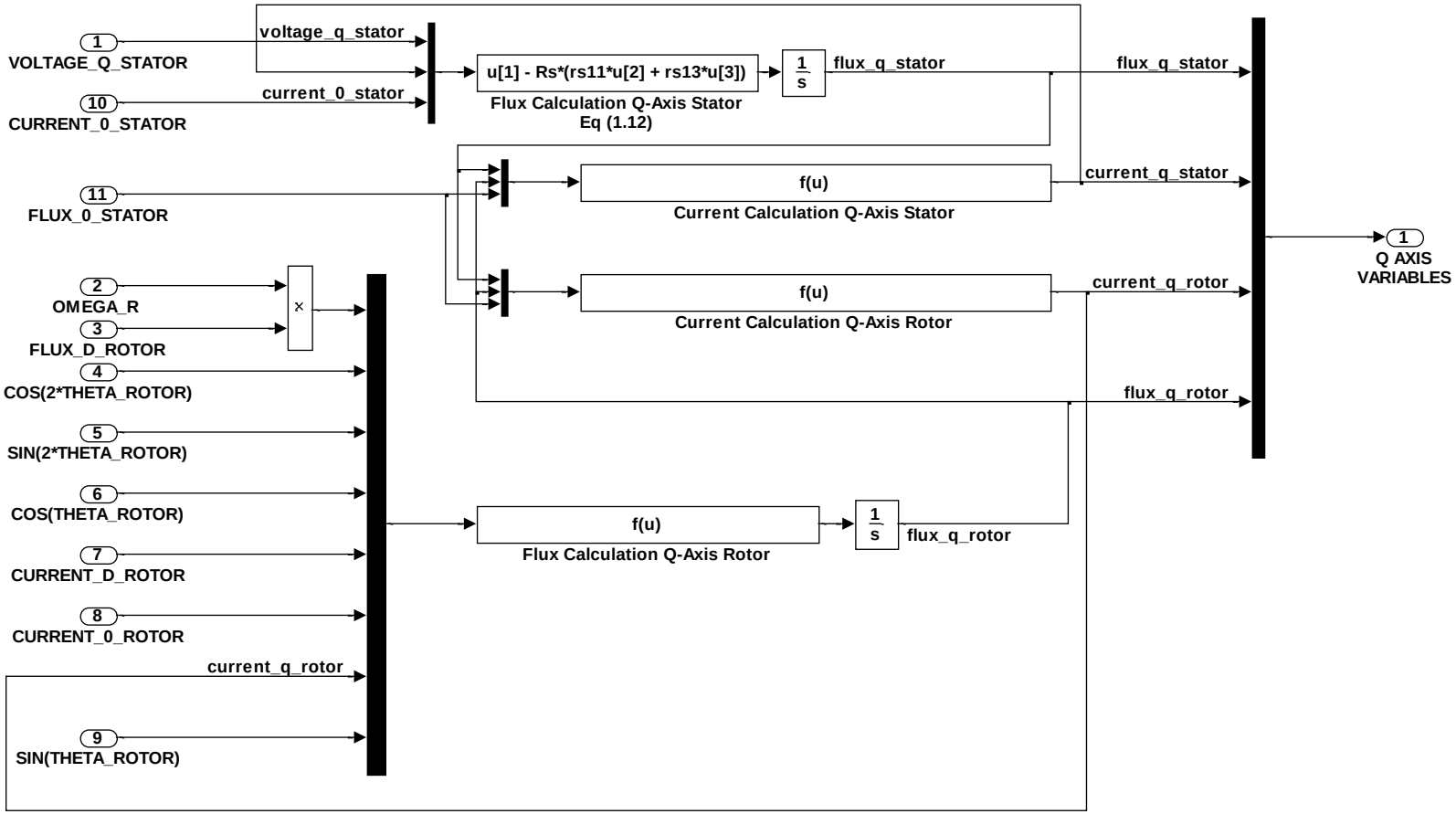

Figure 3.8 'Q' axis calculation block after all algebraic loops have been removed (inputs to the current calculation blocks are now only flux quantities)

3.5 Summary

The development of three induction motor models to be used for induction motor condition monitoring purposes has been presented in this chapter. The basic theory of coupled magnetic circuits has also been presented. The magnetic coupled theory is developed firstly in the 3-phase reference frame with equations being developed on the ‘A’, ‘B’ and ‘C’ axes. On each of these axes voltage and flux equations are developed which describe the electrical characteristics of the stator windings and ‘equivalent’ windings of the rotor.

The first model to be developed based on this theoretical framework was the healthy QD0 reference frame model. This model allows for simulation of induction motors which are electrically balanced. It is for these reasons that this model is limited to simulation of healthy (fault-free) induction motors. If the ‘0’ axis is neglected then this model becomes the ‘QD’ model which, due to the removal of two of the governing equations, is computationally lighter and thus more suited to iterative parameter identification applications. It is important to note that when the inductance and resistance matrices are balanced, excluding the ‘0’ axis leads to no loss in accuracy.

The second model was the QD0 reference frame model with the ability to simulate rotor and stator faults. This model is an extension of the initial model which allows the rotor and stator inductance and resistance matrices to be adjusted. The adjustment to these matrices is based on 2 parameters; the number of shorted turns in a stator winding and the number of broken bars in the rotor cage. These 2 fault parameters are then worked into the equations to allow these types of faults to be simulated.

The final model is an adaptation of the second model (the fault model) in which there are no algebraic loops. The motor equations are converted into a form in which there is no direct feed-through and therefore algebraic loops are eliminated. This is important in terms of the industrial deployment of the algorithm since algebraic loops must be removed to allow the Simulink model to be converted into C code. This final model is now suitable for conversion into C code and thus is ready for deployment onto microprocessor based protection devices and use in a model-driven development process.

The basic model developed here is used for the parameter estimation aspect of the AMRA system and the fault model outputs form a part of the mixed residual set.

Chapter 4. Speed Estimation

This chapter explores the current state-of-the-art for induction motor steady-state speed estimation methods and describes the development of the speed estimation algorithm used as part of this project. The results of the speed estimation are also presented; the algorithm shows good performance when detecting the rotational speed of the test motors at a range of loads.

Accurate speed estimation is crucial for accurate parameter estimation. This allows a variety of different motor sizes and types to be correctly modelled; thus speed estimation is a key contributor to the AMRA strategy.

4.1 Literature review

The area of induction motor (IM) sensor-less speed estimation has attracted a large amount of research interest due to its importance in 2 main areas [102]:

- induction motor control
- induction motor fault detection and diagnosis (FDD)

Sensor-less speed estimation is preferred because it avoids the cost and installation issues associated with additional sensing hardware (e.g. optical encoder) for speed measurement.

Broadly speaking, there are 2 main areas that have been explored in order to provide IM speed estimation. These are:

- model-based estimator methods [97], [103–110]
- model-free spectral methods [102], [111]–[115]

The model-based estimator methods commonly involve using the QD0 reference frame mathematical model of the induction motor. This model is supplied with measured currents and voltages and used to estimate state variables and/or state parameters. If the speed is considered constant it can be estimated as a parameter, if the speed is not treated as a constant then it can be found by comparing 2 state estimates.

The model-free spectral methods involve processing of the spectra of the currents or voltages supplying the motor. These spectra contain frequency components related to the speed of the motor, either due to inherent eccentricity in the machine or the rotor slot harmonics (RSH) generated as rotor bars pass the stator windings. Thus by finding these speed related harmonics the mechanical speed of the rotor can be determined.

4.1.1 Model-based speed estimation

A common form of sensor-less speed detection is the Model Reference Adaptive System (MRAS) [103], [104], [108]**.**

The conventional form of MRAS operates using a mathematical model of the motor. The model commonly used is the simple direct-quadrature (DQ) reference frame 2-axis equivalent model.

The basic premise is to estimate some state variables using a reference model and an adaptive model. The models operate separately but estimate the same state variables. The difference (error) between these estimated state variables is then compared. This error is used to drive an algorithm that controls the adaptive model and attempts to drive the error to zero [103].

The reference model is not a function of speed. The adaptive model is a function of speed. Therefore a value for speed is calculated that minimises the error between the estimated state variables from each of the models (i.e. an estimate of speed is obtained).

There is some choice in which variables to use but rotor flux linkages or back EMF components are commonly used [103].

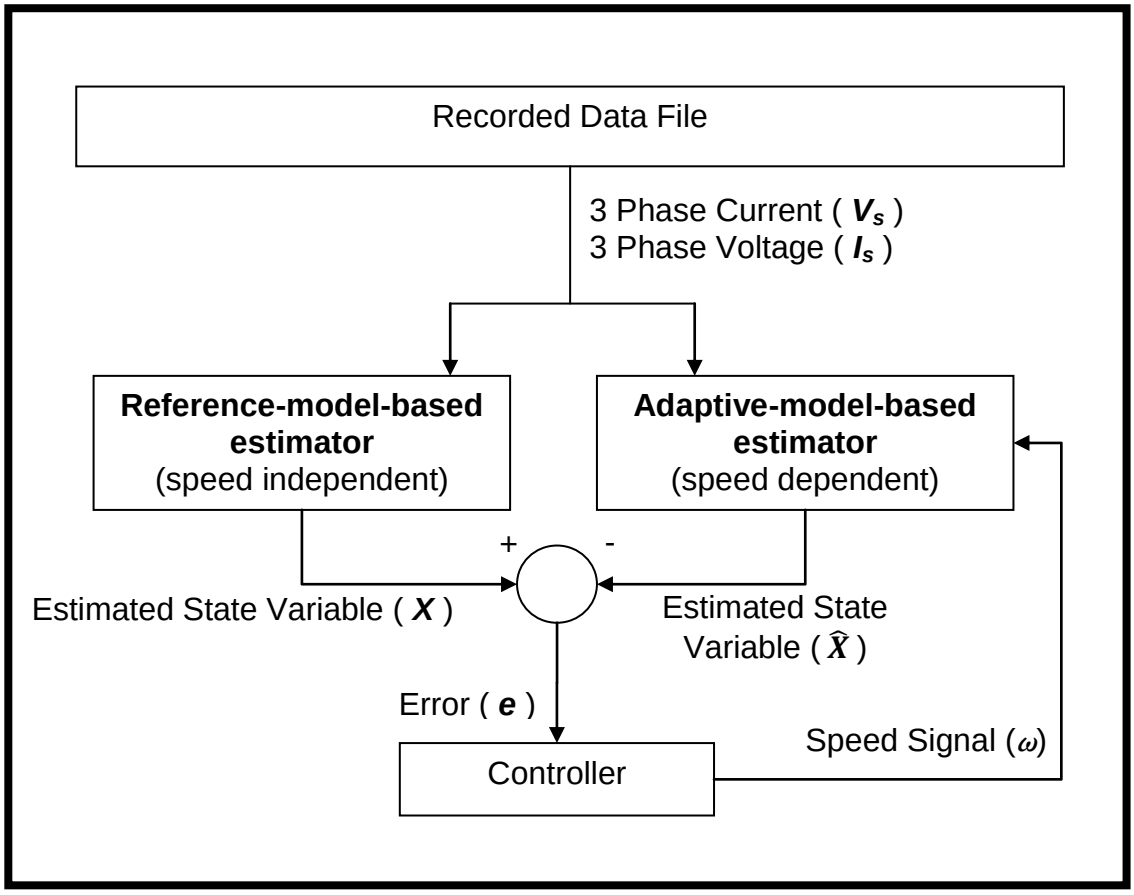

Figure 4.1 The basic Model Reference Adaptive System (MRAS) for speed estimation

Considering the MRAS system configured to estimate rotor flux linkages:

- the stator voltage equation allows calculation of the stator flux linkages (but IS NOT dependent on speed)
- the rotor voltage equation allows calculation of the stator flux linkages (but IS dependent on speed)

So in this case the stator voltage equation is the ‘reference’ model and the rotor voltage equation is the ‘adaptive’ model.

Since the system is model based model parameters are required. These parameter help configure the model to different sizes and types of induction motors. The model parameters are those required for the simple DQ reference frame model:

- Stator resistance, R_s
- Rotor resistance, R_r
- Stator inductance, L_s
- Rotor inductance, L_r
- Mutual inductance, L_m

The accuracy of these parameters is very important for effective speed estimation. MRAS performance has been shown to drop significantly with only slight parameter error. Additionally if the parameters value change during operation (e.g. due to Ohmic heating) then the performance of the speed estimator will dramatically suffer [103]. Simulations have proved that small changes in the machine parameter used in the models can lead the speed estimation to be inaccurate and in some cases unstable.

In one study the effect of parameter variation during operation was minimised by performing online estimation of rotor resistance and employing an artificial neural network (ANN) to replace the adaptive part of the model. This made the process slightly more robust to parameter variations but small deviations in motor parameters still had a significant effect on the accuracy of the speed estimation [103].

A separate study highlights the same required parameter set and goes on to state that the most pressing concern is with knowing the stator resistance and the rotor time constant (Lr/Rr) since these parameters vary due to Ohmic heating [104]. However, before variations during operation are even taken into account the nominal parameter values need to be known for this method to work.

The problem of speed estimation can be approached from a parameter identification point of view [104]. Speed is considered an unknown constant parameter and is identified using a least squares technique. However, the standard motor parameters still need to be known accurately for this method to work.

An alternative method is the Nonlinear Method [104]. This offers improvements over the parameter identification approach because the speed does not have to be considered a constant parameter. Unfortunately it still has the same drawbacks as the other model based methods: it still requires the machine parameters to be known accurately.

The equations used for speed estimation can be rewritten to exclude the stator resistance parameter. This seems attractive however when investigated this technique would not work above 20% of the motors rated load torque [104]. It can be seen that the speed estimation algorithms struggle considerably with parameter inaccuracy in these simulations.

One alternative to the standard MRAS techniques is to use an Extended Kalman Filter (EKF). This requires a model in the form of a state-space equations derived from the DQ reference frame model. But again the electrical parameters of the induction motor need to be known before speed estimation

can take place. The performance EKF can be combined with genetic algorithms to improve the calculation of the EKF weights that control the algorithm operation [110]. In [105] an EKF is utilised which resulted in the error on speed estimation being kept at approximately 3% (unless at very low speeds) and the algorithm showed some ability to work with inaccurate parameters. The most important factor was that the machine parameters used were estimated – however when the parameters are estimated an encoder needs to be fitted for position and speed information [105] (which defeats the point of sensor less speed estimation). Another study, [106], introduces a new sliding mode current observer, the speed is treated as an unknown constant parameter. Like all the other methods discussed thus far it uses stator voltages and currents as inputs. It requires the basic machine parameters to be known.

In [108] several different MRAS techniques are explored. Some of these methods are tested and extensions are proposed in the form of 'mutual estimation' where the rotor speed is estimated at the same time as either stator resistance, rotor inertia or rotor time constant. This would allow the scheme to operate without all machine parameters being known (however the majority of machine parameters would still need to be known). The mutual estimation scheme proposed was untested.

Successful speed estimation has been achieved using another model based approach in which the rotor speed is assumed constant. Again, all electrical parameters are required to be known prior to speed estimation. However, it has been proven that variation in rotor resistance (dependent on temperature) can also be estimated using this scheme [109].

The problem common to all of these methods is that they require most or all of the machine parameters to be known accurately to work correctly.

4.1.2 Model-free speed estimation

Model free methods do not require a detailed knowledge of all the machine parameters. They focus on the current spectrum supplying the induction motor since it contains frequency components whose position depends upon the rotational speed of the motor. In [111] an equation is used that detects eccentricity related sidebands in the current spectrum. These sidebands are a function of slip, so if the sidebands can be detected then the slip (and speed) can then be estimated. The frequency components can be predicted using equation (4.1) below.

$$f_{ecc} = f_0 \pm f_r \tag{4.1}$$

where f_0 fundamental frequency (Hz)

f_r rotor shaft rotational speed (Hz)

This study also goes on to say that the rotor bar harmonics provide more accuracy in speed estimation. The rotor bar harmonics are also known as rotor bar pass frequencies (RBPF). These tend to repeat throughout the spectrum and their position can be predicted. Equation (4.2) shows the method of calculating these frequency components based on the number of rotor bars and the supply frequency. The spectrum is scanned for these harmonics based on the less accurate (eccentricity based) speed estimate and this allows the number of bars to be estimated and then used in future, more accurate, speed estimates.

$$f_{har} = f_0 \left\{ (n.N \pm n_e).\left(\frac{1-s}{p}\right) \pm n_{ws} \right\} \tag{4.2}$$

where f_{har} harmonic frequency (Hz)

N number of rotor bars

p number of pole-pairs

n rotor bar harmonic # = 0,1,2,3,...

n_e rotor eccentricity harmonic # = 0,1,2

n_{ws} stator MMF harmonic # = 0,1,2,3,...

By considering all of these harmonics (using aliasing techniques – combining related frequencies to derive a more significant output) the accuracy and robustness of the FFT based algorithms can be improved [113]. Utilizing the rotor bar pass frequency harmonics is advantageous because it provides an increase in slip resolution over the eccentricity sidebands [116]. Figure 4.2 shows a typical spectrum from a fully loaded healthy motor. The RBPF can be clearly seen to be present in the spectrum and of significant magnitude which makes them a suitable indicator of motor shaft speed.

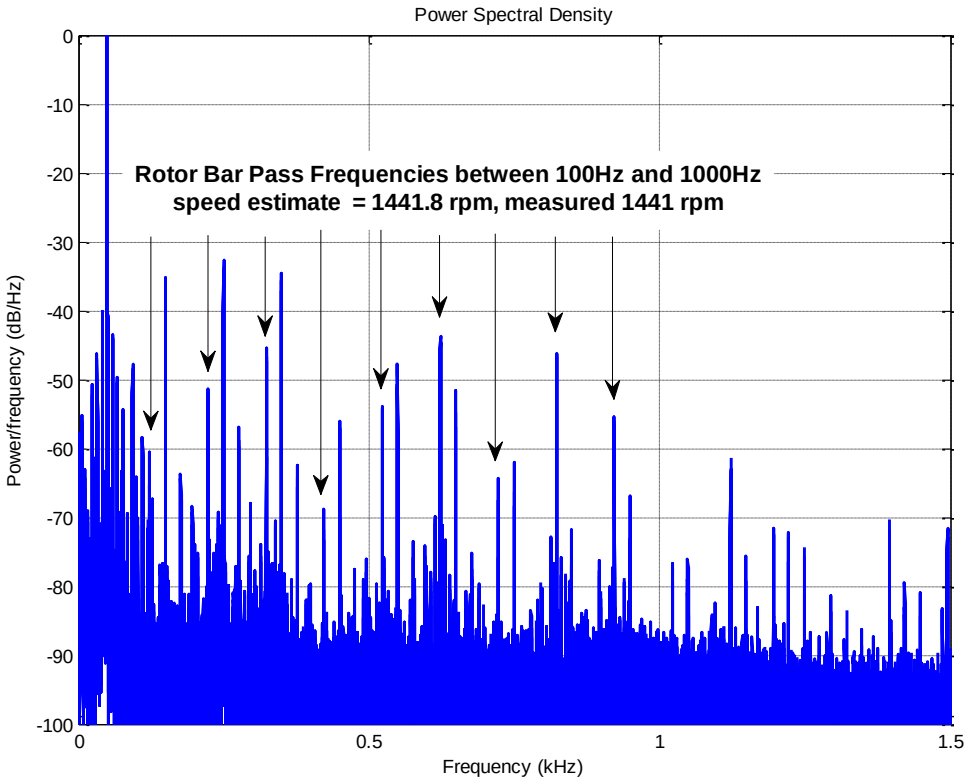

Figure 4.2 Rotor bar pass frequency harmonics (sampled @ 5kHz, 5sec) if correctly detected can provide accurate speed estimation

In [107] the speed of the induction motor is estimated by utilising spectral signatures created by irregularities in the rotor construction. However, this method is only suitable to inverter driven motors since it requires a high frequency carrier signal to be super-imposed on the pulse-width modulated (PWM) supply voltages. This method also requires the number of rotor bars to be known and requires the rotor assemblies to contain manufacturing defects in order to cause a slight imbalance which is then detected.

Figure 4.3 demonstrates the problems with using simple FFT-based spectral methods. Often the speed related frequency components will have a small magnitude in comparison to other content in the spectrum (e.g. load/coupling related sidebands, supply harmonics, etc). In the figure the vertical arrow highlights the component linked to eccentricity (the desired component) however it is clear that there are other frequency components of significantly larger magnitude. This has led to more advanced spectral methods to be developed based on the Park Vector plots [102], [112].

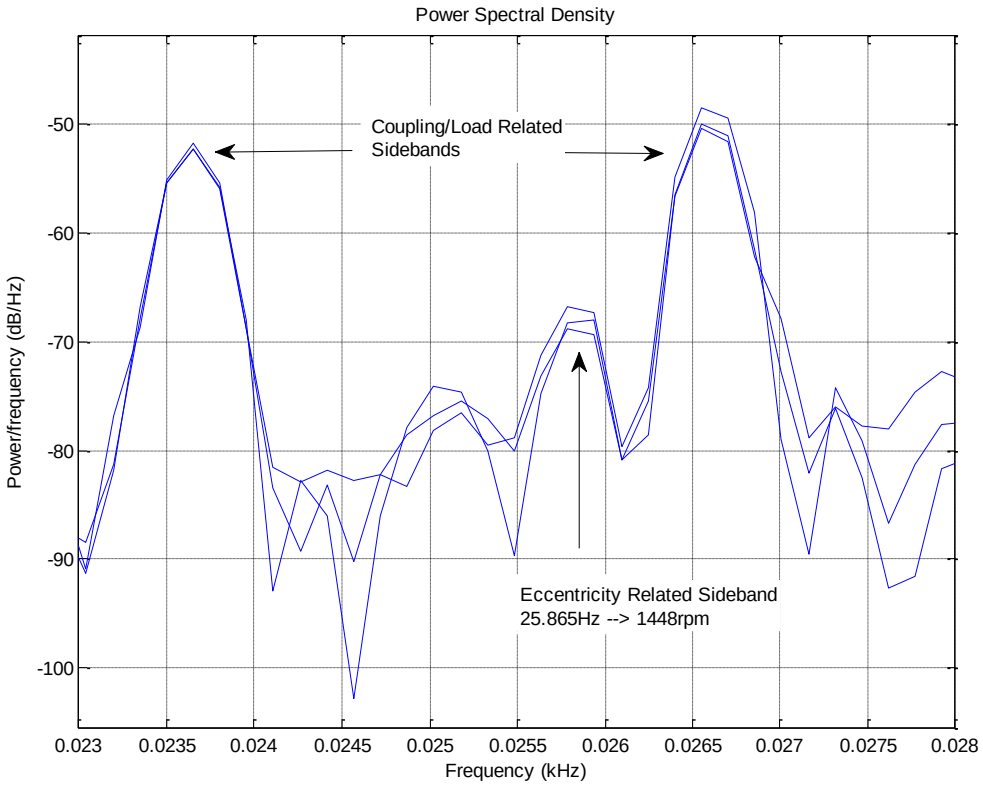

Figure 4.3 Current spectrum for a 7.5kW motor between 23Hz and 28Hz. For smaller motors the magnitude of the eccentric harmonics can make them difficult to detect

Spectral methods based upon Space Vector Angular Fluctuation (SVAnF) offer an alternative to scanning the frequency spectrum [102]. In a similar manner to previously discussed techniques the SVAnF method involves detection of the speed-related current harmonics that are a result of the induction motors inherent levels of static and/or dynamic eccentricity. However, SVAnF uses Park transform plots, specifically the zero crossing times (ZCT). ZCT are used to detect harmonics in the SVAF signal because they are much quicker than running a FFT so can be used for real-time speed tracking. The algorithms showed excellent performance for a 4 pole motor but the authors stated that it was unsuccessful when attempting to detect the speed of a 2 pole motor due to the proximity of the speed related harmonics to the supply fundamental.

In [112] Space Vector Amplitude Fluctuation (SVAmF) is utilised. This is similar to SVAnF except that the amplitude of the Park locus is tracked rather than the instantaneous angle. This method was verified against experimental data on a 2-pole motor and provided very good performance even though the rotational speeds were very close to the 50Hz fundamental. Again, this method is based on detecting the speed-related eccentricity sidebands via the Park transform loci.

The FFT is generally avoided for fast response speed detection due to the time versus frequency resolution problem. Alternative techniques, such as, fast orthogonal search (FOS) have been employed to provide a small frequency resolution for small time-series data segment [114]. Hence, the FOS can extract the same information as the FFT but from much fewer samples.

There are some techniques that do not fall in to either the model-based category or spectral-based category. One of these is artificial neutral network (ANN) based solutions. In [117] neural speed filtering is presented that uses a ANN to solve the problem using non-linear state filtering. This technique neither requires detailed model parameters nor relies on spectral content during operation. However, like all ANN it requires training of some kind. The training set is speed data estimated from RBPF in the current spectrum. So despite appearing to be a ‘new’ solution to the speed estimation problem it is in fact still using the well-understood RBPF spectral method.

In [115] a voltage-based method is developed to estimate speed. Like the other spectral harmonic methods it claims that spectral methods offer advantages in terms of robustness over the model-based (parameter dependent) methods.

Unfortunately, this method can only be used for star connected induction motors and requires access to the motor neutral connection.

4.1.3 Overview of induction motor speed estimation methods

A summary of the papers reviewed in this literature review are displayed in Table 4.1.

Table 4.1 Comparison of several induction motor speed estimation techniques

No.	Author	Description	Type	Techniques Used	Required Data	Required Parameters	Limitations
[106]	DERDIYOK	Uses the DQ model with a sliding mode observer for current and flux states	MODEL	Sliding mode observer	2x Voltage 2 x Current	Rs, Rr, Ls, Lr, Lm	Requires all electrical machine parameters.
[104]	BODSON	Uses 3 model based techniques: adaptive, least squares and non-linear for speed detection	MODEL	MRAS Least squares Non-linear model	3x Voltage 3x Current	Rs, Rr, Ls, Lr, Lm	All 3 methods were highly sensitive to parameter variation and some would only perform at low loading levels. Only tested against simulation.
[108]	CARVALHO	Model Reference Adaptive System (MRAS) approaches to speed estimation	MODEL	Rotor-flux Back EMF Reactive-power Dm observer PI adaption	3x Voltage 3x Current	Rs, Rr, Ls, Lr, Lm	Sensitivity to inaccurate parameters
[109]	LEE	Uses a fourth-order model and converts the problem into a parameter estimation problem for motor speed	MODEL	Parameter estimation	3x Voltage 3x Current	Rs, Ls, Lr, Lm	Requires knowledge of 4 machine parameters
[110]	SHI	An Extended Kalman Filter (EKF) is used on a model where the speed in included as a state. A genetic algorithm is used to optimise the Kalman filter	MODEL	EKF observer GA	3x Voltage 3x Current	Rs, Rr, Ls, Lr, Lm	Requires calibration when measured speed is available.
[103]	YANG	Standard MRAS and ANN MRAS	MODEL/ NEURAL	MRAS rotor flux estimation ANN Stator resistance estimation	3x Voltage 3x Current	Rr, Lr, Ls, Lm	Only validated against simulation. Sensitive to parameter variations.
[105]	LEITE	Reduced order Kalman Filter performing state estimation with estimated parameter set	MODEL	Kalman Filter State estimation	3x Voltage 3x Current	None	Parameters are estimated using measured speed initially.
[111]	SILAGHI	Uses eccentric frequency components to identify speed and then uses this to identify PPF components	SPECTRAL	RBPF Eccentric sidebands FFT/Peak detection	1x Current	None	Not validated against experiment. Unclear description of technique.
[102]	ARKAN	Uses Park (DQ) loci plots and space vector angular fluctuation (SVAnF) to detect speed harmonic components due to eccentricity	SPECTRAL	Park locus SVAnF Zero-crossing	3x Current	None	Did not work for 2-pole motor due to overlapping with supply harmonics
[112]	CHUN	Uses Park loci plots and space vector amplitude fluctuation (SVAmF) to detect sped harmonic components due to eccentricity (validated against a 2 pole machine)	SPECTRAL	Park locus SVAmF STFT High-res STFT	3x Current	None	Was validated against a motor on a reduced voltage (to limit heating due to repeated starts)

[116]	HURST	Uses speed harmonic components due to eccentricity to find PPF rotor-slot harmonics. Harmonics are captured from across the spectrum to improve speed estimation robustness	SPECTRAL	Aliasing detection FFT RBPF/Eccentricity	1x Current	None	If eccentric harmonics are not detectable at any load condition then no. of rotor slots is required.
[114]	MCGAUGHEY	Uses fast orthogonal search (FOS) as an alternative to FFT to detect the RBPF components in the spectrum	SPECTRAL	RBPF FOS	1x Current	nBar (= no. . of rotor bars)	
[115]	PETROVIC	Uses the stator neutral-point voltage harmonics related to pole-passing frequency	SPECTRAL	Peak detection FFT	1x Voltage	nBar	Stator winding must be star-connected. Stator winding neutral point must be accessible.
[107]	DIXON	A high frequency carrier is added to voltage supply to emphasise eccentricity/RBPF related frequency components which are used to indicate speed	SPECTRAL	PWM Peak detection FFT	1x Current	nBar	Requires motor to be controlled by an inverter.
[90], [117]	BHARADWAJ	A neural network is used to perform non-linear filtering to estimate IM speed	NEURAL (SPECTRAL)	ANN State filtering (RBPF for training)	1x Current	None	During operation uses ANN but for training requires RBPF spectral data.

4.1.4 Speed estimation literature review summary

This literature review highlights the fact that there is a reasonable amount of research on the topic of induction motor sensor-less speed estimation but the vast majority of the papers can be classified as one of two distinct methods:

1. Model-based methods
2. Spectral analysis methods

Within these broad areas there are many different techniques that are employed. Some techniques are modified or combined with others but the fundamental method is the same. For model based methods – the speed is either estimated as a state or as a parameter using the measured voltages and currents to drive a model. For the spectral methods – speed related content found in the spectrum is extracted in order to produce an estimate the speed.

The DQ reference frame model is almost universally used, with the equations being manipulated to suit each algorithms different requirement. There are several methods for the parameter/state estimation process (MRAS, EKF, LS, ANN) each of which is proven to have some measure of success. However, for all of these methods there is one fundamental problem: the electrical parameters of the motor need to be accurately defined for them to operate successfully. With only small parameter errors (e.g. 10-15%) the algorithms performance drops and higher errors cause the performance to drop significantly – this cannot be used as part of a robust condition monitoring system and a basic torque/speed estimator based on interpolation using nameplate rated information would provide better performance.

An alternative to this process is to estimate the speed based on speed-related frequency components in the motor's current spectrum. This method is independent of motor parameters. The fact that this method can be conducted completely separately to the motor parameter estimation (source of error) makes it a more attractive solution. However, the majority of these techniques rely on the assumption that all induction motors have an inherent level of eccentricity that will lead to detectable current fluctuations. If induction motor construction improves significantly these fluctuations may become more and more difficult to detect.

Considering the benefits and downsides of both method types, the spectral methods seem to be the most applicable to steady-state, non real-time estimation of induction motor speed to be used for fault detection and diagnosis. The following section describes a comparison of the most suitable spectral speed estimation techniques.

4.2 Speed estimation development and testing

This section describes the testing of a variety of different speed estimation techniques in order to identify the most suitable method for use in the final system. A selection of spectral techniques described in the previous section will be compared in this section in order to find the most suitable solution. The techniques to be compared will be:

1. Basic nameplate based estimation (linear interpolation)
2. Space Vector Amplitude Fluctuation (SVAmF)
3. Space Vector Angular Fluctuation (SVAnF)
4. Primary eccentric sideband detection (upper)
5. Primary eccentric sideband detection (lower)
6. Rotor bar pass frequency detection

The algorithms were tested using a 5kHz sampling rate using the MATLAB FFT function combined with a Hanning window. A dB scale is used throughout normalised to the fundamental frequency. The algorithms were testing using the belt-coupled data set. This involves the 4 different motor units in healthy configuration and with a range of faults (rotor broken bar, stator winding and bearing faults) and fault magnitudes. The belt coupled dataset was used since it contains many additional frequency components due to the belt dynamics thus giving the algorithms the poorest signal-to-noise ratio in order to test them thoroughly. The estimated data can then be compared with the actual rotational speed that was recorded using an optical tachometer during the test.

Appendix E lists the results of the speed estimation performance of the four detection methods. The average and maximum values for speed estimation error are listed at the bottom of the table and displayed in Figure 4.5. The average values give a good indication of the overall accuracy of the algorithm whilst the maximum values provide information on the robustness of the algorithm i.e. will it perform effectively under a range of different conditions.

The SVAF and primary eccentric sidebands methods provide the worst performance. The SVAF methods have a slightly better average error (0.3% and 0.25%) than the eccentric sideband method, but the maximum error is the highest in the test at 1.47%. This equates to a speed estimation error of over 21 rpm. The primary eccentric sidebands methods have slightly improved maximum error (1.44%) but slightly worse average error (0.35%/0.36%).

Surprisingly, the basic nameplate speed estimation performance provided the second best performance in the test with an average error across the whole dataset of only 0.12% (1.78rpm) and a maximum error of 0.43% (6.17rpm). This

method offers a vast improvement over the SVAF and eccentric sideband techniques.

The most accurate method of speed estimation was found to be the rotor bar pass frequency (RBPF) based method. This method had excellent performance with the average error only 0.06% (=0.84rpm) and maximum error limited to 0.23%, which is only 3.46rpm.

Unfortunately the RBPF method requires knowledge of the number of bars making up the rotor cage which will in most cases be unknown (and assumed unknown in this project). Therefore, in order to use this method the number of rotor bars needs to be estimated – this estimation process is covered in the next section.

The fs-fr and fs+fr components are not identical to each other in terms of magnitude due to noise in the spectrum.

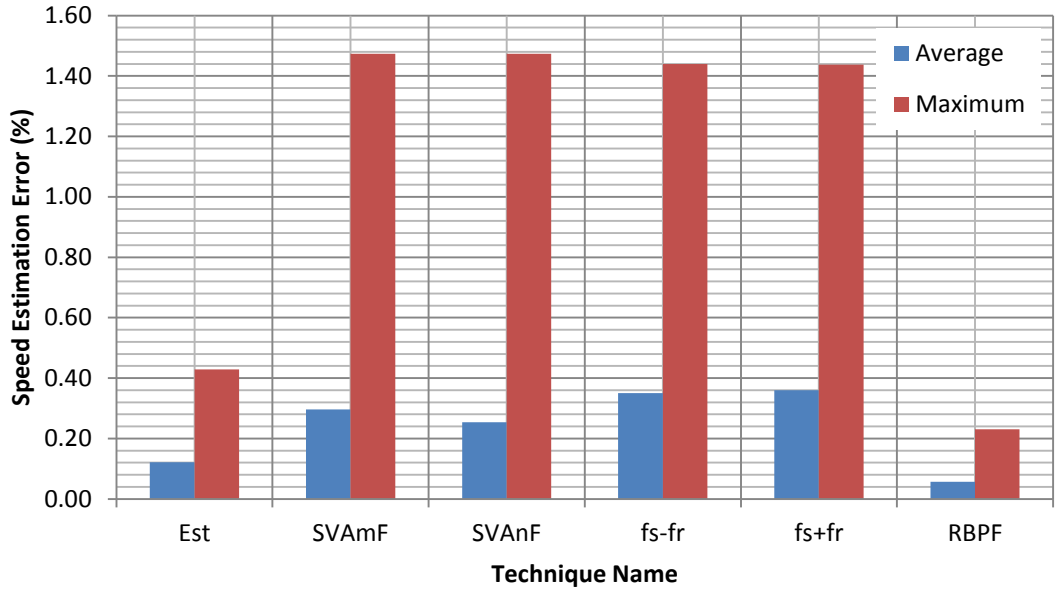

Figure 4.4 Comparison of average and maximum speed estimation errors in RPM

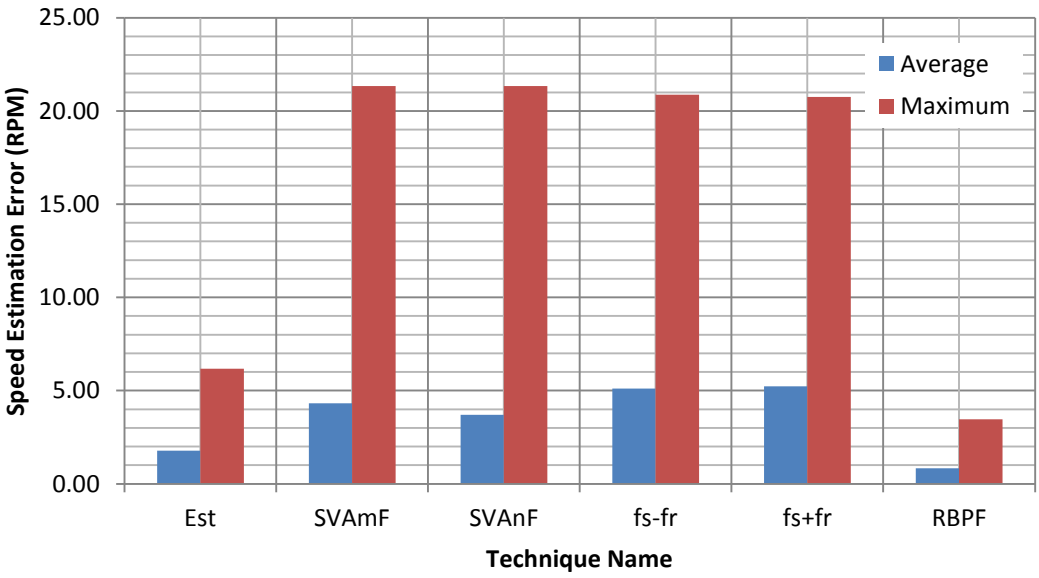

Figure 4.5 Comparison of average and maximum speed estimation errors in percent

4.3 Rotor bar number estimation

This section describes the rotor bar number estimation algorithm developed.

4.3.1 Rotor bar number estimation algorithm

In order to use the RBPF speed estimation method the number of rotor bars needs to be known. Figure 4.6 below explains the process developed as part of this thesis to be used to estimate the number of rotor bars.

The overall concept of this process is to intelligently search through the frequency spectrum for peaks which could be RBPF content. The associated rotational speed of these peaks is then compared with a predicted value based on nameplate rated data and then placed in an array. This array is then sorted in terms of peak magnitude to determine the most probable value of the RBPF. This frequency is then converted to a speed value which is output as the estimated speed.

Initially the data is loaded and following this an FFT is performed to generate the frequency spectrum data, from this the fundamental frequency can be

determined. The next stage is to calculate the approximate speed estimate based on rated nameplate parameters (see section 4.3.3).

At this stage the algorithm enters a loop which cycles through potential bar numbers from a minimum of 10 bars up to a maximum of 80 bars. These numbers were chosen based on typical bar numbers found during literature searches. An extended region was fitted around this initial range in order to account for non-typical bar numbers which may be present.

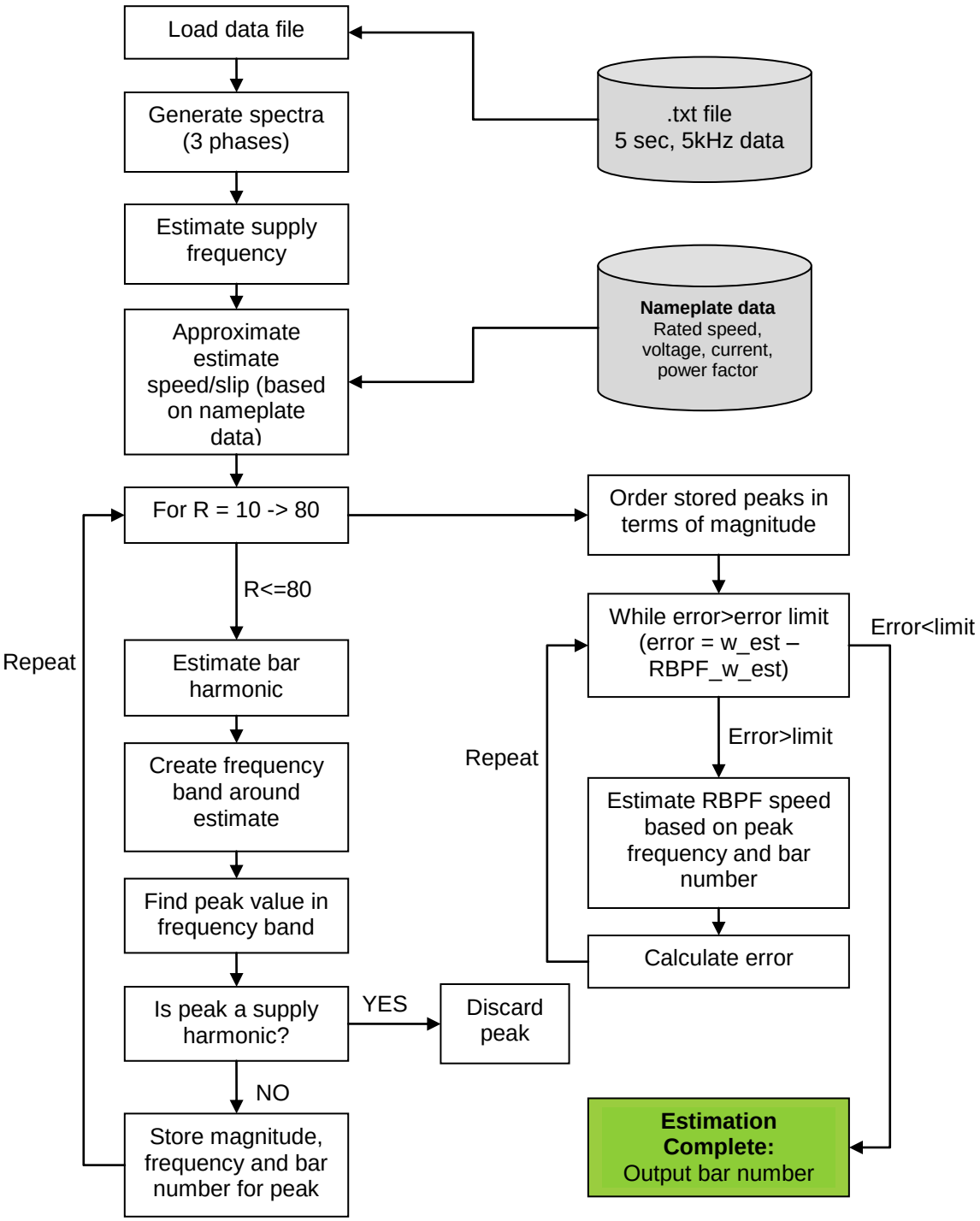

Figure 4.6 Rotor bar number estimation process

For each bar number the following process then occurs; the bar harmonics are estimated, a frequency interval is generated around this predicted harmonic and then the peak value within this band is determined; the magnitude and frequency value of this peak are then recorded.

The theoretical RBPF harmonics given in equation (4.2) are not all included in the analysis since this would result in an excessive amount of data to process. The problem is simplified by setting the rotor bar harmonic to 1, the rotor eccentricity harmonic to 0 and limiting the stator MMF harmonics to ±1 and ± 2. The low value harmonics are those typically of the highest magnitude so limiting the search to these harmonic values allows bar estimations to be made (the most dominant frequency components are still included) without significant computational burden or algorithm complexity. The resulting RBPF equation used is given by equation (4.3):

$$f_{har} = f_0 \left\{ (N) \left(\frac{1 - s_0}{p} \right) \pm n_{ws} \right\} \qquad (4.3)$$

where n_{ws} stator MMF harmonic # = 1, 2

Having found a peak which might possibly be a RBPF the frequency value of the peak is checked against a calculated list of supply harmonics. If the peak is a supply harmonic it is discarded, if not it is stored for the next stage.

Once peak values and their associated frequencies have been determined for all potential bar numbers (up to a maximum bar number of 80) a decision is made to select the most likely bar number based on the frequency content. Each of the supposed RBPF peak values is added to an array and then ordered in terms of magnitude. This puts the largest frequency peaks (i.e. most likely to be a RBPF and not simply noise) first in line to be analysed. This array is then stepped through in order (from highest magnitude to the lowest) each bar number (and RBPF) is used to calculate speed and then this speed is compared with the approximate estimate given by the rated nameplate parameters interpolation method (see section 4.3.3). If the error between the two values is excessive then this frequency component is not likely to be an

RBPF and is discarded. The process moves through all potential bar numbers until a speed is found which is similar (within 5 RPM) to the rated nameplate interpolation value.

This estimated speed and estimated bar number are then outputted from the function. All processes described above take into account all three phases and average the result for the analysis. The nameplate based approximate speed estimate is based on torque and speed estimation, these are covered in the next two sections.

4.3.2 Torque estimation based on nameplate data

The approximate speed value (used to verify the spectral estimates are realistic) is calculated based on an estimated torque which is calculated using the nameplate rated parameters.

For the torque estimation, the first step is to compare the electrical load with the rated electrical load in order to calculate a percentage load (percent full load). The percentage load is therefore given by:

$$L(\%) = P_{IN}/P_{IN.R} \tag{4.4}$$

where P_{IN} Calculated electrical power drawn by the motor
$P_{IN.R}$ Electrical power drawn by the motor at rated load

Furthermore the rated and calculated electrical power values can be calculated as follows:

$$P_{IN.R} = (\sqrt{3}).v_R i_R \cos\varphi_R \tag{4.5}$$

where v_R RMS voltage at motor rated load
i_R RMS current at motor rated load
$\cos\varphi_R$ Power factor at motor rated load

The calculated electrical power is found using equation (4.5) but substituting rated values for measured values. The RMS voltages and currents are

determined using the sampled voltages and currents and the power factor is given by:

$$\cos\varphi = \frac{P_{active}}{P_{apparent}} \qquad (4.6)$$

where P_{active} Active power
$P_{apparent}$ Apparent power

Having calculated the estimated percentage load (equation (4.4)) the absolute load in Nm can be calculated if the rated load torque is known. The rated load torque is calculated using the following relationship:

$$T_R = \frac{P_R}{\omega_R} \qquad (4.7)$$

where T_R Rated load torque (Nm)
P_R Rated power (W)
ω_R Rated speed (rad/sec)

Having determined the rated load and percentage of rated load, based on the measured data, the estimated load in Nm can be calculated.

4.3.3 Speed estimation based on nameplate data

Using the estimated load calculated using the process from the previous section an estimate of the speed can now be found. The relationship between torque and speed over the entire speed range of an induction motor is highly non-linear however if the motor is operating between maximum (rated) load and no-load the relationship is approximately linear (see Figure 4.7). Over this range if the torque is known then the speed can be estimated by interpolating between the rated values of torque and zero torque and the rated value of speed and the synchronous speed (see equation (4.8)).

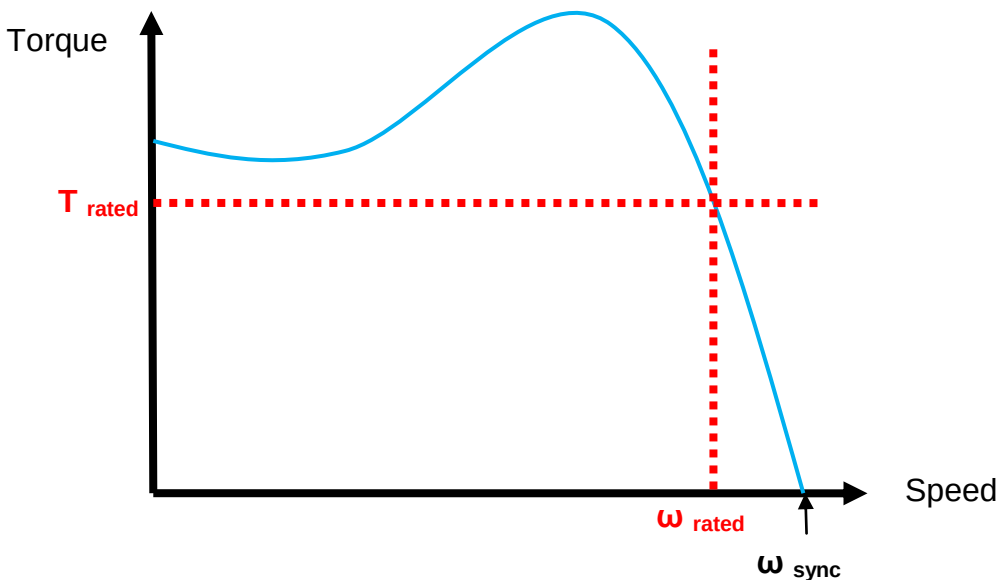

Figure 4.7 A typical induction motor torque vs speed curve

$$\omega_{est} = \omega_{sync} - (\omega_{sync} - \omega_R).\frac{T_{est}}{T_R} \qquad (4.8)$$

where ω_{sync} Induction motor synchronous speed (rpm)

T_{est} Estimated load torque (Nm)

This approximate speed estimate is used to assess the probability that a frequency peak is actually a rotor bar pass frequency in the RBPF speed estimation algorithm.

4.3.4 Bar number estimation results

The results of this bar estimation process are given in Appendix F. Overall, the performance is very good across the dataset with a bar number of 28 being estimated in the vast majority of cases. The algorithm struggles with accuracy when the motor is un-loaded due to the fact that harmonics are either very small or very close to supply harmonics making them almost impossible to detect. This is not an issue for industrial applications since zero loads will not be present and small percentage loads e.g. 0 – 50% will be uncommon.

If the no-load data is included the rotor bar number estimation success rate is 84%. If the no load data is not included then the success rate is 100%. However, even if the number of bars is incorrectly calculated, due to the algorithm design the speed estimate is still accurate (error < 0.21%).

If the no load data is included the average estimated speed error (based on the estimated rotor bar number) is 0.05% (0.78rpm). The maximum error recorded was 0.21% (3.14rpm).

If the no load data is not included the average error drops to 0.04% (0.55rpm), and the maximum error drops to 0.13% (1.96rpm).

4.3.5 Limitations

The rotor bar pass frequency detection algorithm has the following limitations:

- Has only been tested on one size/type of motor
- RBPF cannot be detected at no load
- Algorithm was only tested at no load and >60% of load (needs to be tested at all loading conditions to understand performance)

4.4 Summary

This chapter has assessed the different techniques available for induction motor speed estimation. The algorithms have been applied to the problem of estimating the speed of an induction motor running in steady state.

Using the rotor bar pass frequency was found to provide the most accurate speed estimation, however it required knowledge of the number of rotor bars to be known.

To overcome this problem a rotor bar number estimation algorithm was developed. The algorithm provided excellent performance for the loaded motors with a 100% correct bar number estimation across the test set. However the

algorithm struggled to estimate the number of rotor bars for an unloaded motor. This was not considered a serious flaw since there should never be a situation where a plant is running an unloaded motor.

When the rotor bar number estimation and RBPF speed estimation techniques are combined accurate speed estimation is achieved. Using these techniques resulted in an average speed estimation error of only 0.05% (0.78rpm) and a maximum error of 0.21% (3.14rpm). These results include the no load data. If no only loaded motors are considered then the average error decreases to 0.04% (0.55rpm) and the maximum error decreases to 0.13% (1.96rpm).

This level of accuracy is suitable for steady-state fault detection methods and will be used to improve the accuracy of model parameters, model based fault detection and spectral fault detection techniques.

Chapter 5. Experimental Setup

This chapter describes the experimental setup developed for the project.

5.1 Test rig overview

The test rig was designed in order to allow experiments to be conducted on small to medium sized induction motors. The aim was to provide a system which could control a test motor and a loading motor whilst recording a set of chosen variables. The test rig also needed to be capable of operating with shaft-coupled (flexible bellows coupling) and belt-coupled loads using shaft pulleys. A variable speed drive (VSD) was used for the load motor to allow control over load torque. This piece of research is aimed at fault detection of motors running at steady-state therefore a VSD for the motor under test (driving motor) was not required. The motor under test was run directly off the mains supply, i.e. direct on-line (DOL).

The test rig consisted of the following key components:

1. Three-phase electrical supply
2. Motor controller (for test motor control)
3. Three-phase voltage and current transducers
4. Motor under test
5. Mechanical coupling
6. Load motor
7. Variable Speed Drive (VSD) for load motor control
8. Mechanical structures and fittings
9. PC for data acquisition

The test rig (in direct-coupling configuration) is shown in Figure 5.1.

Figure 5.1 Photograph of the test rig setup

5.2 The test motor

The test motor chosen for this project was the W-DA132MB manufactured by Brook-Crompton Motors. The W-DA132MB is a multipurpose, high-efficiency aluminium motor providing 7.5kW of power at a rated speed of 1445rpm (4-pole). The detailed motor specification is given by Table 5.1.

Table 5.1 Specification of the test motor

Brook-Crompton W-DA132MB	
Rated Power (kW)	7.5
Rated Voltage (V)	415
Connection Type	Delta
Rated Current (A)	15.2
Rated Speed (RPM)	1445
Rated Torque (Nm)	49.6
No. of Poles	4
Rated Power Factor	0.82
Rated Efficiency (%)	87.0

In order for each of the four chosen fault types (stator, rotor, air-gap and bearing) to be tested on separate motors, four identical motors were acquired for use on this project. This type of motor was chosen since it provided a moderate torque and moderate speed which would give a good representation of the type of current and voltage signals that can be obtained from small to medium sized induction motors and it did not exceed the specifications of the test rig.

An overview of the test-rig is shown in Figure 5.2.

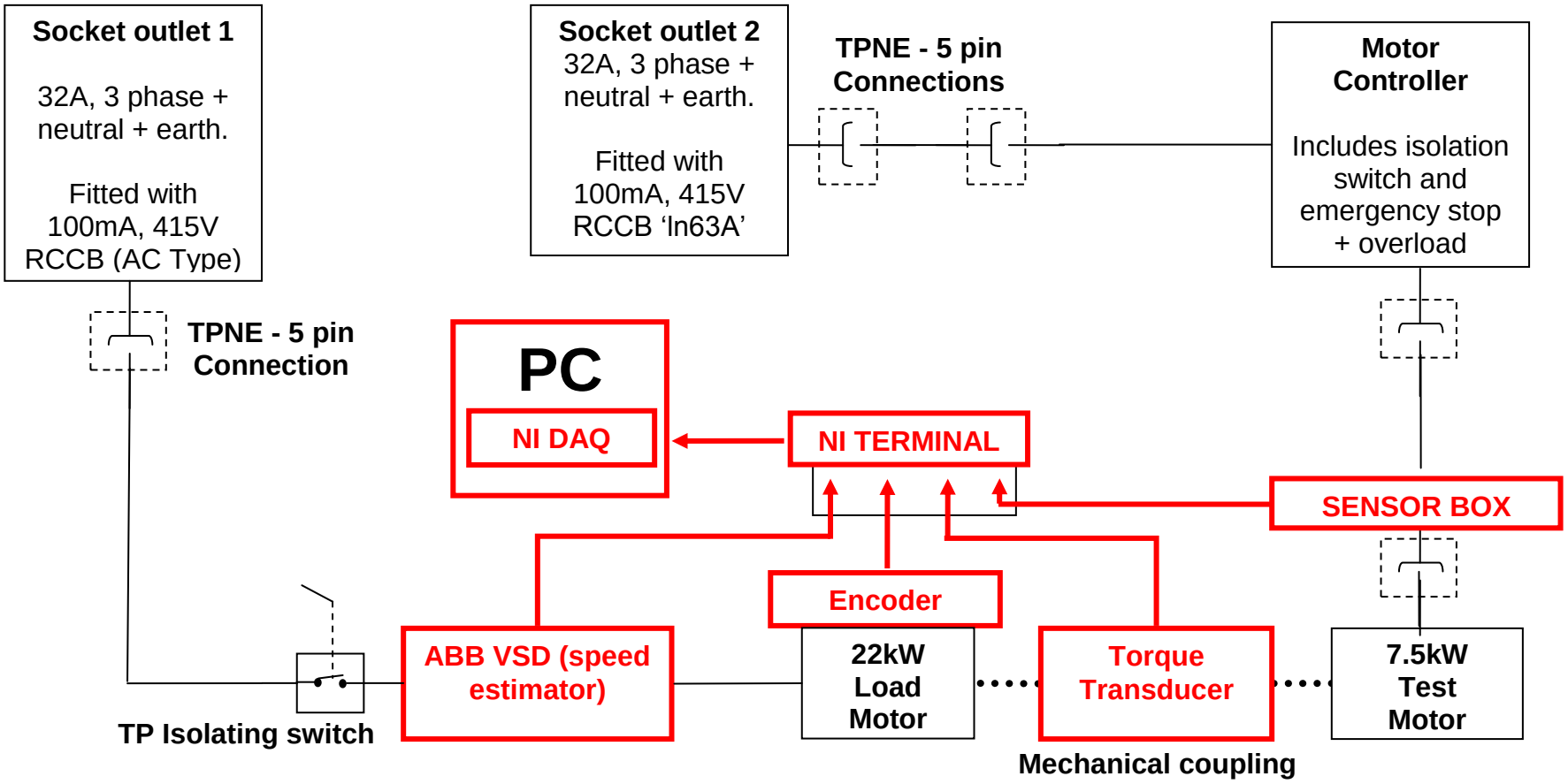

Figure 5.2 Layout of the test rig instrumentation system

Due to limitations in project budget and time-frame motors with different specifications could not be purchased, hence testing was limited to the W-DA132MB motors only.

5.3 Test motor protection and control

The test motor is supplied from a 32A rated supply wall socket. The connections are via 3 phase + earth + neutral (3P+E+N), standard 5 pin, 32A 3 phase plugs. Three-phase cabling connects the supply outlet to the input of the motor protection and control enclosure, shown in Figure 5.3. The output from the enclosure feeds the test motor via a voltage and current measurement box.

The motor protection and control box provides an enclosure to house the motor management device and the switchgear used to isolate the motor. The motor management device provides two functions; control of the motor and protection of the motor. It accepts a 3 phase input and provides a 3 phase output to the motor. The circuit breakers within the enclosure and the motor management software can be configured to protect and control a range of different small-to-medium sized induction motors.

The motor management device used is the ‘Motor Manager 6’, manufactured by Powell Industries.

The protection and control box includes an interlocked isolation switch to prevent access to the enclosure when turned into the ‘ON’ position. In addition to this there is push button emergency stop, on/off key switch and the motor management human machine interface (HMI) for control of the motor and protection functions.

5.4 Motor loading

The motor loading is provided by an ABB ACS800 Variable Speed Drive (VSD) controlling a 22kW ABB induction motor. The VSD (see Figure 5.4) is supplied by a separate three-phase wall outlet and thus provides a feedback path to the supply since the VSD is effectively acting as a generator.

The VSD converts the 3 phase AC currents to DC then back to a modified AC form that will drive the load motor in a specific way. For example, torque or speed can be controlled. For this study the fault detection and diagnosis was aimed at motors running at steady-state, therefore the VSD was operated in torque control mode in order to provide a constant load torque at the motor output shaft. The ABB drive was controlled manually via the front-panel interface.

5.5 Coupling methods

In order to acquire a more representative experimental dataset for different types of coupling methods that may be utilised in industry, tests were carried out with two types of coupling; direct in-line shaft coupling and belt and pulley coupling. The different coupling types can affect the behaviour of the system and introduce different frequency components in the current spectrum. Therefore, it is necessary to test under these different coupling conditions to fully understand the effectiveness of the fault detection and diagnosis algorithms that are developed.

Figure 5.3 The motor protection and control enclosure with 3 phase with three phase cable input and output connected

Figure 5.4 ABB ACS800 variable speed drive (VSD)

The first coupling method is the inline shaft coupling approach using bellows couplings and an inline torque transducer. The bellows couplings are designed to be used specifically with the torque transducer and are rated for torque up to 200Nm and therefore suitable for motors up to 30kW (at rated load). The couplings are of a flexible corrugated metal design and are clamped onto the torque transducer shaft using tightening screws. The opposite end of the bellows couplings are attached to shaft adaptors which are then in turn attached to each of the motor shafts. The adaptors are manufactured with a keyway to fit the specific motor shafts. Both the test and load motor are fitted to a horizontal base-plate and the two shafts are aligned horizontally and vertically. The shaft coupling test rig configuration is depicted in **Error! Reference source not ound.**.

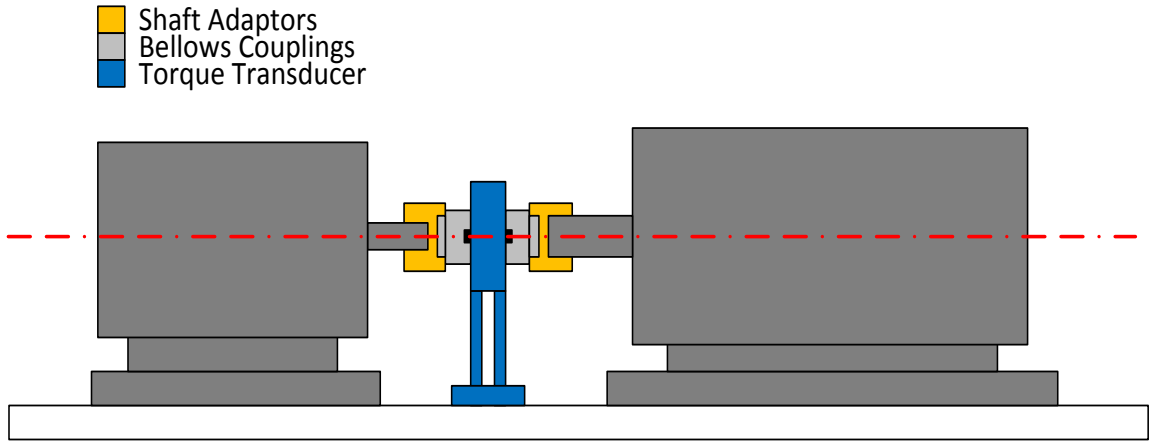

Figure 5.5 Diagram of the direct shaft coupling test rig configuration

The second coupling method is the belt and pulley connection. The load motor is fitted on the base plate and the test motor is bolted to a height-adjustable platform above the load motor. The motor shafts are aligned in the vertical plane and each shaft has a 300mm diameter pulley attached. These pulleys are then linked with a V-belt which is tensioned appropriately by measuring the belt deflection due to a force of known magnitude. Belt tension is modified by either

increasing or decreasing the height of the test motor platform. The belt and pulley test rig configuration is depicted in Figure 5.6.

During the direct shaft coupling stage the torque transducer was continuously compared with the drive torque estimation. The torque estimation performance of the drive was very good with error values of less than 0.1%. In the interests of convenience when the pulley testing was carried out the torque transducer was removed and the VSD torque estimate was used to provide the load torque set point.

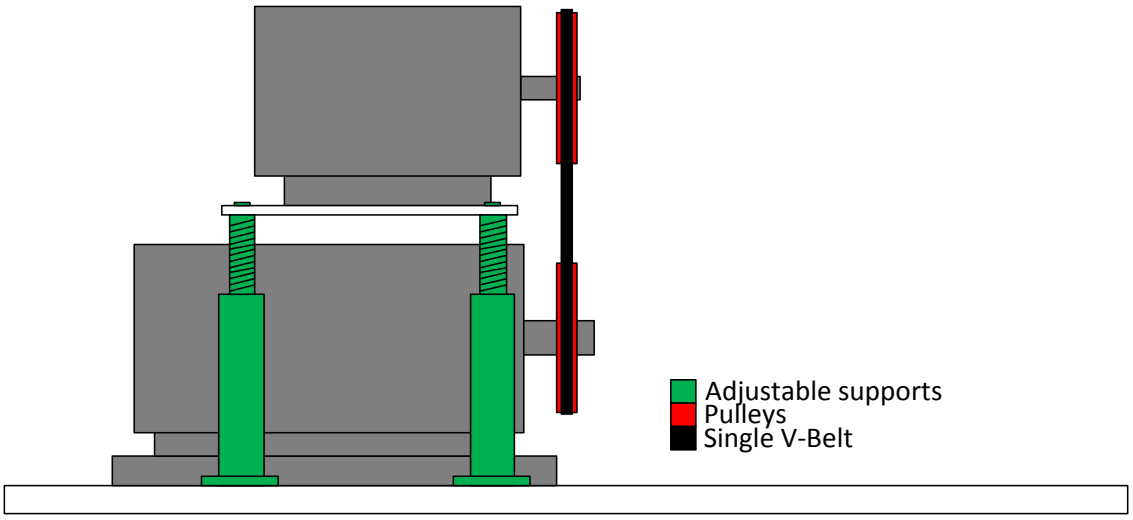

Figure 5.6 Diagram of the belt and pulley coupled test rig configuration

5.6 Instrumentation

The instrumentation system was required to measure the following variables during each data acquisition event:

1. 3 phase motor supply current
2. 3 phase motor supply voltage
3. Shaft speed
4. Load torque

In this application these measurements are made by three different means:

1. S&I Sensor box (voltage and current)
2. British Encoder 755HS shaft Encoder (speed) and laser tachometer (±0.5 RPM accuracy)
3. HBM Torque transducer (load torque)

5.6.1 Voltage & current measurement

The measurement of voltage and current is achieved through the use of a plastic enclosure which includes voltage and current sensors.

The sensor box is fitted between the motor management unit and the motor under test. The 415V power passes directly through the sensor box where the current and voltage transformers produce voltage signals that are proportional to the measured currents and voltages. The sensor box is able to accept 32A and 415V (limited by the socket connectors). The sensor box outputs the measurement signals as voltages in the range ±10V.

5.6.2 Torque measurement

The torque transducer when fitted is located between the motor under test and the load motor. The transducer requires two flexible bellows couplings plus adaptors to allow connection to each of the shafts. The transducer is supported by two threaded rods for alignment purposes connected to the motor base plate.

The transducer is supplied by HBM and measures torques up to 200NM at speeds up to 9000rpm. The connection cable is fitted into the top of the unit and provides 2 functions;

(i) Deliver DC power to the unit

(ii) Produce a voltage signal proportional to the torque being measured

The sensors DC power requirement is 12V and is produced by connecting the input power wires to a controllable stabilised DC power supply. The signal wires output a voltage signal proportional to the measured torque and are connected to the NI DAQ screw terminal unit which in turn supplies measured signals to a measurement PC. The output signals can be currents or voltages, in this case voltages are used – signals are in the range ±5V.

5.6.3 Speed measurement

Speed measurement is measured directly via an encoder fitted to the load motor, measured using a laser tachometer or estimated via the ABB ACS800 drive.

The encoder is fitted to a shaft extension is needed on the non-drive end of the motor. This required removal and modification of the protective vent and extension of the shaft by attaching a spigot into the end of the shaft then a hollow shaft encoder can be fitted onto the spigot. An RTAC-01 module is needed to connect the signal cables into the VSD (via input channels AI1+ and AI1-).

The speed signal output is on the same analogue output channel of the drive, AO1+ and A01-. The output signals are 0 to 20mA, with 0mA being 0rpm motor speed and 20mA being motor nominal speed.

5.6.4 Connection to data acquisition system

Between the NI PXI 6224 card in the measurement PC and the signal cables from the various measurement devices is the NI PXI SCB 68 screw terminal box. The SCB 68 is an I/O connector block with screw terminals for easy connection of signal wires. The unit is connected to the current, voltage, speed and torque outputs of the various sensors. Measurement of up to 32 signals is made possible using this device, enabling additional signals (e.g. accelerometer vibration readings) to be captured if required in the future.

The screw terminal block is then connected directly to the PC to allow analysis and measurement of the signals using National instruments LabVIEW. The DAQ system is described in more detail in the next section.

5.6.5 Data acquisition system

This section will explain the data acquisition aspect of the experimental set-up. The section gives details of the hardware and software required for the project, the integration of these aspects and considerations when using the equipment.

The instrumentation rig will be constructed and data from the sensor box will be described.

The sensor outputs are connected to the National Instruments PXI. PXI 1031 is used with cards PXI 8187 and 6251. The PXI 1031 is a 4 slot chassis which houses the data acquisition cards themselves. The PXI 6251 is a multifunction data acquisition card; it accepts 68-pin cables with up to 24 digital inputs and 16 analogue inputs and is housed within the PXI 1031.

Between the PXI 6251 and the Powell Sensor box is a NI PXI SCB 68. The SCB 68 is a shielded I/O connector block with screw terminals for easy connection of signal wires.

The final part of the NI set-up is the PXI 8187. This is a 2.5GHz 256MB controller which controls the operation of all the NI cards within the 1031 chassis. This controller has USB, Ethernet and GPIB inputs and is loaded with a Windows operating system (XP). The PXI 8187 is connected to the external PC via an Ethernet cable.

The PC allows the user to control the PXI remotely. The LabVIEW programme is created on the PC then uploaded onto the PXI it is then run remotely from the PC. Once the data has been captured it is stored on the PXI hard-drive, the data subsequently needs to be transferred to the PC for analysis. All interactions and data transfer between the PXI and PC are over Ethernet.

The PC is an Intel Pentium 4, 2.80GHz, 512MB RAM with a Windows XP operating system.

The software used to measure and store the signals captured using the sensor box is National Instruments LabVIEW 7. LabVIEW runs on the external PC and PXI. Therefore development can be conducted on the standard PC then the programme is downloaded onto the PXI prior to capturing data.

LabVIEW (Laboratory Virtual Instrumentation Engineering Workbench) is a graphical programming language used for the development of data acquisition, instrument control and automation programmes.

In order to allow the continuous signal to be properly reconstructed in discrete form, the sampling frequency needs to carefully chosen. The criterion for

selecting the sampling frequency is known as the Shannon-Nyquist sampling theorem.

The theorem states that in order for a signal x(t), that contains no frequencies above frequency B, to be completely determined by a number of discrete points, the sampling frequency needs to be at least twice that of the highest frequency in the signal, i.e. 2*B.

In reality a signal does not have a defined cut-off frequency (it is not band-limited) this means that even if the Nyquist criterion is met there will be problems with the reconstruction of the signal. This problem is known as aliasing. In our case a signal is a voltage or current measured from the Powell Sensor Box.

When a signal is reconstructed using sampled data there is a periodic extension of the signal repeating over the frequency spectrum. If the signal is strictly band limited then this is not a problem, but this is not true in reality. This leads to the alias (or repeated elements of the signal) overlapping slightly. This means that any frequency component with a frequency over $f_s/2$ is indiscernible from the lower frequency components.

In order to avoid problems due to aliasing the sampling frequency must be chosen carefully. Since the majority of the current energy is distributed at frequencies well below 2000Hz a sampling rate of 5kHz was selected. In the initial stages of testing the 5kHz data was compared with a heavily oversampled data (20kHz) in order to check for the impact of aliasing. This revealed that over the frequency range of interest (0-2500Hz) aliasing was not a problem.

Chapter 6. Parameter Estimation

This chapter describes the parameter estimation procedure used to determine the basic (healthy) motor model parameters. A review of IM parameter estimation techniques is presented followed by the testing of a variety of algorithms carried out in order to determine the most suitable optimisation algorithm for this type of problem. The selected algorithm is then tested and validated against experimental data.

The AMRA uses accurate parameter estimates to allow adaption to a range of different motor sizes and configurations.

6.1 Problem outline and literature review

In order to simulate and/or control induction motors the parameters of the system need to be known accurately. In some cases the equivalent circuit parameters can be obtained from manufacturers although this information is not usually readily available. An alternative is to perform a set of tests (e.g. no load tests and locked-rotor tests) whilst measuring specific variables, but this requires the motor to be installed on a test-rig with the appropriate instrumentation available. The final option is to use measured data collected from the installed motor to determine the parameters through parameter estimation (also known as system identification) [45]. If the parameter estimation can be done online then this is method of obtaining the system parameters clearly requires the least effort and cost to achieve.

Unfortunately induction motor parameter estimation is a highly complex and challenging task and one which is only effectively possible if a number of

measured variables are available as model inputs, e.g. 3 phase current, 3 phase voltage, load torque, rotational speed, etc. If insufficient measured data is available then the parameter estimates will be of a lower accuracy. This is the first parameter estimation problem with regards to IM.

The second problem with IM parameter estimation is that even if a wealth of measured variables are available to drive the estimation the estimated set of parameters will still not be a unique solution but form one of an infinite number of mathematical solutions. This is due to the fact that the 8 electrical 'primitive' parameters which are used by the basic induction motor models cannot be univocally determined using external measurements (e.g. current, speed, torque) without any other restrictions [118]. This means that if the parameters were estimated twice using a stochastic estimator then two different solutions could be found or if a deterministic estimator was used with different algorithm start vectors then, again, two different solutions would be found.

This would seem to make the parameter identification problem an impossible task. However from a more pragmatic point of view, a unique global solution to the parameter estimation problem is not actually necessary. There are also an infinite number of 'good' solutions which, if motor control is being considered, will provide acceptable performance. A comparison of some different techniques and problem formulations used to identify parameter estimates for induction motor parameter estimation are given in Table 6.1.

Reference	Lead Author	Methods	Known Parameters	Estimated Parameters	Performance Function	Notes
[64]	Ursem	Local search Evolutionary algorithms PSO	Load torque	Rotor resistance Stator resistance *Stator leakage inductance *Rotor leakage inductance Magnetizing inductance Inertia	Current	Uses a simulated reference signal not real data *Lsl and Lsr are said to be linearly dependent so combined into on e parameter
[89]	Karanayil	Neural network	Load torque Stator leakage inductance Rotor leakage inductance Magnetizing inductance Inertia Rotational speed	Stator resistance Rotor resistance	Flux linkage	
[119]	Kim	uDEAS Genetic Algorithm	Rotational Speed	Stator and rotor resistance Stator leakage inductance Rotor leakage inductance Magnetizing inductance Inertia, Friction, Load Torque	Current Rotational Speed	Load torque must be stepped for identification
[120]	Akbaba	Levenberg-Marquardt algorithm	Load torque Rotational speed Stator leakage inductance Stator resistance Core resistance	Rotor resistance Stator leakage inductance Rotor leakage inductance	Torque Power Slip	Explains varying and non-varying parameters e.g. due to non linear magnetization effects
[74]	Bachir	Marquardt algorithm	Speed Stator and rotor resistance Stator leakage inductance Rotor leakage inductance Magnetizing inductance Inertia, Load Torque	Rotor Fault Stator Fault	Current	Requires persistent speed excitation Uses very severe rotor and stator faults
[118]	Corcoles	Levenberg-Marquardt algorithm	Speed Stator resistance Load Torque	Rotor leakage inductance Magnetizing inductance Rotor resistance	Current Speed Torque	Requires a sweep from slip=0 to slip=1
[121]	Moons	Least-squares	Speed Load Torque	Stator and rotor resistance Stator leakage inductance Rotor leakage inductance Magnetizing inductance	Current	
[122]	Zamora	Least-squares	Rotor resistance Rotor leakage inductance Magnetizing inductance	Stator resistance Stator inductance Stator leakage inductance	Current	
[123]	Koubaa	Least-squares		Rotor resistance Rotor leakage inductance Stator leakage inductance		

Table 6.1 Comparison of parameter estimation approaches used for induction motor parameter estimation

Table 6.1 demonstrates techniques which have been successful in identifying induction motor parameters. There are a range of methods which require differing known parameters and measured data to perform estimations and few methods estimate all the required parameters. This is because if the number of known parameters and/or measured variables is small in comparison to the number of estimated parameters then the result will be less accurate parameter estimates.

If an optimisation is carried out using current and voltage as input/outputs and all required parameters are estimated then a repeatable parameter estimate cannot be obtained. There will be some variation in the parameter estimate since there are an infinite number of potential mathematical solutions. This is not a significant problem for fault detection and diagnosis for two reasons; firstly, if the system of optimisers (parameter estimators) are correctly organised the full model optimisation does not occur for fault estimates and only for initial model construction (i.e. fault parameters should not actually be estimated using this procedure), and secondly, since the intention is that the output of the fault detection algorithms will be interpreted by a fuzzy logic system and trended over time, small inaccuracies can be accommodated.

The implementation of the overall optimisation/estimation system will be explained in the next section.

6.2 Parameter estimation implementation

This section explains the system concept and how the optimisation/parameter estimation routines fit within this framework. The basic parameter estimation of the eight induction motor parameters will be referred to as ‘baseline creation’ in the following explanation.

Figure 6.1 depicts the baseline creation stage. Firstly, a maintenance technician or operator inputs the motor nameplate data via the system HMI, this data is then stored. When the motor first runs the data acquisition (DAQ) process captures a 5 second dataset consisting of the motor currents and voltages sampled at 5 kHz. This dataset is then combined with the nameplate information and passed to Optimiser 1 which identifies the healthy motor model parameters via an iterative optimisation process. The basic model's identified parameters are then stored in memory.

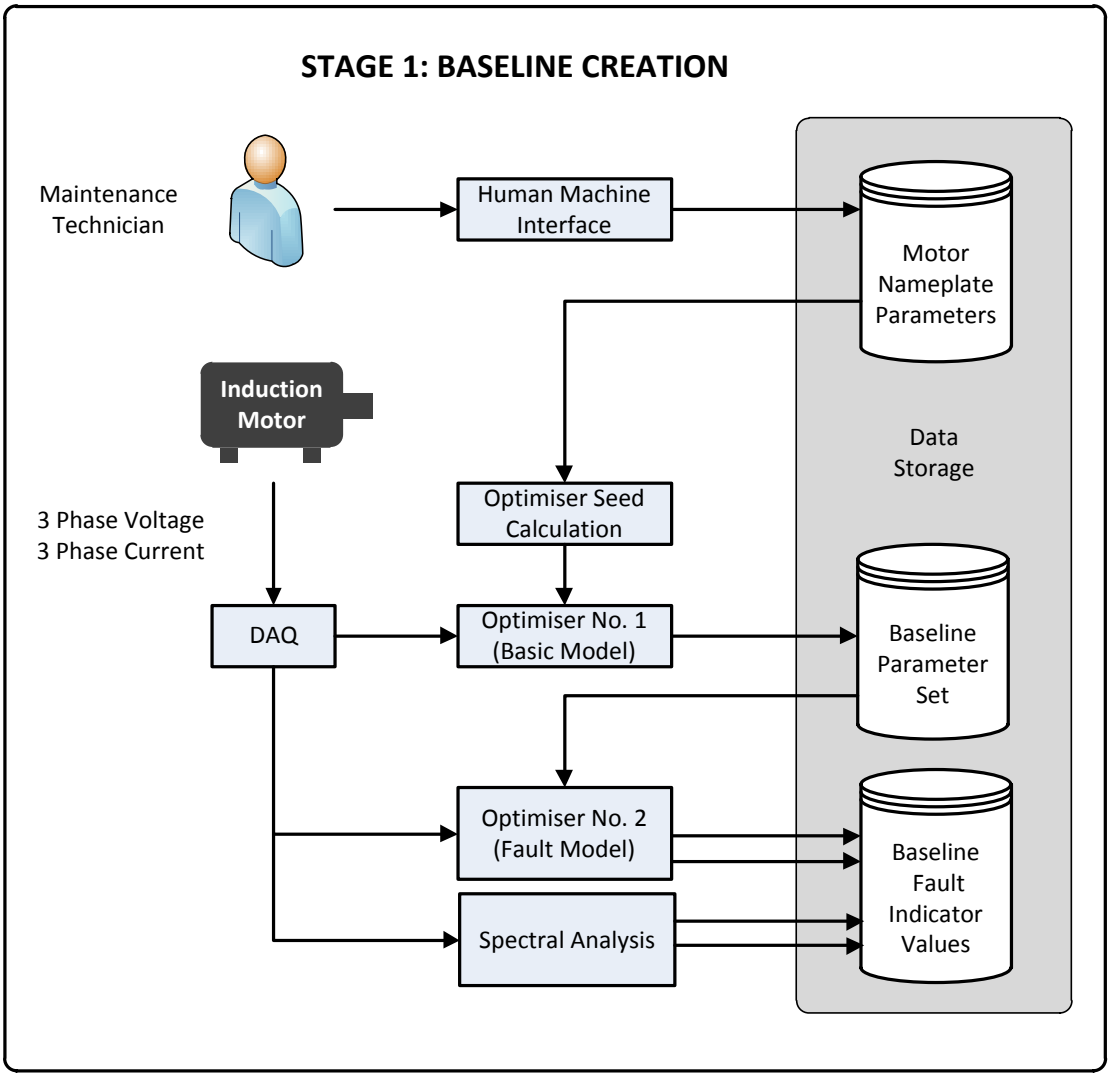

Figure 6.1 An overview of the baseline creation stage

(Note: this means the basic parameters are only estimated *once*. This avoids any problems with the mathematical solutions not being unique since no two

solutions are ever compared. The job of developing the fault residuals (comparisons) is the fault model optimiser (explained below) which uses a deterministic optimiser and a subset of parameters used for fault detection.)

Following this the sampled data is passed with the basic model parameters to the fault model optimiser in order to identify the fault model parameters (a rotor fault parameter and a stator fault parameter). In addition to this the sampled data is passed through the spectral analysis processing. These two subsystems output fault indicator values which are stored in memory and form the motor ‘health baseline’. This is basically a benchmark from which to compare subsequent data captures against.

Figure 6.2 shows the process for the ongoing condition monitoring stage (Stage 2). At each measurement interval (e.g. every 12hrs) the DAQ acquires a data point (5 seconds of 5kHz data). This dataset is then fed to the fault model optimiser and the spectral analyser which calculate the fault indicator values that indicate the condition of the bearings, rotor, stator and air-gap.

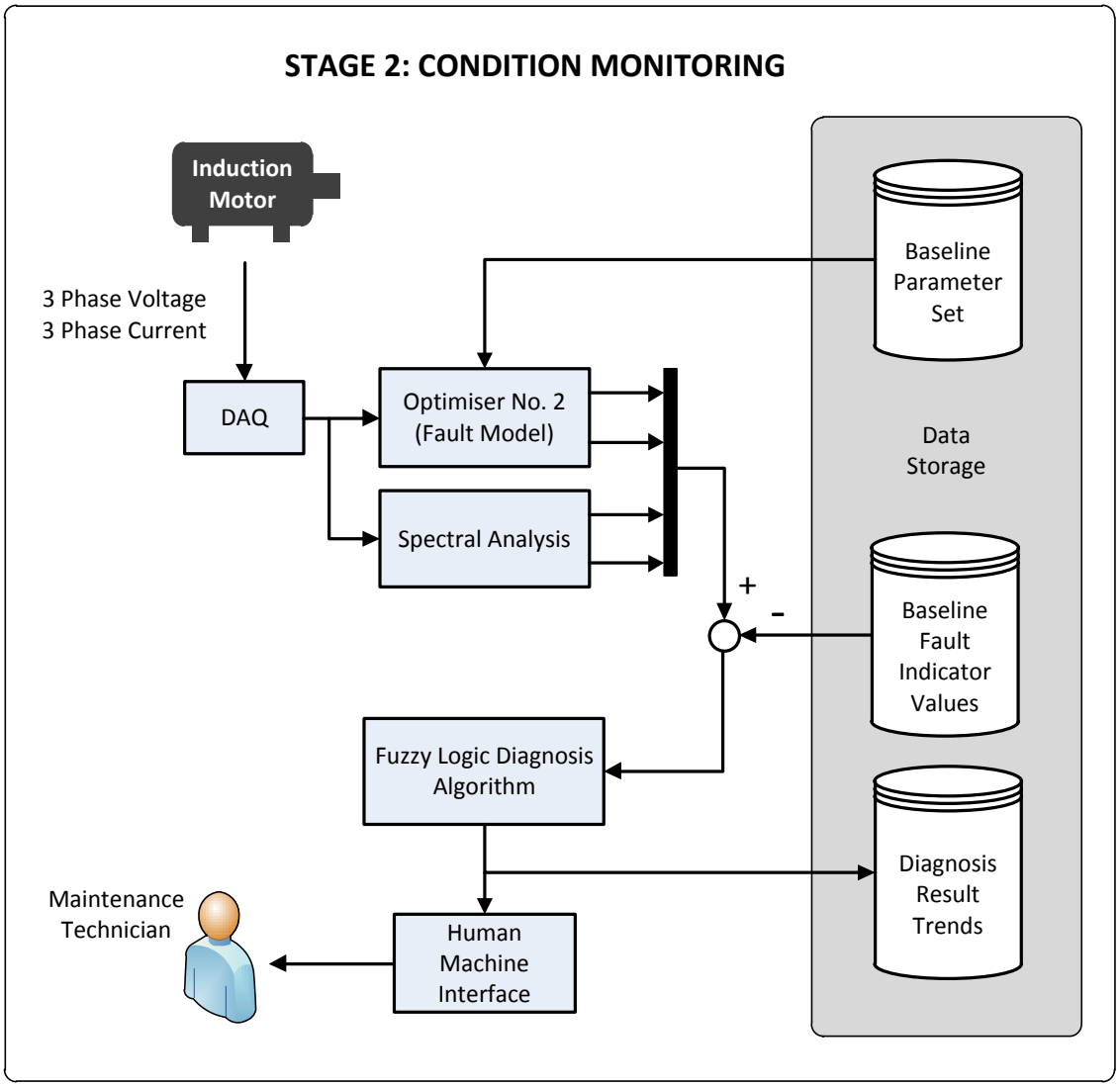

Figure 6.2 An overview of the condition monitoring stage

These fault indicator values are then compared to the values captured for the baseline in order to generate fault residuals. These residuals are fed to the fuzzy logic algorithm which interprets them and provides a diagnosis (a linguistic description plus a numerical value as a measure of damage). The diagnosis data is then fed to the HMI for display to the operator and also stored in order to form a trend over time. The process repeats periodically, e.g. every 12hrs.

The rest of this chapter is devoted to describing the development of ‘Optimiser No. 1’ which performs the estimation of the eight basic model parameters when the system first runs.

Several algorithms were tested in order to determine the most suitable option to be used for the basic model parameter estimation. The optimisation algorithms selected fall into one of three categories:

1. Local Search (LS) Algorithms
2. Evolution Strategies (ES)
3. Particle Swarm Optimisation (PSO)

Descriptions of the algorithms and the testing results are given in subsequent sections.

6.3 Algorithm initialisation

The optimisation routines used for parameter estimation require an initial estimate as a starting point of the optimisation when the direct search methods are used and the stochastic optimisers used in this project use this initial estimate to seed the initial population.

The actual search for the parameter is done by the optimisation routine; this is not the job of the initialisation routine. However, more accurate initial estimates will help focus the search of the optimisation routine towards likely solutions. Manufacturers can provide equivalent circuit parameters but the plant personnel may not have access to this information, therefore a system of deriving a suitable initial guess, based on nameplate data, is developed here.

The process used to calculate the estimates for this system involves using fundamental motor theory with certain simplifying assumptions. The only

information required for the initial estimate calculations is data that is included on every motor nameplate (and therefore freely available):

1. Supply voltage
2. Supply frequency
3. Rated speed
4. Rated power
5. Rated current

Since the motor rated full load power is known this is used as a starting point for the initialisation estimate. When considering the motor equivalent circuit the rotor resistance is commonly rewritten as two separate terms [5]:

$$\frac{\mathrm{R_R}}{\mathrm{s}} = \mathrm{R_R} + \frac{\mathrm{R_R}(1-\mathrm{s})}{\mathrm{s}} \tag{6.1}$$

where $\frac{R_R}{s}$ is the motor output equivalent resistance seen by the stator, R_R is the resistance related to the ohmic losses (actual resistance) of the rotor and $\frac{R_R(1-s)}{s}$ is the resistance equivalent to the mechanical load on the motor.

The rotor resistance, R_R, can therefore be estimated by considering the output power:

$$\mathrm{P_{mech}} = \frac{\mathrm{I_R^2 R_R}(1-\mathrm{s})}{\mathrm{s}} \tag{6.2}$$

where I_2 is the rotor current and P_{mech} is the output power of the motor per phase. The rotor current can be re-written in terms of supply voltage as follows:

$$\mathrm{P_{mech}} = \frac{\left(\frac{\mathrm{V_s}}{\mathrm{Z_{fl}}}\right)^2 \mathrm{R_R}(1-\mathrm{s})}{\mathrm{s}} \tag{6.3}$$

Considering the fact that under normal operating regimes (i.e. the motor has a significant load) the dominant part of the electrical load is the rotor resistance (i.e. useful power generation) so that:

$$\mathrm{Z_{fl}} = \frac{\mathrm{R_R}}{\mathrm{s}} \tag{6.4}$$

Substituting the above into equation (6.3) yields:

$$\mathrm{P_{mech}} = \frac{\mathrm{V_s^2 s(1-s)}}{\mathrm{R_R}} \tag{6.5}$$

When the motor operates in conditions where the load torque does not exceed the rated load torque, slip is very small (i.e. typically < 0.05) which allows the simplification: $(1 - s) \approx 1$. This results in an expression for the total power on all 3 phases:

$$\mathrm{P_{mech}} \approx \frac{\mathrm{3V_s^2 s}}{\mathrm{R_R}} \tag{6.6}$$

Rearranging yields an expression for the estimate of rotor resistance, R_2:

$$\mathrm{R_R} \approx \mathrm{3V_s^2 s/P_{mech}} \tag{6.7}$$

where P_{mech} is the motors full load rated power and V_s is the motor's rated supply voltage.

The initial estimate for the leakage reactances is found by considering the locked rotor current (LRC) of the induction motor. The LRC flows when the rotor is stationary i.e. slip is equal to 1.

Since there is no simple relationship for determining $\mathrm{R_s}$ the following assumption is made:

$$\mathrm{R_s} \approx \mathrm{R_R} = \mathrm{R} \tag{6.8}$$

This assumption is based on the fact that for larger motors both stator and rotor resistances will be small and for smaller motors both stator and rotor resistances will be large. Hence, for a range of induction motors the resistance values can be seen as *approximately* equal.

If the rotor is prevented from rotating then the locked rotor current (LRC) will flow. In this case only a small current flow occurs in the main flux circuit so the exciting current branch can be removed from the equivalent circuit. This leads to the relationship for the LRC which is given by:

$$\mathrm{LRC} = \frac{\mathrm{V_s}}{\sqrt{(\mathrm{X_1} + \mathrm{X_2})^2 + (\mathrm{R_s} + \mathrm{R_r})^2}} \tag{6.9}$$

Then using the commonly used simplification $X_1 \approx X_2 = \mathrm{X}$ (which results only in small errors being introduced [124]) and considering previous assumptions (6.8) the LRC equation can be simplified:

$$\mathrm{LRC} = \frac{\mathrm{V_s}}{\sqrt{4(\mathrm{X})^2 + 4(\mathrm{R})^2}} \tag{6.10}$$

Solving this equation for reactance results in:

$$\mathrm{X_1} \approx \mathrm{X_2} = \mathrm{X} = \sqrt{\frac{\frac{1}{4}\mathrm{V_s^2}}{\mathrm{LRC}^2} - \mathrm{R}^2} \tag{6.11}$$

The LRC of an induction motor is typically 4-8 times the full load rated current of the motor [125]. In order to minimise the possibility of the root becoming negative (due to previous assumptions) the LRC multiplier will be chosen at the lower end of this range i.e. 4 times full load rated current. If the LRC is considered to be 4 times the full load current (FLC) then LRC can be eliminated from equation (6.11), which yields:

$$X_1 \approx X_2 = X = \sqrt{\frac{\frac{1}{4}V_s^2}{(4FLC)^2} - R^2} \tag{6.12}$$

The magnetizing reactance initial estimate requires the following assumptions:

1. All of the reactive power at full load is consumed in the magnetizing reactance (i.e. neglect leakage reactances which are small in comparison to magnetizing reactances).
2. All real power at full load is consumed by R_2/s (i.e. neglect stator losses and other losses).

This results in a two branch equivalent circuit of magnetizing reactance and rotor resistance terms. Since power factor is given by the true power divided by the apparent power:

$$PF = \frac{P}{S} = \frac{I^2R}{I_2Z} = \frac{R}{Z} \tag{6.13}$$

If the appropriate terms are substituted the following equation is obtained:

$$PF = \frac{\left(\frac{R_R}{s}\right)}{\sqrt{\left(\frac{R_R}{s}\right)^2 + X_m^2}} \tag{6.14}$$

Rearranging allows X_m to be obtained:

$$X_m = \sqrt{\left(\frac{R_R}{s}\right)^2 . \left(\frac{1}{PF^2} - 1\right)} \tag{6.15}$$

Then using a typical PF value of 0.8, an approximation of magnetizing inductance can be obtained.

Finally a relationship for calculation of the combined inertia of motor and load is difficult since the as far as the system is concerned the characteristics of the

load are unknown. However, if the motor inertia is considered to be 25% of the total combined inertia of motor and load then an estimation of combined inertia can be made based on typical motor inertia values found in manufacturer catalogues. Considering typical manufacturer data values a simple approximate relationship between combined inertia and motor rated power can be obtained. The calculation for the initial estimate of combined inertia of motor and equivalent load is as follows:

$$J_{eq} = \frac{(P_R)^2}{1000} \tag{6.16}$$

The units of combined inertia and rated power are [kg.m^2] and [kW] respectively.

This completes the calculation of the parameter estimation algorithm starting values. These calculations do not give the result of the parameter estimation stage; they simply provide an *approximate* starting point for the estimation algorithms. It is for these reasons that the extensive simplifications and assumptions can be made.

The importance of these calculations is that they only require full load current, supply voltage, power and full load speed all of which are all available from the motor nameplate.

6.4 Structure of the parameter estimation routine

The basic structure of the basic (healthy) model parameter estimation routine is shown in Figure 6.3.

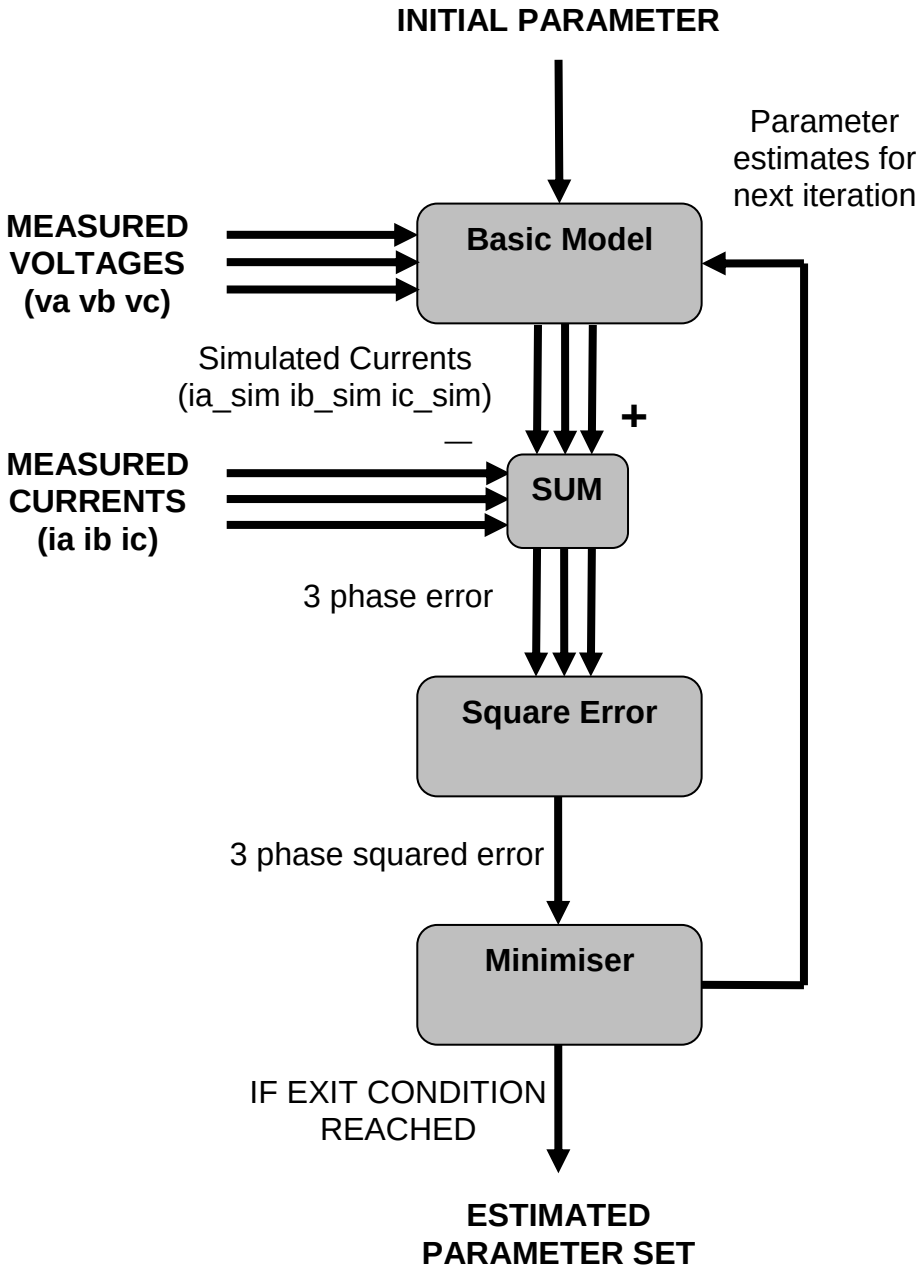

Figure 6.3 An overview of the optimiser structure used for estimation of parameters for the basic motor model

The system captures a segment of measured data then uses the model to simulate the system over the same time period. The model is supplied with the measured voltage as an input and it outputs simulated currents.

The difference between each of the simulated and measured currents is calculated at each time step, squared then added together to give a total squared error. To minimise the error values, the model parameters are varied which in turn modifies the simulated currents to create a better representation of the measured currents.

The current square error objective function is modified by a speed penalty function. This means that if the model running speed is significantly different to the estimated running speed the objective function output increases significantly which drives the optimisation towards a set of parameters which result in accurate simulation of current and accurate simulation of rotational shaft speed.

The speed penalty function is constructed as follows:

$$\mathrm{e_s} = \mathrm{w_1}\left(\omega_\mathrm{r}^{\mathrm{model}} - \omega_\mathrm{r}^{\mathrm{est}}\right)^2 \tag{6.17}$$

where:

e_s	Speed error penalty function modifier
w_1	Speed penalty function weight
ω_r^{model}	Model shaft speed output
ω_r^{est}	Estimated shaft speed (via RBPF estimation algorithm)

This speed error penalty function modifier is then added to the current signal error to provide the overall error objective function which drives the PSO. This results in a multi-objective optimisation (speed and current). The value of $\mathrm{w_1}$ is set to 20 based on optimisation trials.

The algorithm exit conditions are triggered after a certain number of iterations or a certain time limit is exceeded. The optimisation routine can also exit if certain accuracy is reached, i.e. the objective function drops below some predefined value. When this occurs the parameter estimation routine is complete and a

vector, x, and a function value, f, is outputted containing the parameters that best minimise the objective function and the value of the objective function respectively.

6.5 Optimisation algorithms

This section will give a brief description of each of the algorithms which were included in the comparison of optimisation algorithms, and provide the pseudo code which describes each individual algorithm.

6.5.1 Nelder-Mead (NM)

The Nelder-Mead (NM) algorithm is an optimiser which does not require the calculation of function derivatives. This simplifies the construction of the problem and also makes the optimiser more robust to measurement noise. This algorithm is popular for multidimensional problems and forms part of the class of direct (local) search methods. It is based around the concept of changing the shape of a simplex and calculating the function values using the parameters defined by the corners (vertices) of the simplex [126].

The shape of the simplex is modified using a variety of different operators (reflection, expansion, contraction), this transformation results in new positions of each of the vertices. The function value is then recalculated using these new vertices (parameter values).

```
Initialize simplex
        while (not(termination condition)) {
                Calculate function values at each of the simplex vertices
                Transform worst vertex
                Apply termination test
        }
End
```

Figure 6.4 Nelder-Mead algorithm pseudo code

6.5.2 Random-Walk (RW)

Random Walk (RW) is another non-gradient (derivative-free) local search method. A search direction is selected randomly for each iteration of the algorithm.

The algorithm determines the search direction randomly using a random number generator through MATLAB. Once the search direction, S, has been determined the Golden Section algorithm is used to determine the size of the step with which to move in the search direction. The step size chosen is the one which produces the minimum function value. The Golden Section algorithm is a simple technique used to find the minimum value of a function by varying a single parameter and successfully narrowing the range within which the minum exists [127].

If the function value cannot be decreased in the chosen search direction, the step is null and the parameters return to their old values. However if the search direction decreases the function value then the parameters are updated to the new ones.

```
Calculate function value using initial estimate
while (not(termination condition)) {
        Generate random search direction, S
        Determine step size, a
        Xn+1 = Xn + S*a
        If f(Xn+1) < f(Xn)
                set current parameter as Xn+1
        else
                reject Xn+1 and revert to Xn
        Apply termination test
        }
end
```

Figure 6.5 Random Walk algorithm pseudo code

6.5.3 Pattern Search (PS)

The Pattern Search (PS) is a local search method which uses a unit vector to create univariate steps which modify the parameters independently. This provides the search direction and then the Golden Section method is used to find the best step size in this chosen direction to minimise the function. After each of the parameters has been varied independently the final step in each cycle combines the univariate steps into a multivariate step where all parameters are varied at the same time. This prevents the algorithm from zigzagging to the solution.

```
Calculate function value using initial estimate
while(not(termination condition)) {
        for number of variables, n {
                search direction = unidirectional step in n
                Determine step size, a
                Xn+1 = Xn + S*a
                If f(Xn+1) < f(Xn)
                        set current parameter as Xn+1
                else
                        reject Xn+1 and revert to Xn
        }
        search direction = multidirectional combination
        Determine step size, a
        Xn+1 = Xn + S*a
        If f(Xn+1) < f(Xn)
                set current parameter as Xn+1
        else
                reject Xn+1 and revert to Xn
Apply termination test
}
end
```

Figure 6.6 Pattern Search algorithm pseudo code

6.5.4 Simulated Annealing (SA)

Simulated Annealing (SA) is an extension to the RW search method. In a similar fashion to RW the SA algorithm involves generating a random search direction and then determining the correct step length in this direction to minimise the function. However, on certain iterations the algorithm is allowed to accept

inferior solutions. In principal, this allows the algorithm to escape from local minima and hopefully proceed to the global minimum.

The probability of the algorithm permitting a function increase is related to the algorithm temperature. The temperature decreases as time goes by, so that after each iteration the algorithm is less likely to accept an inferior solution.

```
Calculate function value using initial estimate
while(not(termination condition)) {
        Generate random search direction, S
        Determine step size, a
        Xn+1 = Xn + S*a
        If f(Xn+1) < f(Xn) {
                p = 1
        else
                p = exp(-B*delta(f))
        }
        if random[0,1] < p {
                accept change
        else
                reject change
        }
        Apply termination test
}
end
```

Figure 6.7 The Simulated Annealing algorithm pseudo code

6.5.5 (μ, λ) Evolution Strategy (ES)

Evolution Strategies (ES) are based on the principle of survival of the fittest. A detailed introduction to the ES strategies used as part of this project can be found in [128]. These algorithms generate a 'population' of solutions randomly (in this case randomly centred on an initial seed). From this population the best (lowest function values) parents are chosen, the number of parents chosen is μ. Then these parents are paired up at random to generate more potential solutions (known as child solutions). These child solutions share a combination of the properties from their parents. A set number of children, λ, are generated.

From this population of children the best solutions are chosen to become the parents of the subsequent generation.

```
Generate initial population of solutions
while(not(termination condition)) {
        for number of children, λ {
                Select 2 parents randomly
                Perform recombination to generate child
                Perform mutation on child
                Check constraints satisfaction
        }
Select the best μ solutions out of the λ children
Set as parents for the next generation
Apply termination test
        }
end
```

Figure 6.8 (μ,λ) Evolution Strategy

6.5.6 (μ+λ) Evolution Strategy (ES)

The (μ+λ) ES is similar to the (μ, λ) ES but the solutions that are promoted through to the next generation can be either children *or* parents from the previous generation. This allows good solutions to be passed from one generation to the next.

```
Generate initial population of solutions
while(not(termination condition)) {
        for number of children, λ {
                Select 2 parents randomly
                Perform recombination to generate child
                Perform mutation on child
                Check constraints satisfaction
        }
Select the best μ solutions out of the λ children AND the μ parents
Set as parents for the next generation
Apply termination test
}
end
```

Figure 6.9 (μ+λ) Evolution Strategy

6.5.7 Adaptive ES

The two types of evolution strategies can be modified into adaptive ES. Adaptive ES function in a similar way to the standard ES but the strength of the

mutation operator is included as a characteristic of each individual [64]. This means that individuals with the optimum mutation strength survive and pass the optimum mutation strength on to the individuals in subsequent generations. This keeps the level of mutation at the optimum level throughout the length of the optimisation process. The two adaptive algorithms are; Adaptive (μ+λ)-ES and Adaptive (μ, λ)-ES.

6.5.8 Particle Swarm Optimisation (PSO)

The Particle Swarm Optimisation (PSO) is based around the concept of a 'swarm' of possible solutions exploring the search space by sharing information with other solutions in the swarm [16,17].

Each particle in the swarm represents a solution to the problem. A particle changes its parameters by moving around the solution search space; this movement is driven by the particle's velocity. Each of the particles is attracted to its own best solution and the global best solution – these factors dictate the particles velocity for the next iteration. The swarm tends to converge on a solution as the iterations continue. An overview of the PSO process is given in Figure 6.10.

```
Generate initial population of solutions (positions)
Set velocity to zero for each particle
while(not(termination condition)) {
        for number of particles {
                Update velocity
                Update Position
                Update local best position
        }
Store global best position
Apply termination test
}
end
```

Figure 6.10 PSO algorithm pseudo code

6.6 Algorithm control parameters

The following table contains a list of all the control parameters used to configure each of the algorithms used in the parameter estimation tests. These control parameters are used to adjust the way the algorithms operate. The setting of these parameters is problem specific i.e. settings that provide acceptable performance for one problem will not be suited to a different problem. It is for these reasons that the parameters need to be tailored to the specific problem and this is achieved by testing different parameters using trial and error to find adequate control parameters.

As only a limited amount of time was available for this study into parameter estimation, there is no guarantee that these are the optimum control parameters for this problem but they have been chosen since they resulted in the best solutions for each of the particular algorithms.

Table 6.2 Algorithm control parameters

Algorithm Name	Parameter Description	Parameter	Value
Nelder-Mead	Simplex reflection parameter	ρ	1
	Simplex contraction parameter	χ	2
	Simplex expansion parameter	ψ	0.5
	Simplex shrinkage parameter	σ	0.5
Random Walk Pattern Search	Golden Section tolerance	β	0.001
	Initial step size	α_0	0
	Step size increment	α	0.1
	Number of step size trials allowed	n	10
Simulated Annealing	Golden Section tolerance	β	0.001
	Initial step size	α_0	0
	Step size increment	α	0.1
	Number of step size trials allowed	n	10
	Start Temperature	T_{MAX}	1
	End Temperature	T_{MIN}	0
(μ+λ) - Evolution Strategy	Number of parents	μ	100
	Number of children	λ	15
	Design variable range multiplier	r	0.3
(μ+λ) - Evolution Strategy	Number of parents	μ	15
	Number of children	λ	100
	Design variable range multiplier	r	0.3
Particle Swarm Optimisation	Population	P	30
	Personal Weight	C_1	2
	Global Weight	C_2	2
	Initial Inertia	ω_{MAX}	0.7
	Final Inertia	ω_{MIN}	0.3
	Maximum Velocity	v_{MAX}	±0.15
	Design variable range multiplier	r	0.3

6.7 MATLAB implementation

The system is implemented in MATLAB using three M-files:

1. **RunModel.m** provides the code for running the basic Simulink model with a defined set of parameters (chosen by the optimisation algorithm being tested). This m-file is based around the use of the ‘sim’ command which is used to call the Simulink model from within an M-File. **RunModel.m** also loads the measured data (3 voltages and 3 currents) from a .mat file.

2. **ObjectiveFunction.m** calls the **RunModel.m** file. It calculates the total squared error between measured and simulated currents and returns this value. The optimisation routines call **ObjectiveFunction.m** in order to ascertain the potential of a particular parameter set.
3. **Initialise.m** is called from the **RunModel.m** function and it is used to carry out the initial estimate procedure; using basic nameplate to calculate all the parameters required for simulation of the model.

6.8 Optimisation algorithm testing

The algorithms are compared by performing parameter estimations using the 7.5kW Brook-Crompton test motors running at rated load (50Nm). The parameters to be estimated are stator resistance, rotor resistance, magnetising inductance, stator leakage inductance, rotor leakage inductance, combined inertia and load torque; a total of seven parameters.

The motor was run at full rated load for 60 minutes in order to allow standard operating temperature to be reached. During this time the current drawn and operational speed of the motor varies as the electrical characteristics of the machine (temperature dependent) approach their steady-state value. 60 minutes was chosen as the warm-up duration due to observations during initial tests which indicate by this point the motor output has stabilised.

Following the warm-up period, a 5 second (5kHz) measurement (voltages and currents) is taken. The parameter estimation routine utilises a 1 second sub-set of this data. This provides the error minimisation algorithm with 50 cycles of each of the 3 phases to perform the optimisation. It is assumed that the waveforms are recorded in steady-state (in accordance with the problem statement) since this allows model simulation to be limited for a short time span.

This is important as the simulation of the model is the most time intensive part of the parameter estimation process; by minimising the computational effort required for each function evaluation the time required to perform the parameter estimation is minimised.

The initial parameter estimates are calculated as described in section 6.3. The initial parameter estimates are used for the starting point of the direct search routine and are also used to define the seed for the stochastic (PSO and ES) algorithms. The seed defines the centre point of the initial population distribution.

The motor parameters values used for the direct search start point and the stochastic algorithm solution seed is shown in Table 6.3.

Table 6.3 Values for each of the parameters used to initialise the optimisation algorithm

Parameter Name	Parameter	Value
Full Load Speed	N_{RATED}	1445 rpm
Full Load Current	I_{RATED}	15.2 A
Supply Voltage	V_{RATED}	415 V
Rated Power	P_{RATED}	7.5 kW
Stator Resistance	R_S	2.53 Ω
Rotor Resistance	R_R	2.53 Ω
Stator Reactance	X_{LS}	3.17 Ω
Rotor Reactance	X_{LR}	3.17 Ω
Mutual Reactance	X_M	51.67 Ω
Combined Inertia	J	0.056 kg.m^2

6.8.1 Algorithm selection

This section provides the results gathered after performing parameter estimations using the different optimisation algorithms over time periods of 30 minutes and 60 minutes. The experimental data used for these comparisons was recorded at full load with motor M1 in direct coupled configuration.

Algorithms that achieve low function values (i.e. low error) have found more suitable model parameter sets. The function value is the squared error between the samples over the period of simulation. The overall function value results are presented in graphical form in Figure 6.11 and the numerical values and parameters for the 30 minute estimation and the 60 minute estimation are presented in Table 6.4 and Table 6.5 respectively.

Each of the algorithms improves when the algorithm run time is increased from 30 minutes to 60 minutes. This is expected as the algorithm has twice as long to search for optimal parameters and therefore the parameter estimates are more refined. However, the Simulated Annealing (SA) algorithm finds a poorer solution when given 60 minutes. This is thought to be due to difficulties in setting of the algorithm control parameters for the SA algorithm such as the algorithm temperature parameter.

The most notable result is a clear difference in performance between the local search and stochastic algorithms. The local search algorithms (other than SA) can only proceed ‘downhill’ from their current position and is thus funnelled into one solution and not allowed to explore many solutions. Each of the stochastic algorithms out performs the local search algorithms, this is due to their ability to search in a variety of different positions (the ‘population’ consists of multiple solutions) within the search space. This means the stochastic algorithms find better solutions by not being trapped in local minima.

Out of the stochastic search methods the PSO algorithm performs the best; finding minimum function value of 2513 and 2503 for the 30 minute and 60 minute tests respectively. Over 60 minutes all the other stochastic algorithms

provide similar performance, finding values between 3680 and 4020. None of the local search algorithms reached a function value under 5000.

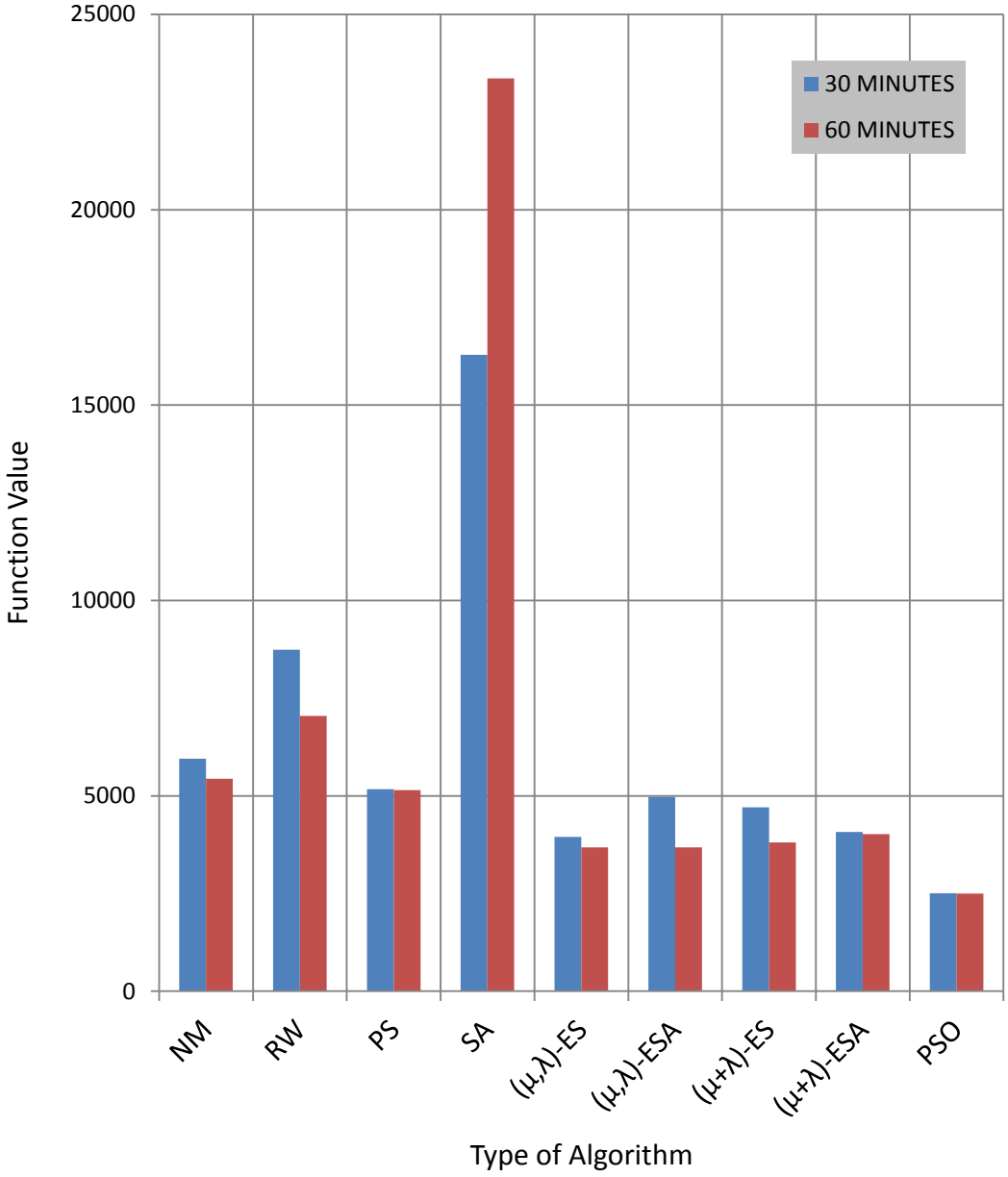

Figure 6.11 Comparison of the minimum function values obtained by the selected optimisation alagorithms

Table 6.4 Algorithm performance over 30 minutes

Type	*Fval*	R_S	R_R	X_{LS}	X_{LR}	X_M	J	T_L
PSO	***2513***	5.846	3.675	6.1	11.205	71.36	0.015	48.91
(μ,λ)-ES	***3948***	6.031	5.156	4.481	3.03	72.338	0.073	48.91
(μ+λ)-ESA	***4078***	3.851	2.792	3.72	4.357	72.99	0.083	48.91
(μ+λ)-ES	***4709***	2.884	4.096	4.726	2.848	72.346	0.128	48.91
(μ,λ)-ESA	***4973***	4.676	4.974	3.74	3.121	74.147	0.042	48.91
PS	***5169***	5.046	6.427	5.466	11.724	72.207	0.018	48.91
NM	***5954***	7.237	4.335	0.713	16.816	76.691	0.022	48.91
RW	***8739***	4.676	4.974	3.74	3.121	74.147	0.042	48.91
SA	***16286***	2.969	2.059	1.677	3.39	75.64	0.095	48.91

Table 6.5 Algorithm performance over 60 minutes

Type	*Fval*	R_S	R_R	X_{LS}	X_{LR}	X_M	J	T_L
PSO	***2503***	5.573	3.284	6.49	9.514	71.022	0.007	48.91
(μ,λ)-ESA	***3680***	3.948	4.528	3.72	4.944	73.598	0.06	48.91
(μ,λ)-ES	***3685***	2.997	3.298	6.877	2.16	70.922	0.058	48.91
(μ+λ)-ES	***3805***	5.073	2.73	4.197	4	74.285	0.04	48.91
(μ+λ)-ESA	***4020***	3.371	2.216	4.328	3.838	73.627	0.114	48.91
PS	***5145***	6.212	8.176	5.169	15.692	72.116	0.02	48.91
NM	***5442***	4.714	4.068	0.486	17.543	77.093	0.016	48.91
RW	***7045***	3.19	4.372	6.484	2.503	71.484	0.059	48.91
SA	***23365***	2.046	1.229	4.154	0.602	75.557	0.063	48.91

By observing the parameter sets each of the algorithms has determined it is apparent that there is some correlation between values determined by each of the algorithms, but there is no clear parameter set that is being produced regularly. This is expected since the local search algorithms will be trapped by local minima and the global search (stochastic) methods will locate one of many ‘good’ solutions to the problem (no unique solution exists – discussed in section 6.1). In addition to this the variation in function value will mean that some of the parameter sets found will be of a lesser accuracy than others.

Providing the error between measured and simulated currents is small these parameter discrepancies are not a significant issue. Since the same parameter sets are used for both baseline and fault case analyses, variations in initial parameter estimates will only affect the *sensitivity* of the rotor and stator fault detection indicators. This only becomes an issue if the repeatability of the

parameter estimation is poor since the sensitivity of the fault indicators will vary significantly and this could lead to the fuzzy logic system misclassifying data. The repeatability of parameter estimates will be considered later in this chapter.

Since the PSO algorithm produced the lowest function value (simulated vs. measured current error) it is chosen as the optimiser for the basic model parameter estimation process. The following section describes the performance of the PSO algorithm in estimating parameters for different motors and different loading conditions.

6.8.2 PSO parameter estimation analysis

The following plots describe the performance of the PSO driven parameter estimation process of the basic induction motor model. The optimisation process is tested on each of the four test motors, under belt coupled and direct coupled loads and also under a variety of load torques. The results are presented with the aim of demonstrating the robustness and flexibility of the parameter estimation process.

Figure 6.12 shows the modelled and experimental line currents using an estimated parameter set of motor M1 directly coupled and supplying its rated loaded torque. There is good agreement between modelled and measured data with only small discrepancies close to the maximum and minimum points of the waveforms.

These errors are due to the fact that the basic model does not take into account the stator winding layout or the detailed construction of the rotor (i.e. location of the individual rotor bars). This theory can be validated by considering the frequency domain comparison of these waveforms (Figure 6.13). The spectrum indicates that supply harmonics are fairly well represented but there are several

frequency components (mainly rotor bar pass frequencies) which are not present in the spectrum for the modelled line current. This is not a serious issue since these frequency components are not required for the model based stator or rotor fault detection methods utilised in this project.

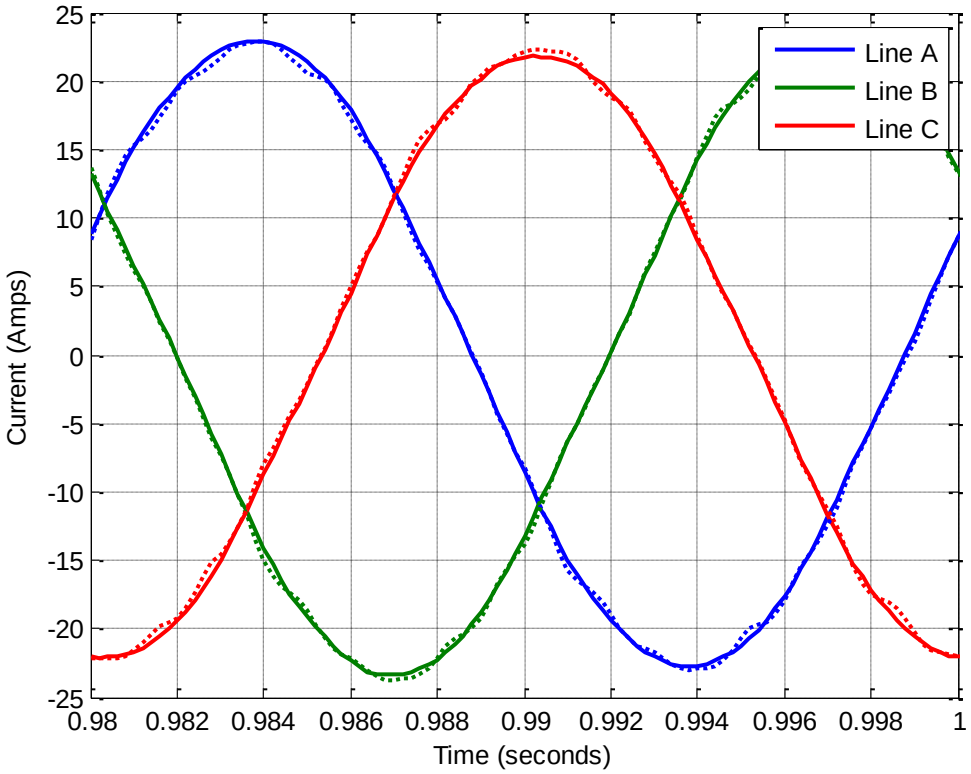

Figure 6.12 Comparison of simulated (solid line) and experimental (dashed line) line currents after estimation (Motor M1 - Direct Coupling)

Similar plots of time-domain and frequency-domain results for a belt coupled load are given in Figure 6.14 and Figure 6.15 respectively. The belt-coupled measured time-domain waveforms contain more distortion than their directly coupled equivalent – this is evident by the deviation of the waveforms from a pure sinusoid. This is also shown in the frequency-domain plot where the low frequency supply harmonics have increased magnitude. The model (and estimated parameters) copes with these differences well – the simulated data still maintaining a good agreement with the measured.

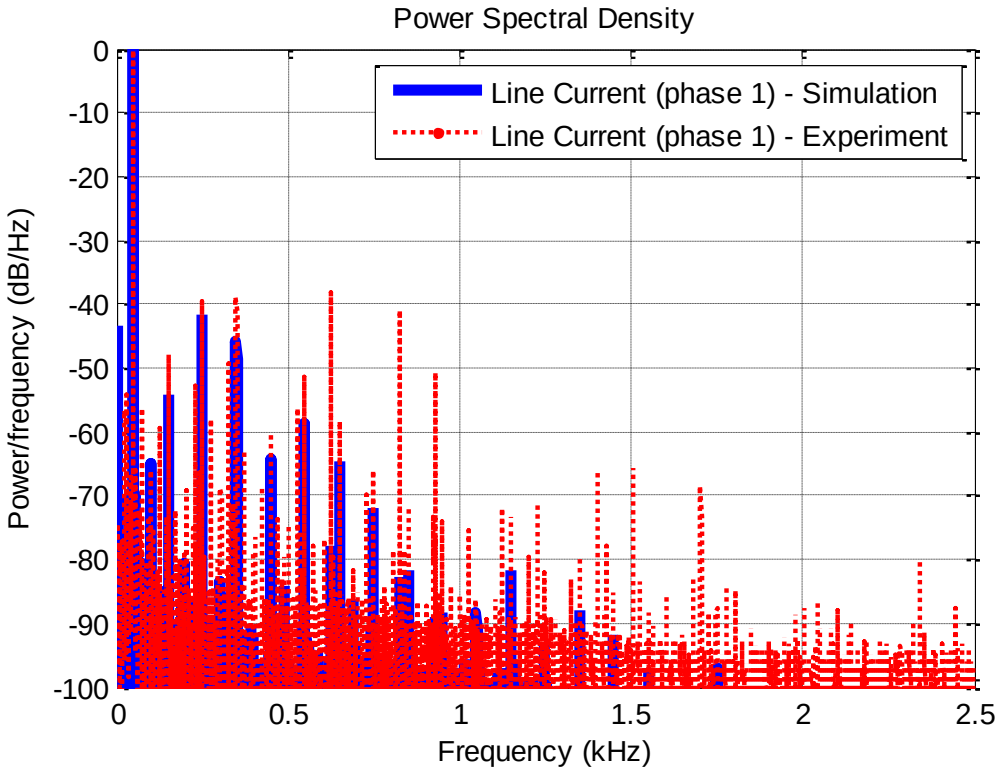

Figure 6.13 Comparison of simulated and experimental line currents in the frequency domain after estimation (Motor M1 - Direct Coupling)

In addition to the changes in supply harmonics there are also several additional frequency components around the supply frequency (0-0.1kHz). These supply sidebands are due to belt oscillation frequencies and therefore are not reproduced by the model.

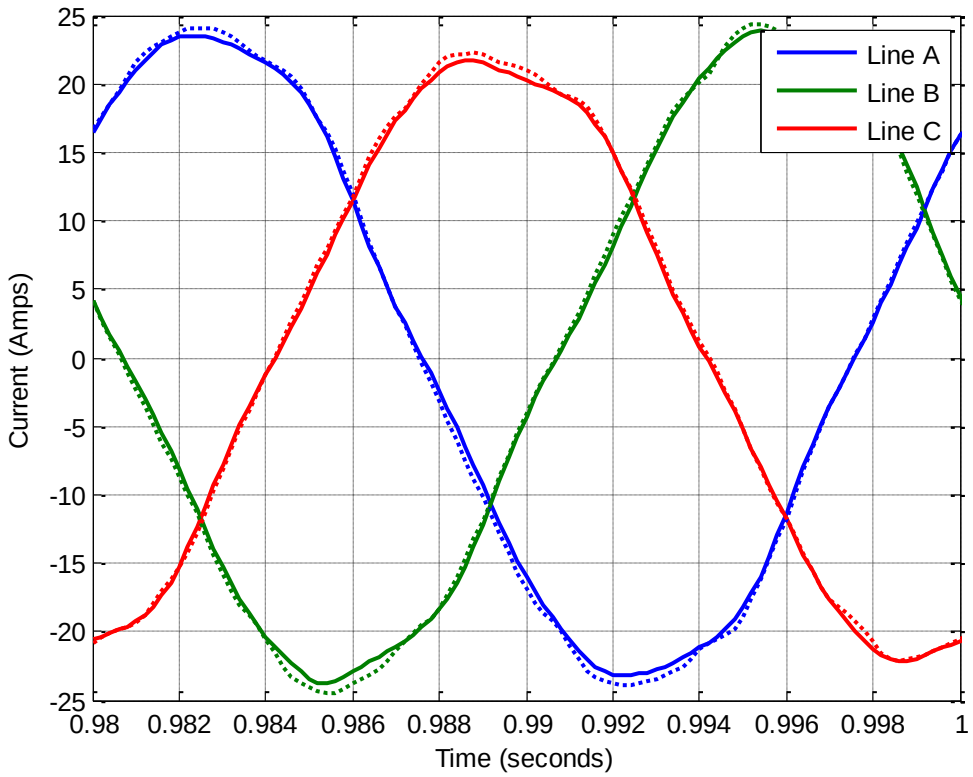

Figure 6.14 Comparison of simulated (solid line) and experimental (dashed line) line currents after estimation (Motor M1 - Belt Coupling)

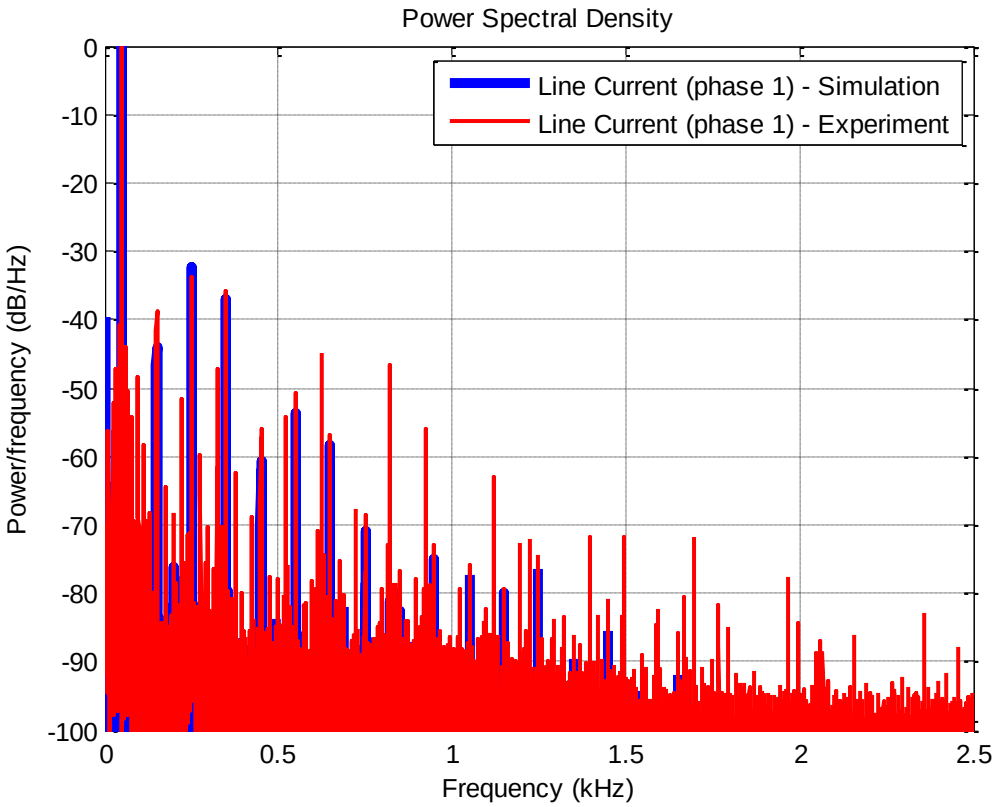

Figure 6.15 Comparison of simulated and experimental line currents in the frequency domain after estimation (Motor M1 - Belt Coupling)

Figure 6.16 and Figure 6.17 compare the modelled and measured line currents for all four of the test motors. Again, the agreement between modelled and experimental results is good.

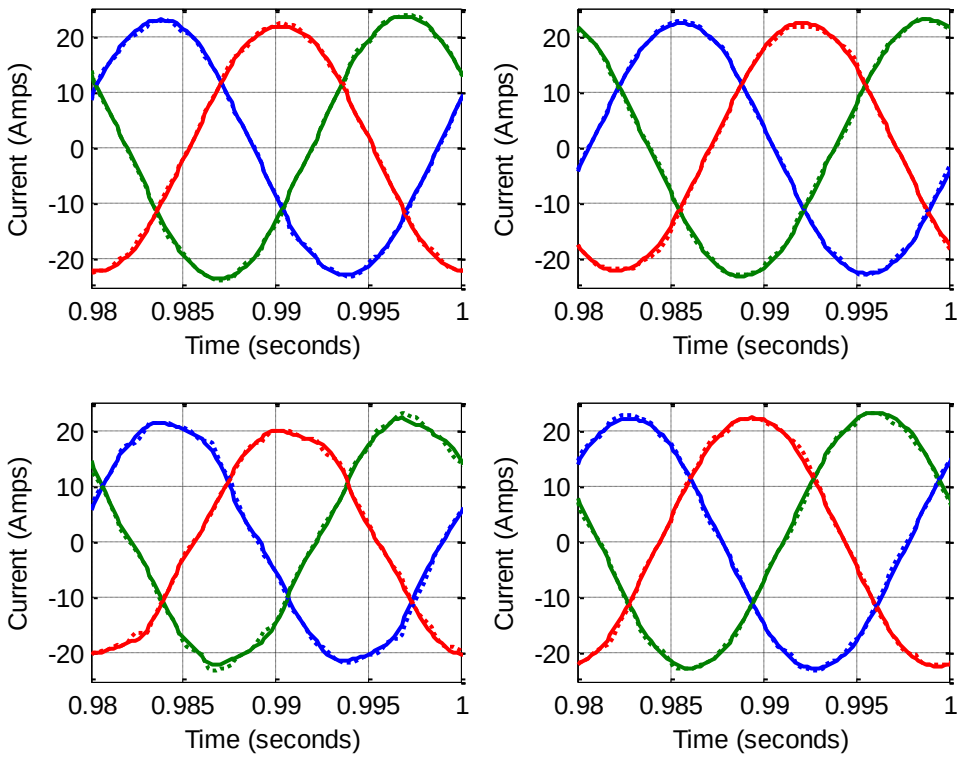

Figure 6.16 Comparison of simulated and experimental line currents in the frequency domain after estimation for all (four) test motors in direct coupling configuration

Figure 6.18 presents the overall results for each of the test motors under both loading configurations. These results are particularly useful since they present the model to experiment average error in terms of amps per sample i.e. the average error between the simulated and measured line currents. In most cases the error is below 0.4A however for motor M3 this value increases up to 0.61A. This is due to the fact the M3 motor in 'healthy' configuration has a modified stator in order to allow turns to be shorted out. The wiring required for the stator tappings adds a small amount of additional impedance on one phase which modifies the currents flowing in that stator winding. This cannot be predicted by

the basic model (thus the increased error) but the fault model used for the fault detection stage can cope with this kind of variation adequately.

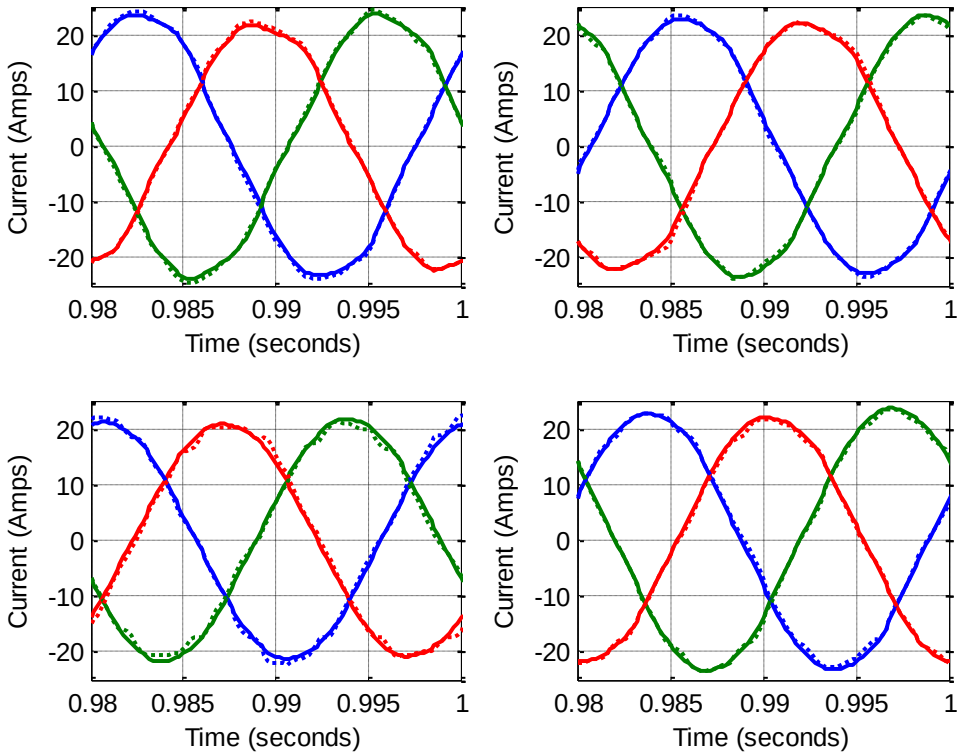

Figure 6.17 Comparison of simulated and experimental line currents in the frequency domain after estimation for all (four) test motors in belt coupling configuration

The progression of the PSO algorithm during a given parameter estimation is shown in Figure 6.19. This plot demonstrates the changes in function value as the optimisation moves through the iterative process for both belt-coupled and direct-coupled load configurations. In general, the objective function is minimised to within 5-10% of its final value after only 10 iterations – the remaining iterations are required to slowly refine the estimate by making small changes.

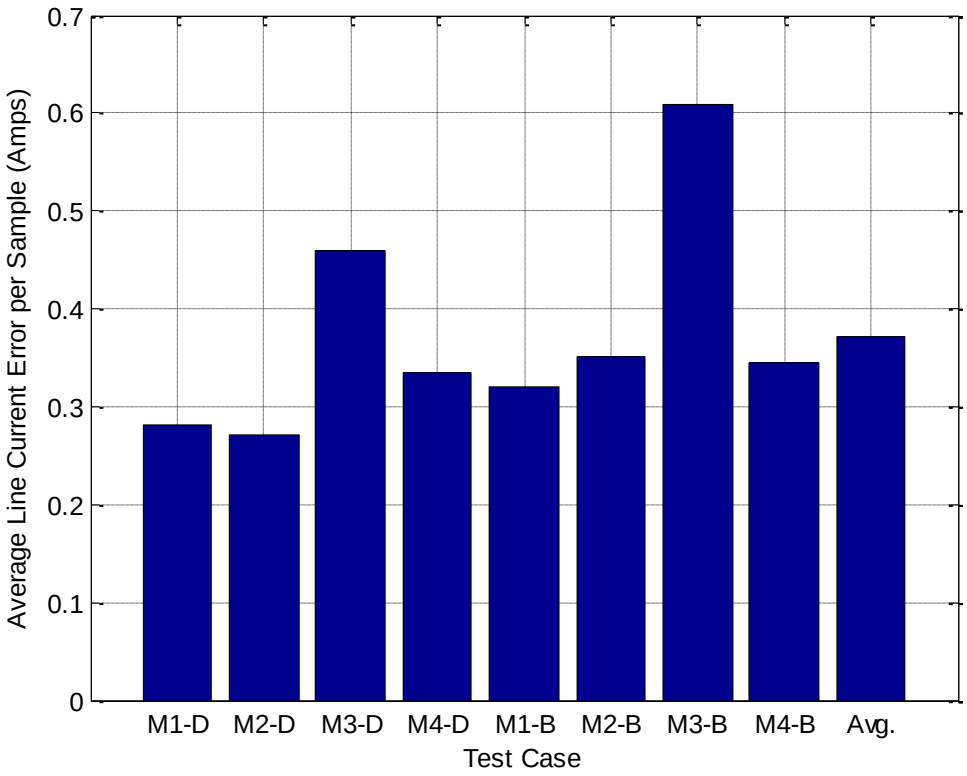

Figure 6.18 Simulated line current error per sample for all test configurations

This refinement process is more suited to one of the local optimisers since the optimal region of the search space has been identified by the global optimiser and now a fast local search can be used to quickly minimise the function further. A two-stage (stochastic-deterministic) optimiser could then be used to find a rough solution and then very quickly refine it. If computational time became an issue this change could be implemented but the algorithm can function adequately without it.

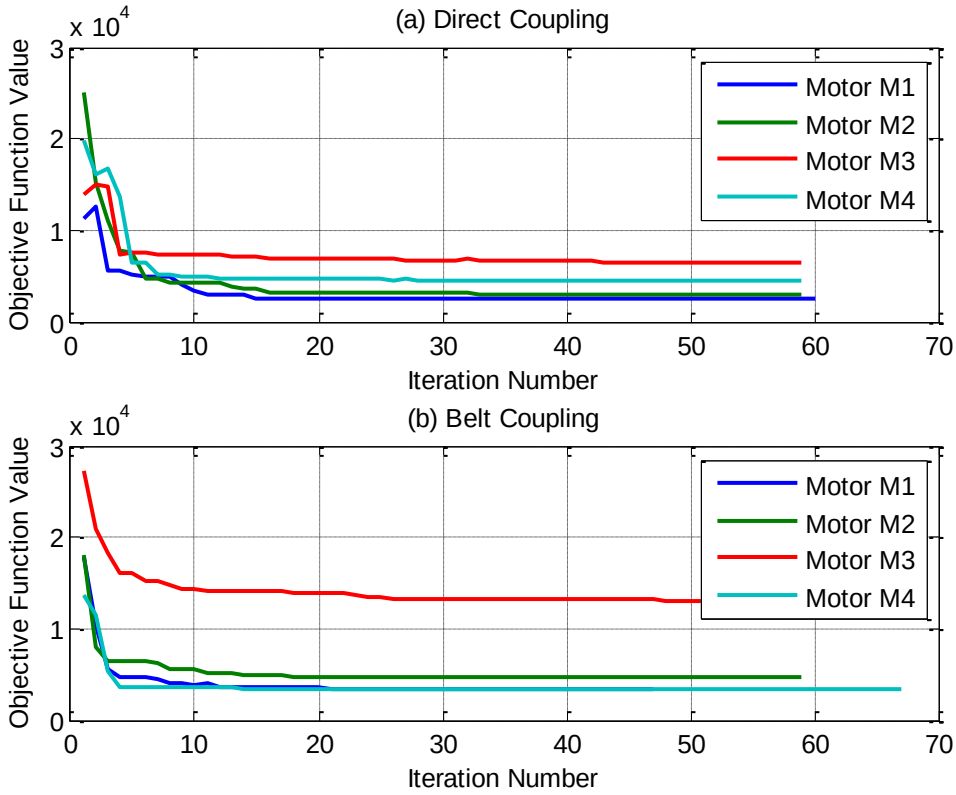

Figure 6.19 Progression of the PSO optimisation algorithm function value for: (a) direct coupled motor configuration, (b) belt coupled motor configuration

Plot (a) of Figure 6.19 indicates that at certain points the function value actually increases. This is impossible with PSO since each particle 'remembers' its own best position (and associated function value) and therefore optimum solutions are never discarded. The reason the function value increases is that the objective function value shown in the plots below (line current error) is combined with the speed driven penalty function. Therefore in some cases in order to reduce the combined function value a worse parameter set (for current matching) is chosen in order to bring the modelled rotational speed closer to the estimated speed. Following this correction it can be seen that the optimiser proceeds to minimise the objective function effectively. It reduces current error whilst simultaneously keeping the model rotational speed close to the estimated value i.e. it performs multi-objective optimisation.

The following tables indicate the parameters that have been estimated by the optimisation algorithms. For each motor four estimation runs were performed which resulted in four sets of estimated parameters. The mean parameter estimate and standard deviation of estimates and the coefficient of variation (CoV) for each of the parameters were calculated. CoV is useful for determining the variability of the parameter estimates since it provides a normalised measure of the dispersion of the estimation of each parameter.

Table 6.6, Table 6.7, Table 6.8 and Table 6.9 indicate the parameter estimation results for motors M1 to M4.

The full load equivalent circuit parameters are obtained empirically and according to the manufacturer's data sheet are as follows:

Rs = 2.08; Rr = 1.66; Xls = 5.36; Xlr = 4.56, Xm = 85.9;

The total equivalent inertia of both motor and load and the load torque applied to the specific motors is as follows:

Jeq = 0.155;

Tl = 49.6Nm (M1,M2,M4) / 45Nm (M3)

A lower load torque was applied to motor M3 since it was to be used for stator testing and the maximum current flowing in the faulty winding (when the fault testing began) needed to be kept to lower values to prevent any permanent damage.

As can be seen from the data most of the parameters are estimated to a reasonable degree of accuracy (for condition monitoring purposes) but the exact parameter values are not obtained. This is due to the reasons discussed

at the beginning of the chapter i.e. there are not enough constraints (measured variables) to allow a single global optimum parameter estimate to be found. In later chapters it will be proved that this level of accuracy for parameter estimates does not prevent successful diagnoses being made.

Table 6.6 Estimated parameters for motor M1

Motor	Coupling Type	Test	Rs	Rr	Xls	Xlr	Xls+Xlr	Xm	Jeq	Tl
M1	Direct	Run 1	4.44	1.50	5.90	3.05	8.95	67.10	0.20	48.91
		Run 2	4.53	1.64	3.68	4.99	8.67	67.28	0.37	48.91
		Run 3	4.44	1.55	4.69	4.42	9.10	68.35	0.10	48.91
		Run 4	4.44	1.50	5.76	3.22	8.98	67.25	0.11	48.91
		Mean	4.46	1.55	5.01	3.92	8.92	67.49	0.19	48.91
		STD	0.05	0.07	1.04	0.94	0.18	0.57	0.12	0.00
		CoV	0.01	0.04	0.21	0.24	0.02	0.01	0.64	0.00
	Belt	Run 1	4.60	1.94	1.37	3.72	5.09	66.94	0.18	50.86
		Run 2	4.60	1.82	3.35	1.58	4.93	64.97	0.18	50.86
		Run 3	4.60	1.90	2.02	3.01	5.03	66.32	0.19	50.86
		Run 4	4.60	1.90	1.98	3.05	5.03	66.33	0.19	50.86
		Mean	4.60	1.89	2.18	2.84	5.02	66.14	0.18	50.86
		STD	0.00	0.05	0.83	0.90	0.06	0.83	0.00	0.00
		CoV	0.00	0.02	0.38	0.32	0.01	0.01	0.01	0.00

Table 6.7 Estimated parameters for motor M2

Motor	Coupling Type	Test	Rs	Rr	Xls	Xlr	Xls + Xlr	Xm	Jeq	Tl
M2	Direct	Run 1	4.50	1.26	8.69	4.61	13.30	80.62	0.14	48.78
		Run 2	4.50	1.35	5.68	7.88	13.56	82.83	0.13	48.78
		Run 3	4.49	1.37	4.94	9.23	14.18	85.31	0.13	48.78
		Run 4	4.51	1.31	7.02	6.52	13.54	82.29	0.13	48.78
		Mean	4.50	1.32	6.58	7.06	13.65	82.76	0.13	48.78
		STD	0.01	0.05	1.65	1.97	0.37	1.94	0.01	0.00
		CoV	0.00	0.04	0.25	0.28	0.03	0.02	0.05	0.00
	Belt	Run 1	4.62	1.67	6.74	1.09	7.83	67.49	0.05	50.26
		Run 2	4.62	1.74	5.19	2.76	7.94	69.10	0.05	50.26
		Run 3	4.62	1.82	3.63	4.42	8.05	70.55	0.05	50.26
		Run 4	4.62	1.72	5.64	2.31	7.95	68.74	0.05	50.26
		Mean	4.62	1.74	5.30	2.64	7.94	68.97	0.05	50.26
		STD	0.00	0.07	1.29	1.38	0.09	1.26	0.00	0.00
		CoV	0.00	0.04	0.24	0.52	0.01	0.02	0.00	0.00

Table 6.8 Estimated parameters for motor M3

Motor	Coupling Type	Test	Rs	Rr	Xls	Xlr	Xls + Xlr	Xm	Jeq	Tl
M3	Direct	Run 1	4.75	1.57	1.99	2.05	4.04	67.53	0.26	45.69
		Run 2	4.74	1.55	2.43	1.59	4.02	67.09	0.26	45.69
		Run 3	4.74	1.56	2.30	2.01	4.32	67.64	0.01	45.69
		Run 4	4.74	1.61	1.15	2.95	4.11	68.37	0.26	45.69
		Mean	4.74	1.58	1.97	2.15	4.12	67.66	0.19	45.69
		STD	0.00	0.03	0.58	0.57	0.14	0.53	0.12	0.00
		CoV	0.00	0.02	0.29	0.27	0.03	0.01	0.64	0.00
	Belt	Run 1	4.85	1.30	7.41	9.13	16.54	99.26	0.05	46.01
		Run 2	4.86	1.22	10.58	5.45	16.03	95.87	0.05	46.01
		Run 3	4.86	1.30	7.26	9.25	16.51	99.07	0.05	46.01
		Run 4	4.86	1.23	10.30	5.77	16.07	96.13	0.05	46.01
		Mean	4.86	1.26	8.89	7.40	16.29	97.58	0.05	46.01
		STD	0.01	0.05	1.79	2.07	0.28	1.83	0.00	0.00
		CoV	0.00	0.04	0.20	0.28	0.02	0.02	0.00	0.00

Table 6.9 Estimated parameters for motor M4

Motor	Coupling Type	Test	Rs	Rr	Xls	Xlr	Xls + Xlr	Xm	Jeq	Tl
M4	Direct	Run 1	4.52	1.68	11.10	5.67	16.77	91.06	0.04	48.88
		Run 2	4.53	2.03	2.84	14.61	17.44	93.94	0.03	48.88
		Run 3	4.54	1.94	5.39	10.79	16.18	89.09	0.07	48.88
		Run 4	4.53	1.98	4.21	12.62	16.83	91.72	0.06	48.88
		Mean	4.53	1.91	5.88	10.92	16.81	91.45	0.05	48.88
		STD	0.01	0.15	3.63	3.83	0.52	2.00	0.02	0.00
		CoV	0.00	0.08	0.62	0.35	0.03	0.02	0.39	0.00
	Belt	Run 1	4.53	1.59	3.98	3.82	7.80	71.46	0.14	50.26
		Run 2	4.53	1.55	4.98	2.73	7.70	70.48	0.04	50.26
		Run 3	4.54	1.55	4.85	2.97	7.82	70.86	0.04	50.26
		Run 4	4.53	1.52	5.75	1.93	7.68	69.75	0.04	50.26
		Mean	4.53	1.55	4.89	2.86	7.75	70.64	0.07	50.26
		STD	0.00	0.03	0.72	0.78	0.07	0.72	0.05	0.00
		CoV	0.00	0.02	0.15	0.27	0.01	0.01	0.72	0.00

To demonstrate that for a given dataset the PSO algorithm produces *similar* estimates, 4 separate parameter estimation runs were compared for each motor and the variation between these estimates using the same dataset are shown in Table 6.10 (intra-dataset). In general the CoV values are very low showing that given a set of data, the stochastic optimiser achieves a repeatable estimate.

The overall inter-dataset repeatability is in the region of two times lower as expected since the different motors will have had slightly different operating temperatures, load torques, manufacturing defects, assembly differences, installation differences and supply conditions.

Table 6.10 Overall parameter estimation results for the four test motors

		Rs	Rr	Xls	Xlr	Xls+Xlr	Xm	Jeq	Tl
Overall - All-dataset results	Mean	4.61	1.60	5.09	4.97	10.06	76.59	0.12	48.71
	STD	0.13	0.23	2.62	3.40	4.67	11.78	0.09	1.83
	CoV	0.03	0.15	0.51	0.68	0.46	0.15	0.74	0.04
Intra Dataset Repeatability	STD	0.01	0.06	1.44	1.56	0.21	1.21	0.04	0.00
	CoV	0.00	0.04	0.29	0.32	0.02	0.02	0.31	0.00

The parameters which showed the highest variation were the combined inertia and the stator and rotor leakage inductances. The inertia is difficult to estimate reliably since the estimate is done during steady load conditions (i.e. minimal or no acceleration) therefore the dynamics of the system are not captured effectively thus the inertia cannot be estimated as accurately as the other parameters. The leakage reactances show more variation because they are linearly dependent [64] and if combined into one parameter (Xls+Xlr) this issue can be reduced to some extent with the CoV dropping slightly from 0.51/0.68 to 0.46.

6.9 Summary

This chapter has demonstrated the ability of various optimisation techniques to solve a parameter estimation problem involving the seven motor parameters of the basic induction motor model (DQ reference frame mode). The parameter estimation was driven by an objective function which outputted the square error between the samples of the three-phase simulated line current waveform and their measured equivalents.

A variety of different optimisation techniques were used to solve this problem, allowing comparisons between local search techniques, evolutionary algorithms and particle swarm algorithms. It is clear that the optimisation landscape for this particular problem is highly multimodal; many of the local search strategies become trapped in local minima. It is for these reasons that the stochastic approaches of the evolution strategies and particle swarm technique showed superior performance. Over 30 minutes and 60 minutes the stochastic techniques outperform the local search techniques. The particle swarm optimisation (PSO) method led to the best (lowest error function value) set of parameters being obtained and thus it was chosen as the optimiser for the baseline parameter estimation stage of the condition monitoring system.

The accuracy of the models derived from the PSO parameter estimation process was analysed. The estimated parameter values show low variability and are similar to the values obtained from the manufacturer (with differences due to the fact that estimating parameters using current only does not allow a unique optimum to be obtained). The time-domain results show good agreement for each of the four test motors with the full-load error per sample less than 0.4A. Frequency-domain results indicate that several frequency components are not reconstructed by the model (e.g. those due to rotor bar passing frequency). This is expected since the simple model does not consider stator winding layout or number of rotor bars. This is not an issue for the chosen fault detection methods since only low frequency components are required.

Chapter 7. Model Validation

This chapter describes the validation of the basic DQ reference frame induction motor model. The model is validated against experimental data collected using the 7.5kW Brook-Crompton test motor.

7.1 Validation method

For each data file the motor parameters are estimated using the estimation method described in the previous chapter. This set of parameters is then used to simulate the motor and the result of the simulation is compared with the measured values recorded during the experiment.

The main variables used for comparison are the three line currents which will be compared in terms of RMS values, time-domain and frequency-domain graphical comparisons and calculation of an average error per sample value for each data set. As a secondary measure of model accuracy the model output shaft speed will be compared with the experimentally recorded shaft speed.

The validation exercise will consider steady-state datasets for motor M1 running under varying load torques ranging from zero up to the rated load torque of the motor. The validation will judge the performance of the model on the steady-state accuracy since the system being developed is aimed at steady-state fault detection and diagnosis only.

The comparisons will be made using data collected on both the direct-coupling test rig configuration and the pulley-coupling test rig configuration.

7.2 Estimated parameters

For each of the datasets the PSO parameter estimation algorithm was used to estimate a set of parameters. The estimation results for each of the test cases (100%, 75%, 50% and 25% of full load rated torque) are given in Table 7.1.

Table 7.1 Estimated parameter values used for the validation process

Load (Nm)	Coupl.	Rs	Rr	Xls	Xlr	Xm	Jeq	Tl
49.6	Direct	4.44	1.49	6.04	2.89	66.92	0.10	48.91
37.2	Direct	4.79	1.32	5.63	3.50	68.64	0.20	36.99
24.8	Direct	4.70	1.28	7.12	2.33	69.85	0.21	25.39
12.4	Direct	3.46	1.32	5.76	4.45	74.06	0.19	14.23
49.6	Belt	4.60	1.84	3.08	1.87	65.24	0.18	50.86
45	Belt	4.77	1.90	2.21	3.01	67.73	0.18	46.38
40	Belt	4.97	1.60	3.53	1.60	67.70	0.15	41.50
35	Belt	5.15	1.83	3.15	2.15	69.79	0.17	36.78

The parameter sets listed here are those used throughout this chapter to derive the model results.

7.3 Time-domain analysis

This section demonstrates the performance of the model in terms of the time-series line current waveforms measured on the test rig and those predicted by the model. The time-domain comparisons of simulated and experimental line currents for (shaft-coupled) load torques of 49.6Nm, 37.2Nm, 24.8Nm and 12.4Nm are shown in Figure 7.1, Figure 7.2, Figure 7.3, and Figure 7.4 respectively. A good agreement between the model and experimental line currents can be seen for each of the four load torque values.

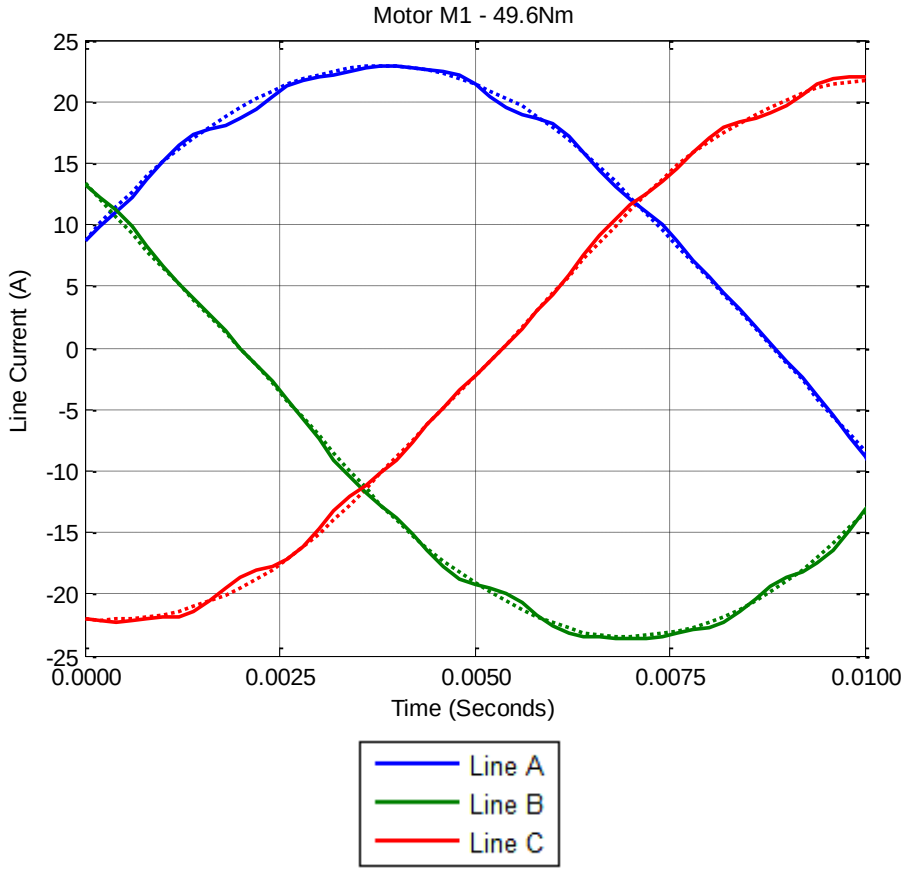

Figure 7.1 Time-domain comparison of modelled and actual line currents – 49.6Nm (full rated load)

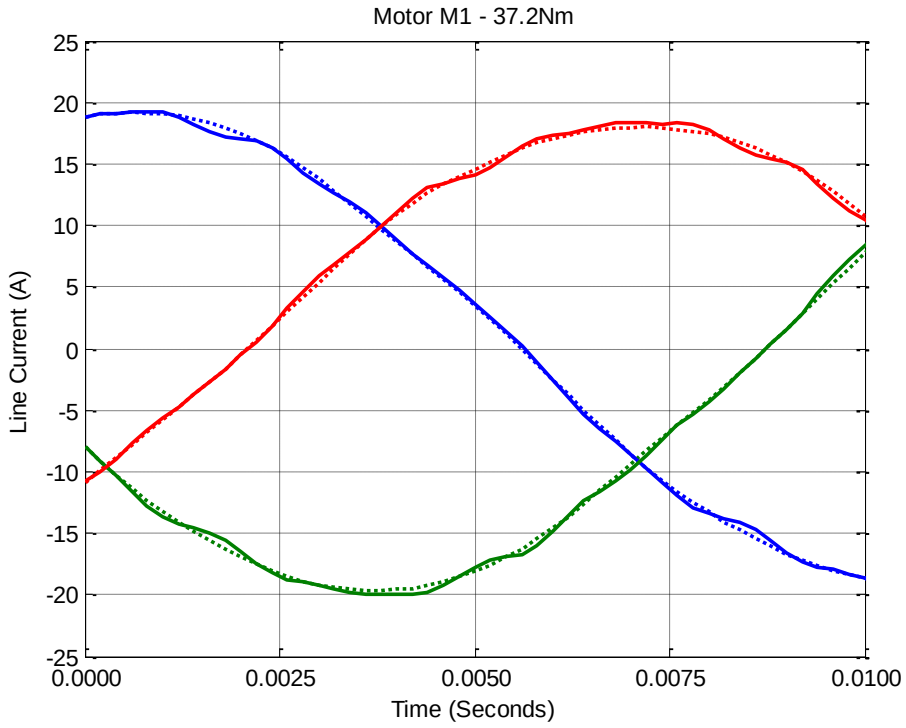

Figure 7.2 Time-domain comparison of modelled and actual line currents – 37.2Nm (full rated load)

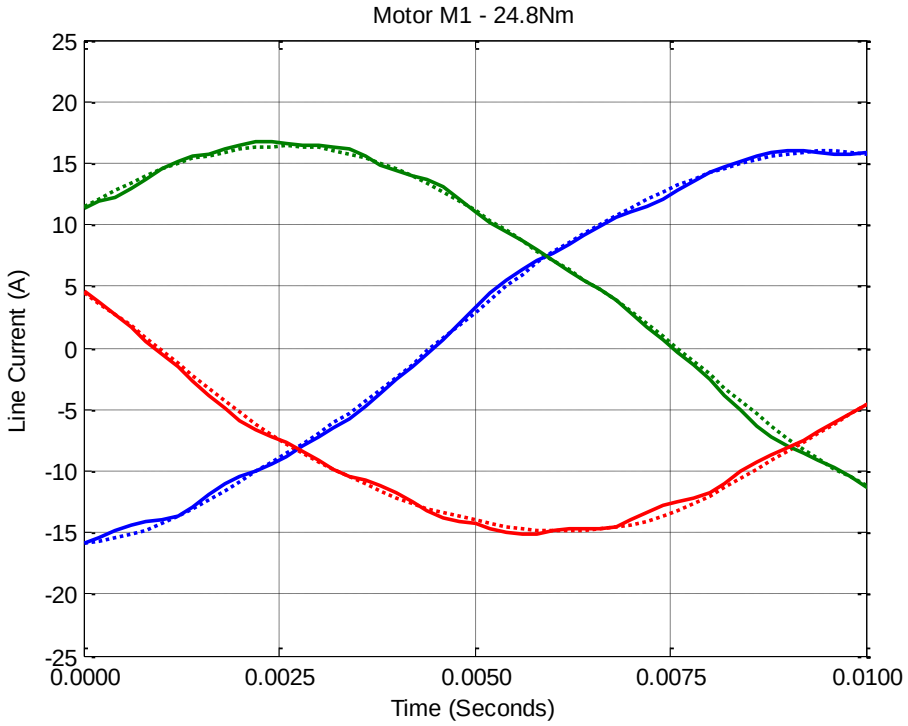

Figure 7.3 Time-domain comparison of modelled and actual line currents – 24.8Nm (full rated load)

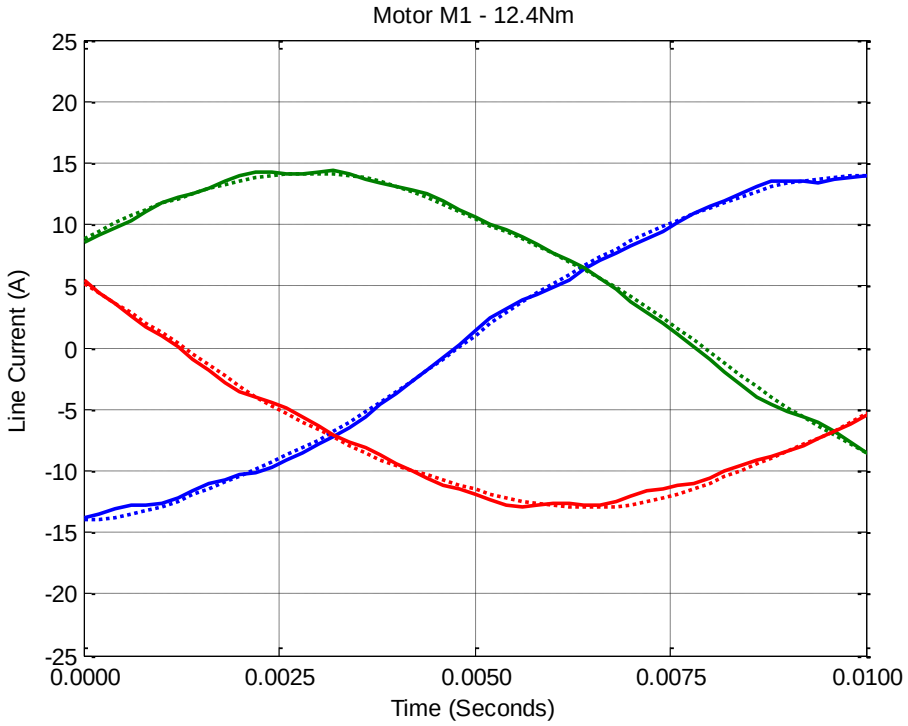

Figure 7.4 Time-domain comparison of modelled and actual line currents – 12.4Nm (full rated load)

Table 7.2 contains data regarding the average error (difference between simulated and measured line currents) in terms of error per sample. The average error per sample is generally quite low, in the region of 0.3 A/sample.

Table 7.2 Averaged sample error for the validation dataset

Load Torque (Nm)	Coupling Type	Average Error (A/sample)
49.6	Direct	0.279
37.2	Direct	0.276
24.8	Direct	0.282
12.4	Direct	0.292
49.6	Belt	0.323
45	Belt	0.309
40	Belt	0.311
35	Belt	0.318

7.4 Frequency-domain analysis

Figure 7.5, Figure 7.6, Figure 7.7 and Figure 7.8 present the frequency-domain comparisons of simulated and measured line current data. The figures include plot of frequencies from 0 to 1.5 kHz and a zoomed plot of the region from 0 to 100 Hz. This is a region of interest for fault detection since this frequency band will contain important fundamental sideband components which can indicate the presence of faults.

As mentioned in the previous section the simulated current cannot replicate all frequency components since the model assumes sinusoidal winding and equivalent winding distributions so stator slotting and rotor bar effects are not replicated. The method of fault modelling used (explained in subsequent chapters) in this project does not utilise stator slotting and rotor bar frequency components so this is not an issue. Other than the aforementioned frequency components the modelled currents show good reproduction of the 50 Hz

fundamental, the supply harmonics and most importantly the low frequency noise floor since this will be critical for the rotor fault detection algorithm to be effective.

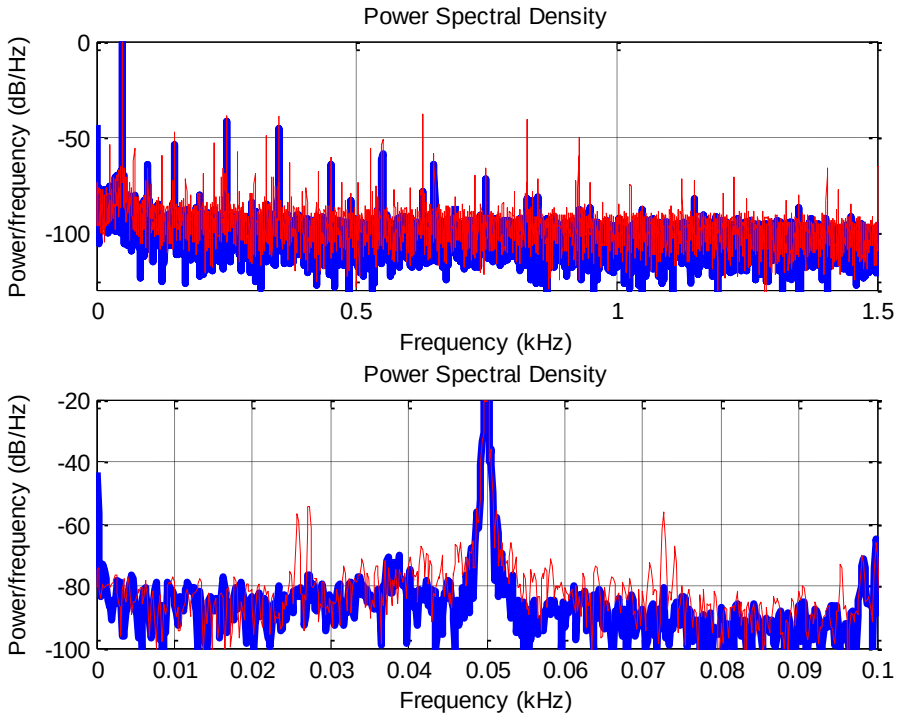

Figure 7.5 Frequency-domain comparison of modelled (blue) and actual line current from line A (red) – 49.6Nm (full rated load)

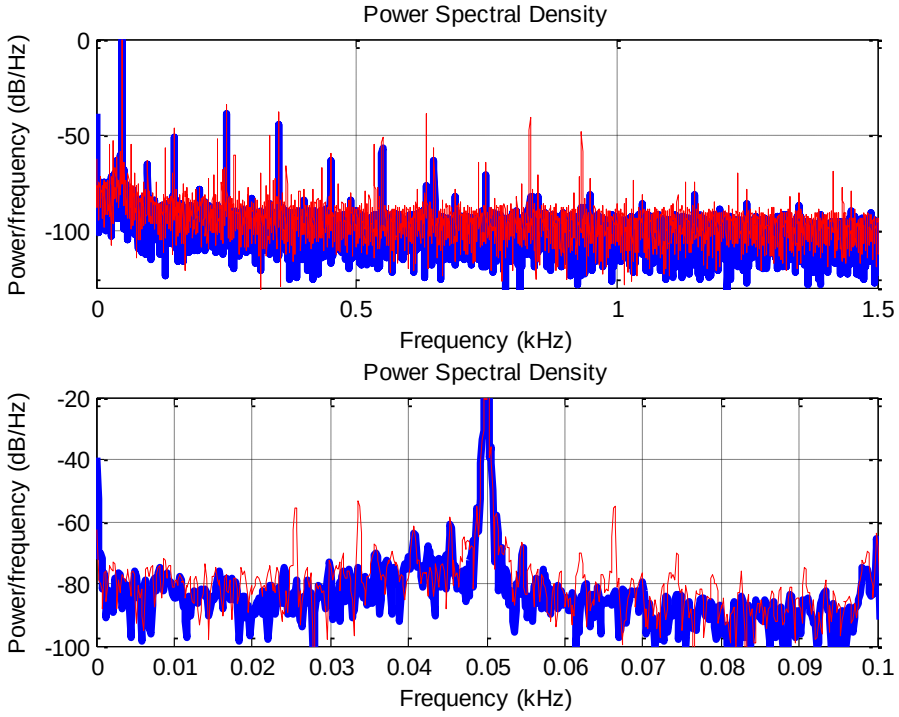

Figure 7.6 Frequency-domain comparison of modelled and actual line current (line A) – 37.2Nm (full rated load)

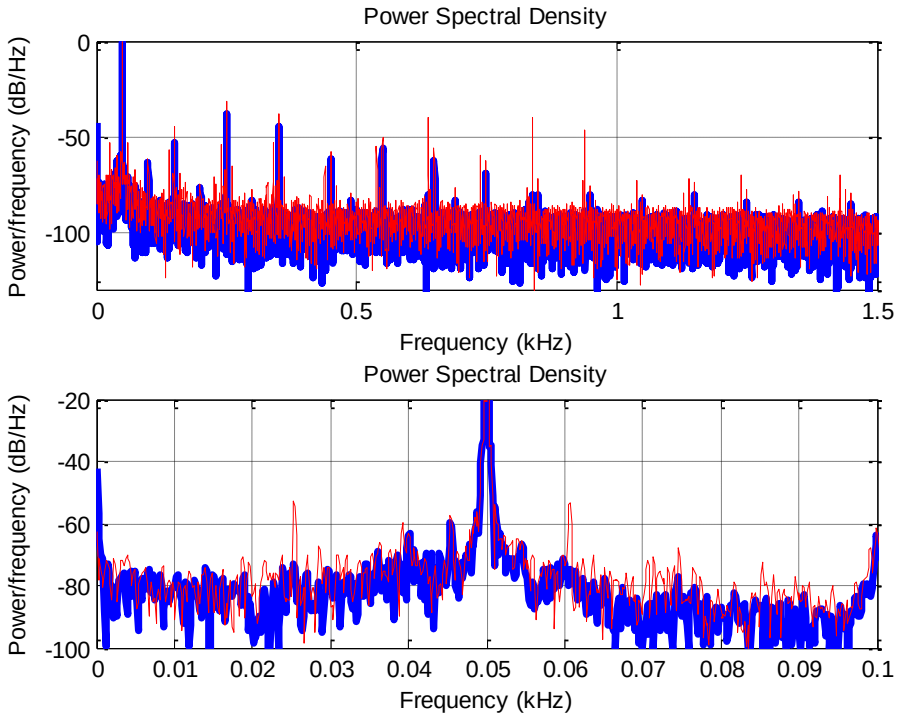

Figure 7.7 Frequency-domain comparison of modelled and actual line current (line A) – 24.8Nm (full rated load)

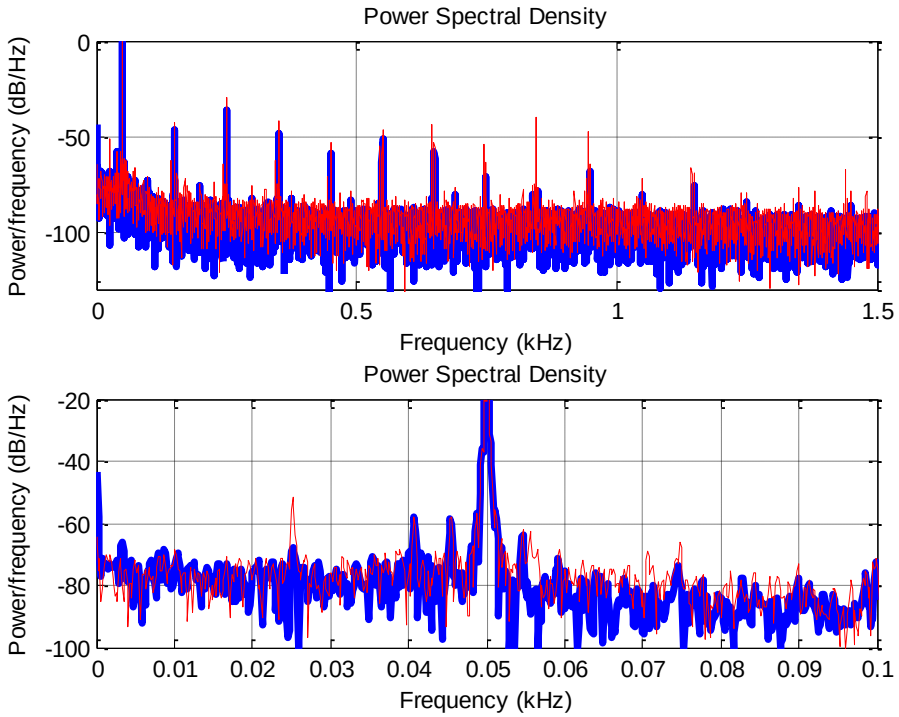

Figure 7.8 Frequency-domain comparison of modelled and actual line current (line A) – 12.4Nm (full rated load)

In terms of the spectrum of the motor current, the model has no ability to predict all of the frequency components, only those due to the voltage. The model is simply interpreting the stator voltage harmonics and predicting their effect on the current harmonics. The major harmonic components of the voltage signal are 150Hz, 250Hz, 350Hz, 450Hz, 550Hz, 650Hz, etc. By observing the simulated and experimental stator current PSDs, it can be seen that these odd harmonics are accurately represented by the model.

7.5 RMS line current comparisons

Table 7.3 gives information on the averaged (across the three phases) RMS line currents for 4 load torque settings for directly coupled loads and 4 load torque settings for belt coupled loads. The RMS values show good agreement particularly for shaft-coupled loads where the error between experiment and simulation is less than 1%. The accuracy decreases slightly for belt-coupled loads due to the presence of additional distortion in the currents due to belt-related frequency components. Even so the error only increases to a maximum of 1.04% for a load torque of 35Nm with a belt-coupled load.

Table 7.3 Comparison of modelled and experimental averaged (3 phase) RMS line current

Load Torque (Nm)	Coupling Type	Average RMS Line Current (A)		Error	
		Experiment	Simulation	Absolute (A)	Percent
49.6	Direct	16.17	16.25	-0.08	-0.49
37.2	Direct	13.41	13.51	-0.10	-0.73
24.8	Direct	11.22	11.31	-0.09	-0.77
12.4	Direct	9.69	9.76	-0.07	-0.72
49.6	Belt	16.82	16.72	0.11	0.64
45	Belt	15.71	15.59	0.12	0.75
40	Belt	14.68	14.55	0.12	0.84
35	Belt	13.58	13.44	0.14	1.04

7.6 Shaft rotational speed comparisons

A comparison of the model predicted rotational speed and actual rotational speed is given in Table 7.4. The maximum error is only 4.48rpm or 0.31% which indicates that the speed estimation algorithm combined with the speed penalty function used in the parameter estimation process is operating effectively. Overall the simulated and measured speeds show very good agreement across the range of load torque settings tested.

Table 7.4 Comparison of modelled and experimental motor shaft rotational speeds

Load Torque (Nm)	Coupling Type	Shaft Rotational Speed (rpm)		Error	
		Experiment	Simulation	Absolute (rpm)	Percent
49.6	Direct	1450	1450.2	-0.20	-0.01
37.2	Direct	1464	1468.3	-4.48	-0.31
24.8	Direct	1476	1479.1	-2.92	-0.20
12.4	Direct	1487	1488.9	-1.57	-0.11
49.6	Belt	1441	1441.4	-0.36	-0.03
45	Belt	1446	1446.9	-0.94	-0.06
40	Belt	1452	1453.0	-0.98	-0.07
35	Belt	1459	1458.7	0.27	0.02

7.7 Summary

The basic DQ0 reference frame model developed as part of this project has been validated against experimental data.

This validation exercise demonstrates that the simulated and measured current waveforms show good agreement under each of the loading cases. The RMS values across the loading range were never further than 1.04% of the actual value. The spectral comparisons indicate that the frequency content of modelled and actual line currents differ slightly – this is as expected since the model does not take into account the asymmetries of the winding distributions and rotor cage bar distributions. However, the model accurately reproduces the supply

harmonics and noise floor which is a key feature of the fault detection techniques described in subsequent chapters.

RMS line current error and rotational speed error are both low with errors of 1.04% and 0.31% respectively.

Overall, the model provides good performance and is fit for purpose to be used as part of the model based fault detection techniques.

Chapter 8. Fault Description

This chapter investigates the different types of faults that can occur in induction motors. The first section will look at each of the faults in detail and the second section explains how these faults were synthetically replicated in the laboratory..

8.1 Bearing faults

The bearings of the induction machines are of the rolling element or ball type and support the shaft at each end whilst allowing it to rotate freely. The balls or rolling elements rotate on metal rings or ‘raceways’. The inner raceway fits on to the shaft whilst the outer raceway sits in the end-plate or end-housing [6].

The rolling elements are lubricated in order to protect the surfaces of the bearing. If the bearing contains too much or too little lubricating grease or contaminated grease then bearing damage can occur, in this situation the bearing can overheat and abrasive mechanisms damage the contact surfaces of the bearing. Small particles that enter the bearing element can also cause a abrasive action and if water, strong alkalis or acids enter the bearing then they can also have a damaging corrosive effect [6].

Bearing faults can often be caused by improper installation of the bearing components, for example, if excessive force is used to fit the bearing onto the shaft or into the motor housing. During motor assembly care must be taken to ensure that the bearings are installed on the shaft and in the end-plates properly and are seated correctly [36].

Bearings can also be damaged by small currents that flow down the induction motor shaft then through the bearings. The current builds up a capacitive

energy between the rolling elements and the raceways, which are separated by a thin film of lubricant. When the capacitive energy reaches a certain value a sPark is created which jumps across the gap and creates pits on the raceway and rolling elements (sPark erosion) [12].

In addition to these faults that can be attributed to a specific cause there can be bearing failures which are simply due to extended use of the bearing. These faults can be caused by vibrations, inherent eccentricity and internal fatigue stresses occurring during normal motor operation [131].

The causes listed in the previous section lead to a change in the physical properties of the bearing elements (raceways and rolling elements); small particles are removed from the surfaces of these components which cause the bearings to operate incorrectly. The process of damage to bearing raceways is known as brinelling [132]. Brinelling occurs when the applied forces within the bearing exceed the material stress limits causing a ‘crater’ or ‘brinell’ mark. For brinelling to occur a small fragment of the bearing surface breaks loose and this fragment can go on to initiate damage elsewhere or reduce the effectiveness of the bearing grease. These process are often also called ‘flaking’ or ‘spalling’ [6].

The types of defects described in the previous paragraph are essentially a small hole or ‘pit’ forming on a bearing surface – and are known as localised or single-point defects [79]. In contrast to this there are distributed defects which affect a whole area and can be categorised by an increase in the ‘generalized roughness’ of a surface rather than specific marks, dents or scratches. These distributed faults are common in industry and can be linked to typical operating life wear, shaft currents and incorrect lubrication [133].

Each of the constituent parts of the rolling element bearing can develop a fault (rolling element, train, inner race and outer race) and these faults cause periodic torque oscillations which cause predictable frequency components in the vibration and current frequency spectrum [8,9].

8.2 Stator faults

The stator of an induction machine consists of a number of coils which distribute the current (and therefore field density) around the circumference of the machine. The stator coils are organised in such a way that when supplied with 3-phase electricity they create a rotating magnetic field. Faults in the stator of an induction motor can be caused by a number of different reasons including thermal, electrical, mechanical and environmental issues. These causes will be summarised in the following paragraphs.

Thermal aging causes the operating life expectancy of the stator conductors' insulation to reduce significantly and this makes the stator winding more susceptible to other types of faults occurring. As a rule of thumb the operational life expectancy of a stator coil will halve for each 10 degree rise in temperature [28]. Thermal stresses can occur due to unbalanced voltages, insufficient cooling, obstructed cooling or a high ambient temperature. Since induction motors draw high currents at start up, multiple starts in a short time frame can also cause thermal stresses within the stator windings. As mentioned previously, the effect of thermal/electrical stresses is to make the stator vulnerable to other stresses (mechanical and environmental) by reducing the physical integrity of the winding potentially leading to short circuits or open circuits [28].

Mechanical stresses occur in the stator due to ever present vibration and electromagnetic forces. Since a current carrying conductor experiences a force when in a magnetic field, each of the stator winding conductors feels a force during operation. The current causes the coils to vibrate radially and tangentially. These vibrations are heightened at start-up as they are proportional to the square of the current. Other mechanical fault causes include objects coming into physical contact with the stator such as faulty rotor assemblies, internal parts of the machine that have become loose or foreign bodies that have entered the machine. Environmental faults such as foreign bodies can also cause stator issues; dust and debris may build up inside the motor insulating surface preventing effective heat dissipation and in some cases cause shorts and grounds [28].

If the stresses mentioned in the previous paragraphs are of a sufficient magnitude and act of a sufficient period of time the stator will initially develop a small turn-to-turn stator winding fault. The turn-to-turn (shorted turn) is an initial small scale fault where the insulation between two adjacent winding turns fails which effectively short circuits part of the stator winding (one or more turns). This fault reduces the resistance of the winding which leads to increased current flow. Excessive current will then lead to heating of the winding (and subsequent thermal ageing) which can eventually result in motor failure [134]. It is thought that these small turn-to-turn faults are the precursors for serious phase-to-phase and phase-to-ground failures [8,1] which if allowed to occur can cause irreversible damage to the stator windings or stator core [135].

8.3 Rotor faults

The rotor of an induction machine consists of a series of straight bars connected by two circular end rings; the entire assembly known commonly as the ‘squirrel cage’. Currents are induced in these bars due to the flux distributions caused by the stator.

Rotor faults are basically breakages or cracking of rotor bars and end rings. There are a number of stresses [6] which act on the rotor conductors (much like those acting on the stator conductors) which are summarised below.

Thermal stresses generated in the rotor can be due to unbalance, sParking and hot-spots developing on the rotor structure. The rotor also suffers from magnetic forces under normal operation but that can be increased due to unbalanced supply, stator faults and also in-built asymmetries. There can also be undue mechanical stresses on the rotor due to poor construction and variation in motor loading (e.g. pulsating loads). Finally, ingress of foreign material into the motor housing can lead to abrasion or corrosion of rotor material due to chemical elements or water being present inside the motor.

If the motor is a DOL starter the stresses on the rotor will be higher due to high currents (high torque) drawn at start-up. The forces experienced at start-up are higher than nominal operating conditions. Therefore, if the motor is started frequently the problems of thermal and mechanical stresses are increased [31].

The main rotor fault mechanism is a breaking or cracking of a rotor bar or end ring. Cracking or breaking of a rotor does not necessarily lead to induction motor failure, and the motor may be able to continue running with multiple cracked or broken rotor bars. However, a broken bar does increase the currents in adjacent bars which can lead to increased thermal stresses and in turn more

damage [136]. The breaking or cracking of the bar leads to a reduction in the conductivity of the rotor bar.

When a rotor bar breaks there is the possibility that it can go on to cause additional mechanical damage within the motor. In some cases parts of the broken bar can be thrown outwards radially into the stator causing serious damage to the stator windings [31].

8.4 Eccentric air-gap faults

Air-gap eccentricity occurs when the rotor is not centred within the stator i.e. rotor and stator centrelines are offset or non-parallel. The eccentricity can be either of the static type (the offset is in a fixed direction) or the dynamic type (the offset rotates as the rotor angular position changes). Eccentricity causes a non-uniform air-gap between rotor and stator and this in turn causes variations in the interaction between rotor and stator magnetic fields and currents. This results in an unbalanced magnetic pull (UMP) which can cause mechanical vibration and, in severe cases, cause the rotor to rub (rotor strike) on the stator which can cause serious damage to the stator and rotor [134].

Static eccentricity can occur due to incorrect installation of bearings or motor end-plates (bearing housings). If the stator winding is not perfectly circular then UMP will exist and cause some degree of static eccentricity. Dynamic eccentricity is usually due to bent rotor shaft, mechanical resonances or worn bearings [20].

8.5 Generation of motor faults

This section describes the methods used to synthetically create faults in the laboratory. These modified motor components are those used in the experimental phases of this project.

8.5.1 Stator fault creation

In order to artificially create the turn-to-turn fault the test motor needed to have the ability to short-circuit a chosen number of windings on a specific phase.

The standard stator winding installed by the motor manufacturers was removed and a new stator was wound. Stator windings (U1, U2) and (W1, W2) were re-wound in the standard ‘healthy’ configuration. The V winding was wound with a number of additional connections or ‘tappings’.

The tappings were points at which the stator winding was passed out of the stator housing, through the terminal box, until there was a length of wire outside of the stator housing (approximately 300mm). A cut was made at this point and then the new section of winding conductor was passed back in through the terminal box and one more turn was wound. The conductor was routed back outside the stator housing and another cut was made. This creates one isolatable turn within the motor.

The process was repeated 15 times to give 15 separate tapping points. By connecting different tappings this allowed a maximum of 14 turns of the stator winding to be shorted circuited. The completed motor is shown in Figure 8.1.

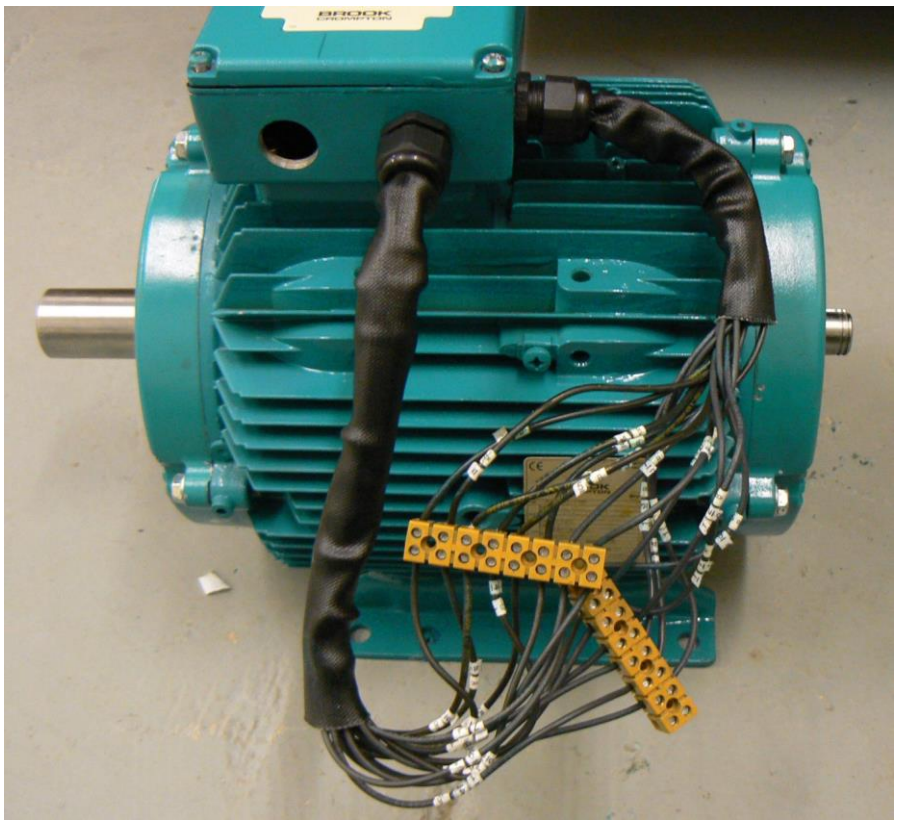

Figure 8.1 Custom stator rewind showing tapping wires and temporary screw terminal connections

A schematic of the winding configuration is given in Figure 8.2. The tappings are labelled with a number and a letter. ‘A’ indicates the start of the turn and ‘B’ indicates the end of the turn. For example, if 1A is connected to 1B, no short is present but if 1A is connected to 2B, one shorted turn is present.

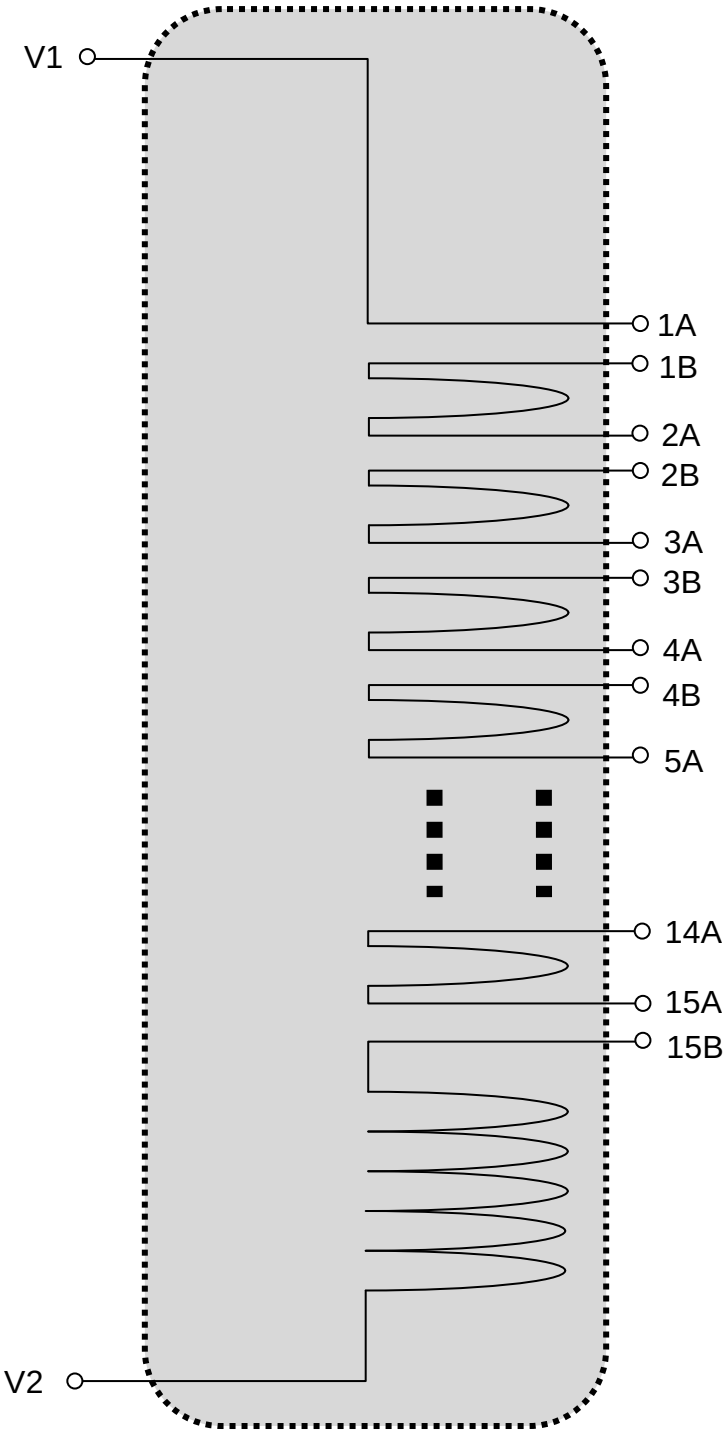

Figure 8.2 Diagram of the tapping configuration used for the stator turn-to-turn fault generation

In order to make it possible for changes to be made to the winding arrangement online (i.e. without stopping and isolating the motor from the supply) additional hardware was installed. This took the form of two Alstom MMLG-01 test blocks and two Alstom MMLB-01 multi-finger test plugs.

The test blocks were installed into a frame which supported the units above the test motor. The winding tappings were fitted with terminations using a crimping tool and then screwed into the terminals on the underside of the test blocks making careful note of the ordering. The test block chassis was then fitted with an earth connection for safety. The completed assembly is shown in Figure 8.3.

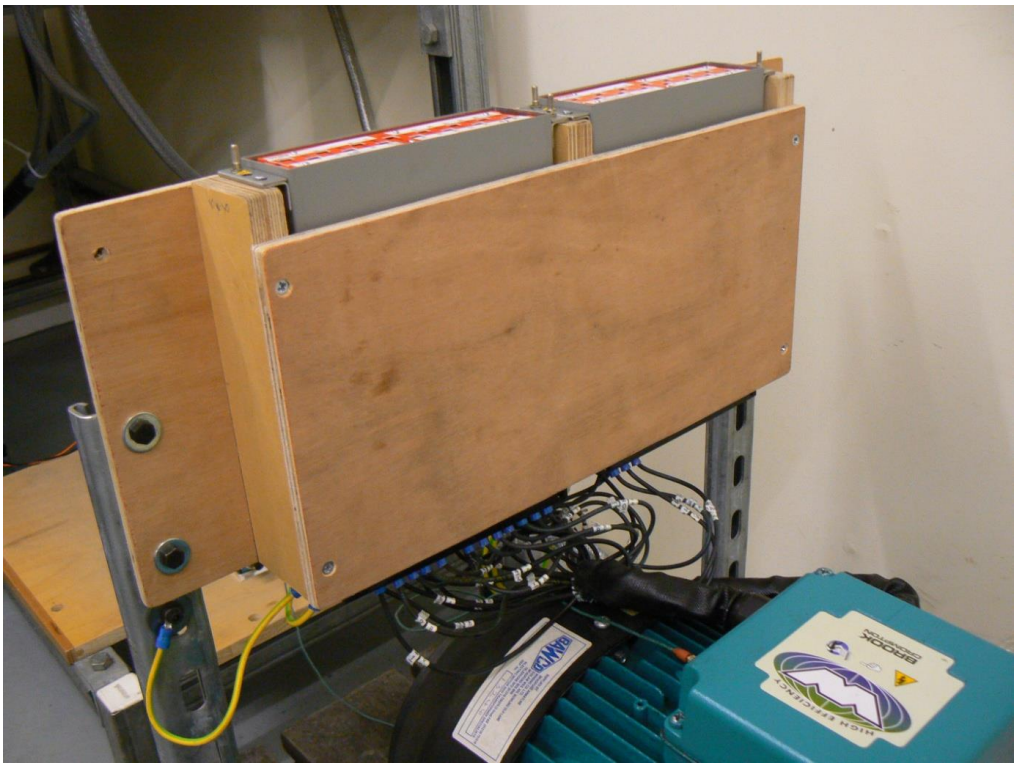

Figure 8.3 Test blocks and mount with screw terminal connection to stator tappings

In the configuration shown in the picture (no test blocks inserted) the winding contains no shorted turns. In order to introduce shorted turns a test block needs to be inserted.

The test block is shown in Figure 8.4 with a number of test leads inserted. By changing the connection of the test leads in the test plug the number of shorted turns can be varied. The finished arrangement with the test plugs inserted into the test blocks is shown in Figure 8.5.

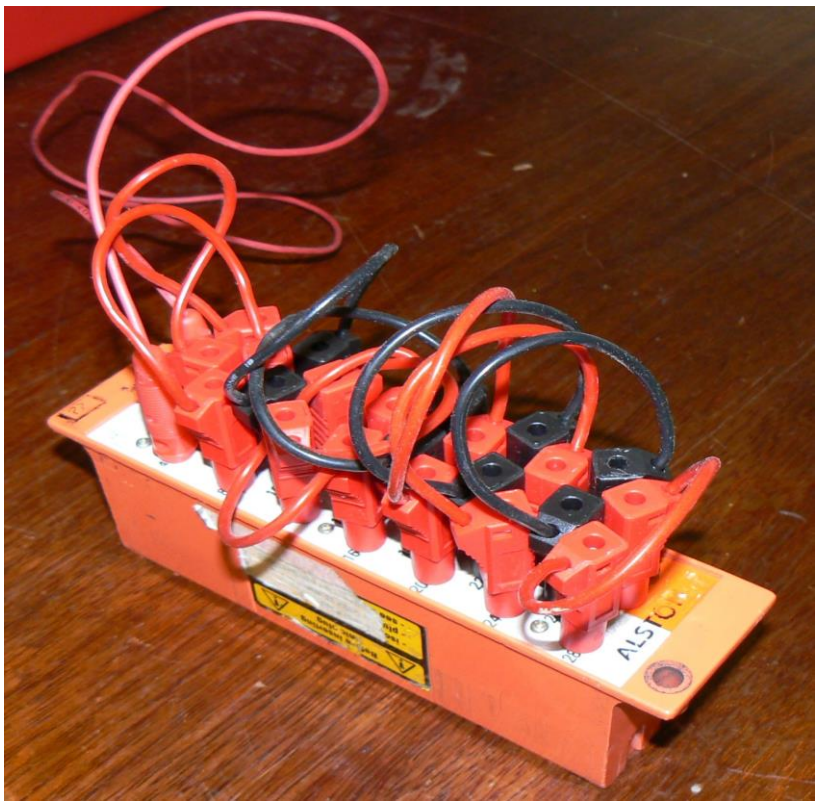

Figure 8.4 Alstom MMLB-01 test plug including test leads

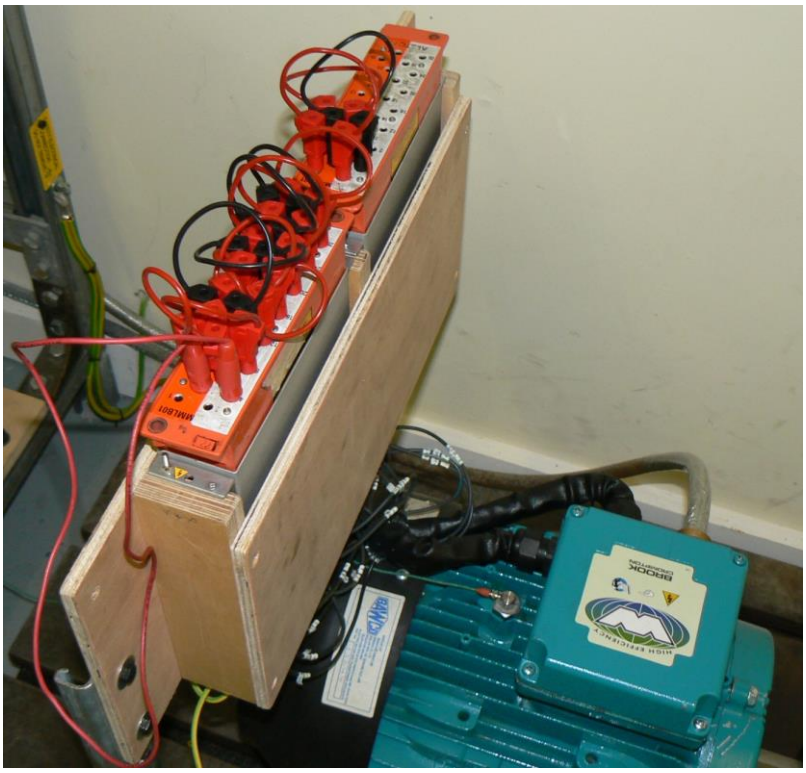

Figure 8.5 The completed stator short fault introduction hardware

8.5.2 Rotor fault creation

In order to re-create the broken rotor bar in the workshop the technique used was to remove portions of a single rotor bar using the pillar drill. Removal of part of the rotor bar material allows simulation of a developing rotor bar crack or a partial break. By removing the full cross-section of one rotor bar allows simulation of a full break i.e. no current can flow. A number of different gradations between these two conditions allow a synthetic re-creation of a propagating crack in the rotor bar. 2.5mm, 3.5mm, 4.5mm and 6mm drills were used to remove increasing amounts of one rotor bar with the 6mm drill-bit leading to a full bar break condition (i.e. the whole cross section of one bar was removed).

Figure 8.6 and Figure 8.7 show the 6mm hole drilled to remove the rotor bar from the rotor. The location of the rotor bars is determined by examining the rotor carefully for the tell-tale skewed lines on the surface of the rotor that indicate the positions of the bars beneath.

The drill depth was determined by drilling through the aluminium bars until steel swarf could be seen. This indicated that the drill had removed the entire aluminium rotor bar. The hole was drilled using a large pillar drill which allowed the rotor assembly to be securely clamped and accurate control of the drill angle and speed.

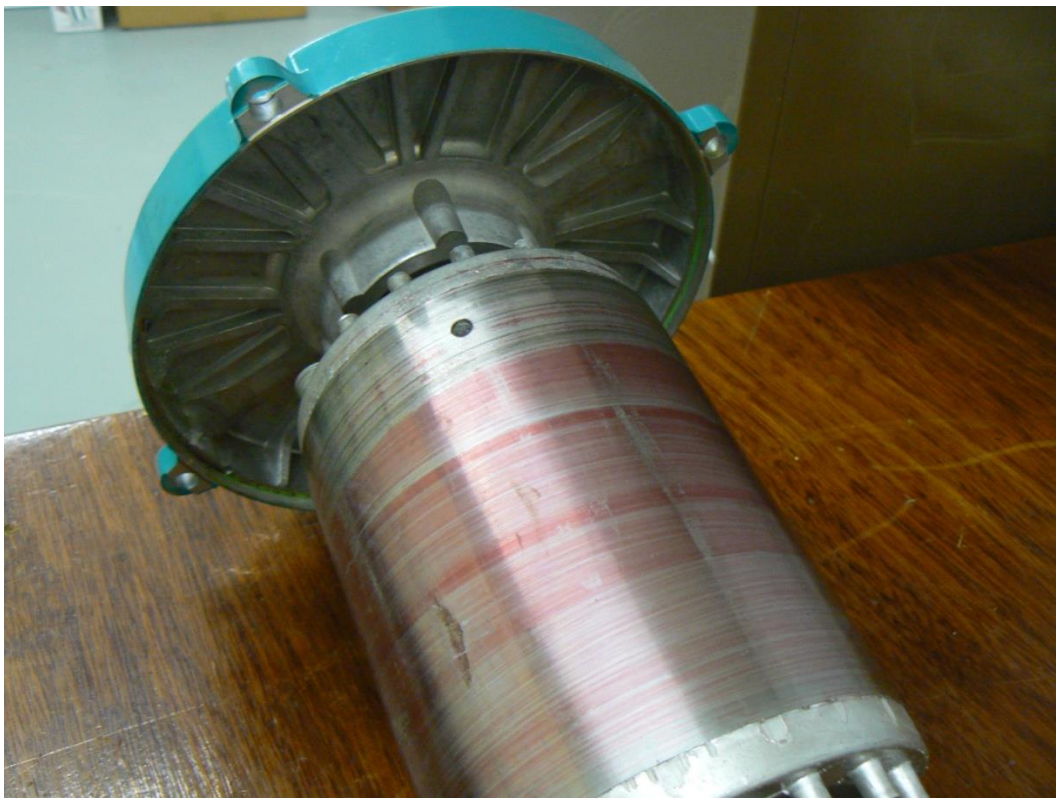

Figure 8.6 The rotor assembly (with end-plate) showing the location of the drilled rotor bar

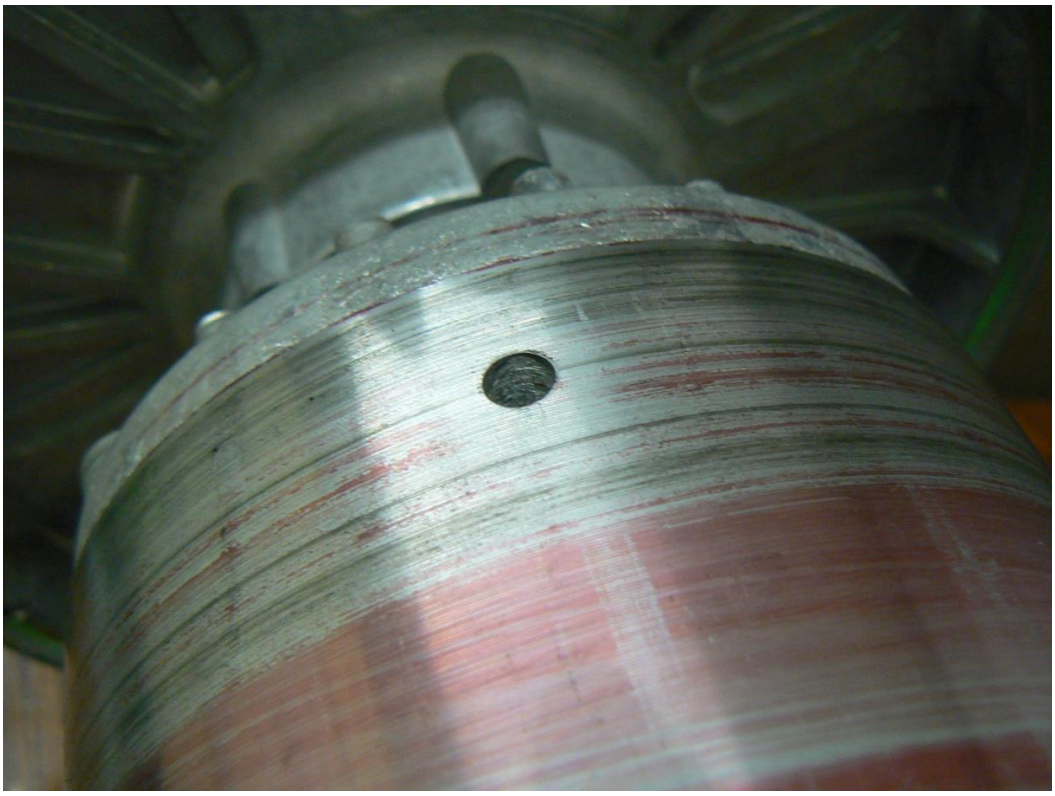

Figure 8.7 Close-up of the hole drilled to remove a section of a rotor bar

8.5.3 Air-gap fault (eccentricity) creation

Motor air-gap eccentricity can either be static (position of rotor axis is fixed) or dynamic (position of rotor axis is rotating), or a mixture of these two cases. When eccentricity reaches its limit (100%) the distance between rotor and stator is zero i.e. the rotator and stator are in physical contact.

In order to re-create an eccentric air-gap in the test motor the process used involved fitting eccentric collars to smaller profile bearings. Firstly, the standard size bearings from the rotor assembly are removed then a smaller bearing plus an internal and external collar are fitted to both the drive end (DE) and non-drive end (NDE) of the rotor shaft. The smaller bearings have a larger inner and a smaller outer diameter which allows fitting of the bearing collars.

The bearing collars are machined so that once the collars and new bearings are fitted they are the same size as the old bearing, thus fitting onto the shaft and into the end plates correctly. The location of the bearing collars for the drive-end bearings is shown in Figure 8.8. The non-drive end bearing collars are similarly located. The rings offset the bearings which in turn mean the rotor shaft is offset making the air-gap eccentric.

If the inner ring fitted to the bearing is eccentric then the air-gap will have dynamic eccentricity. If the outer ring fitted to the bearing is eccentric then the motor will have static eccentricity. If both inner and outer rings fitted to the bearing are eccentric the motor will have mixed eccentricity.

Four eccentric and four concentric rings were created on the lathe to allow the three types of eccentricity to be created. The eccentric rings and bearings can be seen in Figure 8.9.

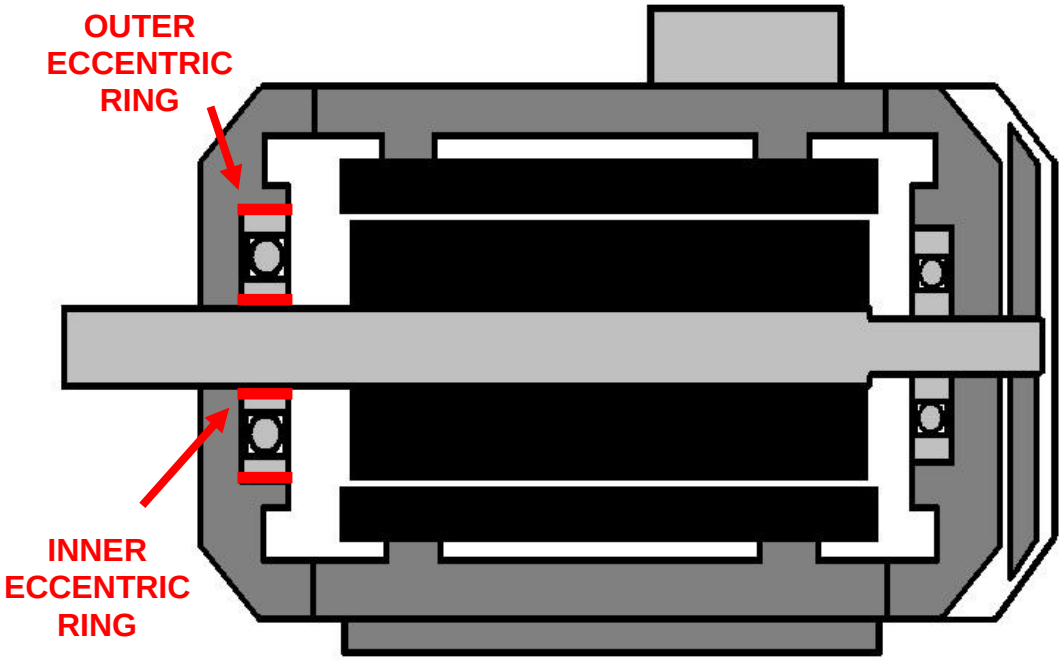

Figure 8.8 Motor cross-section showing position of eccentric rings (NDE would have the same arrangement but is not shown)

Figure 8.9 Exploded view of the bearings and eccentric rings to be fitted.

The eccentric rings were then measured using a coordinate measuring machine (CMM) to verify the level of eccentricity. The results are shown in Table 8.1. The level of air gap eccentricity is equal to twice the value of the ‘d’ parameter (shown in red). Combining eccentric values for all four rings across the motor and averaging gives the following approximate values:

- 46% dynamic eccentricity
- 39% static eccentricity
- 85% mixed eccentricity

The air-gap width as given by the manufacturers is 0.45mm, which leads to the maximum air-gap variation to be:

- 0.207mm (dynamic)
- 0.1755mm (static)
- 0.3825mm (mixed eccentricity)

These faults are of significant magnitude but could not be reduced due to manufacturing tolerances of the machining techniques used to create the eccentric rings. Unfortunately due to the manufacturing and assembly methods used to create the eccentric collars there were variations in the roundness (or ‘form’) of the units when fitted to the bearings meaning that the minimum air-gap in places was decreased further. In addition to this up to 10% variation in air-gap due to manufacturing tolerances which can be expected. This led to the mixed eccentric case being over 100% eccentricity and rotor and stator touching – the mixed eccentricity case could not be used for testing[1]. The other

[1] The mixed eccentricity case is the most severe case of eccentric fault therefore if the milder static and dynamic cases can be detected then detection of the mixed case should be expected.

cases can be considered to be approximately 40% eccentricity (but could vary by as much as 15%).

Part ID	X coord outer	Y coord outer	Dia outer	Form outer	X coord inner	Y coord inner	Dia inner	Form Inner	Concent-ricity	d
H1	-120.878	-48.796	79.951	0.017	-120.840	-48.808	75.026	0.029	0.080	*3.98*
H1	-120.878	-48.796	79.953	0.023	-120.803	-48.803	75.027	0.036	0.079	*7.53*
H1	-120.877	-48.798	79.952	0.011	-120.835	-48.806	75.031	0.039	0.086	*4.28*
H1-Av	***-120.878***	***-48.797***	***79.952***	***0.017***	***-120.826***	***-48.806***	***75.028***	***0.035***	***0.082***	***5.24***
H2	-87.237	2.164	62.001	0.017	-87.246	2.150	55.089	0.013	0.034	*1.66*
H2	-87.237	2.166	62.003	0.015	-87.244	2.152	55.090	0.020	0.031	*1.57*
H2	-87.237	2.163	62.002	0.014	-87.245	2.148	55.089	0.016	0.034	*1.70*
H2-Av	***-87.237***	***2.164***	***62.002***	***0.015***	***-87.245***	***2.150***	***55.089***	***0.016***	***0.033***	***1.64***
H3	-75.308	3.264	44.996	0.016	-75.342	3.313	39.999	0.023	0.120	*5.96*
H3	-75.307	3.261	44.995	0.018	-75.341	3.312	40.000	0.019	0.123	*6.13*
H3	-75.308	3.261	44.993	0.016	-75.34	3.315	40.002	0.028	0.126	*6.28*
H3-Av	***-75.308***	***3.262***	***44.995***	***0.017***	***-75.341***	***3.313***	***40.000***	***0.023***	***0.123***	***6.12***
H4	-72.802	2.147	29.989	0.014	-72.815	2.132	25.009	0.015	0.039	*1.98*
H4	-72.801	2.143	29.992	0.015	-72.814	2.131	25.012	0.019	0.035	*1.77*
H4	-72.802	2.141	29.991	0.017	-72.816	2.131	25.013	0.02	0.036	*1.72*
H4-Av	***-72.802***	***2.144***	***29.991***	***0.015***	***-72.815***	***2.131***	***25.011***	***0.018***	***0.037***	***1.82***
E1	-120.496	-49.276	79.982	0.017	-120.501	-49.38	75.041	0.041	0.209	*10.41*
E1	-120.494	-49.279	79.976	0.022	-120.499	-49.378	75.038	0.046	0.198	*9.91*
E1	-120.497	-49.276	79.977	0.026	-120.499	-49.376	75.036	0.036	0.201	*10.00*
E1-Av	***-120.496***	***-49.277***	***79.978***	***0.022***	***-120.500***	***-49.378***	***75.038***	***0.041***	***0.203***	***10.11***
E2	-62.424	-6.474	62.003	0.018	-62.28	-6.326	55.031	0.026	0.413	*20.65*
E2	-62.426	-6.472	62.001	0.011	-62.285	-6.318	55.03	0.0028	0.418	*20.88*
E2	-62.425	-6.468	62.001	0.013	-62.284	-6.317	55.029	0.021	0.411	*20.66*
E2-Av	***-62.425***	***-6.471***	***62.002***	***0.014***	***-62.283***	***-6.320***	***55.030***	***0.017***	***0.414***	***20.73***
E3	-59.075	-10.01	44.981	0.035	-59.076	-10.193	39.997	0.029	0.366	*18.30*
E3	-59.072	-10.013	44.979	0.041	-59.077	-10.194	40	0.035	0.363	*18.11*
E3	-59.074	-10.008	44.979	0.036	-59.078	-10.191	40.001	0.042	0.367	*18.30*
E3-Av	***-59.074***	***-10.010***	***44.980***	***0.037***	***-59.077***	***-10.193***	***39.999***	***0.035***	***0.365***	***18.24***
E4	-58.499	-8.961	29.979	0.012	-58.495	-8.753	25.007	0.019	0.416	*20.80*
E4	-58.498	-8.962	29.979	0.018	-58.496	-8.75	25.009	0.007	0.423	*21.20*
E4	-58.5	-8.961	29.979	0.015	-58.495	-8.752	25.009	0.007	0.418	*20.91*
E4-Av	***-58.499***	***-8.961***	***29.979***	***0.015***	***-58.495***	***-8.752***	***25.008***	***0.011***	***0.419***	***20.97***

Table 8.1 Dimensions and calculated features of the eccentric rings

8.5.4 Bearing fault creation

Two bearing fault types were created for testing purposes, these were; the generalised roughness fault and the point fault.

The generalised roughness fault is intended to mimic the overall increase in wear of a bearing which could be due to any number of the factors described in the literature review. There is no single failure (e.g. a pit in the race) but just a general wear of the bearing contact surfaces.

This fault was re-created in the workshop by adding an abrasive substance to the bearing. Firstly, the bearing shields were removed then the grease was removed from the bearing using petrol and carburettor cleaner. Once the bearings were clean they were allowed to fully dry. 5 grams of ‘Carborundum’ (Silicon Carbide) valve grinding compound was then applied to the bearing ensuring good coverage of inner and outer race surface. The bearing was then turned on a lathe for a period of 10, 20, 30, 40 or 50 minutes, cleaned out, packed with the correct quantity of new grease and re-fitted to the motor. Figure 8.10 shows the effect of the abrasive past on the outer race of the bearing. The dull portions of the race indicate the wear due to the abrasive action of the contaminant.

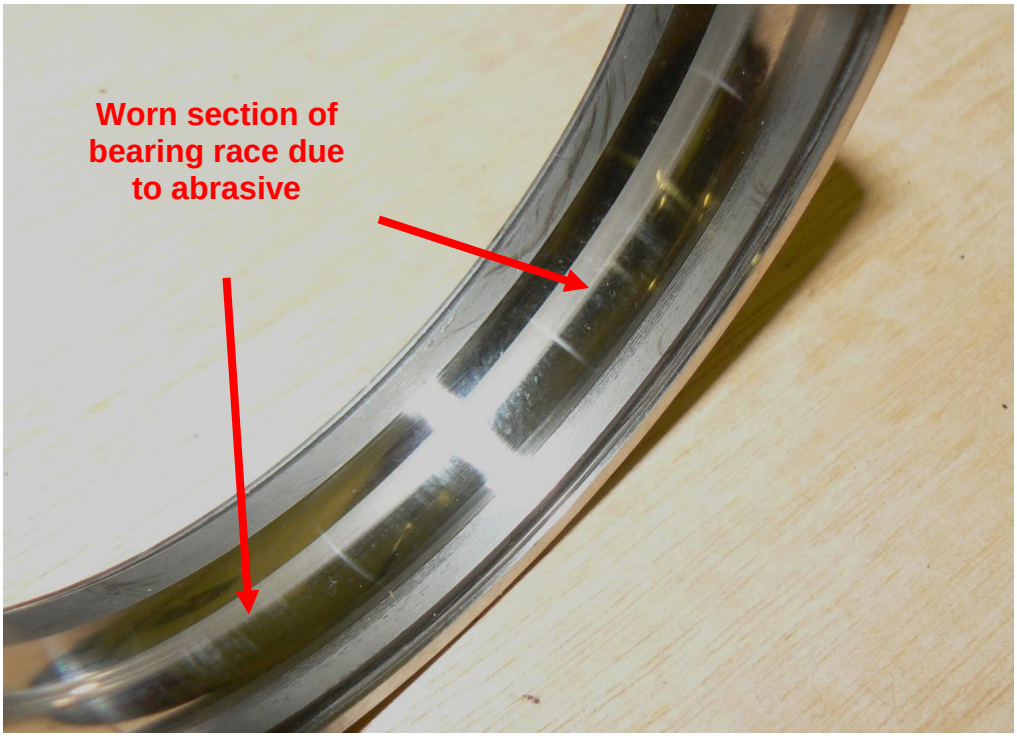

Figure 8.10 Outer race wear following the abrasive test. The dull section indicates the contact path of the rolling element which causes mild surface wear.

For the point defect (pitting fault) a small groove was created in the outer race of the bearing. The groove was created by using an electric erosion machine. A special tip is created to erode a small groove in the bearing outer race. The tip erodes through the bearing from the outside until the groove appears on the race.

There were two groove widths created:

- 0.5mm width
- 1.5mm width

External and internal photographs of the 0.5mm point fault are shown in Figure 8.11 and Figure 8.12 respectively.

These artificial faults attempt to re-create a serious spall or pit in the outer race. The reason a groove was used rather than a hole was to ensure that as the

bearing rotated the rolling elements would always hit the defect. The bearing contact point will not necessarily be in the centre of the race (particularly with the small pre-load applied from the wave-washer in the end-plate and the fact that as the rotor heats up as it expands during operation). With a groove, even if the contact point is off-centre the rolling element will still hit the defect.

8.6 Summary

This chapter has described the most prevalent faults that can occur in the induction motor and how these faults were artificially recreated in the workshop environment.

Figure 8.11 0.5mm bearing groove viewed from outside bearing (groove passes all the way through the bearing outer ring to the outer race)

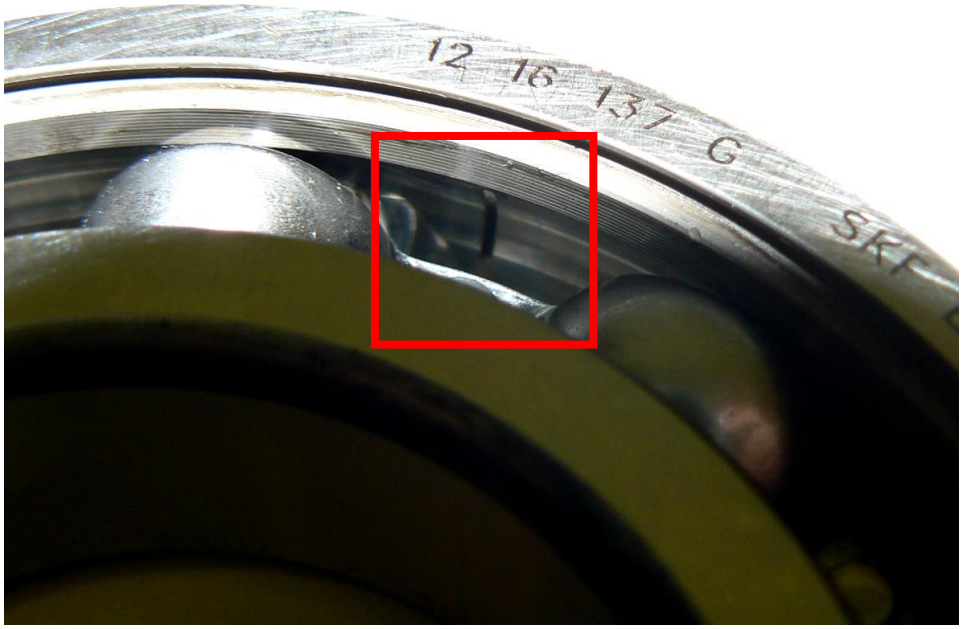

Figure 8.12 A photograph of the 0.5mm bearing fault. The groove can be clearly seen on the outer race of the bearing.

Chapter 9. Fault Detection Methods

This section describes the fault detection methods developed as part of this project. The fault detection methods aim to produce features which are sensitive to one or more faults. These features can then be analysed by some form of diagnosis algorithm (see Chapter 10) to identify the specific type of fault and the fault severity. The chapter is split into two sections: firstly the model-based fault detection methods (used for stator and rotor faults) are explained followed by the model-free or spectral methods (used for air-gap and bearing faults).

9.1 Model-based fault detection

The stator and rotor fault residuals are developed using model-based parameter estimation techniques. These techniques utilise the fault models of the rotor and stator developed in section 3.3. The details of the models will not be reproduced here but rather a description of the model inputs and outputs and how these are used to develop a useful fault detection feature are described here.

Objective functions were created for both the rotor and stator faults. These objective functions are designed to output a value which indicates the goodness of fit of a specific model configuration. The model configuration is altered by varying one parameter; for the rotor case the rotor fault parameter is varied for the stator case the stator fault parameter is varied. The objective function is then repeatedly ‘called’ by an optimiser as part of an iterative process in order to ascertain the optimum fault parameter value for a specific dataset.

The optimiser used for both faults was the ‘fminsearch’ MATLAB function which utilises a Nelder-Mead algorithm. fminsearch is a nonlinear multidimensional

minimiser which was trialled for the basic parameter estimation described in the parameter estimation chapter. The reason the Nelder-Mead algorithm can be successfully used here but not in the basic parameter estimation case is for two reasons. Firstly, for fault parameter estimation the solutions should not be multi-modal which means if a local solution is found then it is the global solution. Secondly, the initial parameter estimate is very close to final solution; incipient faults develop slowly over time therefore only very small changes need to be tracked for fault estimation which makes local-search techniques permissible.

The PSO algorithm used in the basic parameter estimation could be used again here but Nelder-mead is preferred since it can converge on the solution much quicker than the stochastic PSO optimiser.

In order for the rotor and stator fault parameter detection methods to be responsive the objective functions must be focused on specific features in the simulated and measured currents which contain information in relation to that fault.

9.1.1 Rotor fault detection

The rotor fault objective function utilises parts of the current spectrum directly adjacent to the fundamental frequency since these regions are known to contain information relating to rotor faults [39]. The rotor fault objective function will be described in detail below.

Rotor faults will produce characteristic sidebands around the fundamental frequency according to the following equation:

$$f_{rotor} = f_s \pm 2sf_s \tag{9.1}$$

where

f_{rotor}	Rotor fault characteristic frequency (Hz)
s	Slip
f_s	Shaft rotational frequency (Hz)

Therefore, using an estimate of the shaft rotational speed approximate values for the rotor fault characteristic frequencies can be calculated. This value is then used to set up two search regions in the motor current spectrum (for the plus and minus components) and each of these frequency bands is searched for the peak value. The peak value found for the measured and simulated current spectra are then compared and this difference is the value which is output by the objective function. A graphical representation of this process is shown in Figure 9.1 with the detection limits for the search band based on equation (***9.1***) clearly shown (the frequency spike at approximately 46.25Hz is rotor fault dependent).

The peak value within this band for both upper and lower fault frequencies (*Rfault*) is found for the simulated and measured data:

$$\mathrm{Rfault}_1 = \mathrm{SBP}_{\mathrm{line-1U}} + \mathrm{SBP}_{\mathrm{line-1L}} \tag{9.2}$$

where

$Rfault_1$	Rotor fault value, line 1
$SBP_{line-1U}$	Sideband peak value, line 1, upper sideband
$SBP_{line-1L}$	Sideband peak value, line 1, lower sideband

The measured and simulated *Rfault* values are then compared (on each phase) and this value is summed across the phases to give the *Rfault* residual:

$$\mathrm{RF}_{\mathrm{res}} = \sum_{\mathrm{i=1}}^{3} (\mathrm{Rfault}_{\mathrm{i-sim}} - \mathrm{Rfault}_{\mathrm{i-mes}})^2 \tag{9.3}$$

where

RF_{res}	Rotor fault residual (simulated vs. measured error)

The objective function value drives the optimisation toward an optimum value of the model rotor fault parameter, $deltaR$. The optimum $deltaR$ value results in the value of $\mathrm{RF}_{\mathrm{res}}$ being minimised.

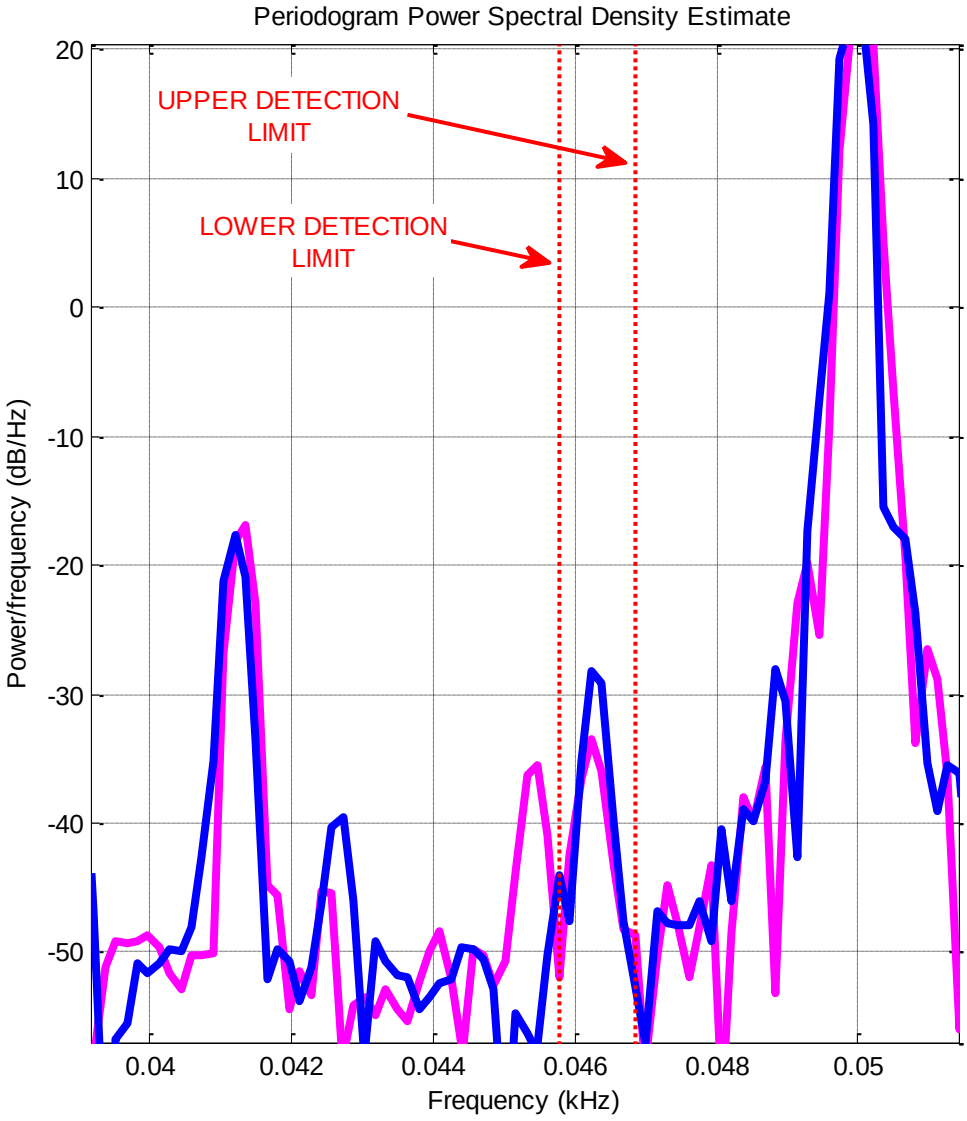

Figure 9.1 Rotor objective function feature detection

Figure 9.2 shows the rotor fault parameter estimates for several test cases with varying degrees of rotor bar damage. Damage to the rotor is replicated by removing increasing amounts of a single rotor bar via drilling (see chapter 8) – this artificially mimics a crack propagating across the rotor bar. The figure shows that the parameter estimation technique successfully detects an increase

in the resistance of the rotor bar (*deltaR*) as more of the rotor bar is removed. The fault value increases from less than 0.01 in the healthy case up to 0.2 in the case of the full rotor bar cross-section being removed.

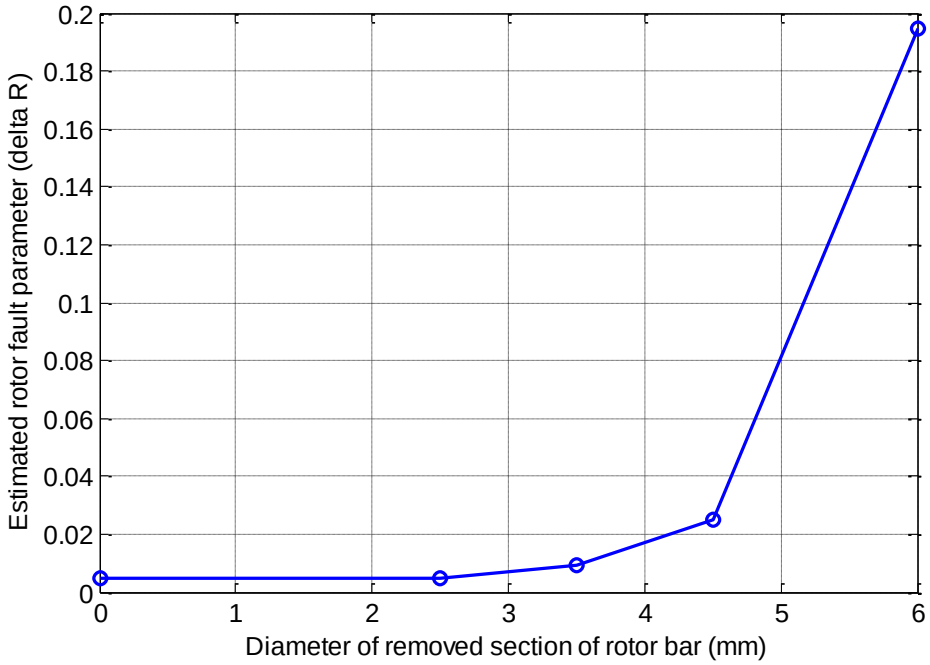

Figure 9.2 Estimated rotor fault parameter plotted against section of rotor bar removed

9.1.2 Stator fault detection

Stator fault detection utilises the same optimiser and minimisation process as the rotor fault but requires a different objective function. The objective function used for stator fault detection process involves simply comparing the samples from the measured data current waveforms with the simulated data points generated by the stator fault model. Since the stator fault can occur on any of the three stator windings the fault has to be simulated on all three windings which results in three fault residuals (one for each phase winding). The model parameter adjusted to minimise the stator fault value is the percentage of shorted turns on a given winding.

The equation used to generate the *Sfault* value is as follows:

$$\mathrm{Sfault} = \sum_{\mathrm{p=1}}^{3} \sum_{\mathrm{t=0}}^{\mathrm{t=n}} \left(\mathrm{i}_{\mathrm{(p,t)-sim}} - \mathrm{i}_{\mathrm{(p,t)-mes}}\right)^2 \qquad (9.4)$$

where $i_{(p,t)-sim}$ t^{th} sample of the simulated current on phase p
$i_{(p,t)-mes}$ t^{th} sample of the measured current on phase p

The phase order of the currents passed to the model is then modified and the process repeated (this effectively simulates the fault occurring on a different phase). Once this has been carried out three times, a value for the percentage of shorted turns on each of the motor windings has been estimated.

Figure 9.3 shows the results of the stator fault detection via parameter estimation. The figure demonstrates that as the motor operates with increasing numbers of shorted turns the estimated fault parameter (percentage of turns shorted) increases. The relationship between the two is approximately linear.

Initially the estimated value is negative; this is caused by an increase in resistance due to the additional wiring required to create the stator tapping modifications and would not be present in reality. The problem is due to the fact that when creating the custom stator winding a large amount of additional wiring is required to bring each turn out of the stator housing and to a connection box. This additional wiring adds to the impedance of the phase. As the test progresses, increasing numbers of turns are shorted out from that phase. Therefore, the machine becomes more balanced (cancellation of additional resistance) before it becomes less balanced (effect of shorted turns). Figure 9.4 describes this trend.

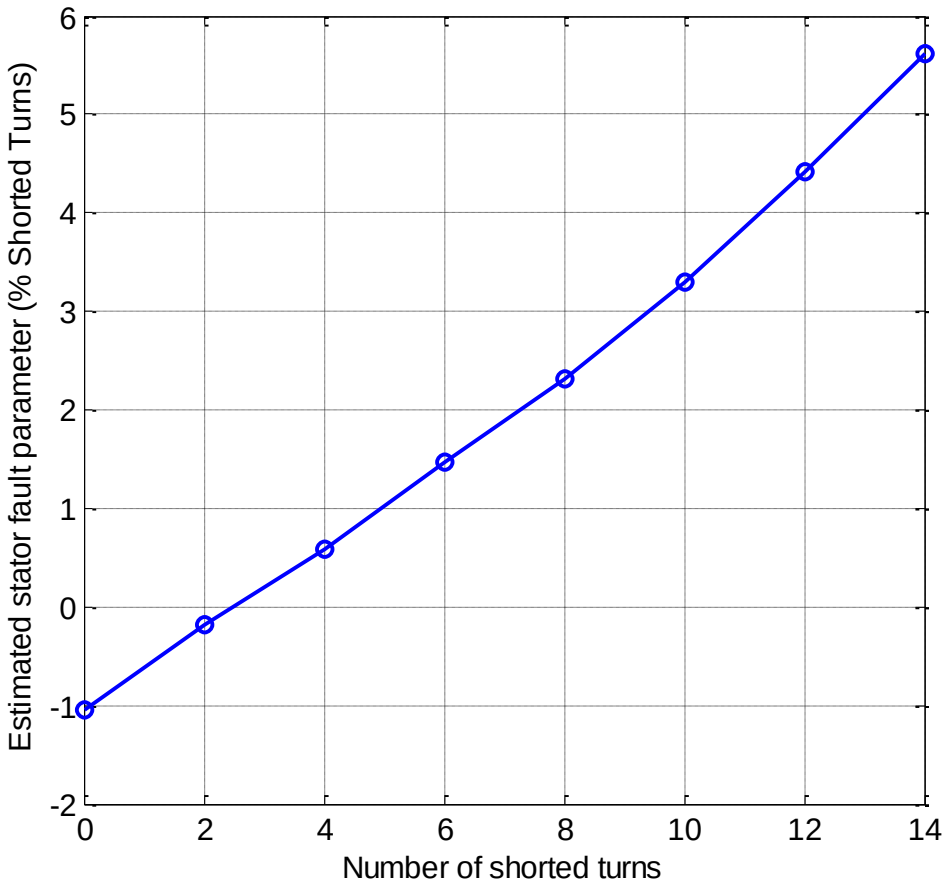

Figure 9.3 A plot of estimated stator fault parameter versus the number of shorted turns on phase A.

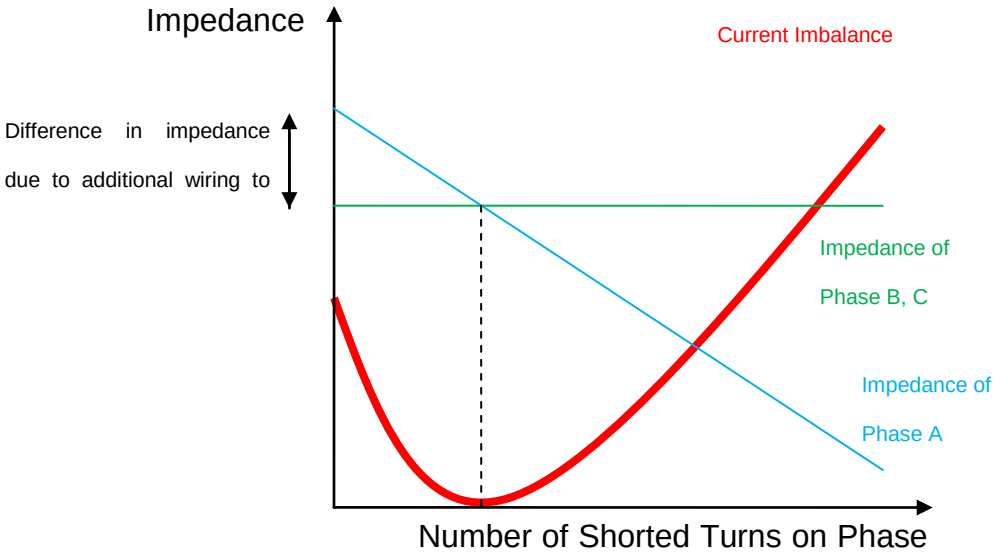

Figure 9.4 Impedance variations due to custom stator winding (tappings)

After four shorted turns there is a small increase in current imbalance (after tapping impedance has been cancelled out).

The problem with the initial impedance increases due to the test methodology would not be present in reality and is therefore not a significant issue. The strong correlation between the actual value of shorted turns and the estimated value (Figure 9.3) indicates that the model based stator fault detection method will be suitable for the condition monitoring system.

9.2 Model-free fault detection

Due to the nature of the problem some aspects of the induction motor prove too difficult to model without a detailed knowledge of the machine construction. For a bearing fault to be modelled, knowledge of the machine operating speed, inner race diameter, outer race diameter, ball diameter and number of balls is required to model the impact frequencies [35]. Additionally if eccentricity is to be modelled, knowledge of the machine winding layout is required (number of coils, coil distribution/overlap, turns per coil, etc) [2,3]. These additional parameters make this type of fault unsuitable for a model-based parameter estimation fault detection technique. To overcome this issue some of the induction motor faults will be detected by other means, i.e. without explicit mathematical modelling of the faults. In this project a wideband total spectral energy method and also speed-based spectral method are developed. Both of these techniques involve converting the time domain data into frequency domain in order to generate more information pertaining to machine condition.

9.2.1 Air-gap fault detection

MCSA will be used to detect the eccentric air-gap faults. In order to detect increases in static or dynamic eccentricity, supply frequency sidebands (offset

by the rotational speed of the machine) can be used. An increase in the energy of these sidebands indicates an increase in the overall level of eccentricity (static combined with dynamic). The frequencies of interest are given by:

$$\mathrm{fecc} = \mathrm{f_s} \pm (\mathrm{kfr}) \tag{9.5}$$

where k 1, 2, 3, ...
$fecc$ Air-gap eccentricity frequency components
f_s Fundamental supply frequency
fr Rotational frequency of motor shaft

Figure 9.5 describes the process used to estimate the eccentric fault level.

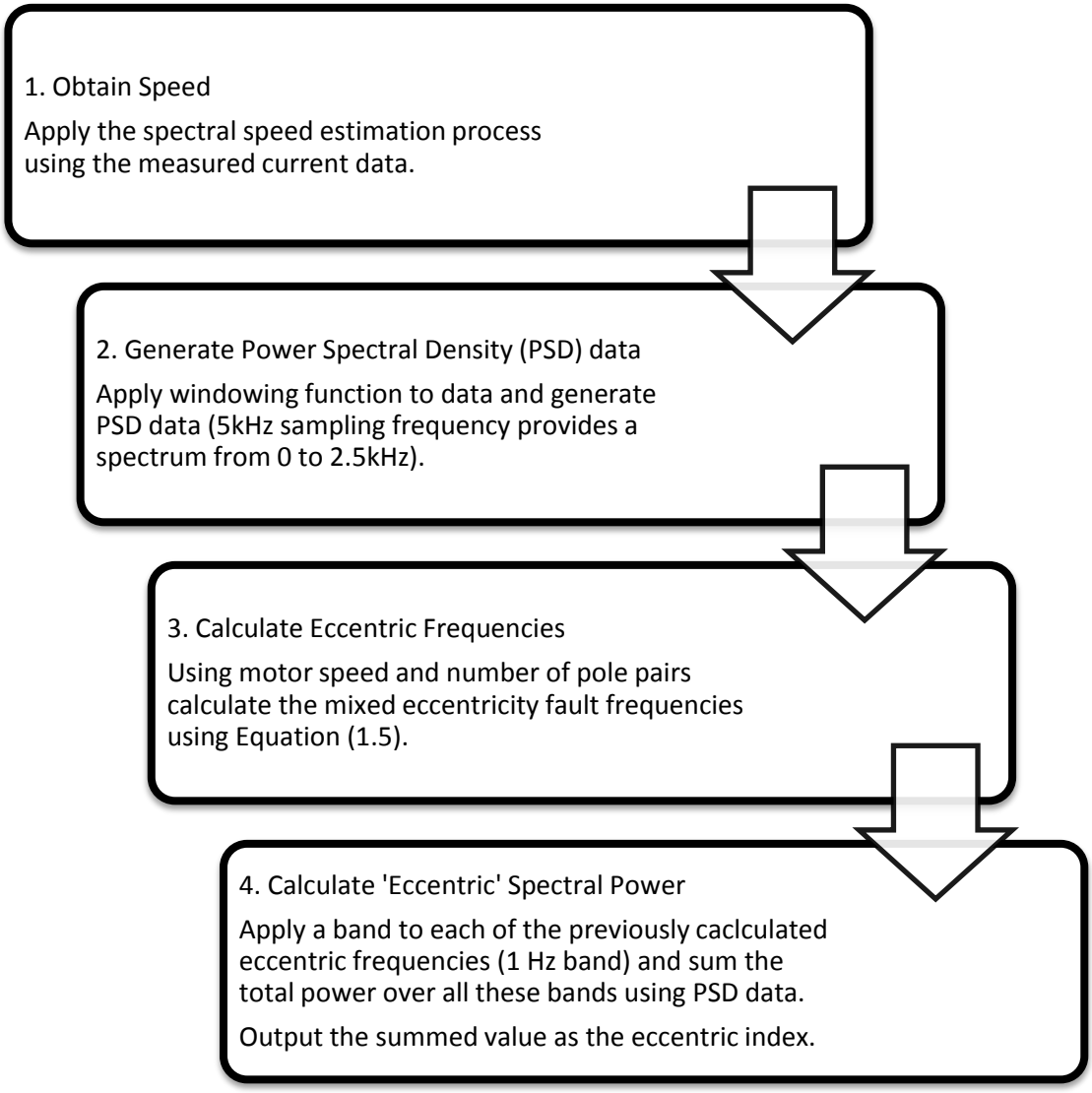

Figure 9.5 Flow chart for eccentric fault level estimation

The process utilises the estimated speed and the measured current data to search through the spectrum for the characteristic air-gap eccentricity fault frequencies. In order to account for any slight errors in the estimated speed a tolerance band is used around each one of these frequencies. This eliminates the need for the speed estimate to be accurate to within fractions of an rpm.

An example of the eccentric air-gap fault frequencies can be found in Figure 9.6. The data recorded with approximately 40% eccentric air-gap (static) shows a clear increase in energy around 26Hz and 74hz – these values are calculated based on equation (9.5). These frequencies will be targeted by the air-gap fault detection algorithm and the increase in energy over the targeted frequency bands indicates a fault is present.

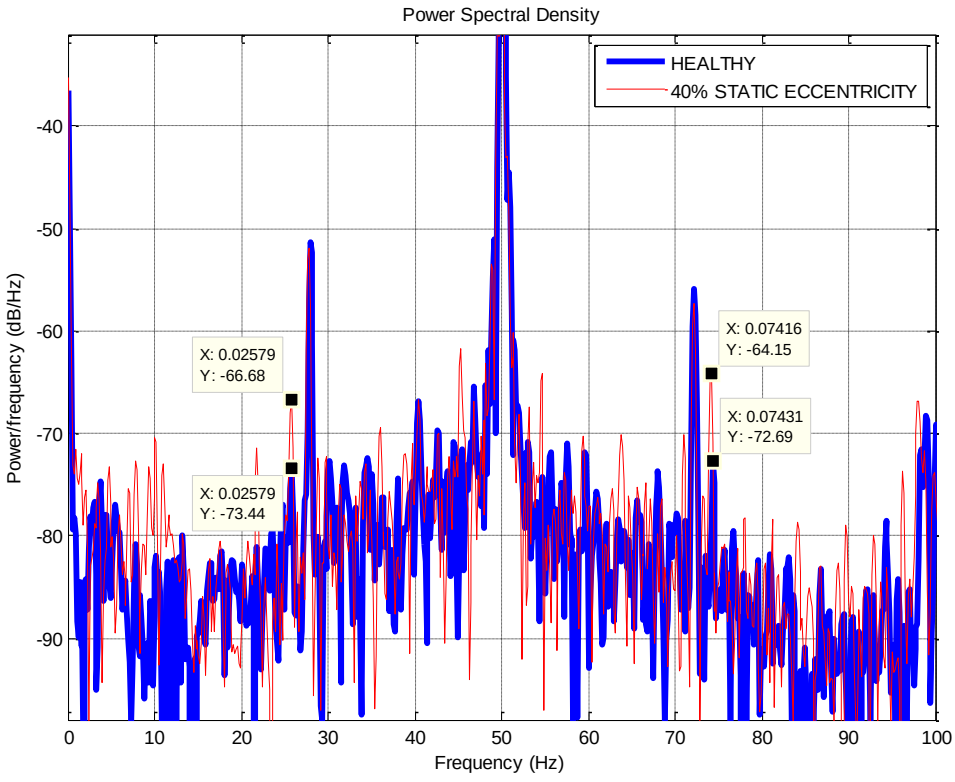

Figure 9.6 Experimental current data of a healthy motor and a motor containing 40% static eccentricity

The results from the airgap fault detection method described above are presented in Figure 9.7 and Table 9.1. Calculated values are shown for both bellows and belt coupled motor tests with positive values indicating an increase in the fault indicator value for the faulty case (i.e. fault detected) and negative values indicating a decrease in the fault indicator value (i.e. fault is not detected) when compared to the healthy baseline value. The upper bar in each pair represents the 40% static eccentricity (SE) case, the lower bar the 40% dynamic eccentricity (DE) case.

The figure indicates that in the majority of cases the eccentric air-gap faults are successfully detected. For the belt coupled data two out of eight of the cases the fault was not detected. This is due to belt vibration frequencies which at this specific load/speed mask the fault frequencies due to both frequency components overlapping. When the fault frequencies overlap non-fault related content can be misclassified as a fault. This problem is a failing of MCSA since the content of the spectrum will differ depending on the motor application, coupling, load and supply conditions so a noise-free spectrum cannot be guaranteed.

In general, the majority of fault frequency will not be masked by other frequency content (fourteen out of sixteen examples in the dataset were not) however in the cases where they are, the algorithm will lose the ability to detect very low level faults. The system will still detect the fault when it becomes more serious since the size of the fault frequency will continue to increase in magnitude.

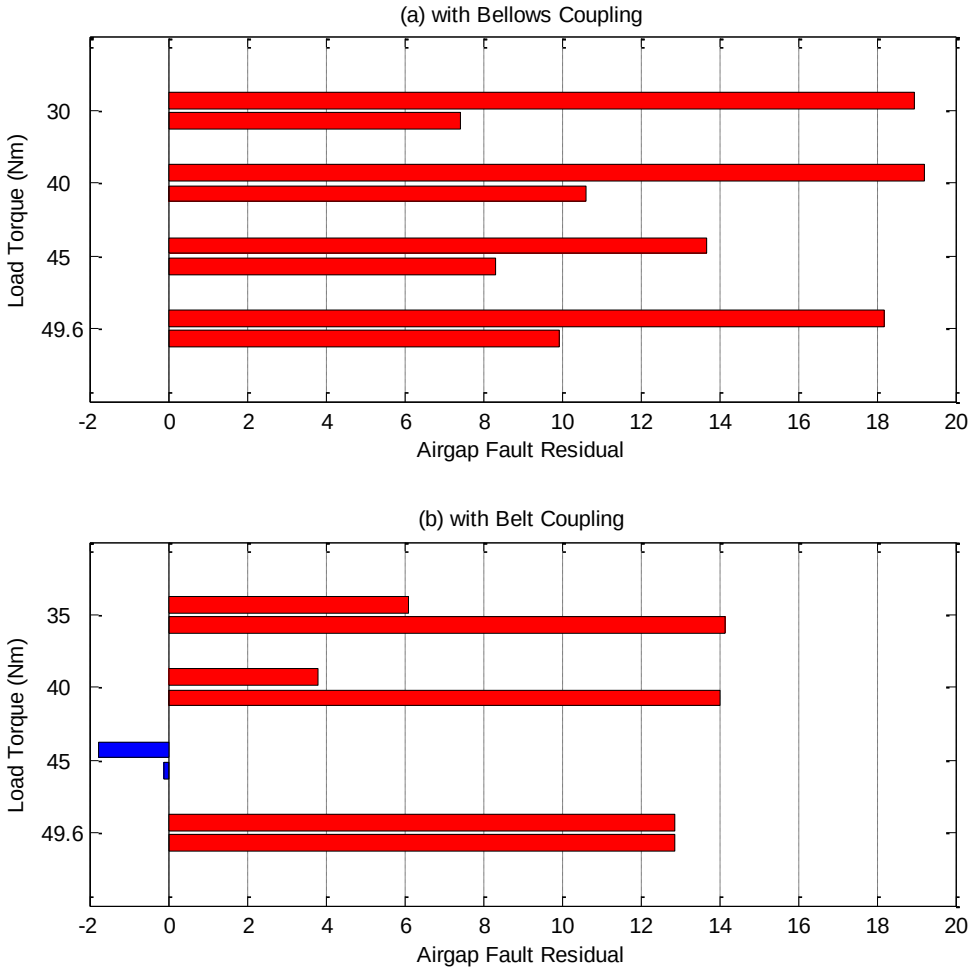

Figure 9.7 Airgap fault indicator residual values (positive values indicate successful fault detection, negative values indicate no fault detected)

Table 9.1 Airgap fault eccentric fault indiactor values and residuals (highlighted 'Del' values indicate correct diagnosis)

Coupling	Load (Nm)	H	SE	**SE Del**	DE	**DE Del**
Belt	50	-74.44	-61.549	**-12.891**	-61.5873	**-12.8526**
	45	-52.7976	-52.9065	**0.108915**	-54.3252	**1.527597**
	40	-72.3701	-58.3548	**-14.0153**	-68.5615	**-3.80866**
	35	-71.8688	-57.7236	**-14.1453**	-65.768	**-6.10079**
	30	-68.7562	-56.4699	**-12.2863**	-61.7188	**-7.03736**
Bellows	50	-75.1291	-65.2078	**-9.9213**	-56.9438	**-18.1853**
	45	-73.4604	-64.9864	**-8.47399**	-59.6185	**-13.8419**
	40	-72.7329	-64.2038	**-8.52914**	-53.442	**-19.2909**
	35	-72.6358	-62.0146	**-10.6213**	-53.442	**-19.1938**
	30	-68.6748	-61.2557	**-7.41916**	-49.7163	**-18.9585**

9.2.2 Bearing fault detection

Many methods used for bearing fault detection involve detecting characteristic fault frequencies in the stator current [79]. When the defects on the race and rolling elements are on the contact surface inside the bearing there is an impact which causes the rotor assembly to change position within the air-gap (because it is supported by the bearings). In addition to this there is a small deviation in the equivalent load torque as the defect passes the contact surface (e.g. the rolling element passing over a small pit or spall on the inner or outer race).

This movement and momentary torque change occurs when a fault on one of the bearing surface is encountered. Both the change in torque and the change in air-gap have an effect on the flux linkages of the machine which allows these small impacts to be detected by examining the IM line currents.

The aforementioned bearing faults are known as point defect faults. In addition to point defects there is another type of bearing fault that can occur known as a ‘generalised roughness’ fault. These faults have seen minimal research interest but are thought to represent a significant proportion of faults found in industry. Generalised roughness faults produce no specific localised damage and therefore no specific characteristic fault frequency; the fault manifests itself as an unpredictable broadband change in machine vibration [138].

machine vibration causes minute changes in the air-gap width which in turn influence the flux and current within the machine thus by tracking the current spectral content the effect of a general or localised bearing fault should be detectable. If the total value of energy in the measured current spectrum is tracked then the increase in this energy due to both localised *and* generalised bearing faults can be monitored and used to differentiate between a healthy and

a deteriorating bearing. This process is similar to the Mean Spectral Deviation method demonstrated in [133].

This provides a value linked to the energy across the spectrum and considers the energy on each of the phases. In theory, any change in the bearing condition will modify the measured spectral energy either by a broadband ‘noise’ level change or presence of increases at specific fault frequencies.

The Spectral Energy Analyser (SEA) process is as follows:

1. Import the sampled signals for
    a. Line Current on Phase A
    b. Line Current on Phase B
    c. Line Current on Phase C
2. For each of the imported signals:
    a. Apply a windowing function to the sampled data (Hanning)
    b. Calculate the FFT of the data
    c. Calculate the energy per point of the FFT
    d. Convert the energy to decibel form
    e. Sum the energy in decibel form across the whole spectrum (0 → Fs/2)
    f. Reduce by a factor of 1000 (to make numbers easier to handle/interpret)
3. Add the value to the total spectral energy value
4. Normalise the current spectral energy against voltage spectral energy (found using the same approach) to account for changes in supply conditions
5. Repeat for all phases and sum together

This provides a value linked to the energy across the whole spectrum and considering each of the phases. In theory, any change in the bearing condition will be detectable in the spectrum. Using this method the location (inner race, outer race, train or rolling element) does not need to be known.

The results of this approach can now be analysed. Figure 9.8 and Table 9.2 show the fault indicator residuals (difference between healthy and faulty cases) for the bearing fault detection method. The 1.5mm outer race fault, 0.5mm outer race fault and abrasive contamination fault (generalised roughness) are represented by the upper, middle and lower bars respectively.

The 1.5mm (serious bearing fault) fault is detected reliably in each case however in some cases the abrasive contamination fault and the 0.5mm fault are sometimes misclassified. These faults are of a low magnitude and thus more difficult to detect than the serious bearing fault (1.5mm). The small scale faults are difficult detect due to a number of factors including inconsistent motor strip-down and rebuild process, motor test-bed installation, presence of other faults (e.g. misalignment) and variations in supply conditions. Since a small scale bearing fault (69% detection rate for this dataset) will eventually develop into a serious fault (100% detection rate) the fault will be detected after a given time period. In addition to this, a trending function in the diagnosis system would improve the ability of a fault detection system to pick up small scale incipient faults since the absolute value and the trend over time provide more information on whether a fault is developing or simply high variability is being observed.

Overall the fault detection method performs well with a high proportion of fault cases successfully detected.

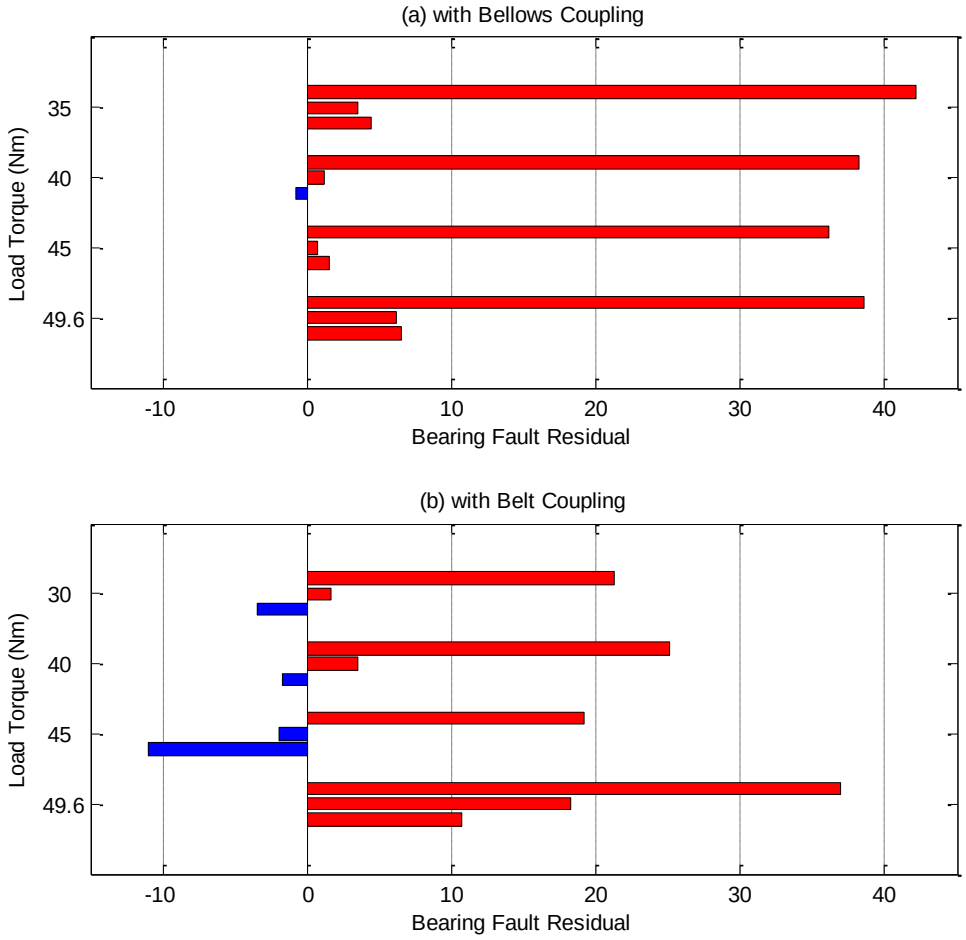

Figure 9.8 Bearing fault indicator residual values (positive values indicate successful fault detection, negative values indicate no fault detected)

Table 9.2 Bearing fault indicator values and residuals (highlighted 'Del' values indicate correct diagnosis)

Coupling	Load (Nm)	H	ABR	**ABR Del**	0.5mm	**0.5mm Del**	1.5mm	**1.5mm Del**
Belt	50	-806.04	-795.32	**-10.72**	-787.79	**-18.25**	-769.06	**-36.98**
	45	-787.08	-798.08	**11.00**	-788.96	**1.89**	-767.90	**-19.18**
	40	-796.78	-798.51	**1.73**	-793.24	**-3.55**	-771.69	**-25.10**
	30	-797.99	-801.49	**3.50**	-796.33	**-1.67**	-776.78	**-21.21**
Bellows	50	-808.16	-801.65	**-6.51**	-801.94	**-6.22**	-769.54	**-38.61**
	45	-806.60	-805.05	**-1.55**	-805.89	**-0.71**	-770.50	**-36.10**
	40	-806.66	-807.41	**0.74**	-805.48	**-1.19**	-768.40	**-38.26**
	30	-810.05	-805.64	**-4.42**	-806.57	**-3.48**	-767.85	**-42.20**

9.3 Summary

This chapter described the different fault detection methods which will be used as part of the overall induction motor condition monitoring system (described in the subsequent chapter). The fault detection methods were split into model-based fault detection and model free fault detection.

The model-based fault detection methods were used for detecting rotor broken bar faults and stator turn-to-turn winding faults. These faults required the use of the QD0 fault model which was described previously in the thesis. The model is then used as part of an objective function which drives a Nelder-Mead based optimisation process in MATLAB. The objective function for the rotor fault utilises rotor fault sidebands around the fundamental frequency in the current spectrum, and the stator fault objective function directly compares the simulated and measured time-series current waveforms in their raw form. Both estimated parameter features (for rotator and stator fault) show a strong response to increasing fault magnitudes at all load levels.

Due to the increased difficulty of modelling the air-gap and bearing faults, model-free methods were used for these fault types. The bearing fault method utilises the spectral content of the line currents to obtain a value on the overall spectral energy. Any noise introduced by bearing point or generalised roughness faults will lead to this value increasing. Since this broadband approach is used specific details on the bearing physical characteristics are not required. The eccentric fault utilises supply harmonic sidebands which have been proven to increase in magnitude when air-gap eccentricity is present. The line current spectrum is scanned for these frequencies (based on an estimated speed value) and the magnitude of these frequencies is used as the fault

feature. The bearing fault detection method could not, in every case, detect the low level abrasive wear fault but since this would eventually develop into a more serious fault (which were detected during the tests) this is not a significant drawback. Overall, the air-gap and bearing fault features respond well to increasing fault methods.

The fault detection methods outlined in this chapter have been proven to be responsive to the relevant fault types by successfully identifying a deviation between a healthy and faulty condition. The next chapter will describe the development of the diagnosis engine which will interpret these outputs of the fault-detection algorithms (features) and use this information to come to a decision on the overall health of the motor and the probable fault location.

Chapter 10. Fuzzy Logic Fault Diagnosis Engine

This chapter will describe the development of the diagnosis system used to interpret the numerical outputs (features) of the fault detection algorithms (developed in the previous chapter) and determine whether any faults are present, which faults are present and also give an estimation of the severity of that fault. The diagnosis system was implemented using fuzzy logic techniques.

10.1 Fuzzy logic background

Fuzzy logic is a technique used to describe and interpret non-precise quantities or information. It can be used to develop approximations when precise data is unavailable and provides a technique that can handle the impreciseness in many situations and still reach a useful conclusion [139].

Fuzzy systems can be simply compared with standard algebraic systems:

- Algebraic System – maps an input variable to an output variable
- Fuzzy System – maps an input ‘group’ to an output ‘group’

By implementing a solution using groups rather than precise values the system develops the ability to approximate system behaviour where strict numerical relations do not exist or are not known. Also, fuzzy logic is useful when exact solutions are not necessary. This allows approximate solutions to problems to be found quickly with minimum computational expense.

Fuzzy logic works around the concept of fuzzy sets – a set in which the boundaries are not precise and membership to the set is to a certain degree (i.e. it does not have to be 0 or 1 only).

Fuzzy logic has several benefits:

- it is a simple concept and easy to understand
- it is flexible and can be adapted and extended easily
- it can be built using the knowledge of experts or by neural training methods
- it can deal with imprecise data
- it is based on human linguistics – uses natural language

In general, fuzzy logic systems are usually applied in two situations [139]:

1. situations involving highly complex systems with behaviours that are not fully understood
2. situations where an approximate, fast solution is warranted

Both these cases are applicable to the problem of induction motor fault FDD and so a fuzzy logic approach will be implemented in this chapter in order to assess its effectiveness for this particular application of IM FDD.

10.2 Application to fault diagnosis

One of the most simple approaches in fault diagnosis or condition monitoring is the checking of some quantity (be it directly measured or calculated) with a set threshold. This predetermined threshold is usually set to provide a compromise between early detection and avoidance of false alarms. For a system that is to interpret a number of different situations where conditions can vary these thresholds cannot be precisely defined. In this situation a fuzzy variable can be used which takes into account the variability or inaccuracy in the process [56].

The process or system which is used to generate the input information in order to make a diagnosis will not always yield exact data – there may be some noise, modelling error or unknown behaviour present. Sources of imprecision added to the process can occur at one of several different stages:

- sensor measurement accuracy
- noise
- model accuracy
- parameter accuracy
- algorithm design

Specifically, with model based approaches it is important to remember that the model is only an *approximation* of reality and the outputs of any model will contain a certain amount of error.

It is apparent that there are several sources of imprecision in the fault diagnosis process. This means the outputs of each stage of the process have a degree of vagueness. Fuzzy sets provide a mathematical method of analysing this vagueness (fuzziness) and dealing with the levels of uncertainty in a given process [139].

This allows key decisions to be made in a computationally efficient manner, even with a degree of uncertainty present making a fuzzy logic algorithm well suited to the problem of microprocessor based online incipient fault diagnosis.

10.3 System overview

Fuzzy logic systems usually consist of 5 stages [56]:

Stage 1: Fuzzification

This is the conversion of precise numeric values (from either sensors or calculation outputs) into fuzzy variables.

Stage 2: Operation

This stage involves combining fuzzy values using fuzzy logic operators (e.g. AND, OR, NOT).

Stage 3: Implication

This stage uses ‘if-then’ statements to link the input of the system to the output.

Stage 4: Aggregation

Aggregation is the process of combining the fuzzy output functions (i.e. taking into account all output fuzzy variables).

Stage 5: Defuzzification

Conversion of the aggregated fuzzy values into a precise (non-fuzzy) numeric value.

An overview of this procedure is given in Figure 10.1.

10.4 Input membership functions

Membership functions perform a vital role in the fuzzy system. They allow the precise input variables to be transformed into fuzzy values. Hence, it is very important that the linguistic fuzzy values are properly set.

Membership functions are part of the ‘Fuzzification’ stage. The membership functions map precise numerical values into fuzzy sets.

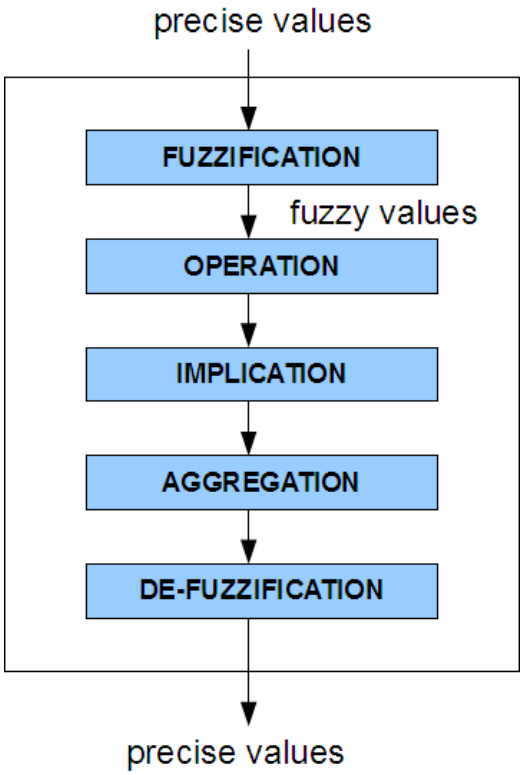

Figure 10.1 Fuzzy logic system overview

There are several ways in which membership functions can be developed [139]:

- Intuition
- Inference
- Rank Ordering
- Neural Networks
- Genetic Algorithms
- Inductive Reasoning

Neural networks are better suited to larger data and test sets and genetic algorithms do not need to be used for a relatively simple system. Inductive reasoning applies entropy minimisation algorithms to define the membership functions so like neural approaches it is more suitable to larger or more complete data-sets.

Due to the fact that the system is being developed using evidence from experiments and literature reviews, ‘inference’ will be the primary method used to define the membership functions. The process of inference involves “deducing or inferring a conclusion based on a body of facts or knowledge” [139]. The body of facts in this case will be the results of the experimental phase of this project and the collection of knowledge from the literature reviews.

Obviously there is insufficient time to test every level of fault severity so the body of experimental facts will contain some small gaps. These gaps in the knowledge will be filled by using the ‘intuition’ method of membership function definition. Intuition is simply the human ‘expert’ designing parts of the membership functions through their own innate understanding of the process in question. It is this human problem solving ability and understanding that the fuzzy logic system is designed to replicate.

Several membership functions are available to use:

- Triangular
- Trapezoidal
- S-shaped
- Gaussian

The fault diagnosis engine will use only trapezoidal and triangular membership functions since they are simple to implement in software and were proven to be effective for this particular application.

The input membership functions analyse the fault residuals. As mentioned previously, the ‘residual’ is the difference in a given variable (or fault feature) between the healthy baseline measurement (time=0) and a measurement at

time=t. This means that the fuzzy logic diagnosis engine is measuring the *deviation* from a known initial state rather than analysing an absolute value from a fault indicator. This makes the system much more flexible by taking into account the initial conditions which differ between motor applications. If an absolute fault measurement was developed in the lab it could not take into account all these differences but by utilising a baseline measurement (initial condition measurement) we can measure deviation from this known reference point. This allows a generic system to be applied to any number of specific motor applications and still provide acceptable performance.

It was decided that the input membership functions would be divided into 5 sets as given in Table 10.1.

Table 10.1 Input fault residual fuzzy sets

Set Name	Set Description
VLOW	A set for non-existent or very low level fault residuals.
LOW	A set for low magnitude fault residuals.
MED	A set for medium magnitude fault residuals.
HIGH	A set for high magnitude residuals.
VHIGH	A set for very high magnitude residuals.

These sets provide sufficient fidelity for subsequent stages of the fuzzy logic system without being overly complex. The linguistic set names are simple which makes the fuzzy logic system easy to program, straightforward to understand and simple to extend or improve in future.

The fuzzy sets are given linguistic terms (VERY LOW, LOW, MEDIUM, etc) that vaguely describe the value of the chosen input variable. The linguistic terms define a region on a scale. For example, if the scale were 1 to 10 then the ‘VERY HIGH’ set might be considered as numbers 8 and above. The membership functions are tested and tailored until acceptable performance is

achieved and the fuzzy algorithm acceptably replicates the vague mappings made by humans effectively.

10.5 Rotor fault membership function

As described previously the membership functions are inferred from the experimental results and intuition is used to make the mapping generic and strike a balance between early detection and false alarm avoidance. The absolute fault values calculated from the test results are given below in Table 10.2.

Table 10.2 Rotor fault test results; raw values and residuals (faulty Rfault value – healthy Rfault value)

Test Condition	RFault Value	Residual
Healthy	0.005	N/A
2.5mm fault	0.006	0.001
3.5mm fault	0.01	0.005
4.5mm fault	0.025	0.02
6mm fault (1 broken bar)	0.2	0.195

The process used to develop the fuzzy input membership function based on these experimental results is now described. A crack which has propagated across the entire cross-section of one bar (1 broken bar case) is considered significant damage therefore the membership function mapping is designed to correctly map Rfault residuals of around 0.2 and above to the ‘VHIGH’ set (see Figure 10.2). Whereas the 2.5mm fault replicates only a developing fracture in bar so not as serious therefore they are mapped to the ‘VLOW’ or ‘LOW’ set. Then intuition and expert knowledge (understanding of the testing process and damage mechanisms and manifestations) is used to develop the other sets to provide a correct classification of the different fault magnitudes. This is an

attempt to build human understanding and interpretation of results into the system.

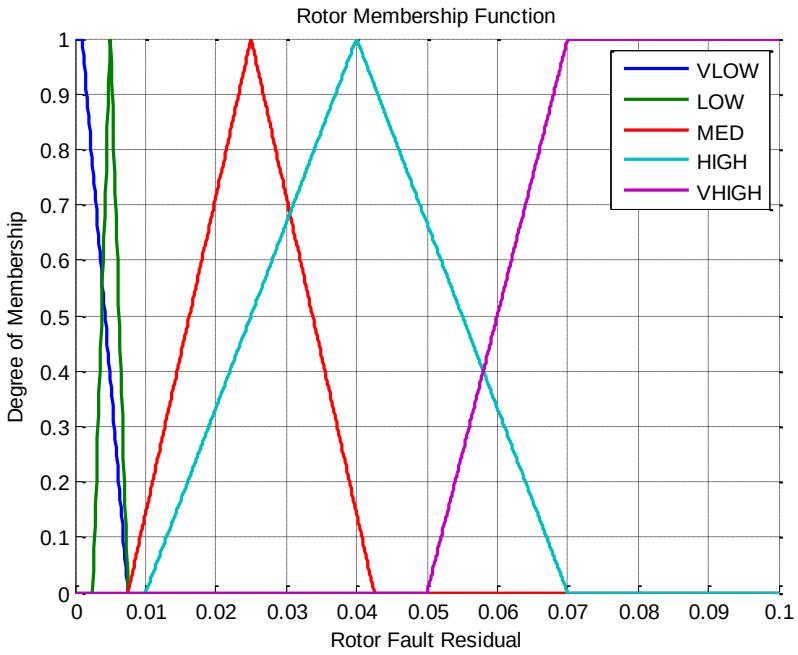

Figure 10.2 Rotor fault membership function

10.6 Stator fault membership function

The stator fault membership function was developed based on the stator fault values obtained from experiment in similar way to the rotor fault membership function. Data recorded on the belt-coupled rig is used to develop the membership function here then validated later in the chapter against data collected on the shaft coupled rig.

The residual values for the stator fault indicator are given in Figure 10.3. The stator fault residual is shown to increase from 0 to almost 0.14 for shorted turn percentages of 0 to 10.4%. This data was then used to create the stator membership function; 2-3% shorted turns of one winding will result in a low level mapping, 3-5% will result in a mid level severity mapping and 5% and above will map to a high or very high fault level set.

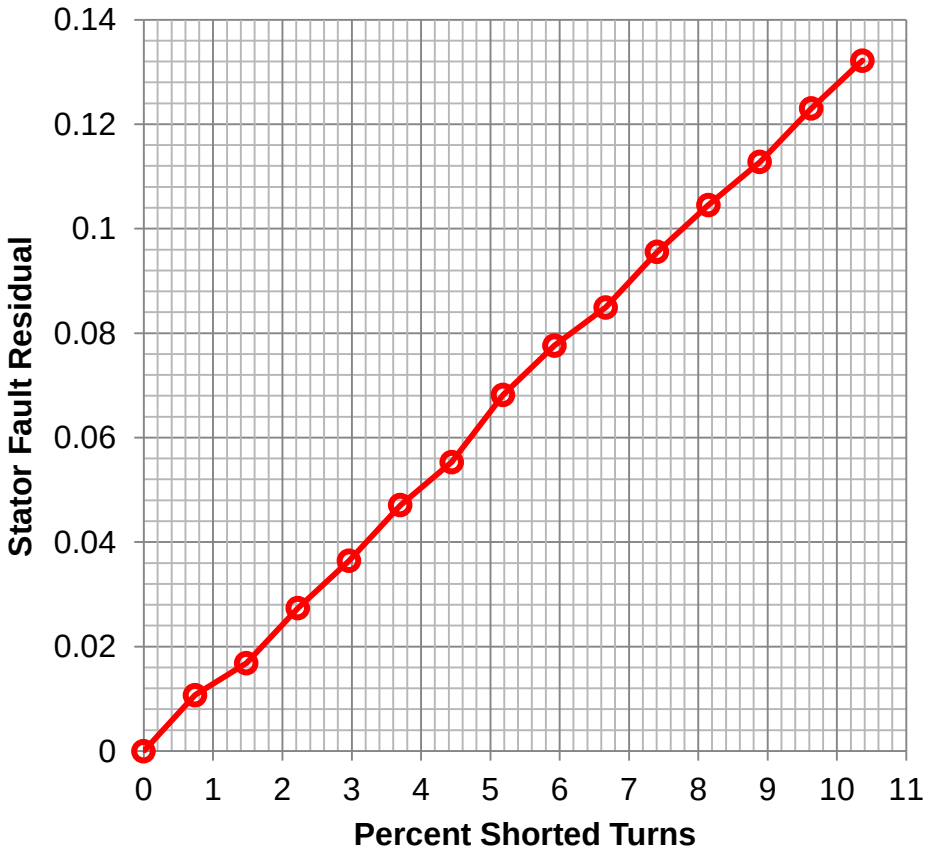

Figure 10.3 Stator fault residual values calcualted for increasing numbers of shorted turns (0 to 10.4% of one winding)

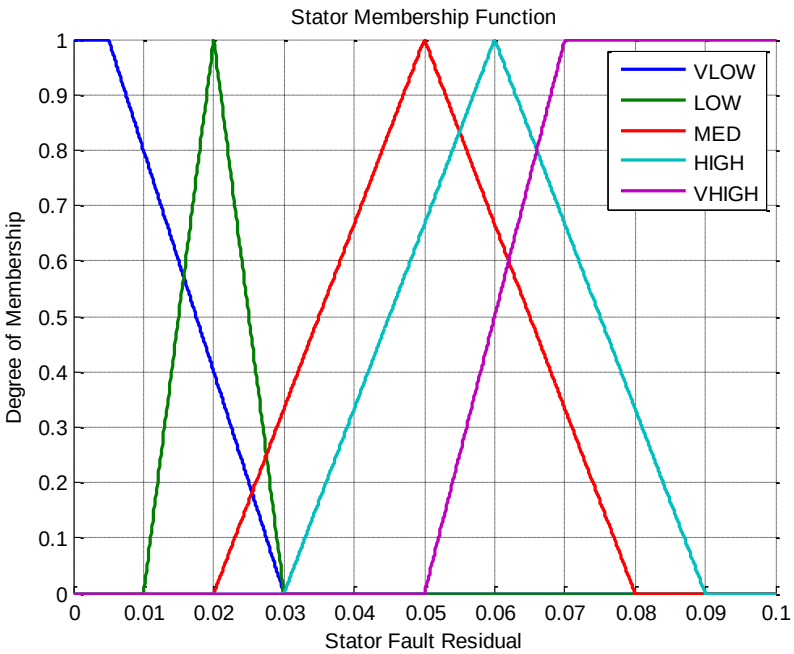

Figure 10.4 Stator fault membership function

10.7 Air-gap fault membership function

Calculated values are shown (Table 10.3) for both bellows and belt coupled motor tests with positive values indicating an increase in the fault indicator value for the faulty case (i.e. fault detected) and negative values indicating a decrease in the fault indicator value (i.e. fault is not detected) when compared to the healthy baseline value.

In a similar way to the previous membership functions, the data on the fault residuals was used to develop the fuzzy membership functions (see Figure 10.5) for the air-gap eccentricity fault types .

Table 10.3 Air-gap fault indicator values and fault residuals

Coupling	Load (Nm)	H	SE	SE Residual	DE	DE Residual
Belt	50	-74.44	-61.549	12.891	-61.5873	12.8526
	45	-52.7976	-52.9065	-0.108915	-54.3252	-1.527597
	40	-72.3701	-58.3548	14.0153	-68.5615	3.80866
	35	-71.8688	-57.7236	14.1453	-65.768	6.10079
	30	-68.7562	-56.4699	12.2863	-61.7188	7.03736
Bellows	50	-75.1291	-65.2078	9.9213	-56.9438	18.1853
	45	-73.4604	-64.9864	8.47399	-59.6185	13.8419
	40	-72.7329	-64.2038	8.52914	-53.442	19.2909
	35	-72.6358	-62.0146	10.6213	-53.442	19.1938
	30	-68.6748	-61.2557	7.41916	-49.7163	18.9585

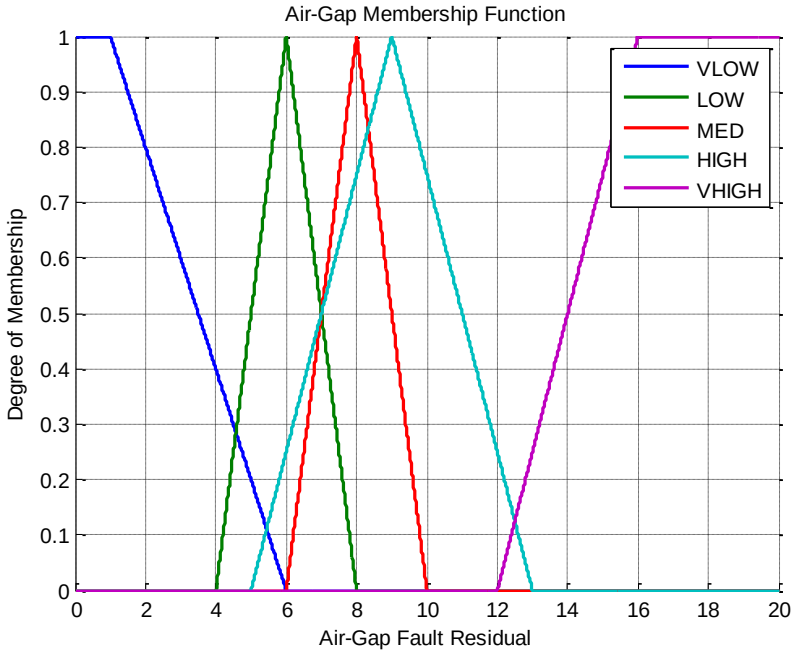

Figure 10.5 Air-gap eccentricity fault membership function

10.8 Bearing fault membership function

Finally, the bearing residual membership function (Figure 10.6) is developed in a similar way to the other fault types.

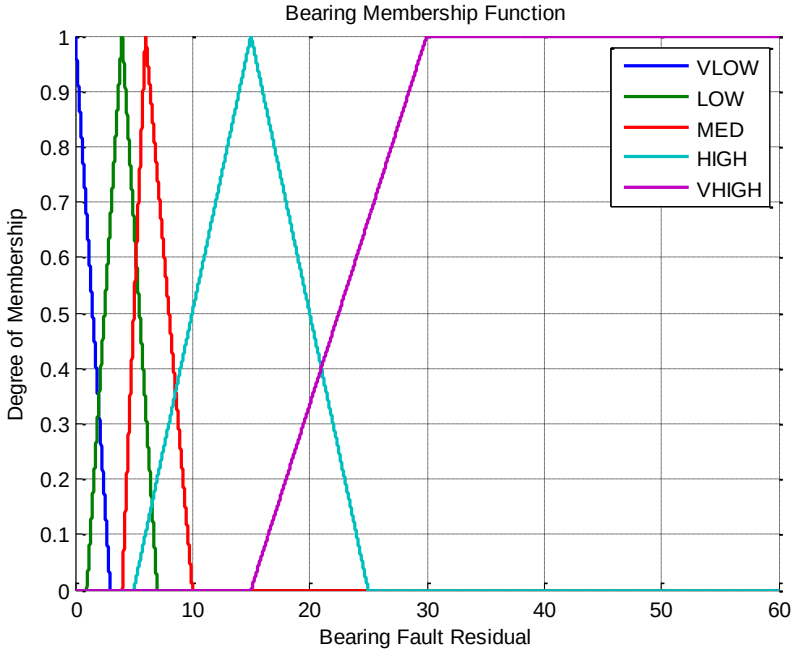

Figure 10.6 Bearing fault membership function

10.9 Output membership functions

Output membership functions are implemented after the IF-THEN statement used in the rule set has been applied (see next section). In a similar fashion to the inputs sets, linguistic descriptions are given to the output sets which give a clear indication of the classification. For example, the output required for a condition monitoring system is some statement on the health of the observed machine or system.

For the system presented in this thesis the idea is to present an output to the end users which clearly describes the condition of the induction motor subsystems, namely the bearings, stator windings, rotor cage and air-gap. Therefore the output function was chosen to firstly describe if the machine was healthy, whether it had some level of mild damage or whether it had a serious fault which could lead to imminent failure.

These output functions were decided based on how this information would be used by staff working in industrial settings. A healthy output would result in the engineer taking no action. A serious fault output would result in the engineer scheduling the machine for maintenance immediately, for example during the next period of plant downtime. A mild damage output would then be used to schedule in (at a lower priority) maintenance at some time in the near future. These simple output sets allow the engineers, technicians and lay people to instantly understand the condition of the motor in simple terms and use this information to effectively manage the ongoing maintenance of the plant.

With this in mind three output sets were defined. The fuzzy output sets were: HEALTHY (motor subsystem has no detectable fault), MILD FAULT (motor

subsystem is thought to have a mild fault), SEVERE FAULT (motor subsystem is thought to have a serious fault).

For each of the four fault types, the same output membership function can be used. The output membership function is given in Figure 10.7.

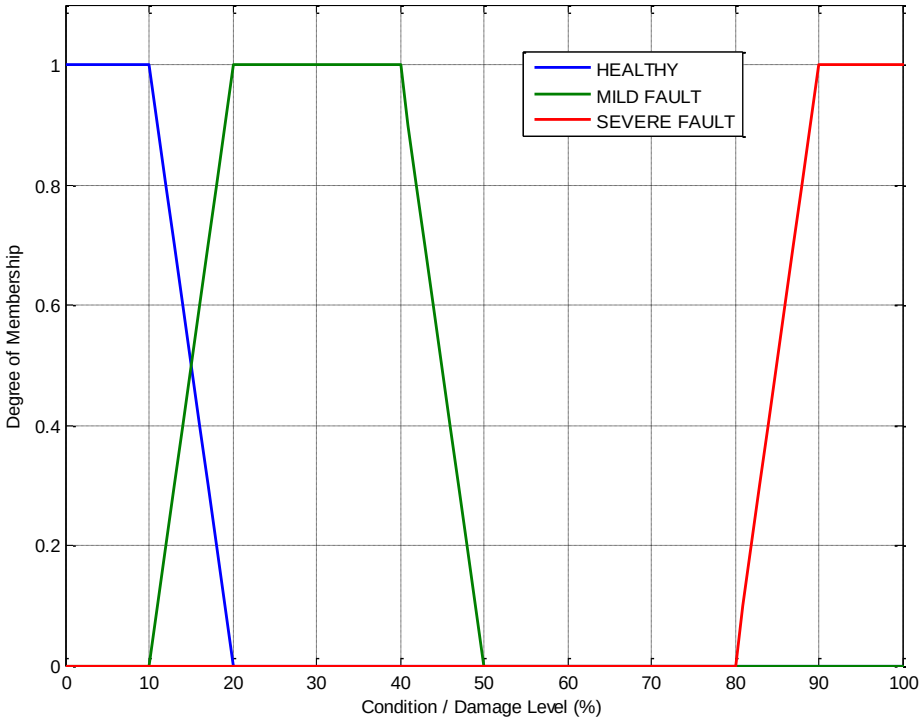

Figure 10.7 Damage level membership function

10.10 Rule sets

The fuzzy quantities constructed in the previous sections are now organised using implications (IF x, THEN y). These statements define how the inputs relate to the outputs via a ‘rule set’. The rule set defines how the diagnosis engine makes its decisions.

The rules are of the form:

IF (antecedent), THEN (consequent)

The antecedent is the input and may involve a logic term (e.g. IF (A is HIGH & B is HIGH)). The consequent is the fuzzy output set, e.g. (rotor condition is POOR) where POOR is the fuzzy output set.

The initial one dimensional rule sets for each of the motor subsystems (rotor cage, stator windings, bearings and air-gap) can now be developed. As an example, the rotor condition rule set is given below:

1. IF (**Rfault** is *Very Low*) THEN (**Rotor Condition** is *Healthy*)
2. IF (**Rfault** is *Low*) THEN (**Rotor Condition** is *Mild Fault*)
3. IF (**Rfault** is *Medium*) THEN (**Rotor Condition** is *Mild Fault*)
4. IF (**Rfault** is *High*) THEN (**Rotor Condition** is *Severe Fault*)
5. IF (**Rfault** is *Very High*) THEN (**Rotor Condition** is *Severe Fault*)

This rule set for this simple case is intuitive; higher Rfault values indicator more rotor damage. This is because the rotor fault indicator was designed to be sensitive to rotor condition. However, when other variables are used (e.g. imbalance, crest factor, RMS, etc) which are not specific to a given fault then the rule set becomes more difficult to develop. In this case a detailed understanding of the process is required (expert knowledge). If the rule sets are set up correctly then this expert knowledge is utilised to make correct decisions on machine condition.

The rules can then be represented in an associative matrix (see Table 10.4). The associative matrices for each of the other fault types are given in Table 10.5, Table 10.6 and Table 10.7 below.

Table 10.4 Rotor IF-THEN associative matrix

IF Rfault is...	THEN Rotor Condition is...
VERY LOW	HEALTHY
LOW	MILD FAULT
MEDIUM	MILD FAULT
HIGH	SEVERE FAULT
VERY HIGH	SEVERE FAULT

Table 10.5 Stator IF-THEN associative matrix

IF Sfault is...	THEN Stator Condition is...
VERY LOW	HEALTHY
LOW	MILD FAULT
MEDIUM	MILD FAULT
HIGH	SEVERE FAULT
VERY HIGH	SEVERE FAULT

Table 10.6 Eccentric IF-THEN associative matrix

IF AGFault is...	THEN Air-Gap Condition is...
VERY LOW	HEALTHY
LOW	MILD FAULT
MEDIUM	MILD FAULT
HIGH	SEVERE FAULT
VERY HIGH	SEVERE FAULT

Table 10.7 Bearing IF-THEN associative matrix

IF BFault is...	THEN Bearing Condition is...
VERY LOW	HEALTHY
LOW	MILD FAULT
MEDIUM	MILD FAULT
HIGH	SEVERE FAULT
VERY HIGH	SEVERE FAULT

KEY:

SFault = stator fault indicator residual
RFault = rotor fault indicator residual
AGFault = air-gap fault indicator residual
BFault = bearing fault indicator residual

These provide the basic fuzzy implications using only the outputs of the primary diagnosis methods (e.g. rotor model, stator model, air-gap eccentric spectral

levels and bearing spectral level). In addition to the specific fault indicators other information can be used to help make the diagnoses more accurate and more robust (the motivation for adding additional variables is covered later in section 10.13.1). The additional information could be RMS current, crest factor, estimated motor speed, total harmonic distortion, maximum/minimum values, variation, current imbalance, etc. Additionally, if at a point in the future, additional hardware becomes available (e.g. accelerometer or thermocouple measurements) then these can be easily added to the rule set.

As an example of adding additional inputs to the rule set, the stator condition diagnosis can be considered. Shorted stator windings leads to an increase in the motor negative sequence current due to an imbalance in the resistance of each of the phases. This understanding of the process can be built into the fuzzy logic system by using negative sequence current as an input to the decision making process (i.e. developing a suitable membership function and modifying the rule set appropriately). The following logic statement can be applied:

IF (**Sfault** is *High*) OR (**Negative Sequence Current** is *High*) THEN (**Stator Condition** is *Severe Fault*)

In this case the OR operator is used. This ensures that a severe stator fault will be flagged if the Sfault residual is high *or* the measured current imbalance is high. By considering additional inputs the robustness and accuracy of the decision making process is improved since a more complete view of the situation is used to reach a decision. In particular, at low fault levels were Sfault values are negligible negative sequence current can be a better indicator of shorted turns.

Since two variables are now considered the associative matrix becomes two dimensional (see Table 10.8).

Table 10.8 Associative matrix for an IF-THEN statmenet using 2 antecedents (e.g. if A *OR* B, then C)

Output Associative Matrix		Negative Sequence Current	
		LOW	**HIGH**
Sfault	**VERY LOW**	***HEALTHY***	***HEALTHY***
	LOW	***HEALTHY***	***MILD FAULT***
	MEDIUM	***MILD FAULT***	***SEVERE FAULT***
	HIGH	***MILD FAULT***	***SEVERE FAULT***
	VERY HIGH	***SEVERE FAULT***	

1. IF (**Sfault** is *Very low*) OR (**Negative Sequence Current** is *Low*) THEN (**Stator Condition** is *Healthy*)
2. IF (**Sfault** is *Very low*) OR (**Negative Sequence Current** is *High*) THEN (**Stator Condition** is *Mild Fault*)
3. IF (**Sfault** is L*ow*) OR (**Negative Sequence Current** is *Low*) THEN (**Stator**
4. **Condition** is *Healthy*)
5. IF (**Sfault** is *Low*) OR (**Negative Sequence Current** is *High*) THEN (**Stator Condition** is *Mild Fault*)
6. IF (**Sfault** is *Medium* OR (**Negative Sequence Current** is *Low*) THEN (**Stator Condition** is *Healthy*)
7. IF (**Sfault** is *Medium*) OR (**Negative Sequence Current** is *High*) THEN (**Stator Condition** is *Severe Fault*)
8. IF (**Sfault** is *High*) OR (**Negative Sequence Current** is *Low*) THEN (**Stator Condition** is *Mild Fault*)
9. IF (**Sfault** is *High*) OR (**Negative Sequence Current** is *High*) THEN (**Stator Condition** is *Severe Fault*)
10. IF (**Sfault** is Very *High*) THEN (**Stator Condition** is *Severe Fault*)

In this scenario the addition of negative sequence data is used to prevent erroneous Sfault values or inaccuracies in the Sfault estimation process leading to a false alarm. If low negative sequence values are detected in addition to intermediate values (LOW, MEDIUM, HIGH) of Sfault then the diagnosis will be reduced to HEALTHY or MILD FAULT. By building in these additional rules, false alarms in the stator fault detection process should be minimised making the whole process more robust.

Additional inputs do not need to be separated into the same number of sets as other inputs nor do all fields of the associative matrix need to be active. For example in the case above an output will always be active since the 1D Sfault rules (whether in combination with negative sequence inputs or not) will always be triggered. Hence, rules do not always need to involve negative sequence current.

10.11 Algorithm operation

Having defined the component parts (input membership functions, rule set, output membership function) of the fuzzy logic system, it can be tested and refined. This section will take the form of an example (using arbitrary values) of how information flows through the fuzzy logic system and how decisions are made.

10.11.1 Example: Classifying stator faults

This example considers a Sfault value of 0.04 and a normalised negative sequence current of 2%. The remainder of the section will indicate how the membership functions and rule sets described in previous sections are used to turn these input variables into a meaningful diagnosis of the stator health (linguistic term) and also to then go on to provide a precise (numeric value) health score to be used for trending purposes (condition monitoring).

The stator fault membership function is shown again in Figure 10.8. The red dotted lines indicate the points where the estimated Sfault value (x-axis) cut the different fuzzy sets (very low, low, medium, high, and very high). The degree of membership of the Sfault value to each of the fuzzy sets can then be obtained by reading across to a point on the y-axis.

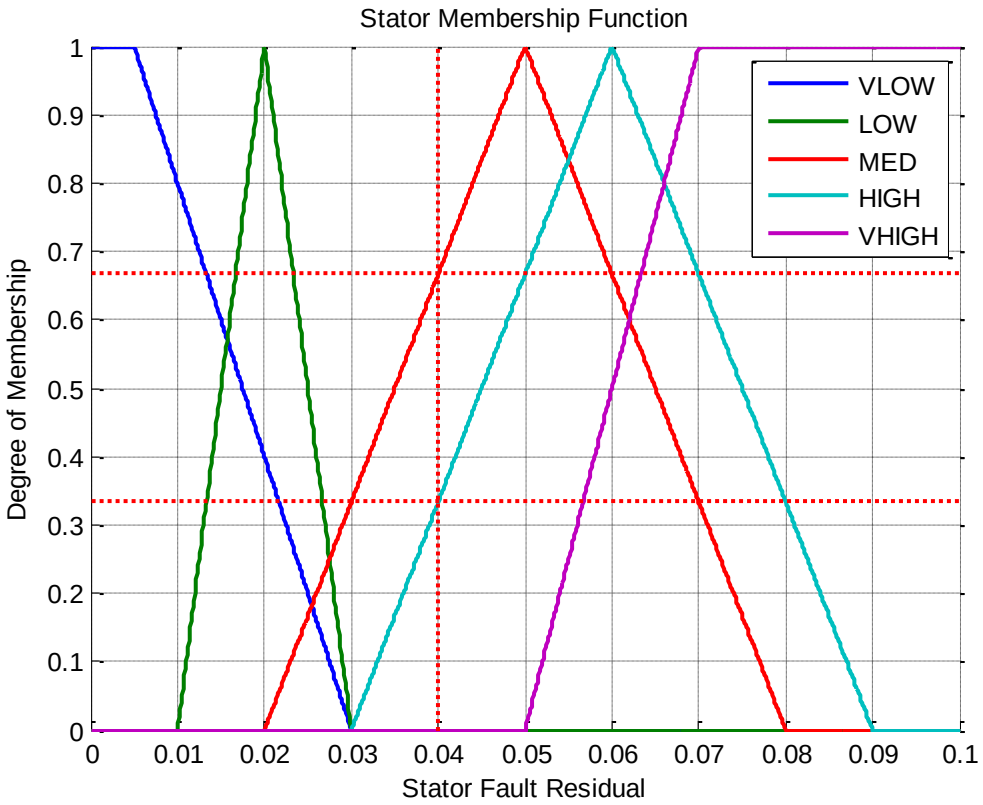

Figure 10.8 Calculating degrees of membership for a 0.04 value of stator fault residual (Very Low = 0, Low = 0, Medium = 0.68, High = 0.33, Very High = 0)

The numerical values of degree of membership (corresponding to the graph above) are given below:

Table 10.9 Degree of memebrship for Sfault value of 0.04

Fuzzy Set	VERY LOW	LOW	MEDIUM	HIGH	VERY HIGH
Degree of Membership	0.00	0.00	0.68	0.33	0.00

The degree of membership (DoM) shown in this table defines how well a specific value belongs to a set, i.e. a value of 1 indicates the value completely belongs to a set, a value of 0 indicates that a value does not belong to a set at all. In standard logic these would be the only allowed values. Any fuzzy set with a DoM of 0 can from this point on be ignored.

Following this the second input for the two dimensional fuzzy system used for stator diagnosis, negative sequence current, can be considered. The membership function is shown below (Figure 10.9):

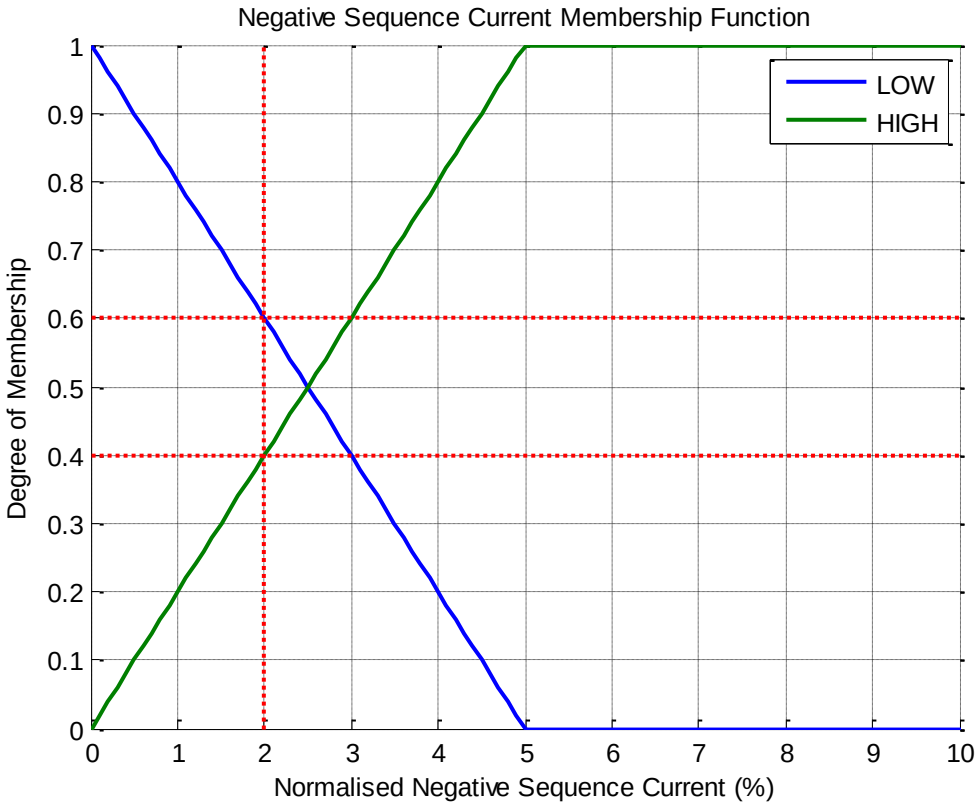

Figure 10.9 The negative sequence membership function with input value of 2% normalised negative sequence current

Having fuzzified the inputs the fuzzy rule set can be applied. Referring to the rule set for stator faults (Table 10.8) we can determine the active rules which are (6), (7), (8) and (9). Considering the rules in order the following results are obtained:

$$\mu_{mild\ fault}(SF \in med \cup NS \in low) = max(SF \in med, NS \in low) = max(0.68,0.6) = 0.68 \quad (10.1)$$

$$\mu_{severe\ fault}(SF \in med \cup NS \in high) = max(SF \in med, NS \in high) = max(0.68,0.4) = 0.68 \quad (10.2)$$

$$\mu_{mild\ fault}(SF \in high \cup NS \in low) = max(SF \in high, NS \in low) = max(0.33,0.6) = 0.6 \quad (10.3)$$

$$\mu_{severe\ fault}(SF \in high \cup NS \in high) = max(SF \in high, NS \in high) = max(0.33,0.4) = 0.4 \quad (10.4)$$

The degree of membership (for the output condition sets) generated by each rule is then summed to give the overall degree of membership for the output function considering the contribution of every rule:

$$\mu_{healthy} = 0.00;\ \mu_{mild\ fault} = 1.28;\ \mu_{severe\ fault} = 1.08; \quad (10.5)$$

Figure 10.10 demonstrates the process of implication, aggregation and defuzzification. Firstly the output fuzzy sets activated by the IF-THEN rules ('mild fault' and 'severe fault') are plotted and scaled according to the degree of membership of the input functions (1.28 and 1.08 respectively). The bottom plot shows the stage of aggregation of active fuzzy sets (taking the maximum). Then the centre of mass or centroid of this aggregated function is calculated (52.6%). This conversion from fuzzy set to numerical value is known as 'defuzzification'.

Figure 10.11 shows the process followed to reach the diagnosis verdict. Figure 10.11 indicates that the 2 diagnosis outputs of the system are:

- Fuzzy – Stator is 'MILD FAULT'
- Precise – Stator has a 52.6% damage score (or through inversion, 'Stator Condition/Health is 47.4%')

This 'damage score' is not an absolute measure of health i.e. if the value reaches 100% the motor has not failed. It is simply an indication of how confident the condition monitoring algorithm is (at a given instant in time) that a fault is present in the motor. For example, if the damage score is 0% the algorithm is confident that there is no fault in the system, if it is 50% a problem

has been detected but at this stage it is only small in magnitude, if it is 100% the algorithm has detected a significant fault.

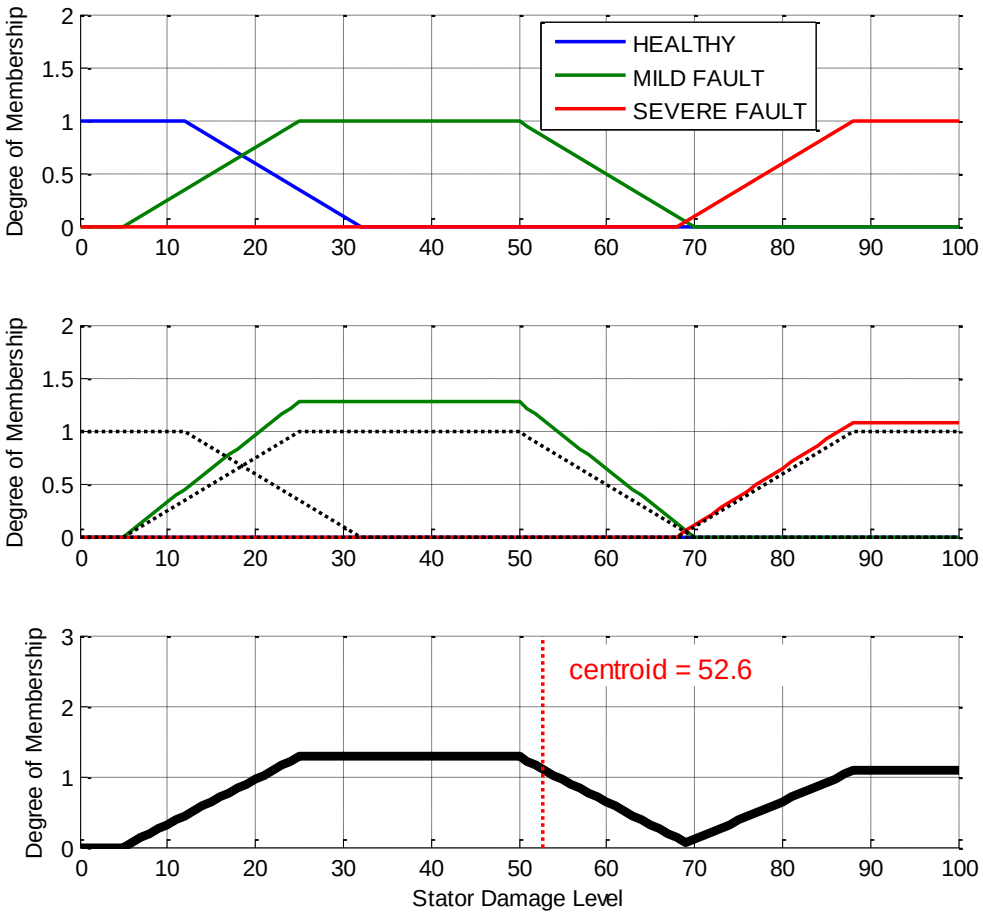

Figure 10.10 Output membership functions (top). Degree of membership of output functions based on active rules (middle). Aggregation of outputs and defuzzification (bottom).

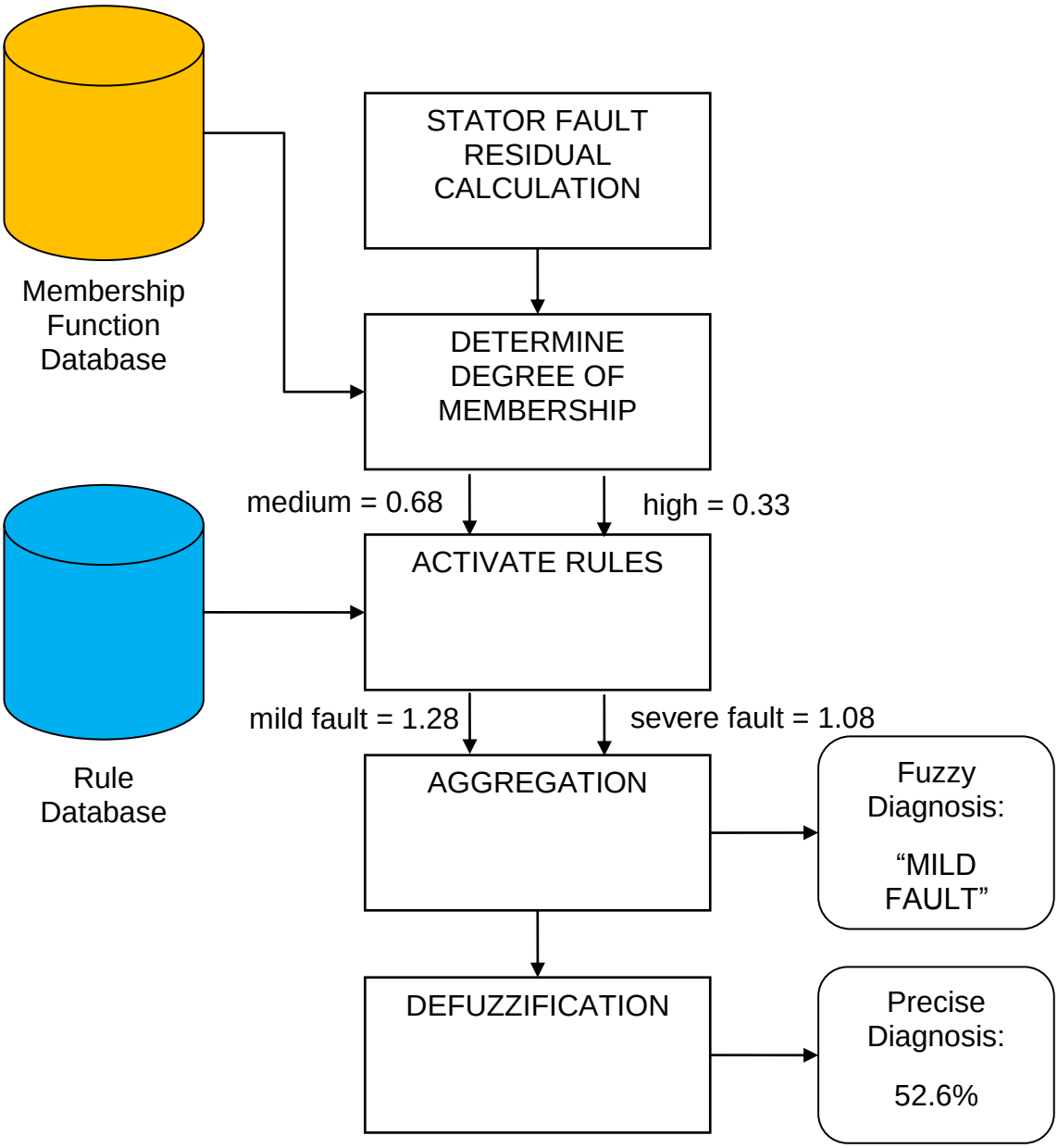

Figure 10.11 An overview of the fuzzy logic diagnosis process

The ability to detect small changes in fault levels is due to the increased fidelity built into the membership functions around low fault levels. Multiple overlapping sets provide the 'sliding scale' that is not possible with standard logic. By using many small sets over critical areas even small changes in variables can be detected and tracked.

10.12 Human machine interface (HMI)

It is envisaged that the diagnosis verdict presented to the technicians on the hardware HMI is in linguistic (fuzzy) form as opposed to the numerical value. This allows easy interpretation by any member of staff without extensive knowledge of the software.

In this example we have used {HEALTHY, MILD FAULT, SEVERE FAULT} however, alternatives could be more useful e.g. {GOOD CONDITION, ADEQUATE CONDITION, POOR CONDITION} or {OK, MONITOR, REMOVE FOR MAINTENANCE} or {HEALTHY, DEVELOPING FAULT, FAULT PRESENT}.

These linguistic terms mean more than a ‘health score’ to the average operator and are a more realistic indication of how accurately the ‘health’ of the machine can be determined. The health score should be used only as a guide or as a trending mechanism.

A percentage score can easily be misinterpreted where as the linguistic terms are more likely to be understandable (as long as they are developed with the end user in mind or preferably with the end users input).

10.13 Results

This section will present the results of the fuzzy logic diagnosis system. These results utilise all the models and algorithms developed in previous chapters and therefore this section represents the overall results of the entire induction motor condition monitoring system.

10.13.1 Initial results & development

Firstly, the initial results will be presented considering only the belt connected data. This initial results phase is still part of the development and includes a description of the changes made to the diagnosis system to improve the algorithm performance. Results are presented after each modification to highlight the effect of the changes. In the following section the results for the entire dataset (including shaft coupled data) will be presented; those results will be the final and overall results of the fault detection and diagnosis system.

Testing Phase 1

The results from the first phase of this initial testing (Phase 1) are shown in Table 10.10 and Table 10.11.

Table 10.10 indicates the raw fault detection method values calculated and Table 10.11 shows the fuzzy logic interpretation and diagnosis of the results. These results are the initial set of results without tailoring of the membership functions, fault detection methods or addition of any combined rules or secondary detection methods (the final membership functions presented in previous sections were a result of this stage of testing).

It is clear that the diagnosis accuracy is fairly unsatisfactory. Out of the 60 individual diagnoses, 22 were incorrectly diagnosed as either ‘MILD FAULT’ or ‘SEVERE FAULT’ when one of the motor subsystems was deemed to be ‘HEALTHY’ (or vice-versa).

Table 10.10 Fault detection method outputs for Phase 1 testing

DETECTION TECHNIQUE OUTPUTS			FAULT ZONE			
			Stator	Rotor	Air Gap	Bearing
EXPERIMENTAL DATAFILE	1	M1 – Healthy – 50Nm	0.0013	0.0000	53.155	820.03
	2	M2 – Healthy – 35Nm	0.0064	0.0000	61.008	822.33
	3	M3 – Healthy – 45 Nm	0.0079	0.0000	56.435	814.34
	4	M4 – Healthy – 50Nm	0.0081	0.0041	61.926	818.59
	5	M1 – Rotor Fault (1 bar)- 50Nm	0.0033	0.0519	46.765	814.88
	6	M2 – Bearing Fault (abrasive) – Start – 35Nm	0.0087	0.0000	54.608	820.66
	7	M2 – Bearing Fault (abrasive) – End – 35Nm	0.0093	0.0000	48.283	813.94
	8	M2 – Bearing Fault (0.5mm point fault) – 35Nm	0.0047	0.0000	59.885	806.57
	9	M2 – Bearing Fault (1.5mm point fault) – 35Nm	0.0063	0.0000	60.328	767.85
	10	M3 – Stator Fault (shorted turns) – 4 turn – 45Nm	0.0135	0.0000	55.005	813.30
	11	M3 – Stator Fault (shorted turns) – 7 turn – 45Nm	0.0269	0.0077	53.970	813.58
	12	M3 – Stator Fault (shorted turns) – 11 turn – 45Nm	0.0468	0.0000	52.688	805.26
	13	M3 – Stator Fault (shorted turns) – 14 turn – 45Nm	0.0626	0.0000	51.452	810.68
	14	M4 – Eccentric Fault (static) – 50Nm	0.0088	0.0000	56.812	815.35
	15	M4 – Eccentric Fault (dynamic) – 50Nm	0.0029	0.0012	50.560	812.27

Note 1: When the abrasive bearing fault was present and the algorithm detected an eccentricity fault this was classed as CORRECT. The reason for this is that at the end of the bearing abrasive test, small amounts of rotor to stator rub was detected indicating that the worn bearing had caused a secondary problem of air-gap eccentricity. In addition, if MCSA is carried out the increase in eccentricity with increasing levels of abrasive bearing wear is clear. Hence, the two faults (bearing wear and eccentricity) are linked.

Note 2: If an eccentric fault was present and the algorithm detected a bearing fault then this was deemed as an INCORRECT diagnosis. This would appear to contradict ‘Note 1’; however, the time taken for an eccentric airgap to

considerably damage the bearing would be much longer than 1 – 2 hrs so the link between airgap eccentricity and bearing damage (for these short term tests) is unidirectional.

Table 10.11 Fuzzy logic diagnosis results for Phase 1 testing

FUZZY DIAGNOSIS		FAULT ZONE							
		Stator		Rotor		Eccentricity		Bearing	
EXPERIMENTAL DATAFILE	M1 – Healthy	HEALTHY	0	HEALTHY	0	SEVERE FAULT	100	HEALTY	15
	M2 - Healthy	HEALTHY	6	HEALTHY	0	HEALTHY	15	HEALTHY	0
	M3 - Healthy	HEALTHY	11	HEALTHY	0	MILD FAULT	45	SEVERE FAULT	84
	M4 - Healthy	HEALTHY	12	HEALTHY	0	HEALTHY	1	MILD FAULT	19
	M1 – Rotor Fault (1 bar)	HEALTHY	0	SEVERE FAULT	100	SEVERE FAULT	100	SEVERE FAULT	63
	M2 – Bearing Fault (abrasive) – 35mins	MILD FAULT	16	HEALTHY	0	SEVERE FAULT	79	HEALTHY	13
	M2 – Bearing Fault (abrasive) – 70mins	MILD FAULT	22	HEALTHY	0	SEVERE FAULT	100	SEVERE FAULT	100
	M2 – Bearing Fault (0.5mm point fault) – 35Nm	HEALTHY	0	HEALTHY	0	MILD FAULT	25	SEVERE FAULT	100
	M2 – Bearing Fault (1.5mm point fault) – 35Nm	HEALTHY	6	HEALTHY	0	MILD FAULT	22	SEVERE FAULT	100
	M3 – Stator Fault (shorted turns) – 4 turn	MILD FAULT	30	HEALTHY	0	SEVERE FAULT	69	SEVERE FAULT	100
	M3 – Stator Fault (shorted turns) – 7 turn	SEVERE FAULT	100	HEALTHY	0	SEVERE FAULT	100	SEVERE FAULT	100
	M3 – Stator Fault (shorted turns) – 11 turn	SEVERE FAULT	100	HEALTHY	0	SEVERE FAULT	100	SEVERE FAULT	100
	M3 – Stator Fault (shorted turns) – 14 turn	SEVERE FAULT	100	HEALTHY	0	SEVERE FAULT	100	SEVERE FAULT	100
	M4 – Eccentric Fault (static)	MILD FAULT	17	HEALTHY	0	MILD FAULT	41	SEVERE FAULT	48
	M4 – Eccentric Fault (dynamic)	HEALTHY	0	HEALTHY	0	SEVERE FAULT	100	SEVERE FAULT	100

Generally speaking, it appears that the major problem with the diagnostic system was the output of the bearing diagnostic method is overly sensitive to all fault types and even some healthy situations. This leads to many bearing incorrect fault diagnoses (many bearing fault false alarms).

Overall, the diagnosis success rate for this phase is 63 %.

Testing Phase 2

In order to improve the diagnosis accuracy further a new source of information was made available: negative sequence current. As mentioned previously, negative sequence current is particularly sensitive to stator winding short faults.

For each of the data files the negative sequence current as a proportion of positive sequence current was calculated (see Table 10.12). By normalising negative sequence against positive sequence current (measured current) this indicator can be used for any size of motor.

Table 10.12 Calculated negative sequence current values for each datafile

Measurement Data file	iP, Positive Sequence Current (A)	iN, Negative Sequence Current (A)	(iN/iP)*100 %
M1 H - 50Nm	22.8079	0.8021	3.517
M2 H - 35Nm	18.0406	0.2179	1.208
M3 H - 45 Nm	21.1464	1.2963	6.130
M4 H - 50Nm	22.5377	0.1435	0.637
M1 Rotor Bar - 50Nm	23.019	0.7124	3.095
M2 Abrasive 35Mins - 35Nm	18.4459	0.3977	2.156
M2 Abrasive 70Mins - 35Nm	18.3962	0.3531	1.919
M2 Bearing 0.5mm - 35Nm	18.0272	0.4617	2.561
M2 Bearing 1.5mm - 35Nm	18.1652	0.1296	0.713
M3 Stator Fault 4T - 45Nm	21.3814	1.4532	6.797
M3 Stator Fault 7T - 45Nm	21.5224	1.8514	8.602
M3 Stator Fault 11T - 45Nm	21.7868	2.8528	13.094
M3 Stator Fault 14T - 45Nm	22.0945	3.7164	16.820
M4 SE - 50Nm	22.7693	0.111	0.487
M4 DE - 50Nm	22.9596	0.2398	1.044

This extra information was involved in the decision making process of the fuzzy logic system by including it in the stator diagnosis fuzzy rule set (see section 10.10 for details). The reason for the implementation of these rules is to help clarify stator faults at low levels. The estimated fault parameter can be inaccurate at very low fault levels so the negative sequence value is utilised to increase the robustness of the algorithm by providing an extra variable to aid with the fault diagnosis calculations.

The results from testing phase 2 (with negative sequence current added to the rule set) are shown in Table 10.13.

Table 10.13 Fuzzy diagnosis results after phase 2

Motor Fault Case	Motor Subsystem							
	Stator		Rotor		Eccentricity		Bearing	
M1 – Healthy	HEALTHY	0	HEALTHY	0	SEVERE FAULT	100	HEALTY	15
M2 - Healthy	HEALTHY	0	HEALTHY	0	HEALTHY	15	HEALTHY	0
M3 - Healthy	HEALTHY	8	HEALTHY	0	MILD FAULT	45	SEVERE FAULT	84
M4 - Healthy	HEALTHY	8	HEALTHY	0	HEALTHY	1	MILD FAULT	19
M1 – Rotor Fault (1 bar)	HEALTHY	0	SEVERE FAULT	100	SEVERE FAULT	100	SEVERE FAULT	63
M2 – Bearing Fault (abrasive) – 35mins	HEALTHY	10	HEALTHY	0	SEVERE FAULT	79	HEALTHY	13
M2 – Bearing Fault (abrasive) – 70mins	HEALTHY	12	HEALTHY	0	SEVERE FAULT	100	SEVERE FAULT	100
M2 – Bearing Fault (0.5mm point fault) – 35Nm	HEALTHY	0	HEALTHY	0	MILD FAULT	25	SEVERE FAULT	100
M2 – Bearing Fault (1.5mm point fault) – 35Nm	HEALTHY	5	HEALTHY	0	MILD FAULT	22	SEVERE FAULT	100
M3 – Stator Fault (shorted turns) – 4 turn	MILD FAULT	21	HEALTHY	0	SEVERE FAULT	69	SEVERE FAULT	100
M3 – Stator Fault (shorted turns) – 7 turn	SEVERE FAULT	100	HEALTHY	0	SEVERE FAULT	100	SEVERE FAULT	100
M3 – Stator Fault (shorted turns) – 11 turn	SEVERE FAULT	100	HEALTHY	0	SEVERE FAULT	100	SEVERE FAULT	100
M3 – Stator Fault (shorted turns) – 14 turn	SEVERE FAULT	100	HEALTHY	0	SEVERE FAULT	100	SEVERE FAULT	100
M4 – Eccentric Fault (static)	HEALTHY	11	HEALTHY	0	MILD FAULT	41	SEVERE FAULT	48
M4 – Eccentric Fault (dynamic)	HEALTHY	0	HEALTHY	0	SEVERE FAULT	100	SEVERE FAULT	100

Now, the stator fault data is the only data that causes a positive stator fault diagnosis to be made. This increases the successful diagnosis rate to 68%.

Initial Testing Phase 3

The issue with the over sensitive bearing fault diagnosis is still apparent. Other faults are incorrectly being classified as bearing faults. This is due to the nature of the primary bearing fault detection method – the Total Spectral Energy (TSE) algorithm. This method tracks the energy across the whole spectrum in order to detect increases in energy due to vibrations caused by the faulty bearings. However, all faults cause an increase in energy across the spectrum at some point, therefore they result a bearing fault being diagnosed.

To overcome this problem the reliable rotor and stator diagnoses can be used. The algorithm is adjusted so that it recognises when a significant rotor or stator fault is present and does not diagnoses this as a bearing fault.

Unfortunately this means that if a bearing fault develops simultaneously with a stator or rotor fault it will not be detected. Due to the nature of the standard motor repair process, missed detection of bearing faults when occurring simultaneously with another fault is not serious flaw of an induction motor condition monitoring system. Standard practice for motor repair is to replace bearings whenever a motor is stripped down (for example to replace/repair a faulty rotor or rewind a faulty stator). Therefore even if the bearing is carrying a fault and this is masked by a stator or rotor fault the bearing issue will still be resolved during the maintenance activity.

The modification to the bearing process is implemented in hard (traditional logic) which overrules the fuzzy logic in the case of positive diagnoses for stator or rotor fault cases in addition to positive bearing diagnoses.

The results from this stage are given in Table 10.14. The change prevents active stator and rotor faults causing a positive bearing fault diagnosis. This increases the diagnosis success rate to 82%.

Testing Phase 4

There are still some incorrectly diagnosed cases in the system with regards to air-gap eccentricity. The fuzzy logic aspect of the system seemed to be fully optimised so it was decided that the air-gap fault detection algorithm would be revisited and improved.

The original eccentric energy algorithm produced the results shown in A modification to the algorithm was included in order to concentrate on the dominant eccentric components situated around the fundamental in an effort to avoid contamination by unrelated energy spikes at higher frequencies. This

eliminated higher harmonics relating to air-gap eccentricity using only the energy levels for the two dominant fundamental frequency sidebands. In addition the variation of the frequency components relating to eccentricity was compared across the phases in order to determine if noise due to other mechanical and electrical factors was interfering with the observed energy values at the eccentric characteristic frequencies. The results from the operation of the algorithm are given in Table 10.16.

Table 10.15. It is clear that there are several cases where supposedly healthy cases lead to a high fault level and vice-versa. For example, the rotor bar fault where the air-gap should be seen as healthy has the lowest (most severe) air-gap fault indicator value of 46.7dB.

Table 10.14 testing results after phase 3: bearing fault isolation

FUZZY DIAGNOSIS		FAULT ZONE							
		Stator		Rotor		Eccentricity		Bearing	
EXPERIMENTAL DATAFILE	M1 – Healthy	HEALTHY	0	HEALTHY	0	SEVERE FAULT	71	MILD FAULT	23
	M2 - Healthy	HEALTHY	0	HEALTHY	0	HEALTHY	0	HEALTHY	0
	M3 - Healthy	HEALTHY	8	HEALTHY	0	MILD FAULT	30	SEVERE FAULT	93
	M4 - Healthy	HEALTHY	8	HEALTHY	0	HEALTHY	0	MILD FAULT	30
	M1 – Rotor Fault (1 bar)	HEALTHY	0	SEVERE FAULT	100	SEVERE FAULT	100	HEALTHY	0
	M2 – Bearing Fault (abrasive) – 35mins	HEALTHY	10	HEALTHY	0	MILD FAULT	36	MILD FAULT	24
	M2 – Bearing Fault (abrasive) – 70mins	HEALTHY	12	HEALTHY	0	SEVERE FAULT	100	SEVERE FAULT	100
	M2 – Bearing Fault (0.5mm point fault) – 35Nm	HEALTHY	0	HEALTHY	0	HEALTHY	14	SEVERE FAULT	100
	M2 – Bearing Fault (1.5mm point fault) – 35Nm	HEALTHY	5	HEALTHY	0	HEALTHY	9	SEVERE FAULT	100
	M3 – Stator Fault (shorted turns) – 4 turn	MILD FAULT	21	HEALTHY	0	MILD FAULT	30	HEALTHY	0
	M3 – Stator Fault (shorted turns) – 7 turn	SEVERE FAULT	100	HEALTHY	0	MILD FAULT	48	HEALTHY	0
	M3 – Stator Fault (shorted turns) – 11 turn	SEVERE FAULT	100	HEALTHY	0	SEVERE FAULT	90	HEALTHY	0
	M3 – Stator Fault (shorted turns) – 14 turn	SEVERE FAULT	100	HEALTHY	0	SEVERE FAULT	100	HEALTHY	0
	M4 – Eccentric Fault (static)	HEALTHY	11	HEALTHY	0	MILD FAULT	30	SEVERE FAULT	68
	M4 – Eccentric Fault (dynamic)	HEALTHY	0	HEALTHY	0	SEVERE FAULT	100	SEVERE FAULT	100

A modification to the algorithm was included in order to concentrate on the dominant eccentric components situated around the fundamental in an effort to

avoid contamination by unrelated energy spikes at higher frequencies. This eliminated higher harmonics relating to air-gap eccentricity using only the energy levels for the two dominant fundamental frequency sidebands. In addition the variation of the frequency components relating to eccentricity was compared across the phases in order to determine if noise due to other mechanical and electrical factors was interfering with the observed energy values at the eccentric characteristic frequencies. The results from the operation of the algorithm are given in Table 10.16.

Table 10.15 Calculated energy (dB) of eccentricity related frequency components (fs±fr) for the measured current on each supply line

Data File	Shaft Speed (rpm)	Fundamental Normalised Amplitude of Eccentricity Related Frequency Components (dB)			
		Line 1	Line 2	Line 3	3-Phase Mean
M1 H - 50Nm	1446	52.683	54.641	52.142	**53.16**
M2 H - 35Nm	1458	60.250	61.211	61.565	**61.01**
M3 H - 45 Nm	1452	55.963	56.390	56.953	**56.44**
M4 H - 50Nm	1446	61.180	60.690	63.907	**61.93**
M1 Rotor Bar - 50Nm	1447	46.613	46.968	46.715	**46.77**
M2 Abrasive 35Mins - 35Nm	1459	54.876	54.185	54.762	**54.61**
M2 Abrasive 70Mins - 35Nm	1457	48.839	48.032	47.978	**48.28**
M2 Bearing 0.5mm - 35Nm	1460	58.728	61.055	59.873	**59.89**
M2 Bearing 1.5mm - 35Nm	1461	60.666	59.942	60.379	**60.33**
M3 Stator Fault 4T - 45Nm	1451	54.758	56.212	54.044	**55.00**
M3 Stator Fault 7T - 45Nm	1452	54.336	54.849	52.725	**53.97**
M3 Stator Fault 11T - 45Nm	1452	53.655	53.428	50.981	**52.69**
M3 Stator Fault 14T - 45Nm	1450	52.268	52.328	49.759	**51.45**
M4 SE - 50Nm	1441	56.945	57.171	56.320	**56.81**
M4 DE - 50Nm	1441	50.449	50.168	51.064	**50.56**

Analysis of the results indicates that the lower sideband (fs-fr) shown in the ‘Lower Mean’ column is more suitable for detecting eccentric air-gap faults since the difference between the healthy and faulty cases (highlighted rows) is the most significant with a difference of 13dB and 19dB for the static and dynamic eccentricities respectively. This is shown by the ‘lower mean’ column which indicates the mean value in dB across all three phases. From this column

it can be seen that the ‘healthy’ cases have a low eccentric energy values (73dB to 63dB) and the eccentricity cases have higher values (61dB to 55dB). Also in the abrasive testing where severe eccentricity was known to be present the values were high too (50dB and 57dB). Note: higher dB values indicate less eccentricity related energy in the line current spectrum.

There is still the issue of other faults generating eccentric frequency energy levels which would incorrectly indicate a fault. This can be seen for the stator faults which show high eccentric energy with lower sideband magnitudes of 60.37dB, 58.27dB, 56.17dB and 54.68dB. This is caused by the modified air-gap flux produced by the stator fault which generates a number of frequency components one of which is the fs±fr sidebands which the detection algorithm uses to indicate air-gap eccentricity faults.

This problem is alleviated by considering the variance between the eccentric fault component magnitudes across the 3 line currents. In addition to causing changes in the frequency spectrum, stator turn-to-turn faults also create a significant current imbalance across the 3 motor windings and therefore a current imbalance in the supply lines. This can be clearly seen by the high values in the ‘Inter Line Variance Lower Sideband’ column (>10). The current imbalance causes differences in magnitude of the frequency components across the 3 line currents; this effect is not seen with eccentric air-gap faults since no significant increase in RMS current imbalance occurs. The difference in this characteristic between stator and airgap faults allows the two cases to be differentiated.

The fuzzy logic rule set for air-gap faults can now be modified based on this information, taking into account the lower eccentric energy sideband and the variance in the energy of that sideband across the three supply lines.

The variance quantity explained in the previous paragraph was converted to a fuzzy quantity using the input membership function shown in Figure 10.12.

Table 10.16 Eccentric energy levels using new algorithm

Data File	Shaft Speed (rpm)	Fundamental Normalised Amplitude of Eccentricity Related Frequency Components (dB)										
		Supply Line 1		Supply Line 2		Supply Line 3		3 Phase Mean Values			Inter-line Variance	
		Lower Sideband	Upper Sideband	Lower Sideband	Upper Sideband	Lower Sideband	Upper Sideband	Mean	Lower Mean	Upper Mean	Lower Sideband	Upper Sideband
M1 H - 50Nm	1446	64.441	53.537	68.838	55.91	64.906	53.196	60.14	66.06	54.21	5.84	2.19
M2 H - 35Nm	1458	66.452	69.990	67.281	69.701	67.432	71.503	68.73	67.06	70.40	0.28	0.94
M3 H - 45 Nm	1452	62.368	58.715	61.959	59.199	63.420	59.560	60.87	62.58	59.16	0.57	0.18
M4 H - 50Nm	1446	81.232	67.194	68.464	69.081	70.777	67.985	70.79	73.49	68.09	46.28	0.90
M1 Rotor Bar - 50Nm	1447	61.944	54.572	59.956	58.685	61.094	55.311	58.59	61.00	56.19	0.99	4.81
M2 Abrasive 35Mins - 35Nm	1459	60.583	57.187	61.236	56.171	58.477	59.317	58.83	60.10	57.56	2.08	2.58
M2 Abrasive 70Mins - 35Nm	1457	54.277	50.583	52.592	50.044	52.188	50.433	51.69	53.02	50.35	1.23	0.08
M2 Bearing 0.5mm - 35Nm	1460	62.262	69.433	64.928	69.418	64.017	71.348	66.90	63.74	70.07	1.84	1.23
M2 Bearing 1.5mm - 35Nm	1461	67.872	65.462	64.406	65.225	66.406	65.996	65.89	66.23	65.56	3.03	0.16
M3 Stator Fault 4T - 45Nm	1451	60.485	57.178	63.616	58.261	57.004	59.077	59.27	60.37	58.17	10.94	0.91
M3 Stator Fault 7T - 45Nm	1452	60.565	56.039	59.707	57.227	54.533	58.443	57.75	58.27	57.24	10.65	1.44
M3 Stator Fault 11T - 45Nm	1452	59.799	55.595	56.481	56.804	52.218	58.808	56.62	56.17	57.07	14.44	2.63
M3 Stator Fault 14T - 45Nm	1450	58.631	55.265	54.644	57.094	50.777	58.339	55.79	54.68	56.90	15.42	2.39
M4 SE - 50Nm	1441	61.496	62.530	60.515	62.394	60.570	62.818	61.72	60.86	62.58	0.30	0.05
M4 DE - 50Nm	1441	55.612	52.395	54.099	52.678	54.349	54.180	53.89	54.69	53.08	0.66	0.92

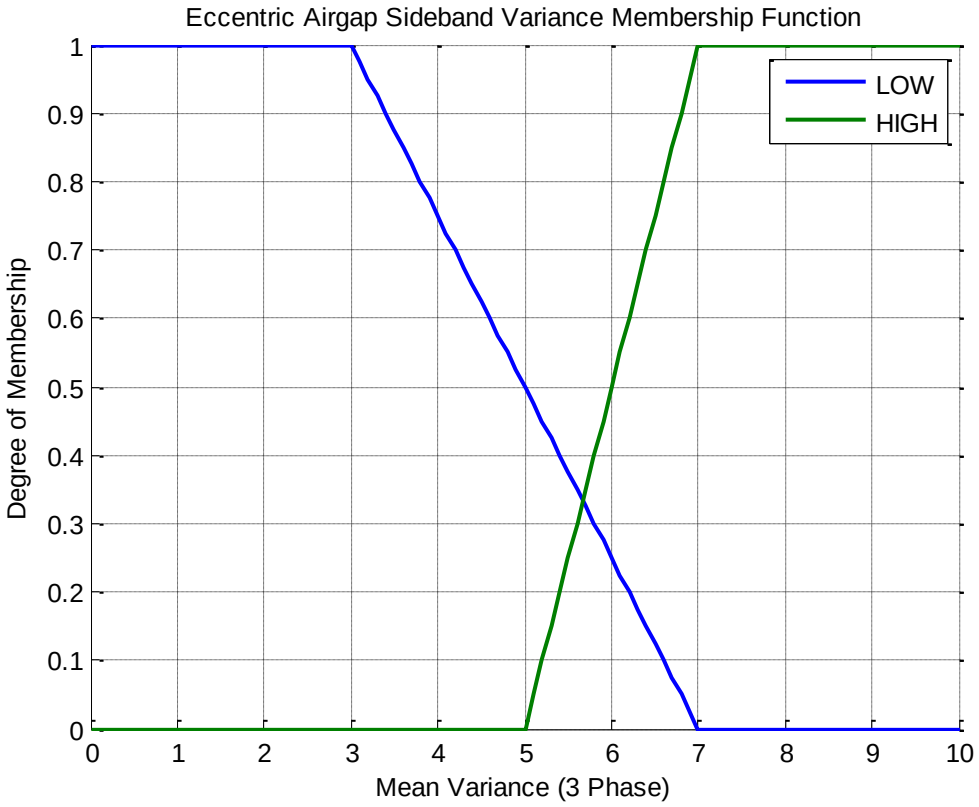

Figure 10.12 Eccentric sideband variance membership function

The rule set for air-gap fault detection is extended from single input to two inputs to take into account the sideband variance quantity. The two dimensional associate matrix taken into account sideband variance is given in Table 10.17. Blank fields in the table indicate the OR operator is not active in this condition, for example, if sideband variance is 'LOW' and AGFault is 'VERY LOW' then the rule used will be from the 1D AGFault table (Table 10.6) for 'VERY LOW' since it was decided that there is no need for an OR statement for this combination of inputs.

Table 10.17 Associative matrix (logic OR) for eccentric air-gap faults (blank fields indicate algorithm uses 1D (AGFault only) rule set i.e. no OR operator)

Input Associative Matrix		Sideband Variance	
		LOW	HIGH
AGFault	VERY LOW		*HEALTHY*
	LOW	*MILD FAULT*	
	MEDIUM	*MILD FAULT*	
	HIGH	*SEVERE FAULT*	
	VERY HIGH	*SEVERE FAULT*	

The results after the new airgap diagnosis rules have been added are shown in Table 10.18. The misclassification of air-gap faults has been significantly reduced for this representative dataset.

Table 10.18 Results after testing phase 4

FUZZY DIAGNOSIS		FAULT ZONE							
		Stator		Rotor		Eccentricity		Bearing	
EXPERIMENTAL DATAFILE	M1 – Healthy	HEALTHY	0	HEALTHY	0	HEALTHY	0	MILD FAULT	23
	M2 - Healthy	HEALTHY	0	HEALTHY	0	HEALTHY	0	HEALTHY	0
	M3 - Healthy	HEALTHY	8	HEALTHY	0	HEALTHY	0	SEVERE FAULT	93
	M4 - Healthy	HEALTHY	8	HEALTHY	0	HEALTHY	0	MILD FAULT	30
	M1 – Rotor Fault (1 bar)	HEALTHY	0	SEVERE FAULT	100	MILD FAULT	30	HEALTHY	0
	M2 – Bearing Fault (abrasive) – 35mins	HEALTHY	10	HEALTHY	0	MILD FAULT	52	MILD FAULT	24
	M2 – Bearing Fault (abrasive) – 70mins	HEALTHY	12	HEALTHY	0	SEVERE FAULT	100	SEVERE FAULT	100
	M2 – Bearing Fault (0.5mm point fault) – 35Nm	HEALTHY	0	HEALTHY	0	HEALTHY	0	SEVERE FAULT	100
	M2 – Bearing Fault (1.5mm point fault) – 35Nm	HEALTHY	5	HEALTHY	0	HEALTHY	0	SEVERE FAULT	100
	M3 – Stator Fault (shorted turns) – 4 turn	MILD FAULT	21	HEALTHY	0	HEALTHY	0	HEALTHY	0
	M3 – Stator Fault (shorted turns) – 7 turn	SEVERE FAULT	100	HEALTHY	0	HEALTHY	0	HEALTHY	0
	M3 – Stator Fault (shorted turns) – 11 turn	SEVERE FAULT	100	HEALTHY	0	HEALTHY	0	HEALTHY	0
	M3 – Stator Fault (shorted turns) – 14 turn	SEVERE FAULT	100	HEALTHY	0	HEALTHY	0	HEALTHY	0
	M4 – Eccentric Fault (static)	HEALTHY	11	HEALTHY	0	MILD FAULT	35	SEVERE FAULT	68
	M4 – Eccentric Fault (dynamic)	HEALTHY	0	HEALTHY	0	SEVERE FAULT	100	SEVERE FAULT	100

After the modifications at this stage are included the successful diagnosis rate is increased to 90%.

Testing Stage 5

The final improvement is to modify the fuzzy logic system to allow it to differentiate a severe rotor fault from a light eccentricity fault.

This problem occurs due to the high levels of energy in the current spectrum at low frequencies (0-100Hz) due to the multiple repeating sidebands produced by the rotor fault. In order for the two to be differentiated the spectrum is searched using narrower frequency bands to prevent the two fault frequencies associated with airgap and rotor faults being misdiagnosed. The reason narrower frequency bands can be used is due to the use of an accurate spectral speed estimation technique (see Speed Estimation chapter).

This change results in the final diagnosis results shown in Table 10.19, increasing the diagnosis accuracy to 92%.

10.14 Utilising the 'birth' histories

The results shown above were obtained based on absolute fault indicator values assuming no knowledge of the machine's initial condition. This method of fault detection is not suitable for a generic system since the environmental and historical conditions under which the motor operates can vary for different motors and different applications. In order for a system to take into account these differences in motor type, assembly, installation, load and supply conditions the fault diagnosis should be relative i.e. the diagnosis at time t is based on a comparison with the condition at time = 0.

Table 10.19 Final stage fuzzy diagnosis results

FUZZY DIAGNOSIS		FAULT ZONE							
		Stator		Rotor		Eccentricity		Bearing	
EXPERIMENTAL DATAFILE	M1 – Healthy	HEALTHY	0	HEALTHY	0	HEALTHY	0	MILD FAULT	23
	M2 - Healthy	HEALTHY	0	HEALTHY	0	HEALTHY	0	HEALTHY	0
	M3 - Healthy	HEALTHY	8	HEALTHY	0	HEALTHY	0	SEVERE FAULT	93
	M4 - Healthy	HEALTHY	8	HEALTHY	0	HEALTHY	0	MILD FAULT	30
	M1 – Rotor Fault (1 bar)	HEALTHY	0	SEVERE FAULT	100	HEALTHY	0	HEALTHY	0
	M2 – Bearing Fault (abrasive) – 35mins	HEALTHY	10	HEALTHY	0	MILD FAULT	52	MILD FAULT	24
	M2 – Bearing Fault (abrasive) – 70mins	HEALTHY	12	HEALTHY	0	SEVERE FAULT	100	SEVERE FAULT	100
	M2 – Bearing Fault (0.5mm point fault) – 35Nm	HEALTHY	0	HEALTHY	0	HEALTHY	0	SEVERE FAULT	100
	M2 – Bearing Fault (1.5mm point fault) – 35Nm	HEALTHY	5	HEALTHY	0	HEALTHY	0	SEVERE FAULT	100
	M3 – Stator Fault (shorted turns) – 4 turn	MILD FAULT	21	HEALTHY	0	HEALTHY	0	HEALTHY	0
	M3 – Stator Fault (shorted turns) – 7 turn	SEVERE FAULT	100	HEALTHY	0	HEALTHY	0	HEALTHY	0
	M3 – Stator Fault (shorted turns) – 11 turn	SEVERE FAULT	100	HEALTHY	0	HEALTHY	0	HEALTHY	0
	M3 – Stator Fault (shorted turns) – 14 turn	SEVERE FAULT	100	HEALTHY	0	HEALTHY	0	HEALTHY	0
	M4 – Eccentric Fault (static)	HEALTHY	11	HEALTHY	0	MILD FAULT	35	SEVERE FAULT	68
	M4 – Eccentric Fault (dynamic)	HEALTHY	0	HEALTHY	0	SEVERE FAULT	100	SEVERE FAULT	100

For example, if a healthy motor is installed in an area where it is exposed to significant environmental vibration this will affect the current signatures, and may lead to alarms being raised regarding its health. However if a birth history is taken then the algorithm is given the ability to account for the fact that this level of vibration is deemed to be acceptable (in this particular case) and only tracks the increase of fault features from this initial set-point.

If the bearing health column is observed (Table 10.19) it can be seen even before any fault (first four rows) has been introduced there can be significant variation in the spectral content of the current drawn by the motors due to a number of unknown factors (motor condition, motor load, supply conditions, installation, etc). These ‘raw’ comparisons lead to incorrect diagnoses. For the

remainder of this thesis a baseline or reference point (dataset acquired at time = 0) will be used for motor condition diagnosis.

The fault indicator values for the healthy baselines and fault conditions are shown in Table 10.20. The first four rows provide the information for the healthy baselines for the four test motors. The fault cases listed below this display the absolute fault indicator values in addition to 'residual' terms which show the difference in each fault indicator between the baseline and current condition).

The fuzzy diagnosis system membership function is adjusted to account for the fact that residuals instead of absolute values are now being analysed. These membership functions now interpret the differences between the healthy 'birth' case and current case rather than simply interpreting the absolute fault values alone.

Table 10.20 Fault indicator method outputs and residual values (healthy baseline comparisons)

Dataset	FAULT ZONE								Additional Data	
	Stator	*Stator Res.*	Rotor	Rotor Res.	Air Gap	AG Res.	Bear.	Bear. Res.	Neg. Seq.	LSB Var.
M1 – Healthy – 50Nm	0.001	*N/A*	0	N/A	66.06	N/A	820.0	N/A	3.517	3.9
M2 – Healthy – 35Nm	0.006	*N/A*	0	N/A	67.06	N/A	822.3	N/A	1.208	0.2
M3 – Healthy – 45 Nm	0.008	*N/A*	0	N/A	62.58	N/A	814.3	N/A	6.13	0.4
M4 – Healthy – 50Nm	0.008	*N/A*	0	N/A	73.49	N/A	818.6	N/A	0.637	30.9
M1 – Rotor Fault (1 bar)- 50Nm	0.003	*0.002*	0.05	0.052	61	5.06	814.9	5.15	3.095	0.7
M2 – Bearing Fault (abrasive) – 35mins – 35Nm	0.009	*0.002*	0	0	60.1	6.96	820.7	1.67	2.156	1.4
M2 – Bearing Fault (abrasive) – 75mins – 35Nm	0.009	*0.003*	0	0	53.02	14.04	813.9	8.39	1.919	0.8
M2 – Bearing Fault (0.5mm point fault) – 35Nm	0.005	*-0.002*	0	0	63.74	3.32	806.6	15.76	2.561	1.2

M2 – Bearing Fault (1.5mm point fault) – 35Nm	0.006	*0.000*	0	0	66.23	0.83	767.9	54.48	0.713	2
M3 – Stator Fault (shorted turns) – 4 turn – 45Nm	0.014	*0.006*	0	0	60.37	2.20	813.3	1.04	6.797	7.3
M3 – Stator Fault (shorted turns) – 7 turn – 45Nm	0.027	*0.019*	0.01	0.008	58.27	4.31	813.6	0.76	8.602	7.1
M3 – Stator Fault (shorted turns) – 11 turn – 45Nm	0.047	*0.039*	0	0	56.17	6.41	805.3	9.08	13.09	9.6
M3 – Stator Fault (shorted turns) – 14 turn – 45Nm	0.063	*0.055*	0	0	54.68	7.9	810.7	3.66	16.82	10.3
M4 – Eccentric Fault (static) – 50Nm	0.009	*0.001*	0	-0.004	60.86	12.63	815.4	3.24	0.487	0.2
M4 – Eccentric Fault (dynamic) – 50Nm	0.003	*-0.005*	0	-0.003	54.69	18.8	812.3	6.32	1.044	0.4

The final results of the diagnosis for the updated system using the baseline comparison method are shown in Table 10.21.

Table 10.21 Fuzzy diagnosis results using healthy 'birth' signatures as a baseline

FUZZY DIAGNOSIS	FAULT ZONE							
	Stator		Rotor		Eccentricity		Bearing	
M1 – Rotor Fault (1 bar)	HEALTHY	0	SEVERE FAULT	100	HEALTHY	1	HEALTHY	0
M2 – Bearing Fault (abrasive) – 35mins	HEALTHY	3	HEALTHY	0	MILD FAULT	24	MILD FAULT	17
M2 – Bearing Fault (abrasive) – 70mins	HEALTHY	8	HEALTHY	0	SEVERE FAULT	100	SEVERE FAULT	73
M2 – Bearing Fault (0.5mm point fault) – 35Nm	HEALTHY	0	HEALTHY	0	HEALTHY	0	SEVERE FAULT	100
M2 – Bearing Fault (1.5mm point fault) – 35Nm	HEALTHY	0	HEALTHY	0	HEALTHY	0	SEVERE FAULT	100
M3 – Stator Fault (shorted turns) – 4 turn	MILD FAULT	21	HEALTHY	0	HEALTHY	0	HEALTHY	10
M3 – Stator Fault (shorted turns) – 7 turn	SEVERE FAULT	85	HEALTHY	0	HEALTHY	0	HEALTHY	7
M3 – Stator Fault (shorted turns) – 11 turn	SEVERE FAULT	100	HEALTHY	0	HEALTHY	0	HEALTHY	0
M3 – Stator Fault (shorted turns) – 14 turn	SEVERE FAULT	100	HEALTHY	0	HEALTHY	0	HEALTHY	0
M4 – Eccentric Fault (static)	HEALTHY	0	HEALTHY	0	SEVERE FAULT	90	MILD FAULT	39
M4 – Eccentric Fault (dynamic)	HEALTHY	0	HEALTHY	0	SEVERE FAULT	100	MILD FAULT	52

Each fault case in this development test set is now correctly identified and false alarms (incorrect diagnoses) have been minimised. The development stage results have the following characteristics:

- 44 diagnoses are made
- Fault detection rate is 100%
- Fault isolation rate is 95.45% (successful diagnosis rate is 95.45%)

The reason that the FDS algorithm did not achieve 100% diagnosis accuracy is that with the implemented fault indicators there is no way to differentiate between the combined bearing and air-gap eccentricity faults and air-gap eccentricity fault acting independently. However, the algorithm can successfully detect a bearing fault if it is the only fault occurring.

Having been developed on this small representative dataset the algorithms can now be validated on a much larger dataset considering a variety of loading conditions and load coupling types. The limitations of the developed FDD method are discussed below and this is followed by the full dataset results which involve applying the FDD system developed by this thesis to the diagnosis of 78 different motor conditions.

10.15 Limitations

The FDS achieves a 100% fault detection rate (i.e. it can always detect a faulty component) however it has some limitations when it comes to isolating faults (detecting which of the 4 faults is present).

The reasons for these limitations are that the bearing fault indicator (total spectral energy) is a wideband method. It sums energy over the entire measureable spectrum (limited by the Nyquist frequency). Therefore if the energy increases at any point in the spectrum this will be detected. Unfortunately this means that although it can detect bearing faults it will be triggered by the other fault types too.

In the following cases the bearing fault may be detected but the diagnosis system would not be able to tell whether the fault (rotor, stator or eccentricity) is operating in isolation or is accompanied by a bearing fault:

- BEARING FAULT AND STATOR FAULT PRESENT
- BEARING FAULT AND ECCENTRIC AIR-GAP FAULT PRESENT
- BEARING FAULT AND ROTOR FAULT PRESENT

Additionally in the following cases the bearing fault may be detected but it might not be present:

- ECCENTRIC AIR-GAP FAULT PRESENT

These scenarios are only a problem if the two faults are developing simultaneously at the same rate. If the faults are developing at a different rate then they will be detected independently.

Although in an ideal world it would be preferable to be able to differentiate between these faults (when combined faults are present) it is not a critical flaw of the system. This is because if a motor is sent to repair it is fitted with a new set of bearings as a matter of course. In this way if a bearing fault is present but undetected the maintenance activity would still result in the motor being restored to its original healthy condition.

It is important to state that if a bearing fault alone *is* present it *will* be detected. However the system will raise alarms on the other faults before the bearing fault if a combined fault situation is encountered.

10.16 Full dataset results

The study into fault detection, fault diagnosis and fault isolation success rate was carried out across the entire dataset which includes stator, rotor, bearing and airgap faults for both bellows coupling (inline) connected loads and belt and pulley connected loads. A list of all the fault conditions included in the validation test set is given by Table 10.22. Each of these conditions was tested under the two load connection types and at a number of different loads. The faults were tested at various loading levels[2]: 30Nm (60% rated load), 35Nm, 40Nm, 45Nm and 50Nm (100% rated load). By testing using different load connection and load torque conditions a through validation of the algorithms should be obtained.

A separate motor was used for each of the four faults (airgap, bearing, rotor, and stator) and initially this motor was run in an unmodified configuration on the test-bed in order to generate a healthy baseline. After this, each of the motors was modified with a particular fault and a new faulty dataset was generated. The baseline and faulty dataset were then compared to generate the condition diagnosis.

The dataset included 78 different motor conditions including two different load connection methods and as mentioned previously included full and moderate load conditions (> 60% rated load) in order to make the test as rigorous as possible. An example of the result format for bellows coupled airgap faults is given below for air-gap faults. For each fault type and loading connection these results were generated by testing the entire condition monitoring system including all the modelling, parameter estimation process, fault detection

[2] Stator fault testing involved only one loading level of 40Nm in order to limit the damaging heating effect of unbalanced winding currents.

methods and fuzzy logic diagnosis system. The fuzzy linguistic terms (e.g. ‘Severe fault’) are presented alongside the health score for each of the 78 diagnosis cases.

Table 10.22 Description of the test cases used in the full dataset testing of the complete system (including fuzzy logic diagnosis engine)

ID	Fault Type	Description
1	Airgap - SE	Eccentric collar fitted to inner race of a smaller bearing in order to produce 40% static eccentricity
2	Airgap - DE	Eccentric collar fitted to outer race of a smaller bearing in order to produce 40% dynamic eccentricity
3	Bearing - ABR	Bearing turned on a lathe for 50 minutes with grease replaced by abrasive paste (to replicate generalised roughness fault)
4	Bearing – 0.5mm	0.5mm width slot in outer race
5	Bearing – 1.5mm	1.5mm width slot in outer race
6	Rotor – 1.5mm	1.5mm of 1 rotor bar removed by drilling (partial bar break)
7	Rotor – 2.5mm	2.5mm of 1 rotor bar removed by drilling (partial bar break)
8	Rotor – 3.5mm	3.5mm of 1 rotor bar removed by drilling (partial bar break)
9	Rotor – 4.5mm	4.5mm of 1 rotor bar removed by drilling (partial bar break)
10	Rotor – 6.0mm	6.0mm of 1 rotor bar removed by drilling (full bar break)
11	Stator – 2 ST	2 of 105 turns in one phase shorted
12	Stator – 5 ST	5 of 105 turns in one phase shorted
13	Stator – 8 ST	8 of 105 turns in one phase shorted
14	Stator – 11 ST	11 of 105 turns in one phase shorted
15	Stator – 14 ST	14 of 105 turns in one phase shorted

Table 10.23 Direct shaft coupling air-gap condition final testing resuts

Load Torque (Nm)	40% Static Eccentricity				40% Dynamic Eccentricity			
49. 6	Component	Condition Diagnosis			Component	Condition Diagnosis		
		Fuzzy				Fuzzy		Precise
	Stator	'HEALTHY'	0	✓	Stator	'HEALTHY'	13	✓
	Rotor	'HEALTHY'	0	✓	Rotor	'HEALTHY'	0	✓
	Airgap	'SEVERE FAULT'	97	✗	Airgap	'SEVERE FAULT'	100	✗
	Bearing	'HEALTHY'	0	✓	Bearing	'HEALTHY'	0	✓
45	Component	Condition Diagnosis			Component	Condition Diagnosis		
		Fuzzy		Precise		Fuzzy		Precise
	Stator	'HEALTHY'	9	✓	Stator	'HEALTHY'	10	✓
	Rotor	'SEVERE FAULT'	100	✗	Rotor	'SEVERE FAULT'	100	✗
	Airgap	'SEVERE FAULT'	71	✗	Airgap	'SEVERE FAULT'	100	✗
	Bearing	'HEALTHY'	0	✓	Bearing	'HEALTHY'	0	✓
40	Component	Condition Diagnosis			Component	Condition Diagnosis		
		Fuzzy		Precise		Fuzzy		Precise
	Stator	'HEALTHY'	0	✓	Stator	'HEALTHY'	20	✓
	Rotor	'SEVERE FAULT'	100	✗	Rotor	'HEALTHY'	0	✓
	Airgap	'SEVERE FAULT'	72	✗	Airgap	'SEVERE FAULT'	100	✗
	Bearing	'HEALTHY'	0	✓	Bearing	'HEALTHY'	0	✓
35	Component	Condition Diagnosis			Component	Condition Diagnosis		
		Fuzzy		Precise		Fuzzy		Precise
	Stator	'HEALTHY'	0	✓	Stator	'HEALTHY'	0	✓
	Rotor	'HEALTHY'	6	✓	Rotor	'HEALTHY'	18	✓
	Airgap	'SEVERE FAULT'	100	✗	Airgap	'SEVERE FAULT'	100	✗
	Bearing	'HEALTHY'	0	✓	Bearing	'HEALTHY'	0	✓
30	Component	Condition Diagnosis			Component	Condition Diagnosis		
		Fuzzy		Precise		Fuzzy		Precise
	Stator	'HEALTHY'	0	✓	Stator	'HEALTHY'	0	✓
	Rotor	'MILD FAULT'	26	!	Rotor	'MILD FAULT'	28	!
	Airgap	'MILD FAULT'	61	!	Airgap	'SEVERE FAULT'	100	✗
	Bearing	'HEALTHY'	0	✓	Bearing	'HEALTHY'	0	✓

The overall dataset results are then combined are presented in Figure 10.13 and Table 10.24. These results are therefore the overall test results for the entire system and are derived by using the entire system from baseline development, system identification, speed estimation, fault detection and finally fault diagnosis. The results presented here aggregate all results (78 conditions in total).

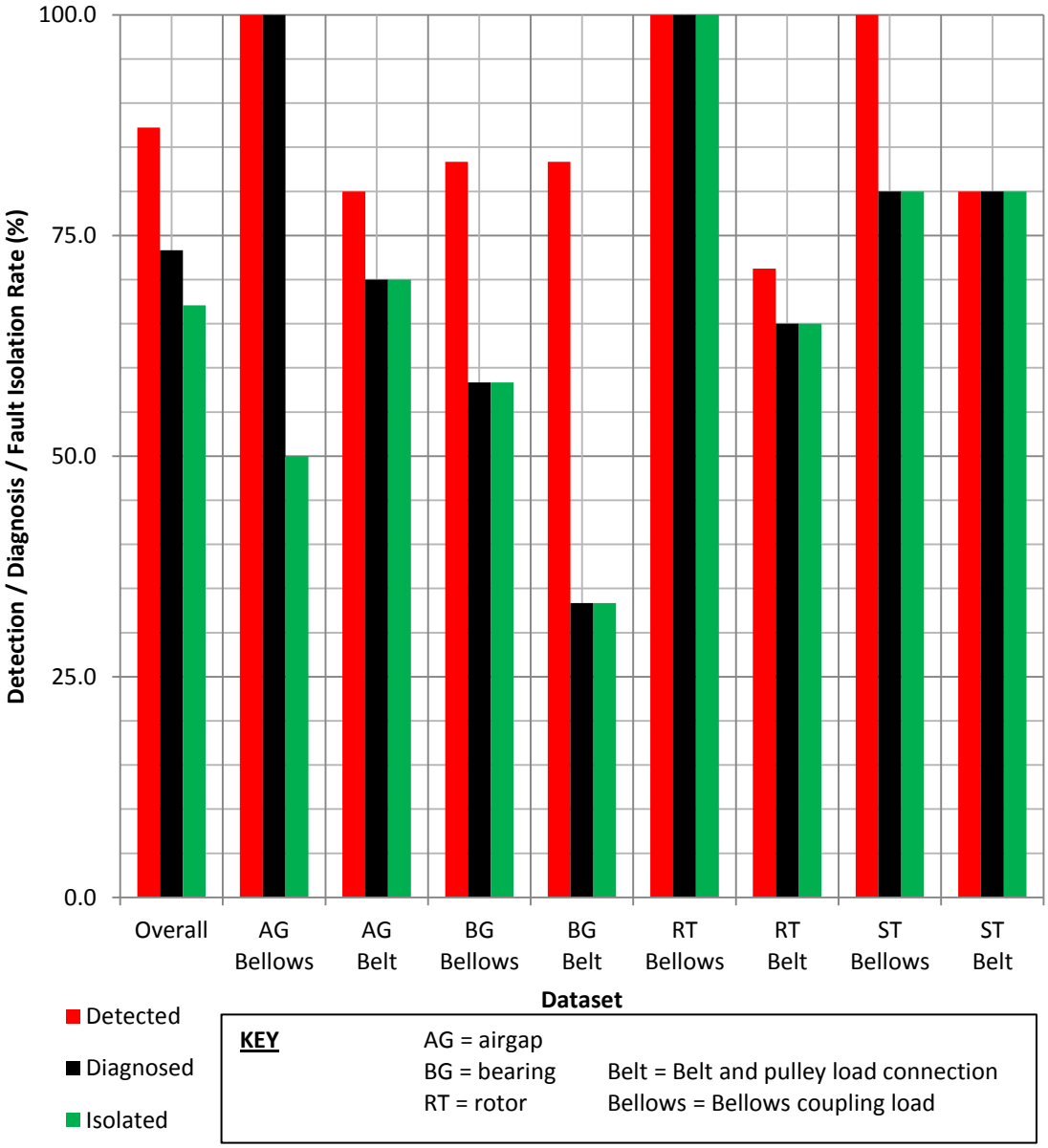

Figure 10.13 Fault detection, diagnosis and isolation results for bearing, airgap, stator and rotor faults

Table 10.24 Fault detection, diagnosis and isolation results

Monitoring Process	**Overall**	AG Bellows	AG Belt	BG Bellows	BG Belt	RT Bellows	RT Belt	ST Bellows	ST Belt
Detected (%)	**87.2**	100.0	80.0	83.3	83.3	100.0	71.3	100.0	80.0
Diagnosed (%)	**73.3**	100.0	70.0	58.3	33.3	100.0	65.0	80.0	80.0
Isolated (%)	**67.1**	50.0	70.0	58.3	33.3	100.0	65.0	80.0	80.0

The success of the detection and diagnosis procedure is measured using three values; detection, diagnosis and isolation. Detection is successfully determining that any of the four faults are present i.e. that the motor is no longer healthy.

Diagnosis is the ability to correctly detect the location of the specific fault that is actually present. Isolation is the ability to correctly detect the fault that is present in isolation i.e. to detect the correct fault and no other faults.

The overall results show that the system provides good performance with an overall detection rate of 87.2% a diagnosis rate of 73.3% and a fault isolation rate of 67.1 %.

The model based fault detection methods (rotor and stator) provide the best performance with isolation rates averaged across these datasets in excess of 80%. Fault detection rates for bearing faults are good (over 80%) but diagnosis and isolation of these faults proves more challenging. This is due to the fact that bearing faults can sometimes be mistaken for other faults due to small magnitude of bearing fault related content in the stator currents.

Air-gap fault detection and diagnosis performance is acceptable with high fault detection and diagnosis rates (in excess of 80% considering both load connections) and an average isolation rate of 60%. In general, the shaft (bellows coupling) connected load datasets have improved detection, diagnosis and isolation rates than the belt connected load. This is due to the increased noise in the low frequency part of the spectrum in the belt-connected case due to the belt-vibration sidebands around the supply frequency.

Overall the fuzzy logic based diagnosis system provides good results and has proved its ability to track the condition of the four major induction motor subsystems effectively.

10.17 Summary

This chapter has described the development and testing of a fault detection and diagnosis system which uses fuzzy logic to reach diagnosis decisions.

The system has been developed in MATLAB using standard MATLAB functionality (as opposed to the Fuzzy Logic toolset). The system takes the outputs from the fault detection methods and uses this information to determine whether the core motor components (stator, rotor, air-gap and bearings) are healthy, mildly faulty or have a severe fault. The system also presents a health 'score' between 0 and 100 which can be used for trending purposes.

The results show that overall the system provides good performance with an overall detection rate of 87.2% a diagnosis rate of 73.3% and a fault isolation rate of 67.1 %.

The limitations of the system have been described; when multiple faults are presents some faults mask/conflict with others so that in a scenario where two faults (one of which being a bearing fault) are present only one can be confirmed with a high level of certainty.

Overall the fuzzy logic based diagnosis system has good performance and has proved its ability to classify the four major internal motor faults in their incipient stages effectively.

Chapter 11. Conclusions and Further Work

11.1 Aims of the thesis

Chapters 1 and 2 contain a critical survey of the existing literature in field of induction motor condition monitoring. The conclusions of this literature review were as follows:

a) Current based monitoring techniques are the most suitable for industrial applications since they require no additional measurement hardware (motor current and voltage will normally already be measured at the MCC) and thus avoid the cost and installation effort associated with other sensors.
b) Model-based techniques offer advantages over other methods in terms of being easily scaled to different motor specifications and also provide a clear link between faults and symptoms (variation in specific parameters). However, model-based techniques require knowledge of machine parameters.
c) MCSA offers a proven method of detecting faults via the current spectrum but requires information on machine construction and operating speed.
d) Diagnosis techniques can be broadly split into two groups; reasoning methods and classification methods. Classification methods require extensive training to 'learn' the problem whereas reasoning methods are limited by strict IF-THEN rules and it can be difficult to obtain the expert knowledge to construct the knowledge-base.

e) Although detection and diagnosis of each fault has been considered extensively in literature very few studies demonstrate detection of multiple faults and isolation of these faults.

Based on literature review the aims of the thesis were decided and a summarised below:

1) Develop a FDD system using only three-phase current and voltage and that can adapt to different ambient conditions. The system must also operate without the need for extensive knowledge of the motor in question; only nameplate data should be used.
2) Develop a parameter estimation process that can identify the main machine parameters based only on the measured three-phase voltages and currents. This will allow the algorithm to adapt to different motors.
3) Develop fault detection methods sensitive to the existence of the most prevalent IM fault types (stator, rotor, air-gap and bearing) simultaneously.
4) Develop a diagnosis algorithm which can interpret the outputs of the fault methods based on a limited amount of information on fault symptoms and are tolerant to the errors generated by other parts of the system (e.g. measurement error or modelling error).

The overall focus of this set of objectives was to develop a practical system that can be readily used in industry to provide a general CM system for IM, capturing the vast majority of machine faults on a variety of motors in different applications. The key factors were the use of a mixed set of residuals (e.g. MCSA and model-based methods) to allow detection of a range of faults, making the algorithm adaptive to allow use on a range of motors and loads and

utilise only current and voltage to make the system suitable for industrial deployment. This resulted in the creation of the adaptive mixed residual approach (AMRA) for current based condition monitoring.

11.2 Achieving the objectives of the thesis

Chapters 3 to 10 of this thesis describe the work done in an attempt to meet these aims.

Firstly, the theoretical background and software implementation of a computationally efficient IM model was given in Chapter 3. This model had the ability to simulate IM in a healthy configuration or with several broken rotor bars or shorted stator turns.

Chapter 4 included a detailed literature review of IM speed estimation, a comparison of popular speed estimation techniques and the development and testing of a novel algorithm based on the rotor bar pass frequencies which was shown to have the ability to estimate the number of rotor bars and shaft speed accurately.

Chapter 5 described the experimental set-up used for this project (including the ability to test both direct couplings and belt and pulley type couplings) and Chapter 6 proposed the construction of a parameter estimation algorithm based on a PSO technique which when coupled with the speed estimation aspect had the ability to estimate machine parameters based on three-phase currents and voltages only. Chapter 7 included the validation of the motor models (including estimated parameters) with the measured and simulated results under different load conditions showing good agreement.

Four fault detection methods were proposed in Chapter 9 including two techniques based on a more detailed fault model of the system supported by a Nelder-Mead optimiser and two methods based on analysis of frequency components in the current spectrum. These fault methods developed a set of residuals (of different types i.e. mixed-residual approach) which when combined together should provide a more robust and effective assessment of machine condition. Finally, the application of fuzzy logic diagnosis algorithms to the diagnosis problem was investigated in Chapter 10. This chapter built on the work included in each of the previous chapters and presented the culmination of this work in terms of presentation of the final results based on 78 different motor conditions being assessed by the overall FDD algorithm. The results show that overall the system provides good performance with an overall detection rate of 87.2% a diagnosis rate of 73.3% and a fault isolation rate of 67.1 %.

11.3 Remarks and recommendations for further work

The basis and initial validation of a current-based IM FDD has been developed through this thesis with the emphasis being on developing an overall system with practical value in industrial applications. With this in mind there is potential for each of the separate aspects of this thesis (e.g. parameter estimation, speed estimation, motor models, fault detection methods, diagnosis techniques) to be studied in isolation and more detail. In addition to this the validation of this system needs to be built upon and fed back into the system design. With these points in mind the following recommendations for future work should be considered:

1) Extension of the fuzzy logic system to include additional features to aid with diagnosis tasks. Potential extensions could be:

a. Inclusion of statistical quantities such as peak factor, kurtosis, skewness, entropy error, etc [10].
b. Inclusion of higher order spectra (higher order statistics) and Cepstrum components [1]
c. Assessment of key features via a PCA technique in order to keep dimensionality of the problem low when additional features are added (important for expert systems)

2) Investigation of the effect of static and dynamic eccentricity on RBPF [75] in the current spectrum and using this information to improve the robustness of the eccentricity fault detection algorithm.
3) A study of machine start-up transients, in particular, time-frequency analysis using STFT or wavelet transforms should be employed. High frequency sampling of transients will become more applicable as processing power improves; at present safety critical tasks take priority at start-up, but as processors become more powerful this will change. Start-up frequency tracking could provide:
    a. Confirmation of the location of characteristic frequencies at steady-state previously masked by other spectral content (e.g. supply harmonics)
    b. Additional information only present during transients.
4) Validation and continued development of the fuzzy membership functions based on test results from a variety of motor power ratings and pole numbers.
5) Extension or modification of the fuzzy logic knowledgebase via the following:

a. Further experimentation into current and voltage based features in the presence of faults. Industrial deployment of a DAQ system would allow real faults as opposed to synthetic laboratory created faults to be captured.
b. Gathering information from maintenance technicians in the field in an attempt to convert their process knowledge into inference rules to be used by the fuzzy logic system (direct capture of expert knowledge)

6) Extension of the PSO optimisation algorithm to a hybrid stochastic-deterministic algorithm to provide improved basic model optimisation speed and accuracy.
7) Repetition of test cases and diagnoses in order to increase confidence in diagnosis verdicts

The key direction for the future of this research would be to acquire data in-situ from a plant or factory on a range of motor types, loads and environments. If this data can be obtained then the system can be fully validated and continual improvement can occur via small changes and additions to the flexible and extendable fuzzy logic diagnosis system.

References

[1] A. Jardine, D. Lin, and D. Banjevic, “A review on machinery diagnostics and prognostics implementing condition-based maintenance,” *Mech. Syst. Signal Process.*, vol. 20, no. 7, pp. 1483–1510, Oct. 2006.

[2] G. Singh, “Induction machine drive condition monitoring and diagnostic research—a survey,” *Electr. Power Syst. Res.*, vol. 64, no. 2, pp. 145–158, Feb. 2003.

[3] R. W. Smeaton, *Motor Application and Maintenance handbook*, Second Ed. New York: McGraw-Hill, 1987.

[4] R. Isermann, “Supervision, fault-detection and fault diagnosis methods - an introduction,” *Control Eng. Pract.*, vol. 5, no. 5, pp. 639–652, 1997.

[5] I. Boldea and S. A. Nasar, *The Induction Machine Handbook*, First Ed. New York: CRC Press, 2002.

[6] S. Nandi, H. a. Toliyat, and X. Li, “Condition Monitoring and Fault Diagnosis of Electrical Motors—A Review,” *IEEE Trans. Energy Convers.*, vol. 20, no. 4, pp. 719–729, Dec. 2005.

[7] V. Venkatasubramanian, “A review of process fault detection and diagnosis Part I: Quantitative model-based methods,” *Comput. Chem. Eng.*, vol. 27, no. 3, pp. 293–311, Mar. 2003.

[8] M. Frankowiak, R. Grosvenor, and P. Prickett, “A review of the evolution of microcontroller-based machine and process monitoring,” *Int. J. Mach. Tools Manuf.*, vol. 45, pp. 573–582, 2005.

[9] S. Chen and R. Zivanovic, “Modelling and simulation of stator and rotor fault conditions in induction machines for testing fault diagnostic techniques,” *Eur. Trans. Electr. Power*, 2009.

[10] V. Tran, B. Yang, M. Oh, and a Tan, “Fault diagnosis of induction motor based on decision trees and adaptive neuro-fuzzy inference,” *Expert Syst. Appl.*, vol. 36, no. 2, pp. 1840–1849, Mar. 2009.

[11] R. A. Collacott, *Mechanical Fault Diagnosis*. London: Chapman and Hall, 1977.

[12] J. R. Stack, T. G. Habetler, and R. G. Harley, “Experimentally Generating Faults in Rolling Element Bearings Via Shaft Current,” *IEEE Trans. Ind. Appl.*, vol. 41, no. 1, pp. 25–29, Jan. 2005.

[13] Z. Gan, M.-B. Zhao, and T. W. S. Chow, “Induction machine fault detection using clone selection programming,” *Expert Syst. Appl.*, vol. 36, no. 4, pp. 8000–8012, May 2009.

[14] C. M. Riley, B. K. Lin, T. G. Habetler, and G. B. Kliman, “Stator current harmonics and their causal vibrations: a preliminary investigation of sensorless vibration monitoring applications,” *IEEE Trans. Ind. Appl.*, vol. 35, no. 1, pp. 94–99, 1999.

[15] B. Y. C. Yung and A. H. Bonnett, “Repair or Replace?,” *IEEE Industry Applications Magazine*, 2004.

[16] V. Purushotham, S. Narayanan, and S. Prasad, “Multi-fault diagnosis of rolling bearing elements using wavelet analysis and hidden Markov model based fault recognition,” *NDT E Int.*, vol. 38, no. 8, pp. 654–664, Dec. 2005.

[17] N. Tandon and A. Choudhury, “A review of vibration and acoustic measurement methods for the detection of defects in rolling element bearings,” *Tribol. Int.*, vol. 32, no. 1999, pp. 469–480, 2000.

[18] J. Vass and C. Cristalli, “Bearing Fault Detection for On-Line Quality Control of Electric Motors,” in *IMEKO Conference on Technical Diagnostics*.

[19] C. Cristalli, N. Paone, and R. M. Rodrı, “Mechanical fault detection of electric motors by laser vibrometer and accelerometer measurements,” vol. 20, pp. 1350–1361, 2006.

[20] L. M. R. Baccarini, B. R. de Menezes, and W. M. Caminhas, “Fault induction dynamic model, suitable for computer simulation: Simulation results and experimental validation,” *Mech. Syst. Signal Process.*, vol. 24, no. 1, pp. 300–311, Jan. 2010.

[21] S. Hamdani, O. Touhami, and R. Ibtiouen, “A Generalized Two Axes Model of a Squirrel-Cage Induction Motor for Rotor Fault Diagnosis,” *Serbian J. Electr. Eng.*, vol. 5, no. 1, pp. 155–170, 2008.

[22] a. Ibrahim, M. El Badaoui, F. Guillet, and F. Bonnardot, “A New Bearing Fault Detection Method in Induction Machines Based on Instantaneous Power Factor,” *IEEE Trans. Ind. Electron.*, vol. 55, no. 12, pp. 4252–4259, Dec. 2008.

[23] M. Zeraoulia, A. Mamoune, H. Mangel, and M. E. H. Benbouzid, “A Simple Fuzzy Logic Approach for Induction Motors Stator Condition Monitoring,” *J. Electr. Syst.*, 2005.

[24] T. G. Habetler, R. G. Harley, R. M. Tallam, S. Lee, and R. Obaid, “Complete Current-based Induction Motor Condition Monitoring: Stator, Rotor, Bearings, and Load,” in *IEEE Power Electronics Congress*, 2002, pp. 3–8.

[25] J. Penman, M. N. Dye, A. J. Tait, and W. E. Bryan, “Condition monitoring of electrical drives,” *Proc. IEE*, vol. 133, no. 3, pp. 142–148, 1986.

[26] K. Bacha, H. Henao, M. Gossa, and G. Capolino, “Induction machine fault detection using stray flux EMF measurement and neural network-based decision,” *Electr. Power Syst. Res.*, vol. 78, no. 7, pp. 1247–1255, Jul. 2008.

[27] W. T. Thomson, D. Rankin, and D. Dorrell, “On-line current monitoring to diagnose airgap eccentricity in large three-phase induction motors - industrial case histories verify the predictions,” *IEEE Trans. Energy Convers.*, vol. 14, no. 4, 1999.

[28] a. Siddique, G. S. Yadava, and B. Singh, “A Review of Stator Fault Monitoring Techniques of Induction Motors,” *IEEE Trans. Energy Convers.*, vol. 20, no. 1, pp. 106–114, Mar. 2005.

[29] A. Bellini, F. Filippetti, and C. Tassoni, “Advances in Diagnostic Techniques for Induction Machines,” in *IEEE Transactions on Industrial Electronics*, 2008, vol. 55, no. 12, pp. 4109–4126.

[30] P. Pillay and P. Hofmann, “Derating of induction motors operating with a combination of unbalanced voltages and over- or undervoltages,” *2001 IEEE Power Eng. Soc. Winter Meet. Conf. Proc. (Cat. No.01CH37194)*, no. C, pp. 1365–1371, 2001.

[31] A. Sasi, F. Gu, Y. Li, and A. Ball, “A validated model for the prediction of rotor bar failure in squirrel-cage motors using instantaneous angular speed,” *Mech. Syst. Signal Process.*, vol. 20, no. 7, pp. 1572–1589, Oct. 2006.

[32] N. Tandon, G. Yadava, and K. Ramakrishna, “A comparison of some condition monitoring techniques for the detection of defect in induction motor ball bearings,” *Mech. Syst. Signal Process.*, vol. 21, no. 1, pp. 244–256, Jan. 2007.

[33] W. T. Thomson and M. Fenger, “Current Signature Analysis to Detect Induction Motor Faults,” *IEEE Industry Applications Magazine*, no. August, 2001.

[34] T. Bishop, “Squirrel Cage Rotor Testing,” in *EASA Convention*, 2003.

[35] L. Eren and M. J. Devaney, “Bearing Damage Detection via Wavelet Packet Decomposition of the Stator Current,” *IEEE Trans. Instrum. Meas.*, vol. 53, no. 2, pp. 431–436, Apr. 2004.

[36] M. El Hachemi Benbouzid, “A review of induction motors signature analysis as a medium for faults detection,” *IEEE Trans. Ind. Electron.*, vol. 47, no. 5, pp. 984–993, 2000.

[37] M. Blodt, M. Chabert, J. Regnier, and J. Faucher, “Mechanical Load Fault Detection in Induction Motors by Stator Current Time-Frequency Analysis,” *IEEE Trans. Ind. Appl.*, vol. 42, no. 6, pp. 1454–1463, Nov. 2006.

[38] P. Pillay, “Motor Current Signature Analysis,” *Read*. 1996.

[39] W. T. Thomson and M. Fenger, “Case histories of current signature analysis to detect faults in induction motor drives,” *IEEE Int. Electr. Mach. Drives Conf. 2003. IEMDC’03.*, pp. 1459–1465.

[40] W. Thomson and R. J. Gilmore, “Motor Current Signature Analysis to detect faults in induction motor drives - fundamentals, data interpretation, and industrial case histories,” in *Turbomachinery Symposium*, 2003.

[41] H. Douglas and P. Pillay, “The impact of wavelet selection on transient motor current signature analysis,” *IEEE Int. Conf. Electr. Mach. Drives, 2005.*, pp. 80–85, 2005.

[42] J. Antoninodaviu, M. Rieraguasp, J. Rogerfolch, F. Martinezgimenez, and a Peris, “Application and optimization of the discrete wavelet transform for the detection of broken rotor bars in induction machines,” *Appl. Comput. Harmon. Anal.*, vol. 21, no. 2, pp. 268–279, Sep. 2006.

[43] H. Douglas, P. Pillay, and A. K. Ziarani, “A New Algorithm for Transient Motor Current Signature Analysis Using Wavelets,” in *IEEE Transactions on Industry Applications*, 2004, vol. 40, no. 5, pp. 1361–1368.

[44] N. Paone, C. Cristalli, and R. M. Rodriguez, “Comparative study between laser vibrometer and accelerometer measurements for mechanical fault detection of electric motors.” .

[45] P. Rodriguez, M. Negrea, and A. Arkkio, “A General Scheme for Induction Motor Condition Monitoring,” in *International Symposium on Diagnostics for Electrical Machines, Power Electronics and Drives*, 2005, no. September.

[46] Z. Ye, B. Wu, and A. Sadeghian, “Current signature analysis of induction motor mechanical faults by wavelet packet decomposition,” *IEEE Trans. Ind. Electron.*, vol. 50, no. 6, pp. 1217–1228, Dec. 2003.

[47] E. Olsson, P. Funk, and N. Xiong, “Fault Diagnosis in Industry Using Sensor Readings and Case-Based Reasoning,” *J. Intell. Fuzzy Syst.*, vol. 15, pp. 41–46, 2004.

[48] E. Olsson, P. Funk, and M. Bengtsson, “Fault Diagnosis of Industrial Robots using Acoustic Signals and Case-Based Reasoning,” in *European Conference on Case-Based Reasoning*, 2004, no. June, pp. 686–701.

[49] A. Fernández, J. Bilbao, I. Bediaga, A. Gastón, and J. Hernández, “Feasibility study on diagnostic methods for detection of bearing faults at an early stage,” in *International Conference on Dynamical Systems*, 2005, vol. 2005, pp. 113–118.

[50] Z. Ye, B. Wu, and A. Sadeghian, “Current Signature Analysis of Induction Motor Mechanical Faults by Wavelet Packet Decomposition,” *IEEE Trans. Ind. Electron.*, vol. 50, no. 6, pp. 1217–1228, 2003.

[51] G. G. Acosta, C. J. Verucchi, and E. R. Gelso, “A current monitoring system for diagnosing electrical failures in induction motors,” in *Mechanical Systems and Signal Processing*, 2006, vol. 20, pp. 953–965.

[52] I. Y. Önel, K. B. Dalci, and İ. Senol, “Detection of bearing defects in three-phase induction motors using Park’s transform and radial basis function neural networks,” *Sadhana*, vol. 31, no. 3, pp. 235–244, Jun. 2006.

[53] J. Faiz and M. Ojaghi, “Different indexes for eccentricity faults diagnosis in three-phase squirrel-cage induction motors: A review,” *Mechatronics*, vol. 19, no. 1, pp. 2–13, Feb. 2009.

[54] J. Zarei and J. Poshtan, “An advanced Park’s vectors approach for bearing fault detection,” *Tribol. Int.*, vol. 42, no. 2, pp. 213–219, Feb. 2009.

[55] R. J. Patton, P. . Frank, and R. Clark, *Fault Diagnosis in Dynamic Systems*. London: Prentice Hall International Ltd, 1989.

[56] R. Isermann, “On fuzzy logic applications for automatic control, supervision, and fault diagnosis,” *IEEE Trans. Syst. Man, Cybern. - Part A Syst. Humans*, vol. 28, no. 2, pp. 221–235, Mar. 1998.

[57] R. Isermann, “Model-based Fault Detection and Diagnosis - Status and Applications,” *Annu. Rev. Control*, vol. 29, pp. 71–85, 2005.

[58] S. Williamson and A. C. Smith, “Induction motor modelling - Choosing the tool to do the job,” *IEE Colloq. Model. Perform. Electr. Mach.*, vol. 166, pp. 1–4, 1997.

[59] M. Boucherma, M. Kaikaa, and A. Khezzar, “Park Model of Squirrel Cage Induction Machine Including Space Harmonic Effects,” *J. Electr. Eng.*, vol. 57, no. 4, pp. 193–199, 2006.

[60] M. Sokola and E. Levi, “A novel induction machine model and its application in the development of an advanced vector control scheme,” *Int. J. Electr. Eng. Educ.*

[61] B. Maria, R. de Menezes, and W. M. Caminhas, “Fault induction dynamic model , suitable for computer simulation : Simulation results and experimental validation,” *Mech. Syst. Signal Process.*, vol. 24, no. 1, pp. 300–311, 2010.

[62] C. Apostoaia, Z. Szekely, and D. Gray, “Feedback Signals Estimation of an Induction Machine Drive,” in *International Conference on Systems*, 2008, no. 4, pp. 53–58.

[63] G. Bossio, C. D. E. Angelo, J. Solsona, G. O. García, and M. I. Valla, “A model for induction motors with non-uniform air-gap,” *Lat. Am. Appl. Res.*, vol. 82, pp. 77–82, 2005.

[64] R. Ursem, “Parameter identification of induction motors using stochastic optimization algorithms,” *Appl. Soft Comput.*, vol. 4, no. 1, pp. 49–64, Feb. 2004.

[65] B. Ozpineci and L. M. Tolbert, “Simulink Implementation of Induction Machine Model - A Modular Approach,” in *Electric Machines and Drives Conference*, 2003, pp. 728–734.

[66] X. Chang, V. Cocquempot, and C. Christophe, “A Model of Asynchronous Machines for Stator Fault Detection and Isolation,” in *IEEE Transactions on Industrial Electronics*, 2003, vol. 50, no. 3, pp. 578–584.

[67] A. L. Orille, G. Sowilam, and J. Valencia, “A new simulation of three phase induction motor under transformations of Park,” *Comput. Ind. Eng.*, vol. 37, pp. 359–362, 1999.

[68] M. Arkan, D. Kosticperovic, and P. Unsworth, “Modelling and simulation of induction motors with inter-turn faults for diagnostics,” *Electr. Power Syst. Res.*, vol. 75, no. 1, pp. 57–66, Jul. 2005.

[69] B. Marungsri, N. Meeboon, and A. Oonsivilai, “Dynamic Model Identification of Induction Motors using Intelligent Search Techniques with taking Core Loss into Account,” in *WSEAS International Conference on Power Systems*, 2006, pp. 108–115.

[70] M. Imecs and I. Incze, “A Simple Approach to Induction Machine Parameter Estimation,” in *Workshop on Electrical Machines’ Parameters*, 2001, no. May, pp. 73–80.

[71] S. Bachir, S. Tnani, J. Trigeassou, and G. Champenois, “Diagnosis by Parameter Estimation of Stator and Rotor Faults Occurring in Induction Machines,” in *IEEE Transactions on Industrial Electronics*, 2006, vol. 53, no. 3, pp. 963–973.

[72] S. Al-Jufout, “Modeling of the cage induction motor for symmetrical and asymmetrical modes of operation,” *Comput. Electr. Eng.*, vol. 29, no. 8, pp. 851–860, Nov. 2003.

[73] G. Didier, H. Razik, and a. Rezzoug, “An induction motor model including the first space harmonics for broken rotor bar diagnosis,” *Eur. Trans. Electr. Power*, vol. 15, no. 3, pp. 229–243, May 2005.

[74] S. Bachir, S. Tnani, J. Trigeassou, and G. Champenois, “Diagnosis by Parameter Estimation of Stator and Rotor Faults Occurring in Induction Machines,” in *IEEE Transactions on Industrial Electronics*, 2006, vol. 53, no. 3, pp. 963–973.

[75] S. Nandi, S. Ahmed, and H. Toliyat, “Detection of rotor slot and other eccentricity related harmonics in a three phase induction motor with different rotor cages,” *IEEE Trans. Energy Convers.*, vol. 16, no. 3, pp. 253–260, 2001.

[76] M. Sahraoui, a Ghoggal, S. Zouzou, and M. Benbouzid, “Dynamic eccentricity in squirrel cage induction motors – Simulation and analytical study of its spectral signatures on stator currents,” *Simul. Model. Pract. Theory*, vol. 16, no. 9, pp. 1503–1513, Oct. 2008.

[77] S. Nandi, R. M. Bharadwaj, H. Toliyat, and A. G. Parlos, “Performance analysis of a three phase induction motor under mixed eccentricity condition,” in *International Conference on Power Electronic Drives and Energy Systems for Industrial Growth*, 1998, pp. 123–128.

[78] D. E. Khodja and A. Kheldoun, “Three-phases Model of the Induction Machine Taking Account the Stator Faults,” *World Acad. os Sci. Eng. Technol.*, pp. 157–160, 2009.

[79] M. Blödt, P. Granjon, B. Raison, and G. Rostaing, “Models for Bearing Damage Detection in Induction Motors Using Stator Current Monitoring,” in *IEEE Transactions on Industrial Electronics*, 2008, vol. 55, no. 4, pp. 1813–1822.

[80] N. Sawalhi and R. B. Randall, “Simulating gear and bearing interactions in the presence of faults Part I . The combined gear bearing dynamic model and the simulation of localised bearing faults,” *Mech. Syst. Signal Process.*, vol. 22, pp. 1924–1951, 2008.

[81] L. H. Chiang, E. L. Russell, and R. D. Bratz, *Fault detection and diagnosis in industrial systems*. London: Springer-Verlag Limited, 2001.

[82] R. Isermann, “Trends in the application of model-based fault detection and diagnosis of technical processes,” *Control Eng. Pract.*, vol. 5, no. 5, pp. 709–719, May 1997.

[83] A. Siddique, G. S. Yadava, and B. Singh, “Applications of artificial intelligence techniques for induction machine stator fault diagnostics: review,” *4th IEEE Int. Symp. Diagnostics Electr. Mach. Power Electron. Drives, 2003. SDEMPED 2003.*, no. August, pp. 29–34, 2003.

[84] F. Filippetti, G. Franceschini, C. Tassoni, S. Member, and P. Vas, “AI Techniques in Induction Machines Diagnosis Including the Speed Ripple Effect,” *IEEE Trans. Ind. Electron.*, vol. 34, no. 1, pp. 98–108, 1998.

[85] V. Venkatasubramanian, “A review of process fault detection and diagnosis Part II: Qualitative models and search strategies,” *Comput. Chem. Eng.*, vol. 27, no. 3, pp. 313–326, Mar. 2003.

[86] V. Venkatasubramanian, “A review of process fault detection and diagnosis Part III: Process history based methods,” *Comput. Chem. Eng.*, vol. 27, no. 3, pp. 327–346, Mar. 2003.

[87] J. W. Hines, *Fuzzy and Neural Appraoches in Engineering - MATLAB Supplement*. New York: John Wiley & Sons, 1997.

[88] L. Kruger, D. Naunin, and C. Garbrecht, “Stochastic and neural models of an induction motor,” *Math. Comput. Simul.*, vol. 46, pp. 313–324, 1998.

[89] B. Karanayil, M. F. Rahman, and C. Grantham, “Identification of Induction Motor Parameters in Industrial Drives with Artificial Neural Networks,” *Adv. Fuzzy Syst.*, vol. 2009, 2009.

[90] R. M. Bharadwaj and A. G. Parlos, “Neural state filtering for adaptive induction motor speed estimation,” *Mech. Syst. Signal Process.*, vol. 17, no. 5, pp. 903–924, 2003.

[91] V. N. Ghate and S. V Dudul, “Expert Systems with Applications Optimal MLP neural network classifier for fault detection of three phase induction motor,” *Expert Syst. Appl.*, vol. 37, no. 4, pp. 3468–3481, 2010.

[92] T. Petsche, A. Marcantonio, C. Darken, S. J. Hanson, G. M. Kuhn, I. Santoso, N. I. S. Scr, and S. Com, “A Neural Network Autoassociator for Induction Motor Failure Prediction.” .

[93] L. Li and C. Mechefske, “Induction Motor Fault Detection and Diagnosis Using Artificial Neural Networks,” *Int. J. COMADEM*, 2006.

[94] Y. Önel, E. Aycicek, and I. Senol, “Detection of Bearing Defects in Inverter Fed Induction Motors Using Park ’ s Transform Approach and RBF Neural Network,” in *International Symposium on Intelligent Manfucturing Systems*, 2006, pp. 863–873.

[95] C. Kowalski, “Neural networks application for induction motor faults diagnosis,” *Math. Comput. Simul.*, vol. 63, no. 3–5, pp. 435–448, Nov. 2003.

[96] B. Ayhan, M. Chow, and M. Song, “On the Comparison of Multiple Signature LDA and Neural Network Based Broken Rotor Bar Detection Schemes in Induction Motors,” no. 5. pp. 3–6.

[97] T. Han, B.-S. Yang, W.-H. Choi, and J.-S. Kim, “Fault Diagnosis System of Induction Motors Based on Neural Network and Genetic Algorithm Using Stator Current Signals,” *Int. J. Rotating Mach.*, vol. 2006, pp. 1–13, 2006.

[98] C. M. Ong, *Dynamic Simulation of Electric Machinery*. Prentice-Hall, Inc, 1998.

[99] N. Mohan, *Advanced Electric Drives*. Minneapolis: MNPERE, USA, 2001.

[100] A. Bellini, F. Filippetti, G. Franceschini, C. Tassoni, S. Member, and G. B. Kliman, “Quantitative Evaluation of Induction Motor Broken Bars by Means of Electrical Signature Analysis,” in *IEEE Transactions on Industrial Applications*, 2001, vol. 37, no. 5, pp. 1248–1255.

[101] P. M. Santos, M. B. R. Correa, C. B. Jacobina, and E. R. C. Silva, “A Simplified Induction Machine Model to Study Rotor Broken Bar Effects

and for Detection," in *IEEE Power Electronics Specialist Conference*, 2006, vol. 9, no. 5.

[102] M. Arkan, "Sensorless speed estimation in induction motor drives by using the space vector angular fluctuation signal," *IET Electr. Power Appl.*, vol. 2, no. 2, pp. 113–120, 2008.

[103] C. Yang and J. W. Finch, "A Comparison of Induction Motor Speed Estimation using Conventional MRAS and AI- Based MRAS with a Dynamic Reference Model," in *World Congress on Engineering*, 2008, vol. I.

[104] M. Bodson and J. Chiasson, "A Comparison of Sensorless Speed Estimation Methods for Induction Motor Control," in *American Control Conference*, 2002, no. 5, pp. 3076–3081.

[105] A. V. Leite, R. E. Araújo, and D. Freitas, "A New Approach for Speed Estimation in Induction Motor Drives Based on a Reduced-Order Extended Kalman Filter," *Ind. Electron. Int. Symp.*, pp. 1221–1226, 2004.

[106] A. Derdiyok, "A novel speed estimation algorithm for induction machines," *Electr. Power Syst. Res.*, vol. 64, pp. 73–80, 2003.

[107] J. Dixon and J. Rivarola, "Induction Motor Speed Estimator Based on a Fixed Carrier Frequency Signal," in *IEEE Transactions on Industrial Electronics*, 1996, pp. 505–509.

[108] C. E. Carvalho, J. W. Lima Nerys, L. R. Lisita, and E. G. Marra, "MRAS techniques Applied to Induction Motor Speed Estimation: A Comparative Anlaysis Based on a LabVIEW Platform." Goiania, Brazil.

[109] G. Lee, D. Lee, T. Yoon, and K. Lee, "Speed and Flux Estimation for an Induction Motor Using a Parameter Estimation Technique," *Int. J. Control. Autom. Syst.*, vol. 3, no. 1, pp. 79–86, 2005.

[110] K. L. Shi, T. F. Chan, Y. K. Wong, S. Member, and S. L. Ho, "Speed Estimation of an Induction Motor Drive Using an Optimized Extended Kalman Filter," *IEEE Trans. Ind. Electron.*, vol. 49, no. 1, pp. 124–133, 2002.

[111] H. Silaghi and V. Spoială, "Induction Motor Speed Estimation by Using Spectral Current Analysis," *J. Comput. Sci. Control Syst.*, pp. 124–127, 2009.

[112] C. Wang, Z. Zhou, P. J. Unsworth, and P. Igic, "Current Space Vector Amplitude Fluctuation based Sensorless Speed Measurement of Induction Machines Using Short Time Fourier Transformation," *IEEE Trans. Ind. Electron.*, pp. 1869–1874, 2008.

[113] K. D. Hurst and T. G. Habetler, "Sensorless Speed Measurement Using Current Harmonic Spectral Estimation in Induction Machine Drives," *IEEE Trans. Power Electron.*, vol. 11, no. 1, pp. 66–73, 1996.

[114] D. R. Mcgaughey, M. Tarbouchi, and K. Nutt, “Speed Sensorless Estimation of AC Induction Motors Using the Fast Orthogonal Search Algorithm,” *IEEE Trans. Energy Convers.*, vol. 21, no. 1, pp. 112–120, 2006.

[115] G. Petrovic, T. Kilic, and B. Terzic, “Sensorless speed detection of squirrel-cage induction machines using stator neutral point voltage harmonics,” *Mech. Syst. Signal Process.*, vol. 23, pp. 931–939, 2009.

[116] K. D. Hurst, T. G. Habetler, G. Griva, and F. Profumo, “Speed Sensorless Field-Oriented Control of Induction machines Using Current Harmonic Spectral Estimation,” in *Industry Applications Society Annual Meeting*, 1994, pp. 601–607.

[117] R. M. Bharadwaj, A. G. Parlos, and H. A. Toliyat, “Neural speed filtering for sensorless induction motor drives,” *Control Eng. Pract.*, vol. 12, pp. 687–706, 2004.

[118] F. Corcoles, J. Pedra, M. Salichs, and L. Sainz, “Analysis of the Induction Machine Parameter Identification,” *IEEE Trans. Energy Convers.*, vol. 17, no. 2, pp. 183–190, 2002.

[119] J. Kim, T. Kim, Y. Park, and S. W. Kim, “On-Load Motor Parameter Identification Using Univariate Dynamic Encoding Algorithm for Searches,” *IEEE Trans. Energy Convers.*, vol. 23, no. 3, pp. 804–813, 2008.

[120] M. Akbaba, M. Taleb, and A. Rumeli, “Improved estimation of induction machine parameters,” *Electr. Power Syst. Res.*, vol. 34, pp. 65–73, 1995.

[121] C. Moons and B. De Moor, “Parameter Identification of Induction Motor Drives,” *Automatica*, vol. 31, no. 8, pp. 1137–1147, 1995.

[122] J. L. Zamora and A. García-Cerrada, “Online Estimation of the Stator Parameters in an Induction Motor Using Only Voltage and Current Measurements,” *IEEE Trans. Ind. Appl.*, vol. 36, no. 3, pp. 805–816, 2000.

[123] Y. Koubaa, “Asynchronous machine parameters estimation using recursive method,” *Simul. Model. Pract. Theory*, vol. 14, no. 7, pp. 1010–1021, Oct. 2006.

[124] P. L. Alger, *The Nature of Induction Machines*. New York: Gordon and Breach Science Publishers, 1965, p. pg 140–141.

[125] M. . Liwschitz-Garik, *Alternating Current Machines*, Second. Princeton: D. Van Nostrand Company, 1961.

[126] T. G. Kolda, R. M. Lewis, and V. Torczon, “Optimization by Direct Search: New Perspectives on Some Classical and Modern Methods,” *SIAM Rev.*, vol. 45, no. 3, p. 385, 2003.

[127] P. Venkataraman, *Applied Optimization with MATLAB Programming*. New York: John Wiley & Sons, 2002.

[128] H. Beyer and H. Schwefel, “Evolution strategies,” *J. Nat. Comput.*, pp. 3–52, 2002.

[129] K. E. Parsopoulos and M. N. Vrahatis, “Particle Swarm Optimization Method for Constrained Optimization Problems,” *Optimization*. .

[130] A. Nikranajbar, M. K. Ebrahimi, and A. S. Wood, “Parameter identification of a cage induction motor using particle swarm optimization,” *Proc. Inst. Mech. Eng. Part I J. Syst. Control Eng.*, vol. 224, no. 5, pp. 841–847, 2010.

[131] M. a. Awadallah and M. M. Morcos, “Application of AI tools in fault diagnosis of electrical machines and drives-an overview,” *IEEE Trans. Energy Convers.*, vol. 18, no. 2, pp. 245–251, Jun. 2003.

[132] M. E. H. Benbouzid, M. Vieira, and C. Theys, “Induction motors’ faults detection and localization using stator current advanced signal processing techniques,” *IEEE Trans. Power Electron.*, vol. 14, no. 1, pp. 14–22, 1999.

[133] J. R. Stack, T. G. Habetler, and R. G. Harley, “Bearing Fault Detection via Autoregressive Stator Current Modeling,” *IEEE Trans. Ind. Appl.*, vol. 40, no. 3, pp. 740–747, May 2004.

[134] M. Sin, W. Soong, and N. Ertugrul, “Induction Machine On-Line Condition Monitoring and Fault Diagnosis - A Survey,” *Current*. .

[135] C. H. De Angelo, G. R. Bossio, S. J. Giaccone, M. I. Valla, J. a. Solsona, and G. O. Garcia, “Online Model-Based Stator-Fault Detection and Identification in Induction Motors,” *IEEE Trans. Ind. Electron.*, vol. 56, no. 11, pp. 4671–4680, Nov. 2009.

[136] T. Boumegoura, J. C. Marques, H. Yahoui, G. Clerc, and H. Hammouri, “Rotor induction machine failure: Analysis and diagnosis,” *Eur. Trans. Electr. Power*, vol. 14, no. 2, pp. 71–84, Mar. 2004.

[137] H. Hamidi, A. R. Nasiri, and F. Taringoo, “Detection and Isolation of Mixed Eccentricity in Three Phase Induction Motor via Wavelet Packet Decomposition,” *Time*. .

[138] J. R. Stack, T. G. Habetler, and R. G. Harley, “Fault Classification and Fault Signature Production for Rolling Element Bearings in Electric Machines,” vol. 40, no. 3, pp. 735–739, 2004.

[139] T. J. Ross, *Fuzzy Logic with Engineering Applications*, 2nd ed. New York: John Wiley & Sons, Ltd, 2004.

Appendices

Appendix A: Motor data

Test motor nameplate data:

Parameter	Value	Unit
Manufacturer	Brook-Crompton	-
Frame reference	W-DA132MB	-
Rated voltage	415	V
Rated power	7.5	kW
Rated speed	1445	rpm
Rated current	15.2	A
Rated output torque	49.2	Nm
Rated power factor (cos φ)	0.82	-
Winding connection	Delta	-
No. of stator phases	3	-

Equivalent circuit parameters (per phase):

Parameter	Value	Unit
Stator resistance	2.08	Ω
Rotor resistance	1.66	Ω
Stator reactance	5.36	Ω
Rotor reactance	4.56	Ω
Magnetizing reactance	85.9	Ω

Datasheet information:

Parameter	Value	Unit
Rotor inertia	0.025	$kg.m^2$
Starting torque	199.0	Nm
Starting current	109.4	A

Load motor data:

Parameter	Value	Unit
Manufacturer	ABB	-
Frame reference	M2BA-180MLB	-
Rated voltage	415	V
Rated power	22	kW
Rated speed	1465	Rpm
Rated current	41.7	A
Rated output torque	143	Nm
Rated power factor (cos φ)	0.83	-
Winding connection	Winding connection	Delta
No. of stator phases	No. of stator phases	3
Rotor inertia	0.13	$kg.m^2$

Appendix B: Removal of algebraic loops from the DQ0 modelling equations

The q-axis stator currents in the DQ0 fault model are given as:

$$i_{qs} = \frac{\psi_{qs}}{L_{11}\omega_b} - \frac{i_{0s}L_{13}}{L_{11}} - \frac{i_{qr}L_{14}}{L_{11}} \quad (0.1)$$

$$i_{0s} = \frac{\psi_{qs}}{L_{11}\omega_b} - \frac{i_{0s}L_{13}}{L_{11}} - \frac{i_{qr}L_{14}}{L_{11}} \quad (0.2)$$

$$i_{qr} = \frac{\psi_{qs}}{L_{11}\omega_b} - \frac{i_{0s}L_{13}}{L_{11}} - \frac{i_{qr}L_{14}}{L_{11}} \quad (0.3)$$

If equation (0.3) is solved for i_{0s} then the following is obtained:

$$i_{0s} = \frac{\psi_{qr}}{L_{43}\omega_b} - \frac{i_{qr}L_{44}}{L_{43}} - \frac{i_{qs}L_{41}}{L_{43}} \quad (0.4)$$

If equation (0.1) is solved for i_{0s} then the following is obtained:

$$i_{0s} = \frac{\psi_{qs}}{L_{13}\omega_b} - \frac{i_{qr}L_{14}}{L_{13}} - \frac{i_{qs}L_{11}}{L_{13}} \quad (0.5)$$

Setting equation (0.4) equal to (0.5) and solving for i_{qs} yields the following:

$$i_{qs} = \frac{\frac{\psi_{qs}L_{43}}{\omega_b} - \frac{\psi_{qr}L_{13}}{\omega_b} + i_{qr}(L_{13}L_{44} - L_{14}L_{43})}{L_{11}L_{43} - L_{13}L_{41}} \quad (0.6)$$

Setting equation (0.2) equal to (0.4) and solving again for i_{qs} yields the following:

$$i_{qs} = \frac{\frac{\psi_{0s}L_{43}}{\omega_b} - \frac{\psi_{qr}L_{33}}{\omega_b} + i_{qr}(L_{33}L_{44} - L_{34}L_{43})}{L_{31}L_{43} - L_{33}L_{41}} \quad (0.7)$$

In equations (0.6) and (0.7) i_{0s} has now been eliminated (one of the two algebraically looped variables) and by setting these equations equal to each other the final loop variable can be eliminated. Setting equation (0.6) equal to (0.7) gives:

$$\frac{\frac{\psi_{qs}L_{43}}{\omega_b} - \frac{\psi_{qr}L_{13}}{\omega_b} + i_{qr}(L_{13}L_{44} - L_{14}L_{43})}{L_{11}L_{43} - L_{13}L_{41}} = \frac{\frac{\psi_{0s}L_{43}}{\omega_b} - \frac{\psi_{qr}L_{33}}{\omega_b} + i_{qr}(L_{33}L_{44} - L_{34}L_{43})}{L_{31}L_{43} - L_{33}L_{41}} \quad (0.8)$$

Re-arranging equation (0.8) in terms of i_{qr} then performing the required expansions and cancellations the expression below is obtained:

$$i_{qr} = \frac{\frac{\psi_{0s}}{\omega_b}(L_{11}L_{43} - L_{13}L_{41}) + \frac{\psi_{qs}}{\omega_b}(L_{33}L_{41} - L_{31}L_{43}) + \frac{\psi_{qr}}{\omega_b}(L_{13}L_{31} - L_{11}L_{33})}{L_{14}L_{33}L_{41} + L_{13}L_{31}L_{44} - L_{14}L_{31}L_{43} - L_{11}L_{33}L_{44} - L_{13}L_{34}L_{41} + L_{11}L_{34}L_{43}} \quad (0.9)$$

The result is an expression for the q-axis rotor current based solely on the flux terms for the q, d and 0 axes and the fixed inductance parameters. This breaks one of the algebraic loops based on current terms (current as an input to this equation has been eliminated). A similar process is repeated for the q-axis current in the stator and this provides the following expression:

$$i_{qs} = \frac{\frac{\psi_{qs}}{\omega_b}(L_{34}L_{43} - L_{33}L_{44}) + \frac{\psi_{qr}}{\omega_b}(L_{14}L_{33} - L_{13}L_{34}) + \frac{\psi_{0s}}{\omega_b}(L_{13}L_{44} - L_{14}L_{43})}{L_{14}L_{33}L_{41} - L_{11}L_{33}L_{44} + L_{13}L_{31}L_{44} - L_{14}L_{31}L_{43} - L_{13}L_{34}L_{41} + L_{11}L_{34}L_{43}} \quad (0.10)$$

These two relationships replace the existing expressions in the q-axis sub-block (which used current terms as inputs) and thus remove the algebraic q-axis loops from the model (i_{qs} , i_{qr} and i_{0s}).

The next stage is to re-write the d-axis current variables in terms of flux only. This process is somewhat easier due to the simpler equations found in the d-axis sub-blocks. The original equations for d-axis stator and rotor currents are as follows:

$$i_{ds} = \frac{\psi_{ds}}{L_{22}\omega_b} - i_{dr}\frac{L_{25}}{L_{22}} \quad (0.11)$$

$$i_{dr} = \frac{\psi_{dr}}{L_{55}\omega_b} - i_{ds}\frac{L_{52}}{L_{55}} \quad (0.12)$$

Solving equation (0.11) for $\mathrm{i_{dr}}$ results in the following:

$$i_{dr} = \frac{\psi_{ds}}{L_{25}\omega_b} - i_{ds}\frac{L_{22}}{L_{25}} \quad (0.13)$$

These two expressions for $\mathrm{i_{dr}}$ can are now used to eliminate $\mathrm{i_{dr}}$ and find an expression for $\mathrm{i_{ds}}$ in terms of flux only. Setting (0.12) equal to (0.13) and solving for $\mathrm{i_{ds}}$ yields:

$$i_{ds} = \frac{\frac{\psi_{ds}}{L_{25}\omega_b} - \frac{\psi_{dr}}{L_{55}\omega_b}}{\frac{L_{22}}{L_{25}} - \frac{L_{52}}{L_{55}}} \quad (0.14)$$

Repeating this process in a similar manner but eliminating $\mathrm{i_{ds}}$ as opposed to $\mathrm{i_{dr}}$ results in a expression for $\mathrm{i_{dr}}$ in terms of flux only:

$$i_{dr} = \frac{\frac{\psi_{ds}}{L_{52}\omega_b} - \frac{\psi_{dr}}{L_{22}\omega_b}}{\frac{L_{55}}{L_{52}} - \frac{L_{25}}{L_{22}}} \quad (0.15)$$

By re-formatting the model in this way all algebraic loops in the model are eliminated. If IM modelling current equations are written in terms of flux (using the method described above) they become suitable for code generation techniques and can therefore be used as part of a model-based development

cycle in order to drive down development time for MATLAB based modelling projects.

The equations in this section are written in terms of flux linkages per second since these terms are compatible with the original model and allow ease of use in the equations when reactance terms are present. However, in this case inductance terms have been used therefore a further simplification can be made by converting the flux linkage per second terms to flux linkage. Equations (0.9), (0.10), (0.14), (0.15) can therefore be re-written:

$$i_{qr} = \frac{\lambda_{os}(L_{11}L_{43} - L_{13}L_{41}) + \lambda_{qs}(L_{33}L_{41} - L_{31}L_{43}) + \lambda_{qr}(L_{13}L_{31} - L_{11}L_{33})}{L_{14}L_{33}L_{41} + L_{13}L_{31}L_{44} - L_{14}L_{31}L_{43} - L_{11}L_{33}L_{44} - L_{13}L_{34}L_{41} + L_{11}L_{34}L_{43}} \quad (0.16)$$

$$i_{qs} = \frac{\lambda_{qs}(L_{34}L_{43} - L_{33}L_{44}) + \lambda_{qr}(L_{14}L_{33} - L_{13}L_{34}) + \lambda_{os}(L_{13}L_{44} - L_{14}L_{43})}{L_{14}L_{33}L_{41} - L_{11}L_{33}L_{44} + L_{13}L_{31}L_{44} - L_{14}L_{31}L_{43} - L_{13}L_{34}L_{41} + L_{11}L_{34}L_{43}} \quad (0.17)$$

$$i_{ds} = \frac{\frac{\lambda_{ds}}{L_{25}} - \frac{\lambda_{dr}}{L_{55}}}{\frac{L_{22}}{L_{25}} - \frac{L_{52}}{L_{55}}} \quad (0.18)$$

$$\mathrm{i_{dr}} = \frac{\frac{\lambda_{\mathrm{ds}}}{\mathrm{L_{52}}} - \frac{\lambda_{\mathrm{dr}}}{\mathrm{L_{22}}}}{\frac{\mathrm{L_{55}}}{\mathrm{L_{52}}} - \frac{\mathrm{L_{25}}}{\mathrm{L_{22}}}} \quad (0.19)$$

Appendix C: ABC to QD0 reference frame transformation of voltage equations

The stator voltage equations are considered as an example. The starting point is the ABC reference frame equation (3.11) included again below for clarity:

$$\boldsymbol{v}_s^{abc} = \frac{d}{dt}\lambda_s^{abc} + \boldsymbol{r}_s^{abc}\boldsymbol{i}_s^{abc} \quad (0.20)$$

The first stage is to replace the voltage, current and flux vectors with the QD0 reference frame equivalents whilst keeping other terms in the ABC frame. To

allow this to happen the inverse of the reference frame transformation is included:

$$\left[T_{qd0}(\theta_d)\right]^{-1}\boldsymbol{v}_s^{qd0} = \frac{d}{dt}\left[T_{qd0}(\theta_d)\right]^{-1}\lambda_s^{qdo} + \boldsymbol{r}_s^{abc}\left[T_{qd0}(\theta_d)\right]^{-1}\boldsymbol{i}_s^{qd0} \qquad (0.21)$$

The next stage is to bring the $\boldsymbol{r}_s^{abc}$ term into the QD0 reference frame. This is done by applying the transformation to both sides of the equation:

$$\begin{aligned}\left[T_{qd0}(\theta_d)\right]\left[T_{qd0}(\theta_d)\right]^{-1}\boldsymbol{v}_s^{qd0} \\ = \left[T_{qd0}(\theta_d)\right]\frac{d}{dt}\left[T_{qd0}(\theta_d)\right]^{-1}\lambda_s^{qdo} \\ + \left[T_{qd0}(\theta_d)\right]\boldsymbol{r}_s^{abc}\left[T_{qd0}(\theta_d)\right]^{-1}\boldsymbol{i}_s^{qd0}\end{aligned} \qquad (0.22)$$

Since $\left[T_{qd0}(\theta_d)\right]\left[T_{qd0}(\theta_d)\right]^{-1} = 1$ and if $\left[T_{qd0}(\theta_d)\right]\boldsymbol{r}_s^{abc}\left[T_{qd0}(\theta_d)\right]^{-1}$ is redefined as $\boldsymbol{r}_s^{qd0}$ then equation (**0**.**22**) can be simplified to give:

$$\boldsymbol{v}_s^{qd0} = \left[T_{qd0}(\theta_d)\right]\frac{d}{dt}\left[T_{qd0}(\theta_d)\right]^{-1}\lambda_s^{qdo} + \boldsymbol{r}_s^{qd0}\boldsymbol{i}_s^{qd0} \qquad (0.23)$$

where:

$$\boldsymbol{r}_s^{qd0} = \left[T_{qd0}(\theta_d)\right]\boldsymbol{r}_s^{abc}\left[T_{qd0}(\theta_d)\right]^{-1} \qquad (0.24)$$

The ABC-QD0 transformation is as follows:

$$\left[T_{qd0}(\theta_d)\right] = \frac{2}{3}\begin{bmatrix} cos\ \theta_d & \cos\left(\theta_d - \frac{2\pi}{3}\right) & \cos\left(\theta_d + \frac{2\pi}{3}\right) \\ -sin\ \theta_d & -\sin\left(\theta_d - \frac{2\pi}{3}\right) & \sin\left(\theta_d - \frac{2\pi}{3}\right) \\ \frac{1}{2} & \frac{1}{2} & \frac{1}{2} \end{bmatrix} \qquad (0.25)$$

The reference frame transformation operates based on the desired angular position of the reference frame. The choice of this frame is arbitrary (in some cases a synchronous reference frame is used e.g. for control purposes) however in this case the reference frame will be set at an angular position of 0

to simplify the following equations. With this in mind θ_d is set equal to zero to obtain the following:

$$[T_{qd0}] = \frac{2}{3}\begin{bmatrix} 1 & -\frac{1}{2} & -\frac{1}{2} \\ 0 & \frac{\sqrt{3}}{2} & -\frac{\sqrt{3}}{2} \\ \frac{1}{2} & \frac{1}{2} & \frac{1}{2} \end{bmatrix} \tag{0.26}$$

Or alternatively:

$$[T_{qd0}] = \begin{bmatrix} \frac{2}{3} & -\frac{1}{3} & -\frac{1}{3} \\ 0 & -\frac{\sqrt{3}}{3} & \frac{\sqrt{3}}{3} \\ \frac{1}{3} & \frac{1}{3} & \frac{1}{3} \end{bmatrix} \tag{0.27}$$

The inverse is now easier to calculate and results in the following:

$$[T_{qd0}]^{-1} = \begin{bmatrix} 1 & 0 & 1 \\ -\frac{1}{2} & -\frac{\sqrt{3}}{2} & 1 \\ -\frac{1}{2} & \frac{\sqrt{3}}{2} & 1 \end{bmatrix} \tag{0.28}$$

Substituting these expressions into equation (**0**.**24**) gives:

$$\boldsymbol{r}_s^{qd0} = \begin{bmatrix} \frac{2}{3} & -\frac{1}{3} & -\frac{1}{3} \\ 0 & -\frac{\sqrt{3}}{3} & \frac{\sqrt{3}}{3} \\ \frac{1}{3} & \frac{1}{3} & \frac{1}{3} \end{bmatrix} \begin{bmatrix} r_s & 0 & 0 \\ 0 & r_s & 0 \\ 0 & 0 & r_s \end{bmatrix} \begin{bmatrix} 1 & 0 & 1 \\ -\frac{1}{2} & -\frac{\sqrt{3}}{2} & 1 \\ -\frac{1}{2} & \frac{\sqrt{3}}{2} & 1 \end{bmatrix} \tag{0.29}$$

Which yields:

$$\boldsymbol{r}_s^{qd0} = \begin{bmatrix} r_s & 0 & 0 \\ 0 & r_s & 0 \\ 0 & 0 & r_s \end{bmatrix} \tag{0.30}$$

Having set the arbitrary reference frame position equal to zero the transformation is no longer a function of θ_d hence equation (**0**.**23**) can be re-written:

$$\boldsymbol{v}_s^{qd0} = [T_{qd0}]\frac{d}{dt}[T_{qd0}]^{-1}\lambda_s^{qdo} + \boldsymbol{r}_s^{qd0}\boldsymbol{i}_s^{qd0} \tag{0.31}$$

The next stage is to solve the derivative product term:

$$[T_{qd0}]\frac{d}{dt}[T_{qd0}]^{-1}\lambda_s^{qd0} = [T_{qd0}]\left\{[T_{qd0}]^{-1}\frac{d}{dt}\lambda_s^{qd0} + \lambda_s^{qd0}\frac{d}{dt}[T_{qd0}]^{-1}\right\} \tag{0.32}$$

Simplifying this expression then substituting back into equation (**0.31**) results in the stator voltage equation in the QD0 reference frame:

$$\boldsymbol{v}_s^{qd0} = \frac{d}{dt}\lambda_s^{qdo} + \boldsymbol{r}_s^{qd0}\boldsymbol{i}_s^{qd0} \tag{0.33}$$

If the same method is followed the rotor voltage equation can also be obtained, however, in this case the angular position of the rotor is required. Considering that θ_d is set to zero the reference frame transformation is modified to:

$$[T_{qd0}(\theta_d)] = \frac{2}{3}\begin{bmatrix} cos{-\theta_r} & \cos\left(-\theta_r - \frac{2\pi}{3}\right) & \cos\left(-\theta_r + \frac{2\pi}{3}\right) \\ -sin{-\theta_r} & -\sin\left(-\theta_r - \frac{2\pi}{3}\right) & \sin\left(-\theta_r - \frac{2\pi}{3}\right) \\ \frac{1}{2} & \frac{1}{2} & \frac{1}{2} \end{bmatrix} \tag{0.34}$$

Using the same method depicted for the stator QD0 reference frame equations (inverting the matrix, inserting the transformation matrices and solving the derivatives) the rotor voltage equation in the QD0 reference frame is finally obtained:

$$\boldsymbol{v}_r^{qd0} = \begin{bmatrix} 0 & -\omega_r & 0 \\ \omega_r & 0 & 0 \\ 0 & 0 & 0 \end{bmatrix}\boldsymbol{\lambda}_r^{qd0} + \frac{d}{dt}\boldsymbol{\lambda}_r^{qd0} + \boldsymbol{r}_r^{qd0}\boldsymbol{i}_r^{qd0} \tag{0.35}$$

<u>Appendix D:</u> ABC to QD0 reference frame transformation of flux equations

Considering the stator component of equation (3.5) gives the following:

$$\boldsymbol{\lambda}_s^{abc} = \boldsymbol{L}_{ss}^{abc}\boldsymbol{i}_s^{abc} + \boldsymbol{L}_{sr}^{abc}\boldsymbol{i}_r^{abc} \tag{0.36}$$

Replacing the flux linkage and current ABC reference frame terms with their QD0 equivalents yields:

$$\left[T_{qd0}\right]^{-1}\boldsymbol{\lambda}_s^{qd0} = \boldsymbol{L}_{ss}^{abc}\left[T_{qd0}\right]^{-1}\boldsymbol{i}_s^{qd0} + \boldsymbol{L}_{sr}^{abc}\left[T_{qd0}(\theta_r)\right]^{-1}\boldsymbol{i}_r^{qd0} \tag{0.37}$$

This is followed by left-multiplying by the ABC-to-QD0 transformation to give:

$$\begin{aligned}\left[T_{qd0}\right]\left[T_{qd0}\right]^{-1}\boldsymbol{\lambda}_s^{qd0} = \\ \left[T_{qd0}\right]\boldsymbol{L}_{ss}^{abc}\left[T_{qd0}\right]^{-1}\boldsymbol{i}_s^{qd0} + \left[T_{qd0}\right]\boldsymbol{L}_{sr}^{abc}\left[T_{qd0}(\theta_r)\right]^{-1}\boldsymbol{i}_r^{qd0}\end{aligned} \tag{0.38}$$

If the relevant matrices are then substituted in:

$$\begin{aligned}&\begin{bmatrix}\frac{2}{3} & -\frac{1}{3} & -\frac{1}{3}\\ 0 & -\frac{\sqrt{3}}{3} & \frac{\sqrt{3}}{3}\\ \frac{1}{3} & \frac{1}{3} & \frac{1}{3}\end{bmatrix}\begin{bmatrix}1 & 0 & 1\\ -\frac{1}{2} & -\frac{\sqrt{3}}{2} & 1\\ -\frac{1}{2} & \frac{\sqrt{3}}{2} & 1\end{bmatrix}\boldsymbol{\lambda}_s^{qd0} = \\ &\begin{bmatrix}\frac{2}{3} & -\frac{1}{3} & -\frac{1}{3}\\ 0 & -\frac{\sqrt{3}}{3} & \frac{\sqrt{3}}{3}\\ \frac{1}{3} & \frac{1}{3} & \frac{1}{3}\end{bmatrix}\begin{bmatrix}L_{ls}+L_{ss} & L_{sm} & L_{sm}\\ L_{sm} & L_{ls}+L_{ss} & L_{sm}\\ L_{sm} & L_{sm} & L_{ls}+L_{ss}\end{bmatrix}\begin{bmatrix}1 & 0 & 1\\ -\frac{1}{2} & -\frac{\sqrt{3}}{2} & 1\\ -\frac{1}{2} & \frac{\sqrt{3}}{2} & 1\end{bmatrix}\boldsymbol{i}_s^{qd0}\\ &+\begin{bmatrix}\frac{2}{3} & -\frac{1}{3} & -\frac{1}{3}\\ 0 & -\frac{\sqrt{3}}{3} & \frac{\sqrt{3}}{3}\\ \frac{1}{3} & \frac{1}{3} & \frac{1}{3}\end{bmatrix}L_{sr}\begin{bmatrix}cos\theta_r & cos\left(\theta_r+\frac{2\pi}{3}\right) & cos\left(\theta_r-\frac{2\pi}{3}\right)\\ cos\left(\theta_r-\frac{2\pi}{3}\right) & cos\theta_r & cos\left(\theta_r+\frac{2\pi}{3}\right)\\ cos\left(\theta_r+\frac{2\pi}{3}\right) & cos\left(\theta_r-\frac{2\pi}{3}\right) & cos\theta_r\end{bmatrix}.\\ &\frac{2}{3}\begin{bmatrix}cos-\theta_r & \cos\left(-\theta_r-\frac{2\pi}{3}\right) & \cos\left(-\theta_r+\frac{2\pi}{3}\right)\\ -sin-\theta_r & -\sin\left(-\theta_r-\frac{2\pi}{3}\right) & \sin\left(-\theta_r-\frac{2\pi}{3}\right)\\ \frac{1}{2} & \frac{1}{2} & \frac{1}{2}\end{bmatrix}\boldsymbol{i}_r^{qd0}\end{aligned} \tag{0.39}$$

The left hand side of the equation simplifies down to the identity matrix:

$$\boldsymbol{\lambda}_s^{qd0} = \begin{bmatrix} \frac{2}{3} & -\frac{1}{3} & -\frac{1}{3} \\ 0 & -\frac{\sqrt{3}}{3} & \frac{\sqrt{3}}{3} \\ \frac{1}{3} & \frac{1}{3} & \frac{1}{3} \end{bmatrix} \begin{bmatrix} L_{ls}+L_{ss} & L_{sm} & L_{sm} \\ L_{sm} & L_{ls}+L_{ss} & L_{sm} \\ L_{sm} & L_{sm} & L_{ls}+L_{ss} \end{bmatrix} \begin{bmatrix} 1 & 0 & 1 \\ -\frac{1}{2} & -\frac{\sqrt{3}}{2} & 1 \\ -\frac{1}{2} & \frac{\sqrt{3}}{2} & 1 \end{bmatrix} \boldsymbol{i}_s^{qd0}$$
$$+ \begin{bmatrix} \frac{2}{3} & -\frac{1}{3} & -\frac{1}{3} \\ 0 & -\frac{\sqrt{3}}{3} & \frac{\sqrt{3}}{3} \\ \frac{1}{3} & \frac{1}{3} & \frac{1}{3} \end{bmatrix} L_{sr} \begin{bmatrix} cos\theta_r & cos\left(\theta_r+\frac{2\pi}{3}\right) & cos\left(\theta_r-\frac{2\pi}{3}\right) \\ cos\left(\theta_r-\frac{2\pi}{3}\right) & cos\theta_r & cos\left(\theta_r+\frac{2\pi}{3}\right) \\ cos\left(\theta_r+\frac{2\pi}{3}\right) & cos\left(\theta_r-\frac{2\pi}{3}\right) & cos\theta_r \end{bmatrix}. \quad (0.40)$$
$$\frac{2}{3} \begin{bmatrix} cos-\theta_r & \cos\left(-\theta_r-\frac{2\pi}{3}\right) & \cos\left(-\theta_r+\frac{2\pi}{3}\right) \\ -sin-\theta_r & -\sin\left(-\theta_r-\frac{2\pi}{3}\right) & \sin\left(-\theta_r-\frac{2\pi}{3}\right) \\ \frac{1}{2} & \frac{1}{2} & \frac{1}{2} \end{bmatrix} \boldsymbol{i}_r^{qd0}$$

Performing the matrix multiplications yields:

$$\boldsymbol{\lambda}_s^{qd0} = \begin{bmatrix} L_{ls}+L_{ss}-\mathrm{L_{sm}} & 0 & 0 \\ 0 & L_{ls}+L_{ss}-\mathrm{L_{sm}} & 0 \\ 0 & 0 & L_{ls}+L_{ss}+2\mathrm{L_{sm}} \end{bmatrix} \boldsymbol{i}_s^{qd0} + \begin{bmatrix} \frac{3}{2}L_{sr} & 0 & 0 \\ 0 & \frac{3}{2}\mathrm{L_{sr}} & 0 \\ 0 & 0 & 0 \end{bmatrix} \boldsymbol{i}_r^{qd0} \quad (0.41)$$

Since the stator phases are displaced by an angle of 120º from one another the mutual inductance between stator windings is given as:

$$L_{sm} = L_{ss}\cos\left(\frac{2\pi}{3}\right) = -\frac{1}{2}L_{ss} \quad (0.42)$$

Thus equation (**0**.**41**) simplifies to:

$$\boldsymbol{\lambda}_s^{qd0} = \begin{bmatrix} L_{ls}+\frac{3}{2}L_{ss} & 0 & 0 \\ 0 & L_{ls}+\frac{3}{2}L_{ss} & 0 \\ 0 & 0 & L_{ls} \end{bmatrix} \boldsymbol{i}_s^{qd0} + \begin{bmatrix} \frac{3}{2}L_{sr} & 0 & 0 \\ 0 & \frac{3}{2}L_{sr} & 0 \\ 0 & 0 & 0 \end{bmatrix} \boldsymbol{i}_r^{qd0} \quad (0.43)$$

Finally, the winding self inductance and magnetizing inductance are related by:

$$L_m = \frac{3}{2}L_{ss} = \frac{3}{2}L_{rr} = \frac{3}{2}L_{sr} \qquad (0.44)$$

If a similar process is followed for the rotor flux and the matrix equations are combined then this results in the QD0 reference frame flux equation given in the main body of text, equation (3.16):

$$\begin{bmatrix} \boldsymbol{\lambda}_s^{qd0} \\ \boldsymbol{\lambda}_r^{qd0} \end{bmatrix} = \begin{bmatrix} L_{ls}+L_m & 0 & 0 & L_m & 0 & 0 \\ 0 & L_{ls}+L_m & 0 & 0 & L_m & 0 \\ 0 & 0 & L_{ls} & 0 & 0 & 0 \\ L_m & 0 & 0 & L_{lr}{}'+L_m & 0 & 0 \\ 0 & L_m & 0 & 0 & L_{lr}{}'+L_m & 0 \\ 0 & 0 & 0 & 0 & 0 & L_{lr}{}' \end{bmatrix} \begin{bmatrix} \boldsymbol{i}_s^{qd0} \\ \boldsymbol{i}_r^{qd0} \end{bmatrix} \qquad (0.45)$$

Appendix D: Derivation of the QD0 electromagnetic torque equation

A detailed description of this derivation is given in [98]. In the ABC reference frame the total instantaneous input power to the three stator windings and the three rotor equivalent windings is given by:

$$p_{in} = v_{as}i_{as} + v_{bs}i_{bs} + v_{cs}i_{cs} + v'_{ar}i'_{ar} + v'_{br}i'_{br} + v'_{cr}i'_{cr} \qquad (0.46)$$

Which when expressed in the QD0 reference frame becomes:

$$p_{in} = \frac{3}{2}\left(v_{qs}i_{qs} + v_{ds}i_{ds} + 2v_{0s}i_{cs} + v'_{qr}i'_{qr} + v'_{dr}i'_{dr} + 2v'_{0r}i'_{0r}\right) \qquad (0.47)$$

Substituting in the voltage expressions given by equations (0.33) and (0.35):

$$\begin{aligned} p_{in} = {} & \omega\lambda_{ds}i_{qs} + i_{qs}\frac{d}{dt}\lambda_{qs} + i_{qs}^2 r_s - \omega\lambda_{qs}i_{ds} + i_{ds}\frac{d}{dt}\lambda_{ds} + i_{ds}^2 r_s \\ & + 2i_{0s}\frac{d}{dt}\lambda_{0s} + i_{0s}^2 r_s + (\omega-\omega_r)\lambda_{dr}i_{qr} + i_{qr}\frac{d}{dt}\lambda_{qr} \\ & + i_{qr}^2 r_r + (\omega_r-\omega)\lambda_{qr}i_{dr} + i_{dr}\frac{d}{dt}\lambda_{dr} + i_{qr}^2 r_r \\ & + 2i_{0r}\frac{d}{dt}\lambda_{0r} + i_{0r}^2 r_r \end{aligned} \qquad (0.48)$$

In this expression the $\omega\lambda i$ terms represent the rate of energy conversion to mechanical work. Thus if these terms are summed and then divided by the rotational speed an expression for torque is obtained:

$$T_{em} = \frac{3}{2}\frac{P}{2\omega_r}\left\{\omega\left(\lambda_{ds}i_{qs} - \lambda_{qs}i_{ds}\right) + (\omega - \omega_r)(\lambda'_{dr}i'_{qr} - \lambda'_{qr}i'_{dr})\right\} \quad (0.49)$$

Considering that the QD0 axis is fixed to the stator A-axis (i.e. ω = 0) the equation can be simplified. If the zero terms are eliminated and the equation is written in terms of current (eliminate the flux linkage terms using equation (3.16)) the final expression for the electromagnetic torque generated is obtained:

$$T_{em} = \frac{3}{2}\frac{P}{2}L_m\left(i'_{dr}i_{qs} - i'_{qr}i_{ds}\right) \quad (0.50)$$

Appendix E: Comparison of speed estimation methods

Filename	w_act	w_est			SVAmF			SVAnF			Fs-fr			Fs+fr			RBPF		
		Speed (rpm)	E (rpm)	E (%)	Speed (rpm)	E (rpm)	E (%)	Speed (rpm)	E (rpm)	E (%)	Speed (rpm)	E (rpm)	E (%)	Speed (rpm)	E (rpm)	E (%)	Speed (rpm)	E (rpm)	E (%)
0703_M2_BELT_50minsAbrasive_0Nm_20kHz_001.txt	1496.0	1493.8	2.2	0.1	1496.8	0.8	0.1	1496.8	0.8	0.1	1501.4	5.4	0.4	1498.3	2.3	0.2	1499.4	3.4	0.2
0703_M2_BELT_50minsAbrasive_30Nm_20kHz_001.txt	1466.0	1464.1	1.9	0.1	1469.3	3.3	0.2	1460.2	5.8	0.4	1464.8	1.2	0.1	1464.8	1.2	0.1	1466.1	0.1	0.0
0703_M2_BELT_50minsAbrasive_35Nm_20kHz_001.txt	1462.0	1460.0	2.0	0.1	1451.0	11.0	0.8	1460.2	1.8	0.1	1464.8	2.8	0.2	1455.6	6.4	0.4	1462.1	0.1	0.0
0703_M2_BELT_50minsAbrasive_40Nm_20kHz_001.txt	1454.0	1453.7	0.3	0.0	1441.9	12.1	0.8	1451.0	3.0	0.2	1446.4	7.6	0.5	1455.6	1.6	0.1	1454.3	0.3	0.0
0703_M2_BELT_50minsAbrasive_45Nm_20kHz_001.txt	1448.0	1448.4	0.4	0.0	1460.2	12.2	0.8	1460.2	12.2	0.8	1455.6	7.6	0.5	1455.6	7.6	0.5	1448.1	0.1	0.0
0703_M2_BELT_50minsAbrasive_49.6Nm_20kHz_001.txt	1442.0	1443.6	1.6	0.1	1423.6	18.4	1.3	1432.7	9.3	0.6	1446.4	4.4	0.3	1440.3	1.7	0.1	1441.9	0.1	0.0
0803_M4_BELT_H_0Nm_20kHz_001.txt	1499.0	1498.5	0.5	0.0	1496.8	2.2	0.1	1506.0	7.0	0.5	1495.3	3.7	0.2	1501.4	2.4	0.2	1502.5	3.5	0.2
0803_M4_BELT_H_30Nm_20kHz_001.txt	1467.0	1465.3	1.7	0.1	1469.3	2.3	0.2	1469.3	2.3	0.2	1464.8	2.2	0.2	1470.9	3.9	0.3	1467.5	0.5	0.0
0803_M4_BELT_H_35Nm_20kHz_001.txt	1461.0	1459.5	1.5	0.1	1460.2	0.8	0.1	1460.2	0.8	0.1	1455.6	5.4	0.4	1464.8	3.8	0.3	1461.2	0.2	0.0
0803_M4_BELT_H_40Nm_20kHz_001.txt	1455.0	1454.4	0.6	0.0	1451.0	4.0	0.3	1441.9	13.1	0.9	1440.3	14.7	1.0	1455.6	0.6	0.0	1454.9	0.1	0.0
0803_M4_BELT_H_45Nm_20kHz_001.txt	1448.0	1449.1	1.1	0.1	1451.0	3.0	0.2	1451.0	3.0	0.2	1446.4	1.6	0.1	1455.6	7.6	0.5	1449.1	1.1	0.1
0803_M4_BELT_H_49.6Nm_20kHz_001.txt	1443.0	1444.2	1.2	0.1	1432.7	10.3	0.7	1441.9	1.1	0.1	1437.3	5.7	0.4	1446.4	3.4	0.2	1444.2	1.2	0.1
0903_M3_BELT_STATOR_0T_45Nm_20kHz_001.txt	1448.0	1448.7	0.7	0.0	1441.9	6.1	0.4	1432.7	15.3	1.1	1428.1	19.9	1.4	1428.1	19.9	1.4	1448.4	0.4	0.0
1003_M3_BELT_STATOR_0T_45Nm_20kHz_001.txt	1449.0	1448.8	0.2	0.0	1460.2	11.2	0.8	1441.9	7.1	0.5	1446.4	2.6	0.2	1443.4	5.6	0.4	1449.1	0.1	0.0
1103_M4_BELT_SE_0Nm_20kHz_001.txt	1495.0	1494.5	0.5	0.0	1496.8	1.8	0.1	1496.8	1.8	0.1	1501.4	6.4	0.4	1492.2	2.8	0.2	1496.7	1.7	0.1
1103_M4_BELT_SE_30Nm_20kHz_001.txt	1464.0	1464.9	0.9	0.1	1469.3	5.3	0.4	1460.2	3.8	0.3	1464.8	0.8	0.1	1464.8	0.8	0.1	1464.8	0.8	0.1
1103_M4_BELT_SE_35Nm_20kHz_001.txt	1458.0	1459.6	1.6	0.1	1460.2	2.2	0.1	1460.2	2.2	0.1	1464.8	6.8	0.5	1455.6	2.4	0.2	1458.5	0.5	0.0

Filename	w_act	w_est			SVAmF			SVAnF			Fs-fr			Fs+fr			RBPF		
		Speed (rpm)	E (rpm)	E (%)	Speed (rpm)	E (rpm)	E (%)	Speed (rpm)	E (rpm)	E (%)	Speed (rpm)	E (rpm)	E (%)	Speed (rpm)	E (rpm)	E (%)	Speed (rpm)	E (rpm)	E (%)
1103_M4_BELT_SE_40Nm_20kHz_001.txt	1452.0	1454.6	2.6	0.2	1451.0	1.0	0.1	1451.0	1.0	0.1	1455.6	3.6	0.2	1446.4	5.6	0.4	1452.7	0.7	0.0
1103_M4_BELT_SE_45Nm_20kHz_001.txt	1446.0	1449.3	3.3	0.2	1441.9	4.1	0.3	1441.9	4.1	0.3	1446.4	0.4	0.0	1437.3	8.7	0.6	1446.8	0.8	0.1
1103_M4_BELT_SE_49.6Nm_20kHz_001.txt	1440.0	1444.3	4.3	0.3	1441.9	1.9	0.1	1441.9	1.9	0.1	1446.4	6.4	0.4	1437.3	2.7	0.2	1440.9	0.9	0.1
1403_BELT_M2_1.5mm_0Nm_20kHz_001.txt	1498.0	1494.2	3.8	0.3	1496.8	1.2	0.1	1496.8	1.2	0.1	1489.2	8.8	0.6	1498.3	0.3	0.0	1501.0	3.0	0.2
1403_BELT_M2_1.5mm_30Nm_20kHz_001.txt	1467.0	1466.2	0.8	0.1	1487.6	20.6	1.4	1469.3	2.3	0.2	1473.9	6.9	0.5	1461.7	5.3	0.4	1468.0	1.0	0.1
1403_BELT_M2_1.5mm_35Nm_20kHz_001.txt	1462.0	1460.4	1.6	0.1	1460.2	1.8	0.1	1460.2	1.8	0.1	1464.8	2.8	0.2	1458.7	3.3	0.2	1462.0	0.0	0.0
1403_BELT_M2_1.5mm_40Nm_20kHz_001.txt	1455.0	1454.2	0.8	0.1	1451.0	4.0	0.3	1451.0	4.0	0.3	1446.4	8.6	0.6	1455.6	0.6	0.0	1454.9	0.1	0.0
1403_BELT_M2_1.5mm_45Nm_20kHz_001.txt	1448.0	1448.9	0.9	0.1	1460.2	12.2	0.8	1460.2	12.2	0.8	1455.6	7.6	0.5	1464.8	16.8	1.2	1449.1	1.1	0.1
1403_BELT_M2_1.5mm_49.6Nm_20kHz_001.txt	1443.0	1443.9	0.9	0.1	1441.9	1.1	0.1	1441.9	1.1	0.1	1446.4	3.4	0.2	1437.3	5.7	0.4	1443.8	0.8	0.1
1503_BELT_M4_DE_0Nm_20kHz_001.txt	1497.0	1494.3	2.7	0.2	1496.8	0.2	0.0	1496.8	0.2	0.0	1495.3	1.7	0.1	1498.3	1.3	0.1	1498.9	1.9	0.1
1503_BELT_M4_DE_30Nm_20kHz_001.txt	1469.0	1466.3	2.7	0.2	1469.3	0.3	0.0	1469.3	0.3	0.0	1473.9	4.9	0.3	1464.8	4.2	0.3	1467.4	1.6	0.1
1503_BELT_M4_DE_35Nm_20kHz_001.txt	1459.0	1459.4	0.4	0.0	1460.2	1.2	0.1	1460.2	1.2	0.1	1455.6	3.4	0.2	1455.6	3.4	0.2	1459.5	0.5	0.0
1503_BELT_M4_DE_40Nm_20kHz_001.txt	1452.0	1454.3	2.3	0.2	1451.0	1.0	0.1	1451.0	1.0	0.1	1455.6	3.6	0.2	1437.3	14.7	1.0	1451.3	0.7	0.0
1503_BELT_M4_DE_45Nm_20kHz_001.txt	1444.0	1449.1	5.1	0.4	1441.9	2.1	0.1	1441.9	2.1	0.1	1446.4	2.4	0.2	1464.8	20.8	1.4	1444.8	0.8	0.1
1503_BELT_M4_DE_49.6Nm_20kHz_001.txt	1438.0	1444.2	6.2	0.4	1441.9	3.9	0.3	1441.9	3.9	0.3	1437.3	0.7	0.0	1437.3	0.7	0.0	1438.9	0.9	0.1
2103_BELT_M1_H_0Nm_20kHz_001.txt	1495.0	1493.9	1.1	0.1	1487.6	7.4	0.5	1496.8	1.8	0.1	1501.4	6.4	0.4	1492.2	2.8	0.2	1497.8	2.8	0.2
2103_BELT_M1_H_30Nm_20kHz_001.txt	1465.0	1464.2	0.8	0.1	1469.3	4.3	0.3	1460.2	4.8	0.3	1464.8	0.2	0.0	1455.6	9.4	0.6	1464.1	0.9	0.1
2103_BELT_M1_H_35Nm_20kHz_001.txt	1459.0	1458.9	0.1	0.0	1460.2	1.2	0.1	1460.2	1.2	0.1	1455.6	3.4	0.2	1455.6	3.4	0.2	1458.2	0.8	0.1
2103_BELT_M1_H_40Nm_20kHz_001.txt	1452.0	1453.8	1.8	0.1	1451.0	1.0	0.1	1451.0	1.0	0.1	1455.6	3.6	0.2	1455.6	3.6	0.2	1453.0	1.0	0.1

Filename	w_act	w_est			SVAmF			SVAnF			Fs-fr			Fs+fr			RBPF		
		Speed (rpm)	E (rpm)	E (%)	Speed (rpm)	E (rpm)	E (%)	Speed (rpm)	E (rpm)	E (%)	Speed (rpm)	E (rpm)	E (%)	Speed (rpm)	E (rpm)	E (%)	Speed (rpm)	E (rpm)	E (%)
2103_BELT_M1_H_45Nm_20kHz_001.txt	1446.0	1448.5	2.5	0.2	1441.9	4.1	0.3	1441.9	4.1	0.3	1437.3	8.7	0.6	1437.3	8.7	0.6	1447.1	1.1	0.1
2103_BELT_M1_H_49.6Nm_20kHz_001.txt	1441.0	1443.6	2.6	0.2	1441.9	0.9	0.1	1441.9	0.9	0.1	1446.4	5.4	0.4	1437.3	3.7	0.3	1441.2	0.2	0.0
2103_BELT_M2_H_0Nm_20kHz_001.txt	1496.0	1494.6	1.4	0.1	1496.8	0.8	0.1	1496.8	0.8	0.1	1492.2	3.8	0.3	1492.2	3.8	0.3	1498.8	2.8	0.2
2103_BELT_M2_H_30Nm_20kHz_001.txt	1465.0	1465.0	0.0	0.0	1478.5	13.5	0.9	1460.2	4.8	0.3	1461.7	3.3	0.2	1464.8	0.2	0.0	1465.1	0.1	0.0
2103_BELT_M2_H_40Nm_20kHz_001.txt	1454.0	1454.6	0.6	0.0	1451.0	3.0	0.2	1451.0	3.0	0.2	1446.4	7.6	0.5	1455.6	1.6	0.1	1454.3	0.3	0.0
2103_BELT_M2_H_45Nm_20kHz_001.txt	1448.0	1449.3	1.3	0.1	1469.3	21.3	1.5	1469.3	21.3	1.5	1464.8	16.8	1.2	1464.8	16.8	1.2	1448.1	0.1	0.0
2103_M2_BELT_H_49.6Nm_20kHz_001.txt	1442.0	1444.2	2.2	0.2	1441.9	0.1	0.0	1441.9	0.1	0.0	1437.3	4.7	0.3	1446.4	4.4	0.3	1443.2	1.2	0.1
2303_M1_BELT_ROTOR2.5mm_0Nm_20kHz_001.txt	1498.0	1494.4	3.6	0.2	1496.8	1.2	0.1	1496.8	1.2	0.1	1492.2	5.8	0.4	1498.3	0.3	0.0	1499.8	1.8	0.1
2303_M1_BELT_ROTOR2.5mm_30Nm_20kHz_001.txt	1466.0	1464.7	1.3	0.1	1469.3	3.3	0.2	1469.3	3.3	0.2	1464.8	1.2	0.1	1467.8	1.8	0.1	1466.4	0.4	0.0
2303_M1_BELT_ROTOR2.5mm_35Nm_20kHz_001.txt	1461.0	1459.5	1.5	0.1	1460.2	0.8	0.1	1460.2	0.8	0.1	1455.6	5.4	0.4	1464.8	3.8	0.3	1460.8	0.2	0.0
2303_M1_BELT_ROTOR2.5mm_40Nm_20kHz_001.txt	1454.0	1454.4	0.4	0.0	1451.0	3.0	0.2	1451.0	3.0	0.2	1455.6	1.6	0.1	1455.6	1.6	0.1	1454.0	0.0	0.0
2303_M1_BELT_ROTOR2.5mm_45Nm_20kHz_001.txt	1447.0	1449.0	2.0	0.1	1441.9	5.1	0.4	1441.9	5.1	0.4	1437.3	9.7	0.7	1437.3	9.7	0.7	1448.4	1.4	0.1
2303_M1_BELT_ROTOR2.5mm_49.6Nm_20kHz_001.txt	1442.0	1444.1	2.1	0.1	1441.9	0.1	0.0	1441.9	0.1	0.0	1437.3	4.7	0.3	1437.3	4.7	0.3	1442.5	0.5	0.0
2403_M1_BELT_ROTOR_3.5mm_0Nm_20kHz_001.txt	1497.0	1494.3	2.7	0.2	1496.8	0.2	0.0	1496.8	0.2	0.0	1492.2	4.8	0.3	1501.4	4.4	0.3	1499.2	2.2	0.1
2403_M1_BELT_ROTOR_3.5mm_30Nm_20kHz_001.txt	1467.0	1464.7	2.3	0.2	1469.3	2.3	0.2	1469.3	2.3	0.2	1464.8	2.2	0.2	1461.7	5.3	0.4	1467.0	0.0	0.0
2403_M1_BELT_ROTOR_3.5mm_35Nm_20kHz_001.txt	1462.0	1459.3	2.7	0.2	1460.2	1.8	0.1	1460.2	1.8	0.1	1455.6	6.4	0.4	1467.8	5.8	0.4	1461.5	0.5	0.0
2403_M1_BELT_ROTOR_3.5mm_40Nm_20kHz_001.txt	1456.0	1454.3	1.7	0.1	1460.2	4.2	0.3	1460.2	4.2	0.3	1455.6	0.4	0.0	1455.6	0.4	0.0	1455.6	0.4	0.0
2403_M1_BELT_ROTOR_3.5mm_45Nm_20kHz_001.txt	1449.0	1448.9	0.1	0.0	1432.7	16.3	1.1	1432.7	16.3	1.1	1428.1	20.9	1.4	1437.3	11.7	0.8	1449.1	0.1	0.0
2403_M1_BELT_ROTOR_3.5mm_49.6Nm_20kHz_001.txt	1443.0	1444.0	1.0	0.1	1441.9	1.1	0.1	1441.9	1.1	0.1	1437.3	5.7	0.4	1446.4	3.4	0.2	1443.8	0.8	0.1

Filename	w_act	w_est			SVAmF			SVAnF			Fs-fr			Fs+fr			RBPF		
		Speed (rpm)	E (rpm)	E (%)	Speed (rpm)	E (rpm)	E (%)	Speed (rpm)	E (rpm)	E (%)	Speed (rpm)	E (rpm)	E (%)	Speed (rpm)	E (rpm)	E (%)	Speed (rpm)	E (rpm)	E (%)
2403_M1_BELT_ROTOR_4.5 mm_0Nm_20kHz_001.txt	1497.0	1494.5	2.5	0.2	1496.8	0.2	0.0	1496.8	0.2	0.0	1492.2	4.8	0.3	1501.4	4.4	0.3	1499.3	2.3	0.2
2403_M1_BELT_ROTOR_4.5 mm_30Nm_20kHz_001.txt	1467.0	1465.0	2.0	0.1	1469.3	2.3	0.2	1469.3	2.3	0.2	1464.8	2.2	0.2	1477.0	10.0	0.7	1467.0	0.0	0.0
2403_M1_BELT_ROTOR_4.5 mm_35Nm_20kHz_001.txt	1461.0	1459.5	1.5	0.1	1460.2	0.8	0.1	1460.2	0.8	0.1	1464.8	3.8	0.3	1455.6	5.4	0.4	1460.5	0.5	0.0
2403_M1_BELT_ROTOR_4.5 mm_40Nm_20kHz_001.txt	1455.0	1454.6	0.4	0.0	1451.0	4.0	0.3	1451.0	4.0	0.3	1455.6	0.6	0.0	1455.6	0.6	0.0	1454.9	0.1	0.0
2403_M1_BELT_ROTOR_4.5 mm_45Nm_20kHz_001.txt	1448.0	1449.3	1.3	0.1	1441.9	6.1	0.4	1441.9	6.1	0.4	1428.1	19.9	1.4	1428.1	19.9	1.4	1448.1	0.1	0.0
2403_M1_BELT_ROTOR_4.5 mm_49.6Nm_20kHz_001.txt	1442.0	1444.4	2.4	0.2	1441.9	0.1	0.0	1441.9	0.1	0.0	1446.4	4.4	0.3	1446.4	4.4	0.3	1443.5	1.5	0.1
2503_M1_BELT_ROTOR_6m m_0Nm_20kHz_001.txt	1496.0	1494.3	1.7	0.1	1496.8	0.8	0.1	1487.6	8.4	0.6	1495.3	0.7	0.0	1480.0	16.0	1.1	1497.4	1.4	0.1
2503_M1_BELT_ROTOR_6m m_30Nm_20kHz_001.txt	1464.0	1464.7	0.7	0.0	1460.2	3.8	0.3	1460.2	3.8	0.3	1464.8	0.8	0.1	1464.8	0.8	0.1	1463.4	0.6	0.0
2503_M1_BELT_ROTOR_6m m_35Nm_20kHz_001.txt	1457.0	1459.4	2.4	0.2	1460.2	3.2	0.2	1460.2	3.2	0.2	1455.6	1.4	0.1	1455.6	1.4	0.1	1457.6	0.6	0.0
2503_M1_BELT_ROTOR_6m m_40Nm_20kHz_001.txt	1452.0	1454.3	2.3	0.2	1451.0	1.0	0.1	1451.0	1.0	0.1	1455.6	3.6	0.2	1446.4	5.6	0.4	1451.3	0.7	0.0
2503_M1_BELT_ROTOR_6m m_45Nm_20kHz_001.txt	1445.0	1448.9	3.9	0.3	1441.9	3.1	0.2	1441.9	3.1	0.2	1446.4	1.4	0.1	1446.4	1.4	0.1	1444.8	0.2	0.0
2503_M1_BELT_ROTOR_6m m_49.6Nm_20kHz_001.txt	1439.0	1444.0	5.0	0.3	1441.9	2.9	0.2	1441.9	2.9	0.2	1437.3	1.7	0.1	1437.3	1.7	0.1	1438.9	0.1	0.0

Average	Est	1.78	0.12	SVAmF	4.32	0.30	SVAnF	3.70	0.25	fs-fr	5.10	0.35	fs+fr	5.24	0.36	RBPF	0.84	0.06
Maximum		6.17	0.43		21.33	1.47		21.33	1.47		20.86	1.44		20.75	1.44		3.46	0.23

Appendix F: Bar number estimation results

Filename	fs	T_act	T_est	w_act	w_est			RBPF_w_est			Rbar_est
					val	err(%)	err(rpm)	val	err(%)	err(rpm)	
0703_M2_BELT_50minsAbrasive_0Nm_20kHz_001.txt	50.0	0.0	4.8	1496.0	1493.8	0.1	2.2	1498.6	0.2	2.6	36
0703_M2_BELT_50minsAbrasive_30Nm_20kHz_001.txt	50.0	30.0	32.0	1466.0	1464.1	0.1	1.9	1466.3	0.0	0.3	28
0703_M2_BELT_50minsAbrasive_35Nm_20kHz_001.txt	50.1	35.0	36.9	1462.0	1460.0	0.1	2.0	1462.1	0.0	0.1	28
0703_M2_BELT_50minsAbrasive_40Nm_20kHz_001.txt	50.0	40.0	41.6	1454.0	1453.7	0.0	0.3	1454.3	0.0	0.3	28
0703_M2_BELT_50minsAbrasive_45Nm_20kHz_001.txt	50.0	45.0	46.4	1448.0	1448.4	0.0	0.4	1448.4	0.0	0.4	28
0703_M2_BELT_50minsAbrasive_49.6Nm_20kHz_001.txt	50.0	49.6	50.9	1442.0	1443.6	0.1	1.6	1442.2	0.0	0.2	28
0803_M4_BELT_H_0Nm_20kHz_001.txt	50.1	0.0	4.3	1499.0	1498.5	0.0	0.5	1502.1	0.2	3.1	12
0803_M4_BELT_H_30Nm_20kHz_001.txt	50.0	30.0	31.5	1467.0	1465.3	0.1	1.7	1467.6	0.0	0.6	28
0803_M4_BELT_H_35Nm_20kHz_001.txt	50.0	35.0	36.3	1461.0	1459.5	0.1	1.5	1461.5	0.0	0.5	28
0803_M4_BELT_H_40Nm_20kHz_001.txt	50.0	40.0	40.9	1455.0	1454.4	0.0	0.6	1455.3	0.0	0.3	28
0803_M4_BELT_H_45Nm_20kHz_001.txt	50.0	45.0	45.8	1448.0	1449.1	0.1	1.1	1449.4	0.1	1.4	28
0803_M4_BELT_H_49.6Nm_20kHz_001.txt	50.1	49.6	50.3	1443.0	1444.2	0.1	1.2	1443.8	0.1	0.8	28
0903_M3_BELT_STATOR_0T_45Nm_20kHz_001.txt	50.0	45.0	46.2	1448.0	1448.7	0.0	0.7	1448.4	0.0	0.4	28
1003_M3_BELT_STATOR_0T_45Nm_20kHz_001.txt	50.0	45.0	46.1	1449.0	1448.8	0.0	0.2	1448.8	0.0	0.2	28
1103_M4_BELT_SE_0Nm_20kHz_001.txt	50.0	0.0	4.2	1495.0	1494.5	0.0	0.5	1496.8	0.1	1.8	16
1103_M4_BELT_SE_30Nm_20kHz_001.txt	50.0	30.0	31.3	1464.0	1464.9	0.1	0.9	1464.8	0.1	0.8	28
1103_M4_BELT_SE_35Nm_20kHz_001.txt	50.0	35.0	36.1	1458.0	1459.6	0.1	1.6	1458.2	0.0	0.2	28
1103_M4_BELT_SE_40Nm_20kHz_001.txt	50.0	40.0	40.8	1452.0	1454.6	0.2	2.6	1452.3	0.0	0.3	28
1103_M4_BELT_SE_45Nm_20kHz_001.txt	50.0	45.0	45.7	1446.0	1449.3	0.2	3.3	1446.4	0.0	0.4	28
1103_M4_BELT_SE_49.6Nm_20kHz_001.txt	50.0	49.6	50.2	1440.0	1444.3	0.3	4.3	1440.6	0.0	0.6	28
1403_BELT_M2_1.5mm_0Nm_20kHz_001.txt	50.0	0.0	4.5	1498.0	1494.2	0.3	3.8	1500.4	0.2	2.4	36
1403_BELT_M2_1.5mm_30Nm_20kHz_001.txt	50.1	30.0	31.6	1467.0	1466.2	0.1	0.8	1467.7	0.0	0.7	28
1403_BELT_M2_1.5mm_35Nm_20kHz_001.txt	50.1	35.0	36.5	1462.0	1460.4	0.1	1.6	1461.8	0.0	0.2	28
1403_BELT_M2_1.5mm_40Nm_20kHz_001.txt	50.0	40.0	41.2	1455.0	1454.2	0.1	0.8	1455.3	0.0	0.3	28
1403_BELT_M2_1.5mm_45Nm_20kHz_001.txt	50.0	45.0	46.0	1448.0	1448.9	0.1	0.9	1449.4	0.1	1.4	28
1403_BELT_M2_1.5mm_49.6Nm_20kHz_001.txt	50.1	49.6	50.5	1443.0	1443.9	0.1	0.9	1443.5	0.0	0.5	28
1503_BELT_M4_DE_0Nm_20kHz_001.txt	50.0	0.0	4.4	1497.0	1494.3	0.2	2.7	1497.6	0.0	0.6	36
1503_BELT_M4_DE_30Nm_20kHz_001.txt	50.1	30.0	31.5	1469.0	1466.3	0.2	2.7	1467.0	0.1	2.0	28
1503_BELT_M4_DE_35Nm_20kHz_001.txt	50.0	35.0	36.4	1459.0	1459.4	0.0	0.4	1459.5	0.0	0.5	28
1503_BELT_M4_DE_40Nm_20kHz_001.txt	50.0	40.0	41.0	1452.0	1454.3	0.2	2.3	1451.2	0.1	0.8	28
1503_BELT_M4_DE_45Nm_20kHz_001.txt	50.0	45.0	45.8	1444.0	1449.1	0.4	5.1	1444.8	0.1	0.8	28
1503_BELT_M4_DE_49.6Nm_20kHz_001.txt	50.0	49.6	50.3	1438.0	1444.2	0.4	6.2	1438.9	0.1	0.9	28
2103_BELT_M1_H_0Nm_20kHz_001.txt	50.0	0.0	4.8	1495.0	1493.9	0.1	1.1	1497.4	0.2	2.4	16
2103_BELT_M1_H_30Nm_20kHz_001.txt	50.0	30.0	31.9	1465.0	1464.2	0.1	0.8	1464.1	0.1	0.9	28
2103_BELT_M1_H_35Nm_20kHz_001.txt	50.0	35.0	36.8	1459.0	1458.9	0.0	0.1	1458.2	0.1	0.8	28
2103_BELT_M1_H_40Nm_20kHz_001.txt	50.0	40.0	41.5	1452.0	1453.8	0.1	1.8	1453.0	0.1	1.0	28

Filename	fs	T_act	T_est	w_act	w_est			RBPF_w_est			Rbar_est
					val	err(%)	err(rpm)	val	err(%)	err(rpm)	
2103_BELT_M1_H_45Nm_20kHz_001.txt	50.0	45.0	46.4	1446.0	1448.5	0.2	2.5	1446.8	0.1	0.8	28
2103_BELT_M1_H_49.6Nm_20kHz_001.txt	50.0	49.6	50.9	1441.0	1443.6	0.2	2.6	1441.2	0.0	0.2	28
2103_BELT_M2_H_0Nm_20kHz_001.txt	50.0	0.0	4.1	1496.0	1494.6	0.1	1.4	1498.7	0.2	2.7	24
2103_BELT_M2_H_30Nm_20kHz_001.txt	50.0	30.0	31.3	1465.0	1465.0	0.0	0.0	1464.8	0.0	0.2	28
2103_BELT_M2_H_40Nm_20kHz_001.txt	50.0	40.0	40.8	1454.0	1454.6	0.0	0.6	1454.6	0.0	0.6	28
2103_BELT_M2_H_45Nm_20kHz_001.txt	50.0	45.0	45.7	1448.0	1449.3	0.1	1.3	1448.1	0.0	0.1	28
2103_M2_BELT_H_49.6Nm_20kHz_001.txt	50.0	49.6	50.3	1442.0	1444.2	0.2	2.2	1443.5	0.1	1.5	28
2303_M1_BELT_ROTOR2.5mm_0Nm_20kHz_001.txt	50.0	0.0	4.3	1498.0	1494.4	0.2	3.6	1498.8	0.1	0.8	36
2303_M1_BELT_ROTOR2.5mm_30Nm_20kHz_001.txt	50.0	30.0	31.5	1466.0	1464.7	0.1	1.3	1466.4	0.0	0.4	28
2303_M1_BELT_ROTOR2.5mm_35Nm_20kHz_001.txt	50.0	35.0	36.3	1461.0	1459.5	0.1	1.5	1460.8	0.0	0.2	28
2303_M1_BELT_ROTOR2.5mm_40Nm_20kHz_001.txt	50.0	40.0	41.0	1454.0	1454.4	0.0	0.4	1454.3	0.0	0.3	28
2303_M1_BELT_ROTOR2.5mm_45Nm_20kHz_001.txt	50.0	45.0	45.9	1447.0	1449.0	0.1	2.0	1448.4	0.1	1.4	28
2303_M1_BELT_ROTOR2.5mm_49.6Nm_20kHz_001.txt	50.0	49.6	50.4	1442.0	1444.1	0.1	2.1	1442.5	0.0	0.5	28
2403_M1_BELT_ROTOR_3.5mm_0Nm_20kHz_001.txt	50.0	0.0	4.4	1497.0	1494.3	0.2	2.7	1498.3	0.1	1.3	36
2403_M1_BELT_ROTOR_3.5mm_30Nm_20kHz_001.txt	50.0	30.0	31.5	1467.0	1464.7	0.2	2.3	1467.0	0.0	0.0	28
2403_M1_BELT_ROTOR_3.5mm_35Nm_20kHz_001.txt	50.0	35.0	36.4	1462.0	1459.3	0.2	2.7	1461.8	0.0	0.2	28
2403_M1_BELT_ROTOR_3.5mm_40Nm_20kHz_001.txt	50.0	40.0	41.1	1456.0	1454.3	0.1	1.7	1455.9	0.0	0.1	28
2403_M1_BELT_ROTOR_3.5mm_45Nm_20kHz_001.txt	50.0	45.0	46.0	1449.0	1448.9	0.0	0.1	1449.2	0.0	0.2	28
2403_M1_BELT_ROTOR_3.5mm_49.6Nm_20kHz_001.txt	50.0	49.6	50.5	1443.0	1444.0	0.1	1.0	1444.2	0.1	1.2	28
2403_M1_BELT_ROTOR_4.5mm_0Nm_20kHz_001.txt	50.0	0.0	4.2	1497.0	1494.5	0.2	2.5	1498.3	0.1	1.3	36
2403_M1_BELT_ROTOR_4.5mm_30Nm_20kHz_001.txt	50.0	30.0	31.3	1467.0	1465.0	0.1	2.0	1467.0	0.0	0.0	28
2403_M1_BELT_ROTOR_4.5mm_35Nm_20kHz_001.txt	50.0	35.0	36.2	1461.0	1459.5	0.1	1.5	1460.2	0.1	0.8	28
2403_M1_BELT_ROTOR_4.5mm_40Nm_20kHz_001.txt	50.0	40.0	40.8	1455.0	1454.6	0.0	0.4	1454.9	0.0	0.1	28
2403_M1_BELT_ROTOR_4.5mm_45Nm_20kHz_001.txt	50.0	45.0	45.6	1448.0	1449.3	0.1	1.3	1448.1	0.0	0.1	28
2403_M1_BELT_ROTOR_4.5mm_49.6Nm_20kHz_001.txt	50.0	49.6	50.1	1442.0	1444.4	0.2	2.4	1443.2	0.1	1.2	28
2503_M1_BELT_ROTOR_6mm_0Nm_20kHz_001.txt	50.0	0.0	4.4	1496.0	1494.3	0.1	1.7	1498.5	0.2	2.5	16
2503_M1_BELT_ROTOR_6mm_30Nm_20kHz_001.txt	50.0	30.0	31.5	1464.0	1464.7	0.0	0.7	1463.1	0.1	0.9	28
2503_M1_BELT_ROTOR_6mm_35Nm_20kHz_001.txt	50.0	35.0	36.4	1457.0	1459.4	0.2	2.4	1457.2	0.0	0.2	28
2503_M1_BELT_ROTOR_6mm_40Nm_20kHz_001.txt	50.0	40.0	41.1	1452.0	1454.3	0.2	2.3	1451.3	0.0	0.7	28
2503_M1_BELT_ROTOR_6mm_45Nm_20kHz_001.txt	50.0	45.0	45.9	1445.0	1448.9	0.3	3.9	1444.5	0.0	0.5	28
2503_M1_BELT_ROTOR_6mm_49.6Nm_20kHz_001.txt	50.0	49.6	50.5	1439.0	1444.0	0.3	5.0	1438.9	0.0	0.1	28

Average	0.12	1.78		0.05	0.78	
Maximum	0.43	6.17		0.21	3.14	
Average (loaded only)	0.12	1.72		0.04	0.55	
Maximum (loaded only)	0.43	6.17		0.13	1.96	

Page left intentionally blank